CONTROL OF A BRUSHLESS PERMANENT MAGNET MACHINE USING AN INTEGRATED TORQUE SENSOR IN PLACE OF A ROTOR POSITION SENSOR

A thesis submitted to the University of Manchester for the degree of
Doctor of Philosophy
In the faculty of Engineering and Physical Sciences

December 2010

By

Fayez Alrifai

School of Electrical and Electronic Engineering

TABLE OF CONTENTS

CHAPTER 4

EXPERIMENTAL VALDITION FOR START-UP ROUTINE

CHAPTER 5

FLUX-LINKAGE ESTIMATION USING MEASURED TORQUE FEEDBACK

The world count for this thesis is 42,382 words

NOMENCLATURE

ψ_α	Flux-linkage in stationary α reference frame	Wb-turns
ψ_β	Flux-linkage in stationary β reference frame	Wb-turns
ψ_{sn}	Flux-linkage generated from v_{sn}	Wb-turns
ψ_f	Flux-linkage established by the permanent magnets	Wb-turns
u_{DC}	DC voltage	Volts
u_α	Stator voltage in stationary α reference frame	Volts
u_β	Stator voltage in stationary β reference frame	Volts
u_w	Phase w stator voltage	Volts
u_v	Phase v stator voltage	Volts
u_u	Phase u stator voltage	Volts
v_d	Stator voltage in rotor d reference frame measured	Volts
v_q	Stator voltage in rotor q reference frame measured	Volts
$v_{hypotheticald}$	Stator voltage in rotor d reference frame calculated	Volts
$v_{hypotheticalq}$	Stator voltage in rotor q reference frame calculated	Volts
v_{as}	Voltage difference between point a and point s	Volts
v_{sn}	Voltage difference between point s and point n	Volts
v_{na}	Voltage difference between point n and point a	Volts
v_{bs}	Voltage difference between point b and point s	Volts
v_{nb}	Voltage difference between point n and point b	Volts
v_{cs}	Voltage difference between point c and point s	Volts
v_{nc}	Voltage difference between point n and point c	Volts
$v_{thirsharmonic}$	Third harmonic voltage	Volts
v_{high}	High frequency voltage	Volts
Δv	Difference between measured and calculated voltages	Volts
u_β	Stator voltage in stationary β reference frame	Volts
u_α	Stator voltage in stationary α reference frame	Volts
i_α	Stator current in stationary α reference frame	Amps
i_β	Stator current in stationary β reference frame	Amps
i_d	Stator current in rotor d reference frame measured	Amps
i_q	Stator current in rotor q reference frame measured	Amps
$i_{hypotheticald}$	Stator current in rotor d reference frame calculated	Amps
$i_{hypotheticalq}$	Stator current in rotor q reference frame calculated	Amps
Δi	Difference between measured and calculated currents	Amps
i_u	Phase u stator current	Amps
i_v	Phase v stator current	Amps
i_w	Phase w stator current	Amps
R_s	Phase resistance	Ω

e_u	Phase u stator back electro magnetic force	Volts
e_v	Phase v stator back electro magnetic force	Volts
e_w	Phase w stator back electro magnetic force	Volts
L_s	Stator winding self inductance	Henry
L_{ls}	Leakage inductance of stator winding	Henry
L_m	Magnetizing inductance due to the fundamental air-gap flux	Henry
L_d	Inductance in rotor d reference frame	Henry
L_q	Inductance in rotor q reference frame	Henry
L_u	Phase u stator synchronous inductance	Henry
L_v	Phase v stator synchronous inductance	Henry
L_w	Phase w stator synchronous inductance	Henry
L_{uv}	Mutual inductance between phase u and phase v	Henry
L_{uw}	Mutual inductance between phase u and phase w	Henry
L_{vu}	Mutual inductance between phase v and phase u	Henry
L_{vw}	Mutual inductance between phase v and phase w	Henry
L_{wu}	Mutual inductance between phase w and phase u	Henry
L_{wv}	Mutual inductance between phase w and phase v	Henry
L_{uu}	Self inductance phase u	Henry
L_{vv}	Self inductance phase v	Henry
L_{ww}	Self inductance phase w	Henry
$\Delta\theta_e$	Difference between measured and calculated electrical position	rad
θ_0	Initial electrical position	Rad
θ_{error}	Error between measured and estimated electrical position	Rad_e
θ_{es}	Estimated electrical position	Rad_e
θ_δ	Load angle position offset	Rad_e
θ_ψ	Flux linkage position	Wb-t
ω_e	Electrical angular velocity	Rad/s
ω_m	Mechanical angular velocity	Rad/sec
P	Pole pairs	
T_{es}	Synchronous torque	Nm
T_{er}	Reluctance torque	Nm
T_e	Electromagnetic torque	Nm
T_l	Load torque	Nm
T_u	Electromagnetic torque for phase u	Nm
T_v	Electromagnetic torque for phase v	Nm
T_w	Electromagnetic torque for phase w	Nm
T_{uv}	Electromagnetic torque for phase u and phase v	Nm
T_{vw}	Electromagnetic torque for phase v and phase w	Nm
T_{wu}	Electromagnetic torque for phase w and phase u	Nm
T_{high}	Largest electromagnetic torque value between two sectors	Nm
T_{sense}	Electromagnetic torque that crosses zero between two sectors	Nm
T_{low}	Smallest electromagnetic torque value between two sectors	Nm
T_m	Maximum electromagnetic torque per electrical period	Nm
d	Distance between sectors	Rad_e
s	The start of the sector	Rad_e

δ	Load angle	Rad_e
P_i	Input power	Watts
P_u	Air-gap power of phase u	Watts
P_v	Air-gap power of phase v	Watts
P_w	Air-gap power of phase w	Watts
J	Inertia of the rotor and connected load	$kg.m^2$
B	Damping coefficient	Nm/ω_m
k_e	Back electro magnetic-force constant	V/ω_e
t	Time	s
k_t	Torque constant	Nm/A

LIST OF TABLES

LIST OF FIGURES

ABSTRACT

The work presented in this thesis proposes the use of measured torque feedback from an integrated, low cost surface acoustic wave (SAW) torque transducer in place of a position sensor to control brushless permanent magnet (BLPM) machines. The BLPM machine closed loop control requires knowledge of the rotor position to control stator current and maximum torque per ampere. The electrical position feedback to control the phase current requires a position sensor or position sensorless technique.

Position sensors such as absolute encoder or resolver are needed for position information, in the absolute encoder, an accurately patterned disk rotates between a light source and a detector giving a unique digital output signal for every shaft position. However, each bit in the digital world represents an independent track on the encoder disk, resulting in a complex and costly sensors. Brushless resolvers operation is based on inductive coupling between stator and rotor winding. The resolver with its resolver to digital converter also gives precise absolute position information, but again the cost is often prohibitive. So the disadvantages of the position sensors are the added cost and size to the machine. The position sensorless techniques for the BLPM machine are based on obtaining position from the terminal voltages and currents based on estimating the back electro-magnetic force (EMF), flux-linkage or inductance which from position can be estimated. The disadvantages of the back-EMF and flux-linkage techniques are (1) that they behave poorly at zero and low speed (2) behave poorly for load disturbances since load torque is estimated from machine parameters which can change. The inductance techniques work at zero and low speed, however the disadvantages are (1) in a surface mounted machine there is no saliency so any variation of winding inductances with rotor position arises from magnetic saturation; (2) the back-EMF dominates the rate-of-change in the current; (3) the variation of incremental inductances with rotor position undergoes two cycles per single electrical cycle of the brushless pm machine causing an ambiguity in sensed position; (4) the distortion due to the nonlinearities in the inverter; (5) the load offsets and the noise caused by signal injection.

This thesis develops a start-up routine and operation algorithms that enhance the performance of position sensorless control of brushless permanent magnet machines at all speeds, including zero speed, and loads by using a machine integrated, low-cost, SAW torque transducer in place of the rotor position sensor.

DECLARATION

No portion of the work referred to in this thesis has been submitted in support of an application for another degree or qualification of this or any other university or other institution learning.

COPYRIGHT STATEMENT

i. The author of this thesis (including any appendices and/or schedules to this thesis) owns certain copyright or related rights in it (the "copyright") and he has given The University of Manchester certain rights to use such Copyright, including for administrative purposes.

ii. Copies of this thesis, either in full or in extracts and whether in hard or electronic copy, may be made **only** in accordance with copyright, designs and Patents Act 1988 (as amended) and regulation issued under it or, where appropriate, in accordance with licensing agreements which the university has from time to time. This page must form part of any such copies made.

iii. The ownership of any certain copyright, patents, designs, trade marks and other intellectual property (the "Intellectual Property Rights") and any reproductions of copyright works in the thesis, for example graphs and tables ("Reproductions"), which may be described in this thesis, may not be owned by the author and may be owned by third parties. Such Intellectual Property and Reproductions cannot and must not be made available for use without the prior written permission of the owner(s) of the relevant Intellectual Property Rights and/or Reproductions.

iv. Further information on the conditions under which disclosure, publication and commercialisation of this thesis, the Copyright and any Intellectual Property and/or Reproductions described in it may take place is available in the University IP Policy(see http://www.campus.manchester.ac.uk/medialibrary/policies/intellectual-property.pdf), in any relevant Thesis restriction declarations deposited in the University Library, The University Library's regulations (see http://www.manchester.ac.uk/library/aboutus/regulations) and in The University's policy on presentation of Theses. from the Head of School or Electrical and Electronic Engineering (or the Vice-President) and the Dean of the Faculty of Life Sciences, for Faculty of Life Sciences' candidates.

ACKNOWLEDGEMENTS

The author acknowledges with thanks and wishes to express his sincere gratitude to Dr Nigel Schofield for his guidance and encouragement during this project and valuable help during the preparation of the thesis.

A special note of thanks goes to Danny and John of the Mechanical Workshop for their fine work on setting up the test rig and to the rest of the Power Conversion Group for their friendship and support. The author is grateful to Public Authority of Applied Education in Kuwait for their financial support of this thesis and to Sensor Technology Ltd (ST), Banbury, UK for providing the experimental devices needed.

Finally, I would like to thank my Mom and my Wife for there love and support which has been much appreciated.

CHAPTER 1

BRUSHLESS PERMANENT MAGNET SERVO DRIVES

1.1 Introduction

When used to control variable torque or speed, brushless permanent magnet (PM) drive systems require rotor position (angle) feedback to effectively control phase current and optimise torque per ampere. To obtain rotor position information with the required angular resolution, position sensors, for example, absolute or incremental optical encoders, resolvers or Hall-effect based sensors are required. These devices add cost to the drive system and are, generally, susceptible to electrical noise, mechanical damage and ambient temperature. Consequently, there has been much research effort to remove these sensors and determine position via other techniques, so-called 'sensorless schemes'. These are in fact position sensorless schemes since they generally utilise other sensors within or around the drive system, as will be reviewed later in this Chapter. This thesis follows on from earlier research investigating the feasibility of utilising a non-contact, integrated, surface acoustic wave (SAW) torque sensor to enhance the dynamic performance of a brushless PM servo drive [1-7], and discusses the potential utilisation of such a device for estimation of rotor angular position. Given that an integrated torque sensor is an additional sensor, albeit a potentially more robust and reliable one then a typical position sensor, the interest of the sponsoring company, Sensor Technology Ltd., Banbury, Oxfordshire, UK, is removal of the rotor position sensor, thus making the torque sensor based system more commercially attractive. The study of position sensorless drive systems is still a very active research area and a review of methods published to date is made in the next section. This

review has tried to be exhaustive in scope so as to clarify the novelty contributed by this thesis. Here, a non contact SAW torque transducer embedded within the PM machine is used to enable position sensorless machine control from zero speed up to speeds where by traditional flux-estimator (for example) may take over the position estimation function. Fig. 1.1 presents an overview of the control of brushless PM machines, illustrating industry and research developments in relation to this thesis study.

The in-line torque transducer is therefore briefly discussed in Chapter 1 and then characterized in Chapter 3. Position sensorless schemes are reviewed in Chapter 1 to set the scene for the thesis study. Chapter 2 presents a position sensorless start-up routine for brushless permanent magnet machines. Chapter 3 discusses machine characterisation and test facilities designed for experimentation and validation of machine control schemes discussed in Chapters 4 and 5. Finally, Chapter 6 will draw the overall conclusions from the research study.

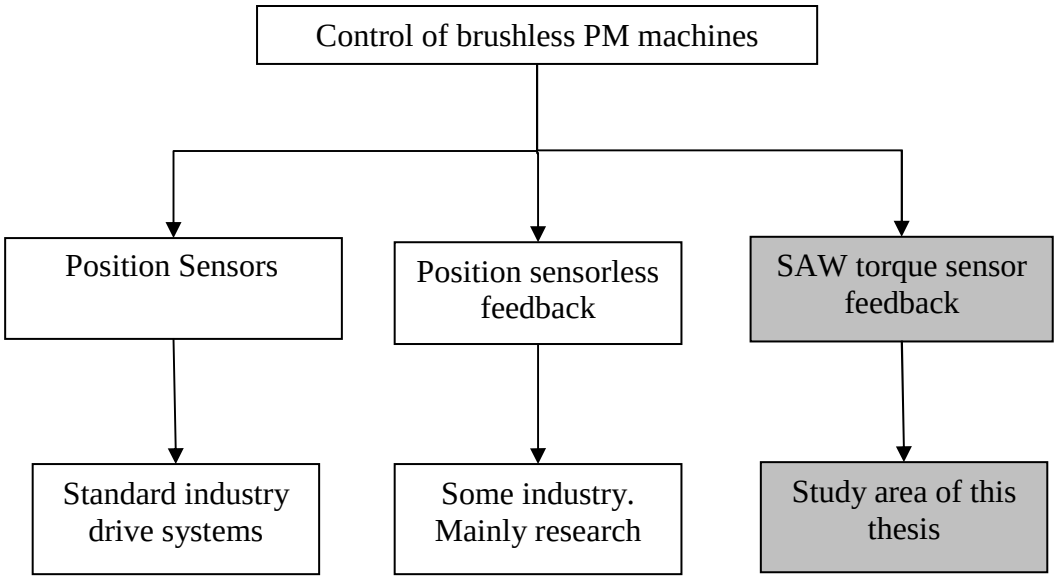

Fig. 1.1 Control of brushless PM machines.

1.2 Surface Acoustic Wave (SAW) Torque Transducer

The SAW torque transducer has been used to enhance the dynamic performance of servo-drive systems by the use of measured shaft torque feedback [1-7]. Common torque transducer measures torque based on the relationship between torque and angle of twist in a shaft, and/or the change of material characteristics when subject to torsional stress. However, in a rotating shaft system, torque measurement is difficult to obtain because supporting circuitry has to contact to a rotating body. Optical torque transducers measure the angle of shaft twist, but that requires a long slender shaft that will lower the system stiffness. Magneto-elastic torque transducers can yield greater system stiffness because they are responsive to torsion stress rather then strain. However, torque measurements that are due to stress induced variation are generally effected by external influences such as magnetic and thermal conditions. Thus, the main deficiencies in most common torque transducer technologies are summarised below [1]:

- high cost.
- reliability and high-repair costs: typically due to excessive torque applied.
- size and space required: transducer size and extra couplings required.
- limited bandwidth: generally around 500Hz.
- impact on control system performance: due to the inherent torsional compliance of the torque transducer.

Therefore, there is great interest in low cost, high performance, non-contact torque measurement and SAW transducers have emerged as a candidate technology for application in high performance electro-mechanical drive-systems [1-5], since they do not significantly affect system stiffness, exhibit high sensitivity, have high bandwidth (≈2.0 kHz) and are relatively unaffected by servo-machine generated electromagnetic noise [1]. Hence, the sensing elements can, in principle, be integrated directly within the servo-machine assembly. The SAW elements and instrument transducer are discussed in further detail in Appendix A1.

Fig. 1.2 schematically illustrates the SAW torque sensor mounted inside an electro-magnetic machine (a). Note, the machine technology is not constrained to brushless PM and could be applied to other brushless machine technologies, i.e. induction, synchronous and switched reluctance machines. However, these are outside the scope of this research study. Fig. 1.2 also illustrates the prototype PM machine with integrated SAW torque sensor and display unit (b) and a cross-section of SAW machine showing the location of the sensing device (c).

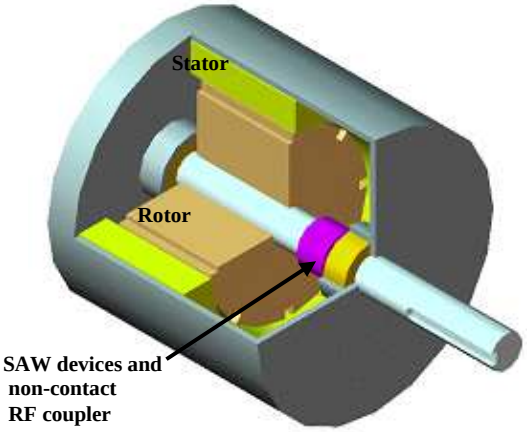

(a) SAW torque sensor inside the prototype PM machine [1].

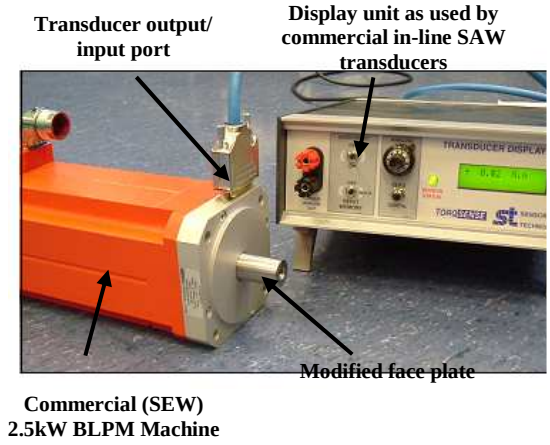

(b) Prototype PM machine with integrated torque transducer [1].

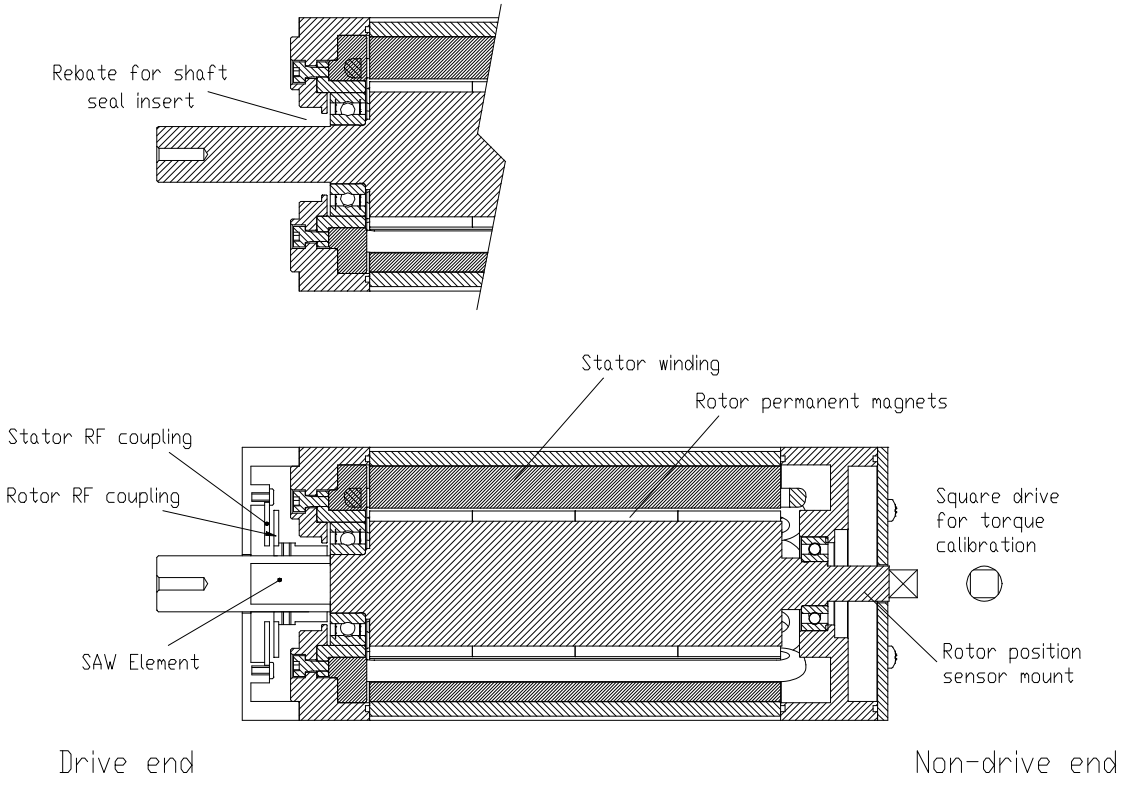

(c) Engineering drawings of the prototype PM machine [1].

Fig. 1.2 Brushless PM machine and integrated SAW torque sensor concept.

1.3 Literature Review of Position Sensorless Control

1.3.1 Introduction

Position sensorless torque controlled drives for machines excited with sine waves (brushless AC) or rectangular phase currents (brushless DC) is not a new research subject with many papers published in the field. For example, the idea of position sensorless torque controlled drives was discussed by Frus and Kuo [13] in the mid 1970's, where they designed control circuitry for a self-synchronously driven step motors under closed-loop control. They determined rotor position via analysis of the phase current waveforms, a technology referred to as 'waveform detection'. This was followed by 'indirect position sensing', so named because the position estimation was due to observation of voltage and current waveforms. Other authors have used the term 'direct position sensing', because the position was sensed directly from measurements at the machine terminals and not via a separate encoder. These drives are now referred to as 'sensorless drives', although the terminology could be considered misleading. The technique should be known as position sensorless which refers to only speed and position sensors, i.e. current and voltage sensors are still required to implement closed loop control [14]. Large drive manufactures (Control Technquies Plc, Siemens, Hitachi, Yaskawa, Eurotherm, etc.) are very interested in sensorless control, some having introduced sensorless induction machine drives [14]. However, at very low speeds these machines can not operate without speed or position sensor feedback. In general, rotor position is measured by a position sensor; Hall-effect sensors, optical encoders and resolvers being the must commonly used devices. Hall-effect sensors require one sensor per phase symmetrically mounted around the machine stator to detect the magnetic field due to the main rotor magnets or an auxiliary magnetised disk. The output signals are processed to provide the logic signals required for the inverter [15].
Brushless AC controlled drives require a high resolution in rotor position for good control of machine phase currents. The position sensor maximum speed of operation is limited by the high-frequency characteristics of the electronics, and particulary by the opto-electronics. The resolution of the disc will determine the speed of operation in which the higher the resolution the higher the cost [8]. Position sensors such as electromagnetic resolvers or digital optical encoders are used when continuous position sensing is required. An electromagnetic resolver and resolver-to-digital converter electronics yield absolute position and is based on transformer coupling between the device stator and rotor windings. Disadvantages are the cost and size of the resolver and associated electronics [9, 10, 14].

Optical encoders are, by far, the most widely used sensors for servo drive systems. There are basically two types of encoders, either incremental or absolute. Incremental optical encoders do not keep track of position all the time and information can be lost when the drive system is turned off. On the other hand, absolute encoders have a specific position output regardless of drive system excitation. As with resolvers, optical position sensors, have a cost disadvantage but, more importantly, they are highly susceptible to external mechanical damage to the sensor and associated cabling, introduce an element of noise to the drive system due to cable lengths, ground loops and screening issues etc. [11, 12, 14]. Consequently, a goal of position sensorless control is to eliminate these sensors, thus reducing the total hardware cost while improving mechanical robustness (and hence reliability) and noise immunity. Many high performance drives require the system to have a small inertia, thus these sensors increase the system inertia and damping. In small drives it is impossible to use such sensors since the cost of the position sensor can be close to that of the machine. Further, the machine and hence associated position sensors may have to be mounted in a hostile environment, again limiting suitability. In summary, the main advantages of position sensorless drives are [14]:

- cost reduction
- hardware reduction
- operation in hostile environments
- higher reliability
- decreased maintenance requirements
- increased noise immunity
- unaffected machine inertia
- application to off-the-shelf machine

It is accepted by many in research and industry that in the future, speed- and position-sensorless drives will emerge and find wide industrial application [14]. For completeness, Appendix A2 discusses the resolver and optical position sensing technologies in greater detail.

1.3.2 Brushless PM machines and drive systems

The simple equivalent circuit for one phase of a brushless PM machine consists of a phase voltage that supplies the phase current to a series resistance, inductance and back-EMF as illustrated in Fig. 1.3 (a). The phase back-EMF voltage is generated by the rotation of the rotor permanent magnet and is therefore dependent on rotor position relative to the stator coils and speed which determines amplitude as will be discussed later. The generated back-EMF vs. electrical position for of a brushless AC (sinusoidal) machine is illustrated in Fig.1.3 (b). If the PM machine inductance exhibits saliency the phase inductance will also vary with rotor electrical position and have a direct mechanical relationship to the machine back-EMF as illustrated in Fig. 1.3 (c).

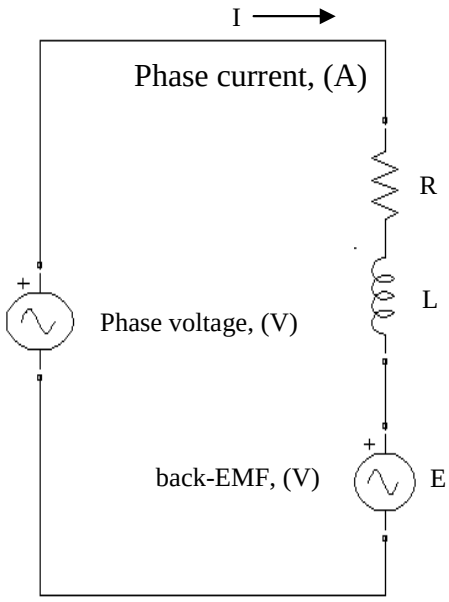

(a) Circuit diagram for one phase

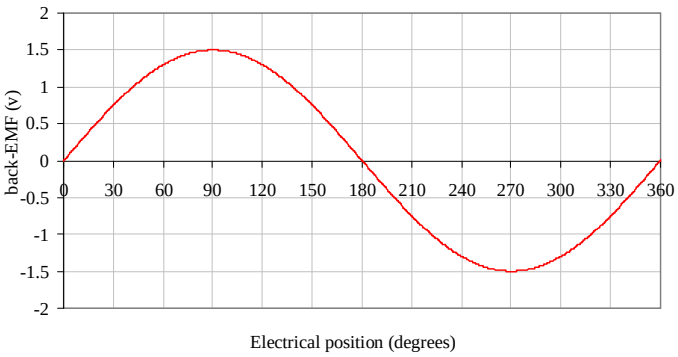

(b) Phase back-EMF voltage.

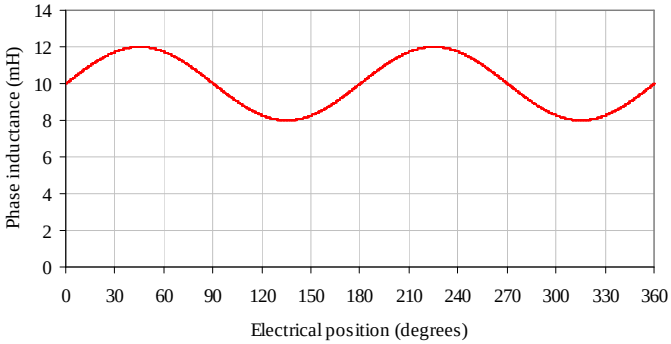

(c) Phase inductance variations.

Fig. 1.3 Simple equivalent circuit representation of one phase of a brushless PM machine.

The machine air gap power is developed when phase current supplied via the drive system power electronic inverter interacts with the machine back-EMF. Since phase inductance and back-EMF vary with rotor position, they both effect the machine current for a known supply voltage waveform. Thus, it is intuitive that by analysis of the machine phase voltage and resultant current waveforms, the inductance, back-EMF or phase flux-linkage can be extracted, from which rotor position can be estimated. These concepts form the cornerstone of most position sensorless control schemes, as illustrated by the flow chart of Fig. 1.4.

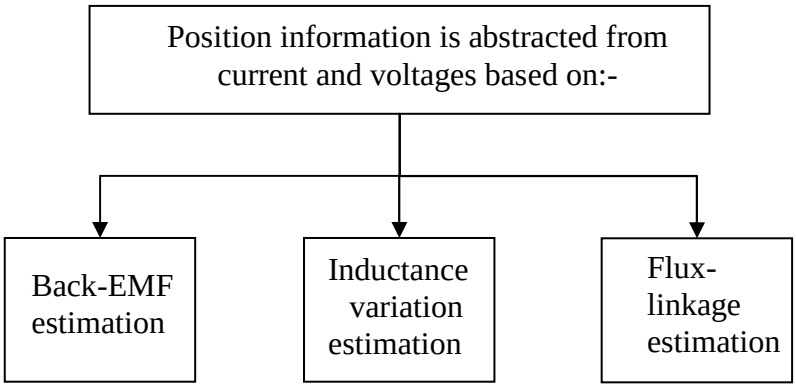

Fig. 1.4 Scope of position sensorless techniques for BLPM machine.

In brushless drive system the machine phase currents are controlled to yield torque output over a speed range dictated by the system DC link voltage. For motor operation, this voltage has to be greater then the back-EMF to achieve fast control of the current. Rated speed is the maximum speed that the machine can operate to without employing flux weakening schemes that allow operation at higher speeds by injecting a negative direct-axis current in the field opposing that of the permanent magnets [16-17]. Position sensorless brushless PM drive systems can be classified into (i) brushless DC and (ii) brushless AC control.

Control of a brushless DC drive requires only two of the three machine phases to be excited at any instant in time. For example, current may flow in phases U and V during one commutation period of 60 electrical degrees, and then in phases U and W for the next 60 electrical degrees. During these commutation events, one phase is not switched by the power electronic inverter (i.e. phase W and V respectively in the preceding discussion) and is allowed to float to a phase terminal voltage determined by the inverter bridge electronics and circulating currents, as disused in much greater detail in [18]. Brushless DC drive

system designs aim towards trapezoidal back-EMF's to reduce excitation torque ripple during commutation events. However, inherent cogging torques usually adds harmonics to the electro-magnetic design. Excitation and cogging torques will be discussed and illustrated later in the thesis. Because one phase of the brushless DC machine is not switched by the power inverter, the back-EMF voltage in the unexcited phase can be detected to establish a switching sequence for commutation of the power devices. Based on the rotor position, the power devices are commutated sequentially every 60 degrees electrical to continually synchronize the phase voltage excitation with the back-EMF. The electrical phase of the back-EMF should be the same as the stator currents for optimal and maximum torque per ampere. Brushless AC control requires sinusoidal phase currents to flow to produce a constant torque with low ripple. To achieve sinusoidal phase currents the machine control algorithm requires continuous rotor position feedback. At any instant in time, three power devices of the three-phase bridge inverter are conducting, thus back-EMF sensing techniques reported to date cannot be employed. Techniques for position sensorless brushless DC control are illustrated by the schematic overview of Fig. 1.5. The position sensorless techniques will be discussed in section 1.3 in more detail.

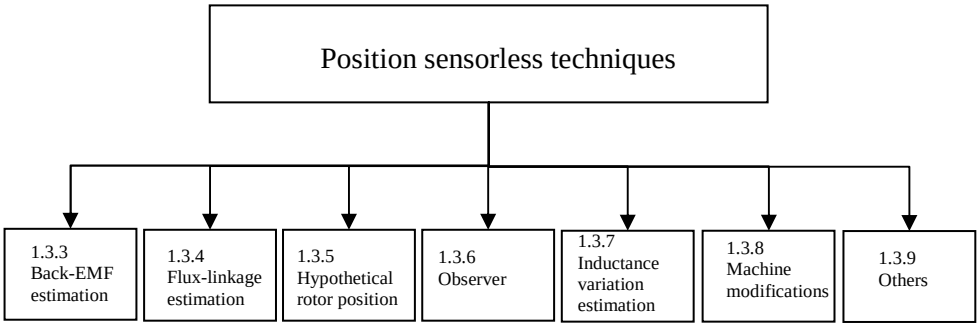

Fig. 1.5 Overview of position techniques published to date.

1.3.3 Back-EMF detection methods: zero crossing sensing

As mentioned for brushless DC control, the back-EMF of the unexcited phase can be detected to establish a switching sequence for commutation of the drive system inverter [18-20], as illustrated in Fig. 1.6, showing the time relationships between the three idealised phase back-EMF voltages a, b, and c, the back-EMF zero crossing instants and zero crossing shifted by 90 degrees electrical. Kenichi proposed in [18] to monitor the three terminal voltages V_a, V_b and V_c and a neutral voltage V_n via a comparator circuit, as shown in Fig. 1.7. At the instant of a zero crossing one of the three terminal voltages is equal to the neutral voltage. This position of point D, this position shown in Fig 1.6, needs to be delayed by 90 electrical degrees to generate the switching signal to be used in the inverter. They used this method in air conditioning systems. The disadvantages of this method are that it has phase differences between the actual position and the estimated position signal resulting from speed variation of the brushless DC machine; it does not work at low speeds; and requires additional circuitry to as a comparator for the neutral voltage. Jianwen Shao proposed in [19] a zero crossing sensing technique without the neutral point and utilizing the inverter by a proper pulse width modulation (PWM) strategy. The method was for an automotive fuel pump application. Starting of the motor was aachieved by an open loop ramp that was predetermined experimentally. The phase locked loop method proposed in [20, 21] works by firstly detecting the rotor position through the unexcited phase and outputs a pulse to the communication control logic based on the speed setting. This method has a narrow speed range due to the limited capabilities of the phase detector and is sensitive to PWM switch noise which may lead the system to be unstable. To summarize, technique based on the back-EMF zero crossing in [18-21], do not work at zero and low-speed. They all require three voltage and two current sensors and a comparator circuit to sense the neutral voltage. The schemes are also sensitive to load changes which tend to lead to some instability.

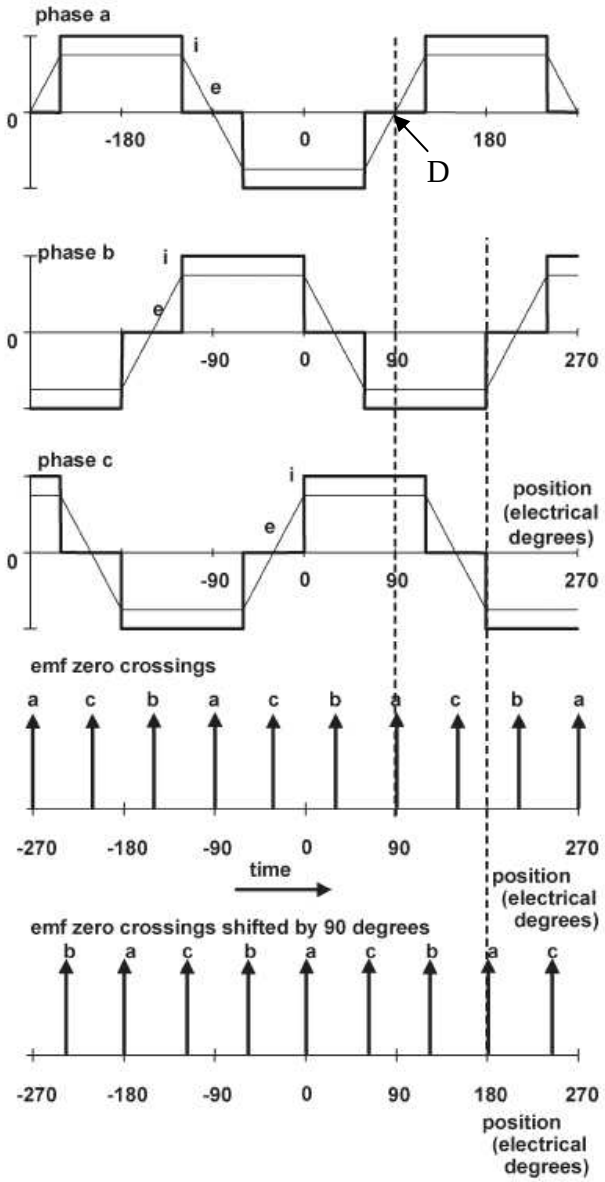

Fig. 1.6 Zero crossing sensing to derive commutation signals [16].

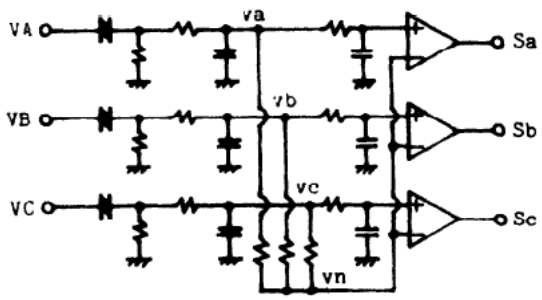

Fig. 1.7 Comparator circuit for zero crossing [18].

1.3.4 Back-EMF detection methods: third harmonic voltage sensing

A number of authors has proposed position sensorless using the stator EMF third harmonic voltage component, as discussed in [22-24]. The PM machine must be designed to be have an air-gap flux-density with an induced third harmonic voltage component. To acquire the third harmonic voltage a set of resistors are connected across the two neutrals used to determine the third harmonic voltage, as illustrated in Fig. 1.8. Moreria showed in [24] that:

$$v_{as} + v_{sn} + v_{na} = 0 \tag{1.1}$$

$$v_{bs} + v_{sn} + v_{nb} = 0 \tag{1.2}$$

$$v_{cs} + v_{sn} + v_{nc} = 0 \tag{1.3}$$

Thus when adding (1.1) to (1.3) the result is:

$$(v_{as} + v_{bs} + v_{cs}) + 3v_{sn} + (v_{na} + v_{nb} + v_{nc}) = 0 \tag{1.4}$$

For a balanced three phase winding, the sum of the stator currents is zero. Similarly the summation of the voltages is also zero which leads to:

$$v_{sn} = \frac{1}{3}[v_{thirdharmonic} + v_{high}] \tag{1.5}$$

The rotor flux can be estimated from the third harmonic voltage signal by integration of:

$$\psi_{sn} = \int v_{thirdharmonic} dt \tag{1.6}$$

Thus, the third harmonic voltage is integrated and input to the zero crossing detector. The output of the zero crossing detectors determine the switching sequence for turning on and off the power inverter switches, as illustrated Fig. 1.9. This method is not as sensitive to phase delay as the zero crossing method. Since the third harmonic frequency is three times that of the fundamental, the filtering requirement when using a low pass filter is

advantageous. The third harmonic approach was implemented by Shen [25] in the high speed flux-weakening region with current flowing in all three phases. The disadvantages of this method are that they do not work at stand still and low speed, require three voltage sensors and two current to achieve control.

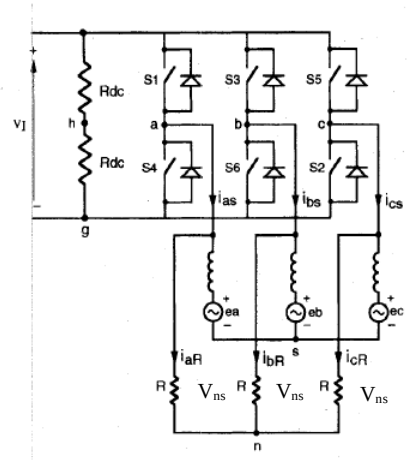

Fig. 1.8 Third harmonic signal circuit [23].

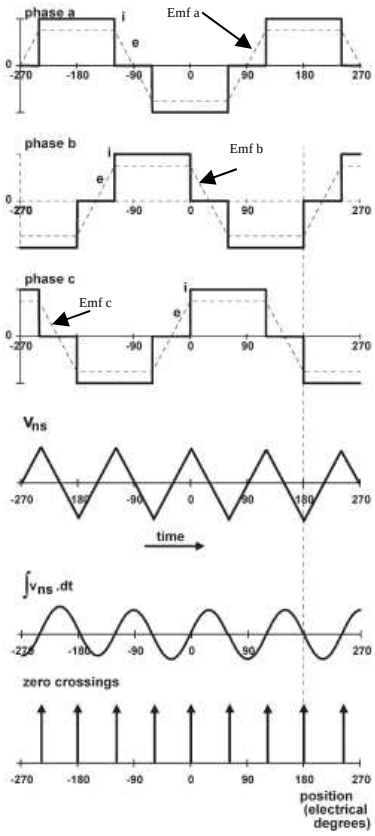

Fig. 1.9 Third harmonic signal to drive commutation signals [16].

1.3.5 Back-EMF detection methods: integration

When the back-EMF crosses zero an integrator takes the absolute value of the back-EMF and starts integrating [26-27] as illustrated in Fig. 1.10. The integrated absolute back-EMF waveform reaches a predetermined threshold voltage which provides a commutation pulse. The threshold value and the integrator constant depend on the machine and the alignment of the phase current waveform with the back-EMF voltage. The threshold is set to stop the integration and thus corresponds to a commutation instant. The threshold is kept constant throughout the drive system speed range. To advance the current the threshold voltage is changed. Once the integrated value reaches the threshold voltage, a reset signal is asserted to zero. The reset signal is kept on long enough to prevent the integrator from starting to integrate until the current in the open phase has decayed to zero, as illustrated in Fig. 1.10. The advantages of this technique are reduced switching noise and automatic adjustment of the inverter switching instants to changes in rotor speed. The disadvantages are that this scheme does not work at stand-still and low speed, requires three voltage sensors and three current sensors. Further the threshold voltage must be known before operating.

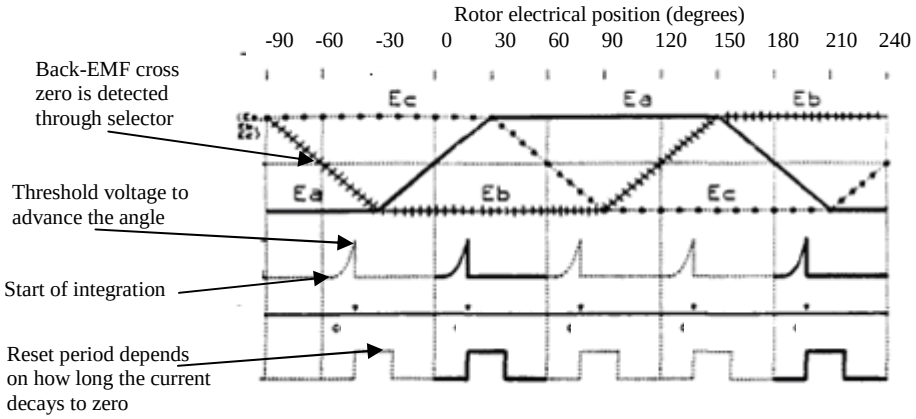

Fig. 1.10 Back-EMF integration [27].

1.3.6 Inverter free-wheeling diode current

Rotor position information can be determined from the conduction state of free-wheeling diodes in the unexcited phases [28-29]. For a short period after opening the machine phase there still remains current circulating in the winding via the inverter bridge free-wheeling diodes. This open phase current becomes zero at the same time in the commutation interval, which corresponds to the point when the back-EMF of the open phase crosses zero. This method can be explained by considering Fig. 1.11; when the bridge upper switching device Ta+ and switch Tb- are turned on, current will flow through phase a and phase b while phase c is open. When Ta+ is turned off current continues to flow through the diode, D_a, and decreases. The detecting circuit consists of a resistor and diode which are connected to a comparator for voltage clamping. The reference voltage is smaller then the free wheeling current voltage drop and the detecting circuit needs two isolated power supplies as shown in Fig. 1.12. The biggest downfall for this method is the requirement of six additional isolated power supplies for each of the comparator circuits.

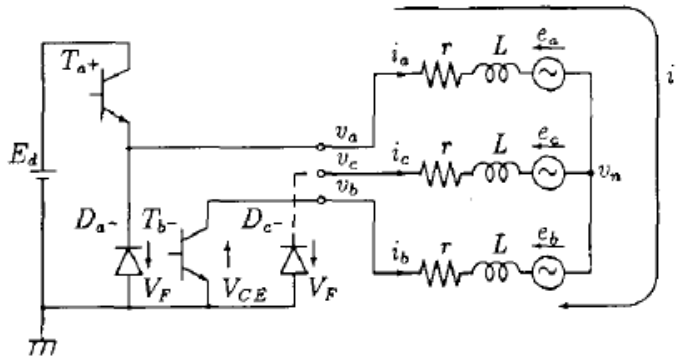

Fig. 1.11 Simplified circuit on free wheeling diode operation [28].

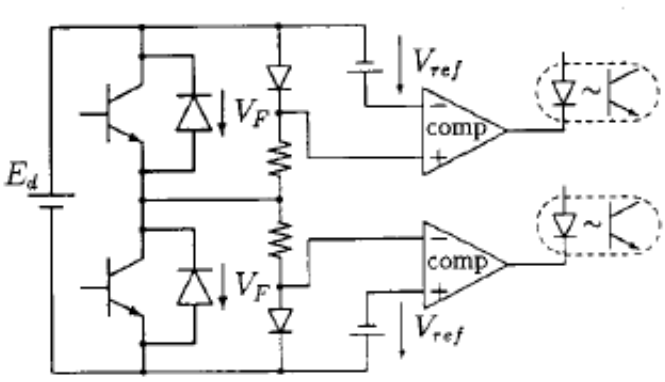

Fig. 1.12 Free wheeling diode circuit [28].

1.3.7 Flux-linkage estimation

The position information is determined from the machine line voltages and phase currents with the aim of estimating flux-linkages [30-34]. The stator flux-linkage is firstly estimated in a stationary reference frame then the rotor position is calculated from the estimated flux linkages. The flux linkage can be estimated [34]:

$$\psi_\alpha = \int u_\alpha - R_s i_\alpha dt \tag{1.7}$$

$$\psi_\beta = \int u_\beta - R_s i_\beta dt \tag{1.8}$$

An estimate of flux-linkage can be produced by subtracting the resistive voltage drop from the phase voltage and then integrating the result. The flux linkage position can be calculated as:

$$\theta_\psi = \tan^{-1} \frac{\psi_\beta}{\psi_\alpha} \tag{1.9}$$

Flux-linkage estimation techniques can be divided into two categories:

- Open-loop flux estimation is a method without feedback, but by direct flux estimation. The open-loop flux estimation can initially be used with a pure integrator circuit to estimate the flux as detailed in [30]. However, the pure integrator has drift problem and initial value problems explained in [16]. The drift problems are caused from small offset signals which are summed over time, ultimately causing the integrator to saturate. The initial value problem is due to the pure integrator, if a sine wave is integrated a cosine will appear. This is true only if the sine wave is input at its peak, otherwise a DC offset will appear [35]. This DC offset does not exist during machine operation, but can be generated, for example, when there is a rapid change in the input. The integration drift is a problem when using (1.7) and (1.8), but can be reduced by using a low pass filter [35].
- Closed-loop flux estimations there are two ways of implementing closed-loop flux estimation either with a mechanical model or a look-up table. In the mechanical model, torque is calculated from the flux-linkage and current, as shown in [36], where the machine three phase currents are calculated from an assumed initial position this is

then used to estimate flux-linkage. Torque is calculated from the current and calculated flux, and the predicted position corrected by the difference between the calculated current and the actual current error. The estimated flux-linkage is corrected using the corrected rotor position from the error between the measured stator current and calculated current. The second method is when the flux-linkage is calculated from the measured currents and voltages, and a look-up table containing the flux-linkage versus position and current characteristic is used to estimate current and position [16, 37]. Position estimation using flux-linkage may be viewed as an combination of sensing back-EMF and inductance, so a lot of authors have researched the idea of an extended back-EMF estimator that includes rotational back-EMF and inductance terms [38-40]. In the flux-linkage based methods, machine parameters are required. The methods are therefore sensitive to parameter variations. Moreover, the stand-still and low speed position prediction is not possible.

1.3.8 Hypothetical rotor position

In this method, the difference between the measured state variables and the estimated state variables is used to obtain positional information. The ideal voltage is calculated using the instantaneous voltage equation of the machine and the measured current. The difference between the actual and ideal values is proportional to the angular difference between hypothetical and actual rotor positions. Here,

(i) Rotor position is assumed.
(ii) The machine variables are calculated in the rotor reference frame.
(iii) The measured variables are also transformed to the rotor reference frame using the assumed position.
(iv) The difference between the calculated and measured values is proportional to the true rotor position and the assumed rotor position shown as:

$$(\Delta v = v_{dq} - v_{hypotheticaldq}) \propto \Delta\theta_e \tag{1.10}$$

$$(\Delta i = i_{dq} - i_{hypotheticaldq}) \propto \Delta\theta_e \tag{1.11}$$

The machine variables for the hypothetical method are voltage and current. Studies on this method concluded that applying current values is better than applying voltage values.

The disadvantages are computational intensity requiring fast processors with high resolution; the technique does not work at low speed and it is also dependent on parameter variations [41-43].

1.3.9 State observers for rotor position estimation

In the state observer method, the dynamic model of the machine is used in the state observers as illustrated in Fig. 1.13. These dynamic models are driven with the same inputs as for the real machine. The state of the modelled machine follows the state of the real machine to check and ensure the accuracy. The observer corrects any error arising from the difference between the output of the real machine, which is measurable, and the output of the modelled machine in the estimated state. Since state observers are model based, parameter variations in the system can be expected to affect observer performance. There are many observer schemes published such as full order observer [44-46], reduced order observer [47-48], non linear [49], disturbance [50-52], sliding mode observer [53-60] and Kalman filter [61-63]. The fundamental idea of the basic full-order state observer was developed by Luenberger of Stanford University in 1964 [16] and the theory can be applied to brushless PM machine control. The PM model is driven by voltages and currents that are transformed into the rotor reference frame using an estimate of the rotor position. Therefore, the difference between the estimated output of the model and the measured currents transformed into the estimated frame is not correct, generating an error that can be used to correct the preceding position estimate. The performance of the observer depends on appropriate choice of gains. For a given set of gains, the stability of the observer can be predicted. The Full-Order Observer discussed in [44-46] is a basic observer, which estimates all states. Reduced-Order-Observer depends on system outputs being linear transformation of the system states. The observer can be reduced by coupling some of the system states to the output of the observer through a linear transformation (or the actual measurements if the states are readily available for measurement). Only the states of interest need be estimated by the lower order observer. Voltages and currents are easily measurable, helping to reduce the order and therefore reducing the number of states needed for the reduced observer [47-48]. In [47] the observer was constructed to use only two measured phase currents and thus reduced the number of sensors. Non-Linear-Observer take into account rotor position and velocity estimates that best fit the available data to the back-EMF function [49]. Disturbance-Observer implemented in [50-52] are basically reduced order observers used with the system states that assume quasi-static (fast sampling) calculating times. The slight variation of the state variables from one sample to

the next is termed a disturbance, which results in observations of small changes in rotor position angle, this observer usually monitors the flux-linage. The Sliding-Mode-Observer [53-60] is basically an observer with inputs as discontinuous functions of the error between the estimated and measured outputs. The system dynamic behaviour in the sliding mode is only decided by the surface chosen in the state space and is not affected by the matched uncertainty. The performance of the Sliding-Mode-Observer position estimation depends on the quality and accuracy of the measured values of voltages and currents. The Kalman-Filter is an optimum state observer estimator [61-63]. A Kalman-Filter provides an optimum observation of noisy sensed signals and parameter variations. The measured voltages and currents are transformed to stationary frame components using the state equations and a Kalman-Filter; the missing states (rotor position and velocity) are estimated. The estimated rotor position is used for commutation. The filter estimation is constantly corrected by an additional term originating from the measurement. The function of the filter is to correct the estimation in recursive manner. The filter constantly works on the output and corrects its quality in a recursive manner based on the measured values. In [63] two observers, a Sliding-Mode-Observer and a Kalman-Filter where implemented. The Sliding-Mode-Observer was used to detect the instantaneous value of the motor back-EMF and the Kalman-Filter was cascaded and employed to identify the rotor speed and the back-EMF fundamental shape, from which position can be estimated. The critical step in designing the observer is to select the gains to yield the best position.

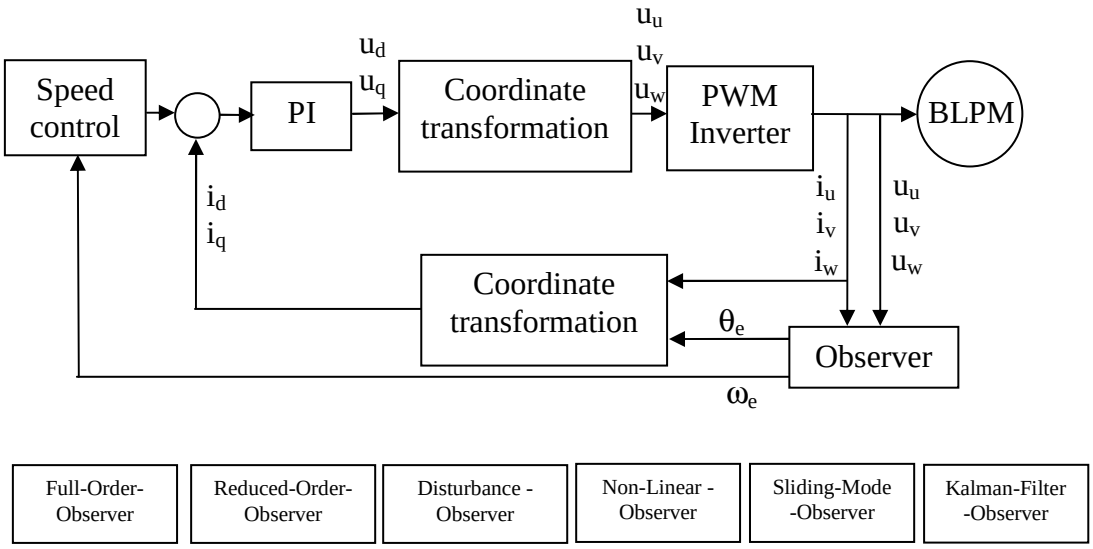

Fig. 1.13 State observer for rotor position estimation.

To illustrate some of these observers the brushless PM stator reference frame can be written as [52]:

$$\begin{pmatrix} \frac{di_\alpha}{dt} \\ \frac{di_\beta}{dt} \end{pmatrix} = \begin{pmatrix} \frac{-R_s}{L_s} & 0 \\ 0 & \frac{-R_s}{L_s} \end{pmatrix} \begin{pmatrix} i_\alpha \\ i_\beta \end{pmatrix} + \begin{pmatrix} 0 & \frac{\omega_e}{L_s} \\ \frac{\omega_e}{L_s} & 0 \end{pmatrix} \begin{pmatrix} \psi_\alpha \\ \psi_\beta \end{pmatrix} + \begin{pmatrix} \frac{1}{L_s} & 0 \\ 0 & \frac{1}{L_s} \end{pmatrix} \begin{pmatrix} u_\alpha \\ u_\beta \end{pmatrix} \tag{1.12}$$

The flux-linkage is considered to be a disturbance state that satisfies a known differential equation which is:

$$\begin{pmatrix} \frac{d\psi_\alpha}{dt} \\ \frac{d\psi_\beta}{dt} \end{pmatrix} = \begin{pmatrix} 0 & -\omega_e \\ \omega_e & 0 \end{pmatrix} \begin{pmatrix} \psi_\alpha \\ \psi_\beta \end{pmatrix} \tag{1.13}$$

Combining the disturbance state vector with the state variables yields:

$$x = \begin{pmatrix} i_\alpha & i_\beta & \psi_\alpha & \psi_\beta \end{pmatrix}^T \tag{1.14}$$

The input vector *u* is the applied phase voltages in the α-β coordinates:

$$u = \begin{pmatrix} u_\alpha & u_\beta \end{pmatrix}^T \tag{1.15}$$

The output vector *y* is the measurable currents in the α-β coordinates:

$$y = \begin{pmatrix} i_\alpha & i_\beta \end{pmatrix}^T \tag{1.16}$$

Thus, the brushless PM state and output equations are:

$$\frac{dx}{dt} = A_\omega x + Bu \tag{1.17}$$

$$y = Cx \tag{1.18}$$

The state model flux-linkages ψ_{α} and ψ_{β} are not measurable therefore instead of a complex full order observer a reduced observer can be used for stable estimation of the flux linkage, and instead of the measurable phase voltages, the reference voltage are used as the estimator input and is shown in detail [52]. The disadvantages of observers are that they do not work at stand-still and low speed, this is a common problem for all observers. The mechanical model 2-axis rotor reference frame must have correct parameters, if the sense parameters are wrong then flux and torque control will be lost. At low speed the observer becomes very sensitive to stator resistance. A loss of the observer stability will results in erratic and destructive motor operation.

1.3.10 Inductance variation with rotor position

The rate of change of machine winding current depends on the inductance of the machine winding, variation of which may be a function of rotor position and winding current. Rotor position can be calculated from analysing the rate-of-change in winding current of the machine [64-67]. The main advantage of this method is that position can be estimated at low and zero speed where there is no rotational back-EMF. Rotor position estimation from inductance variations is not straight forward and complicated by:

(i) in a surface mounted magnet machine there is no or virtually no saliency so any variation of winding inductances with rotor position arises only from magnetic saturation [16],
(ii) the back-EMF dominates the rate-of-change in the current and
(iii) the variation of incremental inductance with rotor position undergoes a two cycle per electrical cycle of the machine back-EMF, as illustrated in Fig. 1.14 causing an ambiguity in sensed position.

There are four known ways to use inductance variation to estimate rotor position, the first solution is to consider the effect of magnetic saturation on the winding incremental inductance. The principles of this method can be understood by referring to the flux-linkage characteristics illustrated in Fig. 1.14, where it can be observed that if the current is at zero or 180 degrees electrical the incremental inductance of a phase is at its minimum value. Now, the effect of a positive pulse of current if the rotor is aligned with zero degrees position is to increase the total positive flux-linked with the phase, but if the rotor is at the 180 degrees position, the current reduces the total negative flux-linkage. Therefore, there is a difference between the flux amplitudes for the two alternative rotor positions and

consequently, difference in the level of magnetic saturation. If magnetic saturation increases, the incremental inductance is lower and so the amplitude of the current pulse is larger at one of the two possible rotor positions [16], as illustrated in Fig. 1.15. Magnetic saturation has small but significant influence on incremental inductance even in a surface mounted BLPM machine having no inherent saliency. The variation arises in surface mounted magnets due to the saturation in the stator teeth. In [68], the magnetic saturation on the incremental inductance has been investigated and an error of 18 electrical degrees was reported.

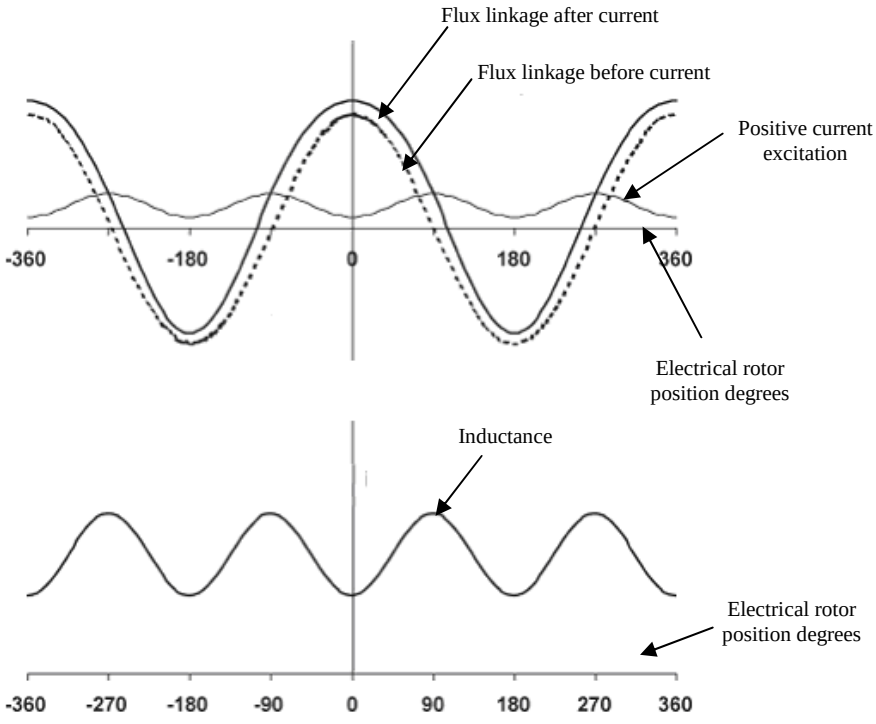

Fig. 1.14 Flux-linkage and inductance variation with electrical position [16].

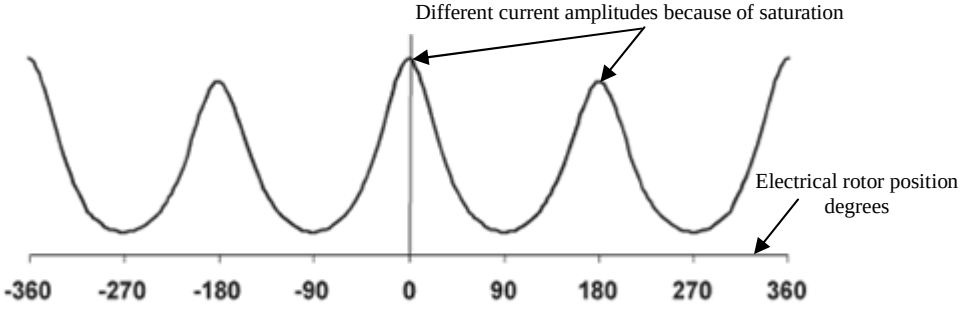

Fig. 1.15 Current amplitude due to saturation [16].

The second method of rotor position sensing using inductance variation is applicable to interior and inset brushless PM machines where the direct and quadrature axis inductances are different, thus $L_q > L_d$. This inductance variation is explained due to the fact that the quadrature axis of the rotor is only iron while the direct axis encompasses the PM material which having a recoil permeability close to 1.0 (i.e. 1.07 for sintered NdfeB) is similar to air. Thus, the reluctance in the quadrature is less then that in the direct axis to $L_q > L_d$. The L_q and L_d inductances can be expressed as [14]:

$$L_d = L_{ls} + \frac{3}{2}(L_m - L_s) \tag{1.19}$$

$$L_q = L_{ls} + \frac{3}{2}(L_m + L_s) \tag{1.20}$$

The stator voltage for phase u is [14]:

$$u_u = R_s i_u + L_u \frac{di_u}{dt} + e_u \tag{1.21}$$

The phase synchronous inductance for phase u can be written in terms of voltages and currents as :

$$L_u = \frac{u_u - R_s i_u - e_u}{\frac{di_u}{dt}} \tag{1.22}$$

The phase synchronous inductance is also related to the quadrature and direct inductance as :

$$L_u = \frac{L_d + L_q}{2} + \frac{L_d - L_q}{3}\left[\cos(2\theta_e) - \cos\left(2\theta_e - \frac{2\pi}{3}\right)\right] \tag{1.23}$$

$$L_v = \frac{L_d + L_q}{2} + \frac{L_d - L_q}{3}\left[\cos\left(2\theta_e - \frac{2\pi}{3}\right) - \cos\left(2\theta_e - \frac{4\pi}{3}\right)\right] \tag{1.24}$$

$$L_w = \frac{L_d + L_q}{2} + \frac{L_d - L_q}{3}\left[\cos\left(2\theta_e - \frac{4\pi}{3}\right) - \cos(2\theta_e - 2\pi)\right] \tag{1.25}$$

By using equations (1.23) - (1.25), a look up table can be implemented to estimate rotor position. The reason for using the three inductance measurements is to overcome the problem due to the inductance variation at twice the rotor angle.

The third inductance based scheme for detecting rotor position due is implemented by injecting high frequency voltages to the stator windings. These produce high frequency currents which are modulated by with rotor position [14]. By detecting these currents a signal is produced which is proportional to the difference between the actual rotor position and the estimated rotor position. This method is only applicable for salient brushless PM machines.

The fourth way to utilize the variation was considered in [69], where the current derivative can be obtained more easily over the relatively longer zero state in the low and zero speed regions. No extra test signal injection is required. This methods works by firstly analysing the stator voltage equation system expressed in the rotor reference frame as in (1.26) and (1.27) under high frequency or transient excitation. The inductance parameters L_d and L_q are different due to the machine saliency, caused by the mechanical rotor construction and/or magnetic saturation.

$$v_d = R_s i_d + L_d \frac{di_d}{dt} \tag{1.26}$$

$$v_q = R_s i_q + L_q \frac{di_q}{dt} + k_e \omega_e \tag{1.27}$$

When a zero voltage vector is applied, the inverter shorts the motor terminals driving both v_d and v_q to zero. The stator voltage equation (1.26) and (1.27) can then be simplified to (1.28) and (1.29) which reveals two different time constants dependent on the difference in L_d and L_q of the machine.

$$\frac{di_d}{dt} = \frac{R_s i_d}{L_d} \tag{1.28}$$

$$\frac{di_q}{dt} = \frac{-1}{L_q}\left[R_s i_q + k_e \omega_e \right] \tag{1.29}$$

A number of recent conferences papers have focused on the extracting position information from the variation in machine inductance. Salt et al in [70] proposes compensation of non-linear distortion effects for signal injection. The non-linear distortions are introduced by

the pulse width modulation switching of the drive system power inverter and lead to distortion of the high frequency carrier signal which in turn, causes a degradation of the position detection accuracy. The carrier signal can be injected open-loop onto the three phase reference frame or onto the d- or q- axis voltages. The resulting measured high frequency current can then be demodulated and used to track the saliency and position of the machine. There are generally, three ways of implementing frequency injection and the compensation strategies:

(i) The three phase voltages injection results showed the error between the estimation rotor position when compared to measured rotor position obtained from mechanical resolver is 5% degrees electrical, there was an observation also that the extra error is due to non ideal saliency [70].

(ii) The q-axis voltage injections are inherently more robust to non-linear distortion effects. Reported compensation strategies show negligible improvement. The distortion is mainly due to non-sinusoidal q-axis inductance [70].

(iii) The d-axis voltage injection is beneficial as it does not interfere with the torque producing current unlike the q-axis voltage injection. This mode of injection does not increase the peak current through the inverter IGBTs because the injected current is modulated such that it is zero at the peak of the fundamental current and is a maximum when the fundamental crosses zero. The positional error when using this method is within 10 degrees electrical.

Budden et al in [71] focus in the injection of a balanced set of high frequency, low magnitude sinusoidal voltages into the machine terminals using a PWM based drive. This reports to be a simple method for detecting the variation in saliency, followed by a simple and robust correction procedure achieved using a look-up table. There are two possible means of producing this table. First the table can be derived based on a comparison of sensorless and measured results. Alternatively, a self commissioning test based on voltage injection and synchronous machine drive requiring no position feedback, allows the entire saliency profile to be captured. The disadvantage of this procedure is that it has to be done for each machine. El-Murr et al in [72] propose a solution to a problem that arises when load is applied to the machine. A problem arises due to the cross-coupling inductance which increases and causes a saliency, or anisotropy angle, which is delayed from the actual rotor position. To estimate rotor position accurately the inductance has to be known at various operating points. The paper proposes an algorithm to compensate for the error due to the load angle. The technique has been theoretically analysed and demonstrated experimentally. However, if misalignment occurs between the rotor and the anisotropy

positions, the effectiveness of sensorless control is reduced. Saturation and cross-coupling inductance effects are found to be a reason for the saliency misalignment in brushless PM machines. The phase error between the rotor and the anisotropy position appears in the negative sequence of the carrier current and is related to the self- and cross-coupling incremental inductance. Therefore, the paper calculates these inductances to find the amount of anisotropy angle shift. Nonlinearity effects in high frequency signal injection are discussed in [73]. The paper shows the use of high frequency rotating voltage or current vectors superimposed on the fundamental excitation and present analysis of the resulting high frequency current (or voltage) to track spatial saliencies that have has been widely studied as a variable option to estimate the rotor or flux position. The paper addresses in detail the non-linearities caused by the non-ideal behaviour of switching devices these can be summarized as:

(a) Dead-time: also known as shoot-through delay, dwell-time, or inter-lock time. Dead-time is needed to prevent the DC link from being short-circuited when the two devices of an inverter phase leg are switched simultaneously. When the switch state of a leg changes, a delay time is given for the switch to initially turn-on or turn-off. This delay time generates short voltage error pulses of a constant amplitude and width in the output voltage of one inverter phase leg, with respect to the commanded voltage value. The sign of the error pulse is the opposite of the current polarity in that phase leg.

(b) Turn-on and Turn-off times: are the times required to turn-on or off the inverter power devices (e.g. IGBTs). Some of the proposed compensation methods used for dead-time includes solutions to the problem though in other cases its effects are neglected.

(c) Parasitic capacitance of and around power semiconductor devices cause changes in the slope of the rising and falling edges of the output voltages when the current is very small. This is due to the fact that the changing currents charge up the parasitic capacitances of the diode or switches prior to flowing through the diode. Turn-on and Turn-off are also affected by these capacitances in such a way that switching times and parasitic capacitances combine to produce a unique distortion effect in the output voltage in the low current region [73].

(d) Zero current clamping occurs when a phase current nears zero during the dead-time and is caused by the extinction of the current in the free-wheeling diode resulting in the phase leg being disconnected from the bus during a portion of the dead-time period. Secondly, by the larger commutation times at low current levels arise due to

the non-ideal nature of the power diodes. This is an important consideration for low frequency signals [73].

(e) Voltage drops in the semiconductor are another source of error in the injected voltages. They can be modelled by a constant voltage source plus an equivalent series resistor and compensated for by using models or look-up tables.

(f) Short-pulse suppression: appears when the commanded current pulse is shorter than the dead-time. This not generally an issue in self sensing methods since they are typically only employed in low speed applications where modulation indexes are far from the inverter voltage limit.

(g) Voltage distortion: can arise due to poor design of power board components.

Leidhold in [74] proposes using the high frequency zero-sequence generated by the inverter to detect weak saliencies. The saliency methods are mainly classified by the signal being injected in:

(i) revolving carrier,

(ii) alternating voltage carrier,

(iii) voltage plus pattern,

(iv) without injecting a specific signal by evaluating the derivative of the current resulting from the standard PWM.

In all cases, the voltage signal is injected in the non-zero sequence. The response of the injected signal is usually acquired by measuring the non-zero sequence current or the zero sequence voltage. Leidhold in [74] proposed to inject a carrier in the zero sequence so a position dependent signal can be obtained and may be four times higher than injecting a carrier in the non zero sequence with equal voltages. The high frequency (HF) is 50 times higher then the fundamental frequency. The disadvantages of estimating position from the variation of inductance are the distortions due to the non-linearities in the inverter, the load offsets and the noise caused by signal injection.

1.3.11 Modifications to machine electro-magnetics

Another way to estimate rotor position is to modify the machine as proposed in [75-76] by the pasting of a non-magnetic material on to the rotor surface. This method uses the change of phase currents due to eddy currents that change according to rotor position. This method is used at stand-still and after the threshold speed uses another position sensorless control.

In [75] currents were monitored to extract position. However, it was found difficult to monitor the current, so in [76] the voltages were monitored. To simplify non-magnetic material was pasted 360 degrees electrical on the surface of the rotor surface with a width of 180 degrees electrical to increase the saliency than electrical position is extracted. An error of 19 electrical degrees was reported. In [77] a similar method was applied to a surface mounted permanent magnet. Here, a complete loop of cooper wire is wound around the rotor permanent magnet as illustrated in Fig. 1.16.

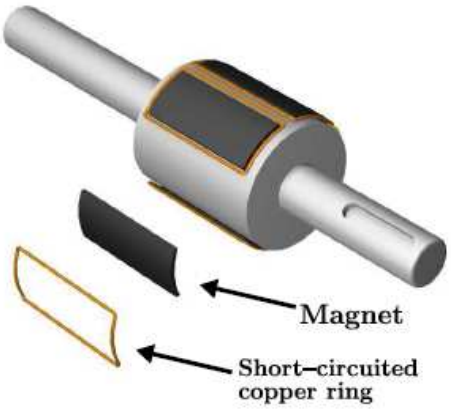

Fig 1.16 Copper ring wound around each rotor magnets pole [77].

In [78] rotor non-magnetic material was replaced with an electrical winding to increase the variation of the stator winding inductance as a function of rotor position, this variation was subsequently used to estimate rotor position, as illustrated in Fig. 1.17 where the conventional amortisseur windings (usually used on synchronous machines) have been added to a surface mounted rotor. The amortisseur winding is designed to increase the variation of the inductance as a function of rotor position so make it easer to track.

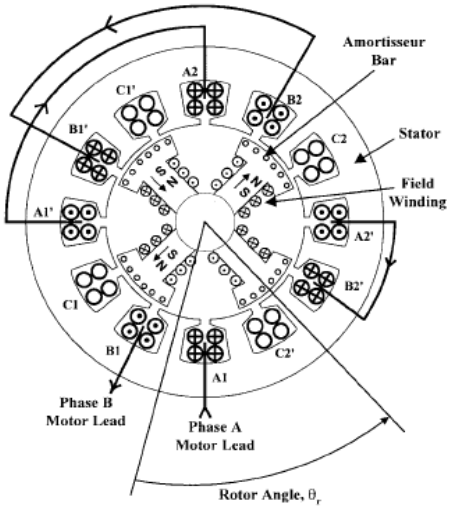

Fig. 1.17 Amortisseur windings added to brushless PM machines [78].

In [79-82] the authors propose a closed slot stator configuration shown in Fig. 1.18, where a saturable yoke is placed between the main teeth of the stator core. The yoke will affect the self-inductance of the stator with partial magnetic saturation. Thus, an increase the variation of inductance as a function of position is achieved making it easer to track.

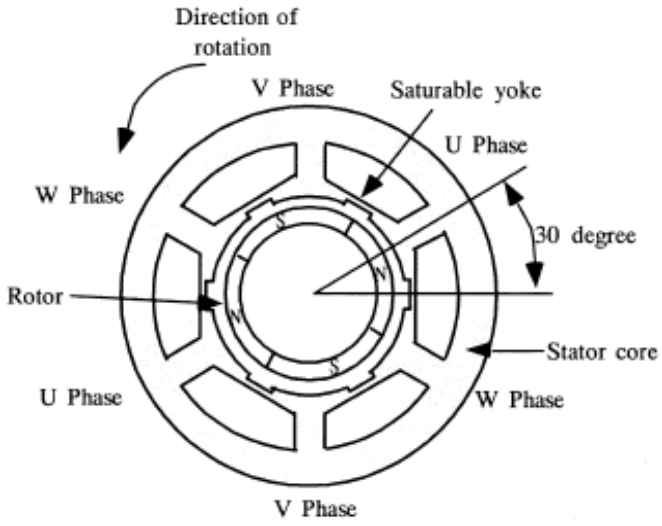

Fig. 1.18 Closed slot stator configuration [82].

In [83-86] the machine is assembled with additional stator lamination having equally spaced slots around the periphery. These slots contain a sensing coil, as illustrated in Fig. 1.19. As the machine rotates the magnetic circuit for each coil varies. Using the injected frequency method the generated signal is analyzed at the terminal of the sensing coil to estimate rotor position.

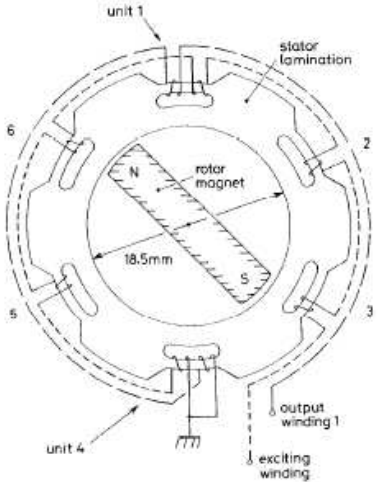

Fig. 1.19 Sensing coil in the stator lamination section [86].

In [87] the stator winding were tapped as illustrated in Fig. 1.20. The taps are thin since they do not carry high current and thus contribute only a minor modification to the machine stator. The taps are used to make voltage measurements and thus to estimate the electrical position.

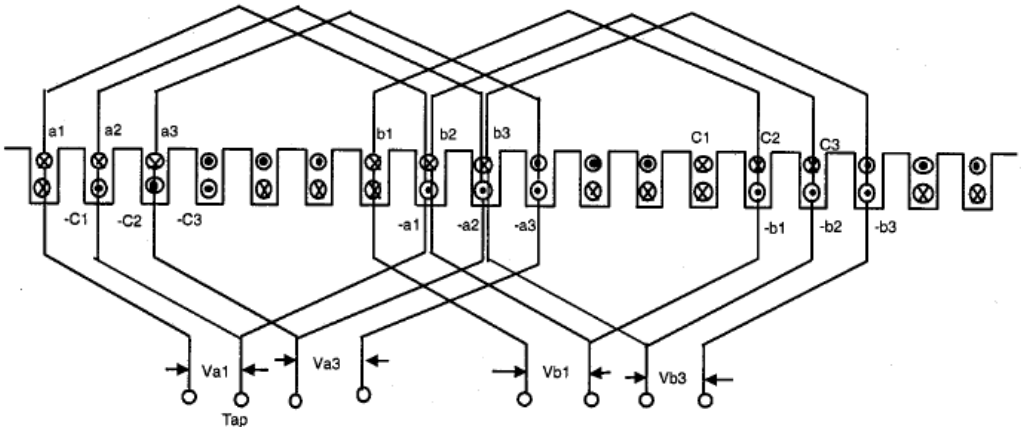

Fig. 1.20 Tapped stator winding [87].

1.3.12 Other miscellaneous techniques

Neural networks have been proposed to estimate rotor position, as presented in [88, 89]. A back propagation neural network (BPN) was presented in [88], where the BPN provided a non-linear mapping between measured voltages and currents to estimate rotor position. The rotor position was used to calculate the flux-linkage vector which was then compared to the flux-linkage estimated from the measured voltages and currents. The difference was used as an error which was back propagated to modify the BPN weights; experimental results where shown in [89]. However, an initial rotor position is required and the sensorless scheme does not work at low speed.

In [90-92] a fuzzy logic system was proposed, comprising of two subsystems; a fuzzy logic observer used the measured currents and voltages to estimate rotor position; a second fuzzy system used the estimated position and produced reference current values for two different drive strategies, unity power factor and maximum torque per amp. However, an initial rotor position is required and the sensorless scheme does not work at low speed.

In [93] the irregularities in measurables was analysed, this method utilize small deviation or inherent properties of the shapes of the current waveforms to obtain position information. In [93] the DC current shape is utilized. Here, the author showed that the DC

current varies depending on the alignment of the phase current and back-EMF. The leading and lagging pattern was analyzed and the differences examined. There was a clear distortion difference between both patterns. The method of control is to count the number of samples on a consecutive rising and falling half cycle of the DC current ripple. When they are equal, the machine back-EMF is aligned with the respective current. When unaligned, the difference in the rising and falling counts is used as a multiplier in the DC link voltage incremental update.

The matrix converter has been used in the position sensorless technique in [94-99]. The matrix converter is an array of controlled semiconductor switches that directly connects the three-phase source to the three-phase load, as shown in Fig. 1.21. The difference between a matrix converter and a conventional inverter is that it provides a bigger choice of voltage vectors. The unique topology of the matrix converter provides additional advantages over a two-level inverter in that it is capable of applying smaller input voltages to the machine, for example when additional position measurements are needed at low speed.

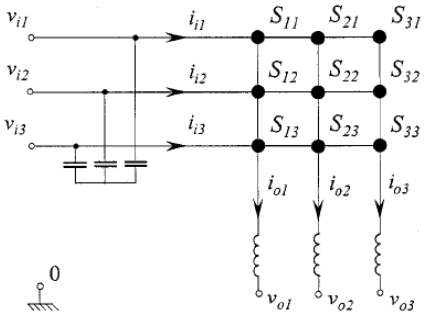

Fig. 1.21 Matrix converter schematic [94].

The open-loop controller is a constant amplitude variable frequency source of excitation. The machine is started by providing a rotating stator field which is increased in amplitude and frequency. Then the rotor field begins to be attracted to the stator field and torque developed which, when of suitable magnitude starts to overcome friction and inertia and hence the rotor begins to turn. This controller may be enough for certain applications, e.g. pumps and fan drives. The disadvantages of open-loop control are that it produces a torque sense ripple, may resulting reverse of direction and that its initial rotor position is not predictable. So for applications that require unidirectional motion, like disk drives, this method is inadequate [100].

Knowing a starting position, this method operates by stopping the rotor at a known initial position. One way to operate this method is to excite current into one phase and thus cause

the rotor to shift and lock into a position which always provides the initial position. The disadvantages of this method is that when the machine is excited with current to lock the position, the rotor freely rotates in either direction and stops at the known starting position. If there is load torque then the rotor position will be offset [101-103].

Direct torque control (DTC) is sensorless after a threshold speed, explained in detail in [104-109]. DTC was initially applied to induction machines [104], and recently for PM machines [105-109]. The operation of a DTC scheme is based on directly selecting voltage vectors to control the flux and torque of the machine as illustrated schematically in Fig. 1.22. The stator flux-linkage is usually calculated by integrating the stator back-EMF and the torque estimated from the measured currents and estimated flux. DTC possesses advantages to the implementation of high-performance, low-cost, machine control mainly due to the fact that only one parameter is involved, the stator resistance. The PWM comparator is removed and the rotor position is not needed. Although DTC is a sensorless scheme by itself, an approximated initial rotor position is required in order to start and get it to threshold speed.

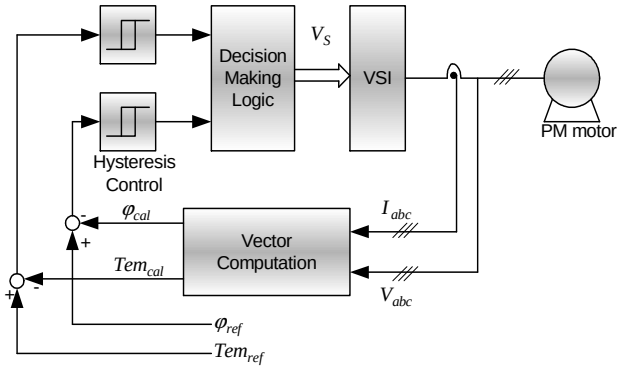

Fig. 1.22 Sensorless direct torque control [113].

1.4 Summary of Position Sensorless Literature Review

When used to control variable torque or speed, BLPM drive systems require rotor position (angle) feedback to effectively control phase current and optimise torque per ampere. The position feedback schemes reported in the literature are summarized in the flowchart illustrated in Fig. 1.23. Sensorless control strategies for the BLPM machines are generally based on calculating position from the machine parameters, via measurement of terminal voltages and currents. All of the main sensorless control strategies for detecting rotor position have been reviewed in this Chapter, as presented in Table 1.1. The table left-hand column links to the relevant references in the right-hand column. The compilation of this table was undertaken to try to collect the main techniques, the applicable drive systems (BLDC or AC), the existence of experimental validation and an audit of the required sensors into one overview. The table is not claimed to be exhaustive, but serves to highlight prior research effort with that of the research reported in this thesis. Position sensors such as absolute or incremental encoders, or resolvers and there associated circuitry have disadvantages in that they contain delicate parts that makes them sensitive to mechanical abuse and temperature. Oil, dirt or dust can harm or contaminate the encoder disk. Gratings, may also be broken by shock loads or sustained vibrations. The LED and photo detectors are also sensitive to mechanical and electrical disturbances. Brushless resolvers are relatively robust, but the associated resolver-to-digit converter electronics is complex and generally a high cost components in the drive system.

The main issue with back-EMF detection schemes is that they do not work at zero and low speeds, they require at least three voltage and two current sensors and a comparator circuit to sense the neutral voltage, or free wheeling diode circuit which necessitates additional isolated power supplies. These techniques are sensitive to speed and load changes which can cause instabilities. There is also is a delay between actual and estimated positions which must be predetermined.

In the flux-linkage estimation methods the main disadvantages are used: the machine parameters, hence sensitivity to parameter variations due to temperature load (saturation) etc. These estimation techniques require two current and two voltage sensors. The load torque must be estimated by a look-up table or torque estimation technique to estimate the load angle offset. Moreover, zero and low speed operation is not possible.

The disadvantage of observers is that they do not work at zero and low speed. The common problem for all observers is that if the currents and voltages are DC there will not be enough information for position estimation. The need for a detailed electrical model of the machine so that the error signal can be constructed from the measured and estimated

states leads to increased computation requirements. The machine electrical parameters, the inductance, resistance and back-EMF coefficient are required, but load torque information is also necessary to consider the steady-state error due to parameter perturbations. A loss of the observer stability will results in erratic and possibly destructive machine operation.

The variation in inductance and machine modifications techniques are similar since they require machines to be specifically designed or modified to exhibit saliency. The main advantage of this method is that position can be estimated at zero and low speed. However, inductance variation for rotor position estimation is complicated: in a surface mounted magnet machine since there is no saliency so any variation of winding inductances with rotor position arises from magnetic saturation, the back-EMF dominates the rate-of-change in the current, the variation of incremental inductances with rotor position undergoes two cycles per electrical cycle causing an ambiguity in sensed position, the distortion due to the nonlinearities of the inverter, and due to load offsets and noise caused by signal injection.

Other techniques such as fuzzy logic and neural networks have similar issues to observers techniques. The unique topology of the matrix converter provides additional advantages over a two-level inverter in that it is capable of applying smaller input voltages to the machine when the position measurement is needed at low speed, but not at zero speed. Finally, direct torque control is similar to closed-loop flux-estimator schemes. Sensorless position techniques behave poorly, if at all, at zero and low speeds (0-300rpm) and load torque must be estimated to know the load angle offset. In all the position sensorless techniques researched [18-110], at least two current and one voltage sensor are required to establish closed-loop control and for estimation of position.

This thesis reports the results of a research study investigating position sensorless operation of a BLPM at all speeds by using measured torque feedback from a machine integrated, low-cost, SAW transducer. The in-line torque transducer is briefly discussed in Chapter 1 and then characterized in Chapter 3. Chapter 2 presents a position sensorless start-up routine for BLPM machines. Chapter 3 discusses machine characterisation and test facilities designed for experimentation and validation of machine control schemes discussed in Chapters 4 and 5. The start-up routine is discussed in Chapter 4 both without and with measured torque feedback. The use of one DC current, one DC voltage sensor and measured torque feedback is presented in Chapter 5. It is normal that at least two or possibly three current and voltage sensors are typically used in sensorless closed-loop drive systems, hence the current and voltage sensor reduction complements the reduction cost of the torque sensor. Chapter 5 also discuses the use of flux estimators to control speed over

a predetermined threshold speed which, for the system studied in this thesis is between 150-300 rpm. Finally, Chapter 6 will draw the overall conclusions from the research study.

					Experimental		Sensors			
	Scheme	Notes	Application	Drive	Steady	Dynamic	Voltage	Current	Sensor	Ref
Back-EMF detection		All of the reported schemes do not work at zero and low speed. They require three voltage and two current sensors and require comparator circuit to sense the neutral voltage They are sensitive to load changes which, if sudden causes instability.								
	Zero crossing sensing		Air condition	Brushless dc	Y	N	3	3	Comparator circuit	18-21
	Third harmonic		Fuel pump	Brushless dc	Y	N	3	3	Comparator circuit	22-25
	Integration of back EMF		Pump and fans	Brushless dc	Y	N	3	3	Comparator circuit	26-27
	Free wheeling diode		Pump and fans	Brushless dc	Y	N	3	3	Diodes	28-29
Flux-estimation	Open loop pure integrator	In the flux linkage based methods, machine parameters are used, the methods therefore is sensitive to parameter variations. Moreover, the stand still and low speed position is not possible.		Brushless dc and ac	Y	N	2	2		30-34
	Open loop low pass filter			Brushless dc and ac	Y	N	2	2		35
	Closed loop without lock up table			Brushless dc and ac	Y	Y	2	2		36
	Closed loop with lock up table			Brushless dc and ac	Y	Y	2	2		37
	Enduced elf			Brushless dc and ac	Y	Y	2	2		38-40
Observer	Full order observer	The main disadvantage of observers is that they do work at stand-still and low speed. This is a common problem for all observers; if the current and voltages are DC there will not be enough information for position estimation. Techniques need a mechanical model of the machine and load.		Brushless dc and ac	Y	Y	2	2		44-46
	Reduced observer			Brushless dc and ac	Y	Y	2	2		47-48
	Non linear observer			Brushless dc and ac	Y	Y	2	2		49-50
	Disturbance observer			Brushless dc and ac	Y	Y	2	2		51-52
	Sliding mode observer			Brushless dc and ac	Y	Y	2	2		53-60
	Kalaman filter			Brushless dc and ac	Y	Y	2	2		61-63
	Sliding mode and Kalaman observer			Brushless dc and ac	Y	Y	2	2		64
Inductance	Magnetic saturation	1) Surface mounted magnet (no saliency) 2) The inductances variation is twice per electrical cycle 3) Inverter nonlinearities 4)Load offsets.		Brushless dc and ac	Y	Y	2	2		65-68
	Inductance variation with look up table			Brushless dc and ac	Y	Y	2	2		69-72
	Inductance variation injecting frequency			Brushless dc and ac	Y	Y	2	2		72-73
	The decay of current			Brushless dc and ac	Y	Y	2	2		
Machine modification	Non magnetic material	These schemes aim to increase machine saliency. Or take more voltage measurements at low speed to estimate rotor position.		Brushless dc and ac	Y	Y	2	2		74-76
	Electrical winding in the rotor			Brushless dc and ac	Y	Y	2	2		77-78
	Slot stator configuration			Brushless dc and ac	Y	Y	2	2		79-83
	Sensing coils in stator			Brushless dc and ac	Y	Y	2	2	Sensing coils	84-85
	Tapped stator winding			Brushless dc and ac	Y	N	2	2		86
Others miscellaneous techniques	Neutral network	Similar to observer.		Brushless dc and ac	Y	N	2	2		87-89
	Fuzzy logic	Similar to observer.		Brushless dc and ac	Y	N	2	2		90-92
	Irregularities in measurable	Shape of current.		Brushless dc and ac	Y	N	2	2		93
	Matrix converter	Nine switch bidirectional.		Brushless dc and ac	Y	Y	2	2		94-99
	Open loop V/f technique	Load has to be known. Could go into reversal at start-up.		Brushless dc and ac	Y	Y	2	2		100
	Know starting position	Offset problem due to load.		Brushless dc and ac	Y	Y	2	2		101-103
	Sensorless DTC	Similar to a closed loop flux estimator.		Brushless dc and ac	Y	Y	2	2		104-110
	Hypothetical rotor position	Depends on machine parameters. Does not work in stand-still and low speed.		Brushless dc and ac	Y	Y	2	2		41-43
	Torque feedback	Enhances the performance of sensorless technique from stand-still to high speed. Need only one current and one voltage sensor.		Brushless dc and ac	Y	Y	1	1	Torque sensor	111-113

Table 1.1 Summary of position sensorless schemes reported in the literature.

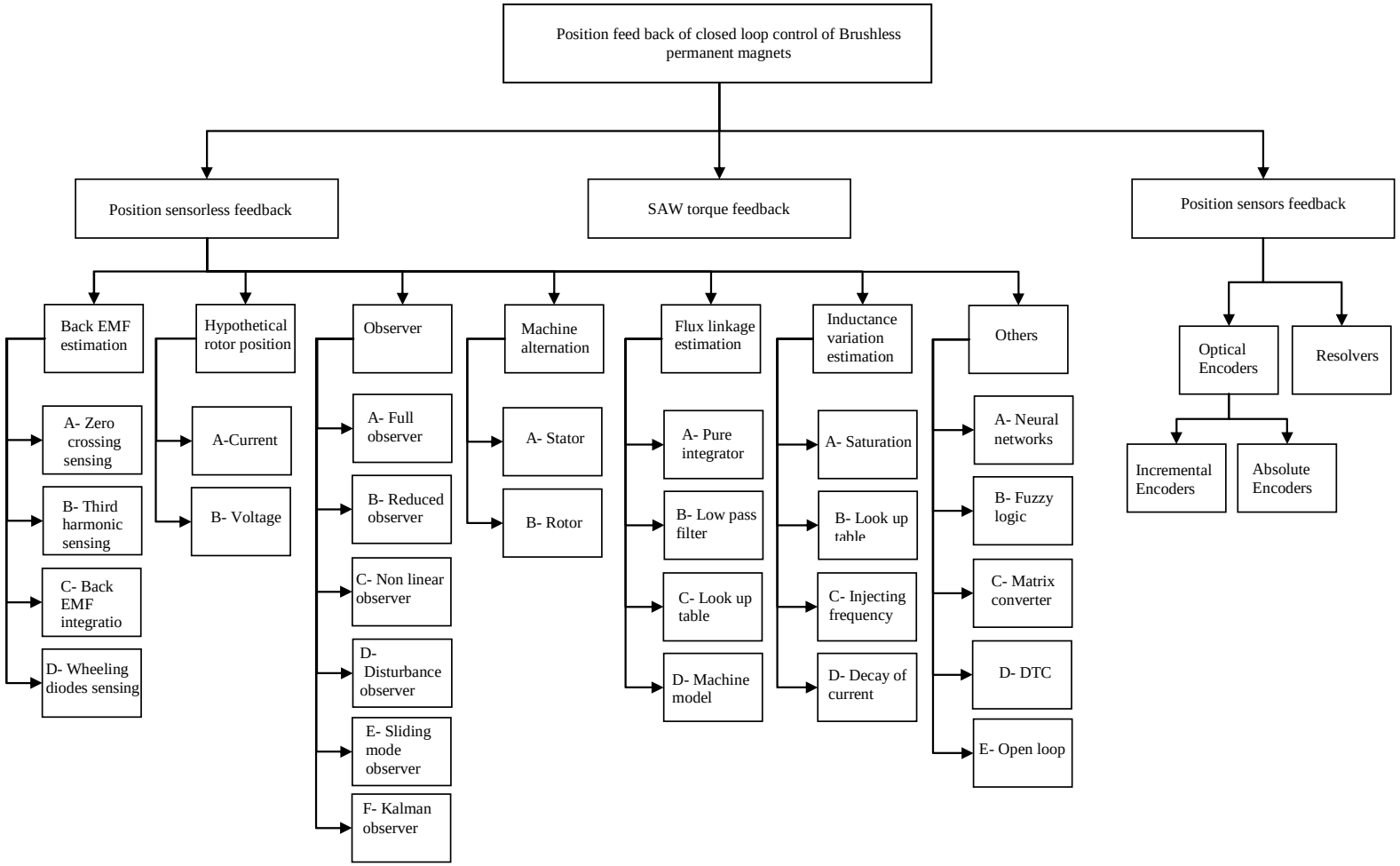

Fig. 1.23 Flowchart of position feedback schemes reported in the literature.

CHAPTER 2

BLPM START-UP ROUTINE

2.1 Introduction

The literature review of Chapter 1 highlighted a problem common to all position sensorless schemes, that of poor control from zero to low speeds, typically 0-300 rpm. This Chapter will therefore investigate the utilisation of measured torque feedback for the starting of BLPM machines from zero speed and the control thereof up to speeds of around 300 rpm. The choice of this higher speed will be discussed in later Chapters as being a suitable speed point at which other schemes, for example flux-estimator, may take over from the measured torque start-up routine. This Chapter will firstly analyse the relationship between electromagnetic torque and electrical rotor position in section 2.2. Three electromagnetic torque excitation form the base for zero speed position estimation in section 2.3. A flow chart to extract position from measured torque at zero speed is discussed in section 2.4. The flow chart has four routines; the first routine for when the electromagnetic torque is less than load torque at all rotor positions; the second routine is for when there is no-load attached to the machine shaft; the third routine is for when the electromagnetic torque is larger than the load on the shaft, but less than the threshold torque; and finally the fourth routine is for when the electromagnetic torque is larger than the load torque and the load is larger than the threshold torque. All of these routines can be used to estimate rotor position based on three phase current excitations. The preferred routine is the first routine because the brushless PM can start from stand-still, while for the other three routines the machine may rotate in either direction. In section 2.5 brushless DC control will be discussed and developed to an open-loop control strategy similar to the commutation strategy used in

brushless DC, but similar in manner to scalar *V/f* control. The advantages and disadvantages of open-loop control are discussed in section 2.6. The use of measured torque feedback to account for load conditions and how it will be implemented is discussed section 2.7.

2.2 Electromagnetic Torque

The mechanical dynamics of BLPM machines including rotor position and speed information can be determined from the electromagnetic torque equation [114]:

$$T_e = J\frac{d\omega_m}{dt} + B\omega_m + T_l \tag{2.1}$$

The electromagnetic torque is derived from the machine voltage matrix (2.2) by examining the various components, such as resistive losses, mechanical power and the rate of change of stored magnetic energy. The rate of change of stored magnetic energy can only be zero in steady state. Hence the output power is the difference between the input power and the resistive losses in steady-state. Assuming that saturation effects and iron losses can be neglected the derivation of the electromagnetic torque is (2.2) [114]:

$$\begin{pmatrix} u_u \\ u_v \\ u_w \end{pmatrix} = \begin{pmatrix} R_s & 0 & 0 \\ 0 & R_s & 0 \\ 0 & 0 & R_s \end{pmatrix} \begin{pmatrix} i_u \\ i_v \\ i_w \end{pmatrix} + \begin{pmatrix} L_{uu} & L_{uv} & L_{uw} \\ L_{vu} & L_{vv} & L_{vw} \\ L_{wu} & L_{wv} & L_{ww} \end{pmatrix} \begin{pmatrix} \frac{di_u}{dt} \\ \frac{di_v}{dt} \\ \frac{di_w}{dt} \end{pmatrix} + k_e \begin{pmatrix} \sin(\omega_e t + \theta_0) \\ \sin(\omega_e t + \frac{2\pi}{3} + \theta_0) \\ \sin(\omega_e t - \frac{2\pi}{3} + \theta_0) \end{pmatrix} \omega_e \tag{2.2}$$

Multiplying (2.2) by the transpose current vector, the instantaneous power is:

$$p_i = i^t u = i^t [R] i + i^t [L] \frac{di}{dt} + i^t k_e \left[f^n \theta_e \right] \omega_e \tag{2.3}$$

Here, the stator and rotor resistive losses are $i^t[R]i$ and the rate of the change of stored magnetic energy is $i^t[L]\frac{di}{dt}$. Therefore the third component of (2.3) must be equal to the air-gap power, given by the term $i^t k_e \omega_e f^n \theta_e$.

The air-gap power is the product of the mechanical rotor speed and electromagnetic torque. Hence, the electromagnetic torque is derived from the terms involving the mechanical rotor speed ω_m and P, the pole-pairs [114]:

$$p_i = \omega_m T_e = i^t k_e \left[f^n \theta_e \right] \omega_m = i^t k_e \left[f^n \theta_e \right] P \omega_e \tag{2.4}$$

Cancelling speed on both sides of the equation leads to an electromagnetic torque that is

$$T_e = P i^t k_e \left[f^n \theta_e \right] \tag{2.5}$$

the *d-q* rotor reference frame [115]:

$$T_e = \frac{3}{2} P[\psi_f + (L_d - L_q) i_d] i_q \tag{2.6}$$

Another way of deriving the electromagnetic torque is by multiplying the *d-q* voltages with the d-q currents and then representing the instantaneous power of the machine [114]:

$$P_i = \frac{3}{2}[u_q i_q + u_d i_d] \tag{2.7}$$

$$P_i = \frac{3}{2}[R_s[(i_q)^2 + (i_d)^2] + \left[L_q i_q \frac{di_q}{dt} + L_d i_d \frac{di_d}{dt} \right] + \omega_r \left[\psi_f + (L_d - L_q) i_d \right] i_q \tag{2.8}$$

From the (2.8) the stator resistance losses, the rate of change in magnetic stored energy, and the air-gap power can be determined. The air-gap torque can be computed by dividing the air-gap power by the mechanical speed. The factor 3/2 has been introduced to account for the power invariance of the three-phase to two-phase machine transformation [114]. The machine torque function for a steady-state characteristics for a salient pole BLPM machine when excited by stator current is [114]:

$$T_e = \frac{3}{2} P[\psi_f I_m \sin(\delta) + (L_d - L_q) I_m^2 \sin(2\delta)] \tag{2.9}$$

The torque angle influences the air-gap torque directly. There are also two distinct terms of the electromagnetic torque equation. The first term results from the interaction of the q-

axis stator current and the rotor magnet, referred to as the synchronous or excitation torque, T_{es}. The second term is due to the machine saliency variation and is known as the reluctance torque T_{er}. These two terms complete the electromagnetic torque equation:

$$T_{es} = \frac{3}{2} P \psi_f I_m \sin(\delta) \tag{2.10}$$

$$T_{er} = \frac{3}{2} P[(L_d - L_q) I_m^2 \sin(2\delta)] \tag{2.11}$$

$$T_e = T_{es} + T_{er} \tag{2.12}$$

For brushless PM machines, excited by a stator phase current of 1 p.u. magnitude, the sum of the synchronous and reluctance torques represent the electromagnetic torque, as illustrated in Fig. 2.1 for an illustrative machine discussed in [116]. The Fig. 2.1 shows that the torque angle for peak torque is more than 90 degree electrical due to the reluctance torque component. The reluctance torque increases the peak electrical torque in the region from 90-180 electrical degrees but also reduces the electrical torque in the region from 0-90 electrical degrees. Therefore, if there is saliency machine operation should be in the 90-180 electrical degrees region [116].

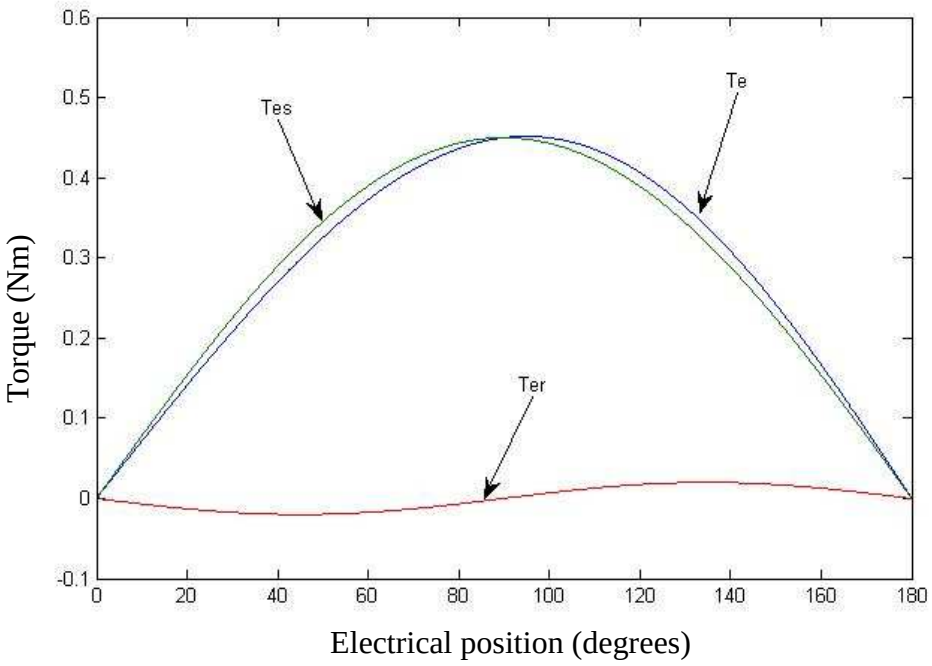

Fig. 2.1 Simulated electromagnetic torque [116].

2.3 Electromagnetic Torque vs. Electrical Position Variation

As discussed in section 2.2, the electromagnetic torque for a BLPM machine is a function of electrical position and stator current excitation (2.9). This section begins, therefore, with a method of extracting position from the electromagnetic torque excitation. The electromagnetic torque can be simulated (for example in Excel), assuming that the brushless PM machine has a balanced, three phase, sinusoidal, 120 electrical degrees distributed winding, there is no cogging torque and no saliency. Hence, the electromagnetic torque is due the synchronous torque. When the brushless PM machine is excited with a constant DC current between two phases, the electromagnetic torque is related to phase air-gap power for phase *U* by:

$$P_u = T_u \omega_m = e_u i_u = k_e \sin(\omega_e t)\omega_e i_u \tag{2.13}$$

$$T_u = \frac{k_e \sin(\omega_e t) P \omega_m}{\omega_m} i_u = k_e P \sin(\omega_e t) i_u \tag{2.14}$$

Similarly the electromagnetic torque for phase *V* and *W*:

$$T_v = \frac{k_e \sin(\omega_e t + 120) P \omega_m}{\omega_m} i_v = k_e P \sin(\omega_e t + 120) i_v \tag{2.15}$$

$$T_w = \frac{k_e \sin(\omega_e t) P \omega_m}{\omega_m} i_w = k_e P \sin(\omega_e t - 120) i_w \tag{2.16}$$

The excitation torque due to current excitation of phases *U* and *V* can be calculated from (2.17) as illustrated in Fig. 2.2, showing the machine stator winding connection schematic (a) and the torque versus rotor angle due to DC excitation of *U* and *V* (b). To demonstrate the process an illustrative machine with a phase current of 1 A and a phase back-EMF, e_u, of 1.5 V peak is used. The back-EMF is assumed sinusoidal, thus by multiplying the phase current i_u and the phase back-EMF, e_u, the resultant phase torque, T_u, is calculated. Similarly for phase *V* where the phase current here is -1 A due to the switching sequence of the power inverter where current flows from phase *U* to phase *V* now. The back-EMF, e_v, is 120 degrees lagging phase U. Multiplying the phase current i_v by the back-EMF, e_v, yields the resultant torque, T_v as summarized by the following:

$$T_{uv} = T_u + T_v = k_e P \sin(\theta_e) i_u + k_e P \sin(\theta_e + 120) i_v \tag{2.17}$$

$$i_u = -i_v \tag{2.18}$$

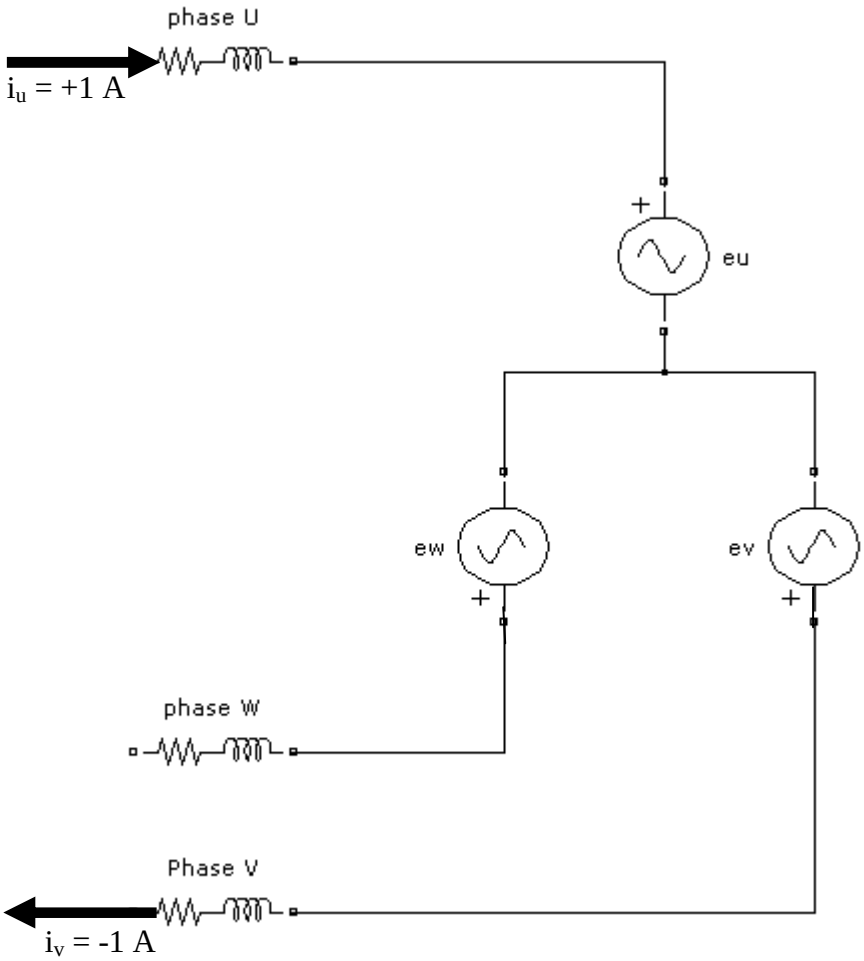

(a) Schematic of stator winding.

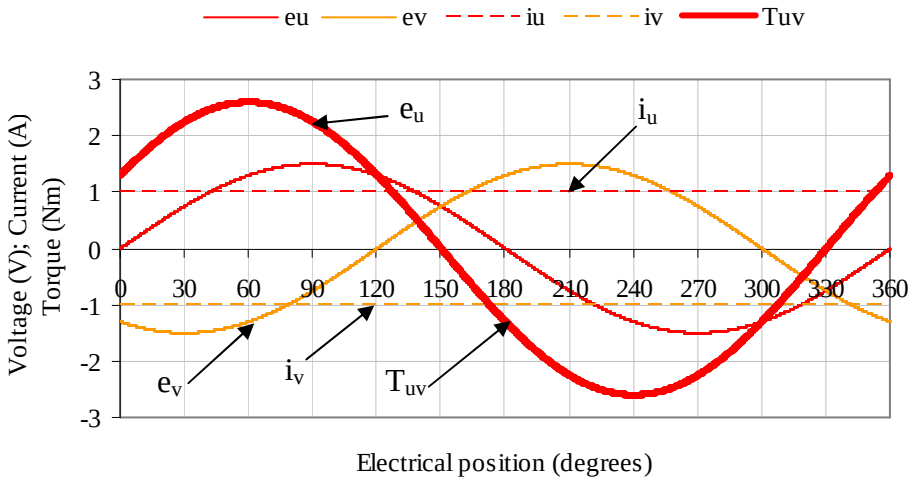

(b) Phase relationship of voltage, current and torque.

Fig. 2.2 Calculation of electromagnetic torque T_{uv} due to 1 A DC excition.

Similarly, Fig. 2.3 illustrates the electromagnetic torque excitation of phases *V*-*W* using the same procedure as for phase *U* and *V*. Phase *V* and *W* are 120 degrees and 240 electrical degrees respectively from the reference phase *U*. The torque calculation is therefore:

$$T_{vw} = T_v + T_w = k_e P \sin(\theta_e + 120) i_v + k_e P \sin(\theta_e - 120) i_w \tag{2.19}$$

$$i_v = -i_w \tag{2.20}$$

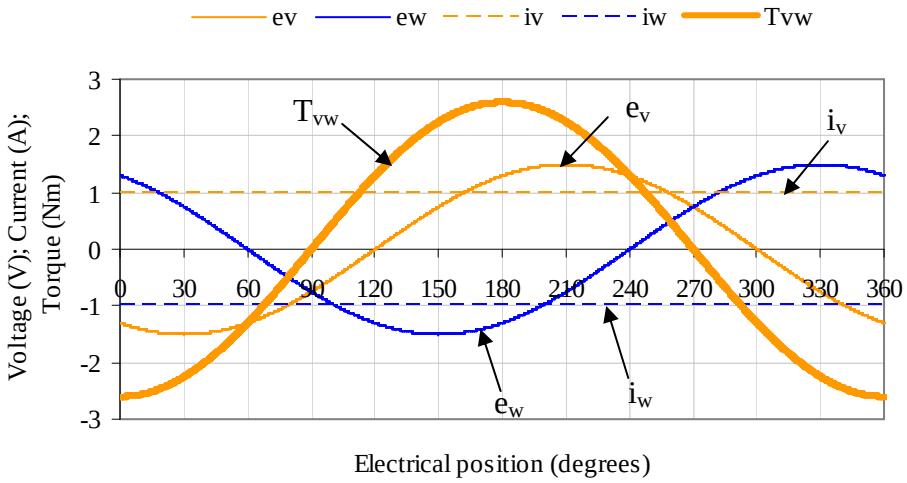

Fig. 2.3 Calculated electromagnetic torque T_{vw} due to 1 A DC excitation.

Finally, Fig 2.4 illustrates the electromagnetic torque due to 1 A excitation current through phases *W* and *U*. The torque calculation is now:

$$T_{wu} = T_w + T_u = k_e P \sin(\theta_e - 120) i_w + k_e P \sin(\theta_e) i_u \tag{2.21}$$

$$i_w = -i_u \tag{2.22}$$

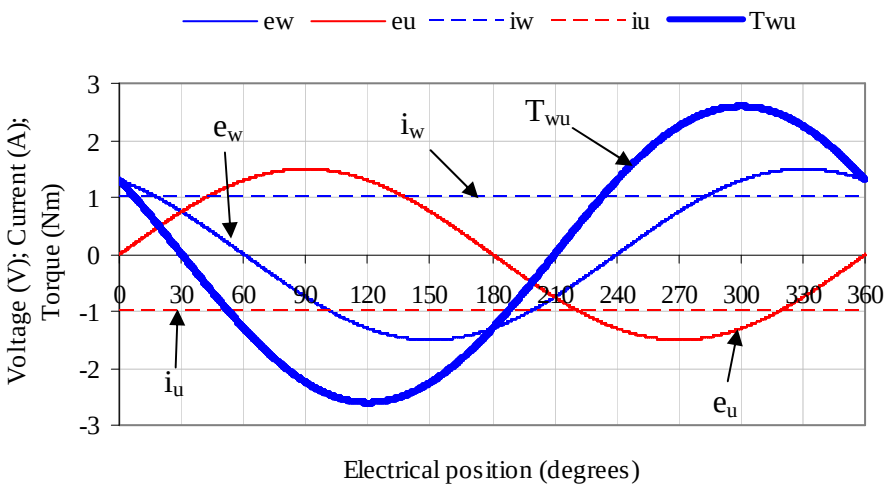

Fig. 2.4 Calculated electromagnetic torque T_{wu} due to 1 A DC excitation.

The electromagnetic torque waveforms illustrated in Fig. 2.2 to Fig. 2.4 are plotted in Fig. 2.5 for comparison. Here, the threshold torque, T_{th}, is defined and will be discussed later. Fig. 2.6 illustrates the change in torque amplitude for current excitation of 1 A, 2 A and 3 A amplitudes and illustrates that the rotor position does not change for different amplitudes. The three torque waveforms T_{uv}, T_{vw}, and T_{wu} are examined for calculating rotor position via measured torque feedback in the next section.

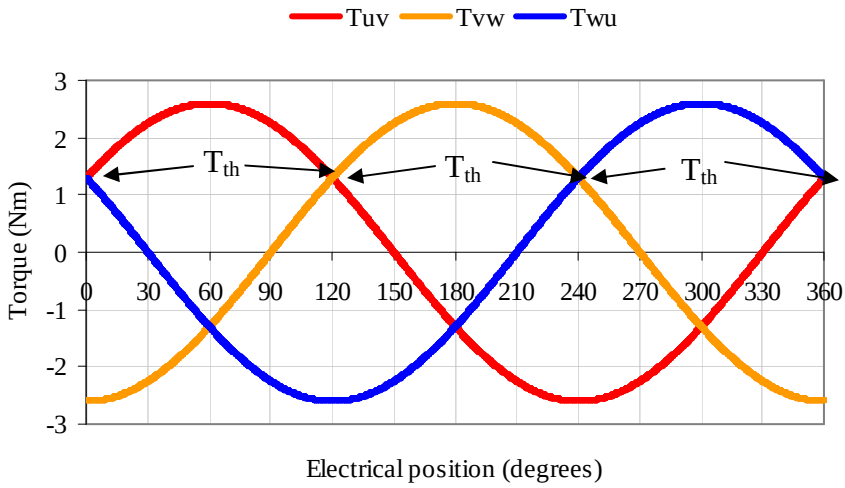

Fig. 2.5 Calculated electromagnetic torques and threshold torque.

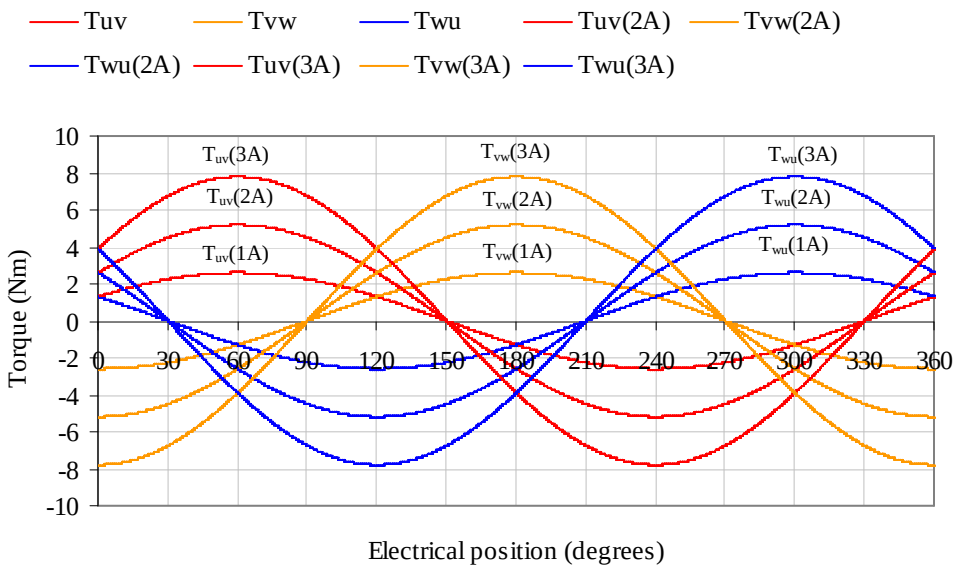

Fig. 2.6 Calculated electromagnetic torque for current amplitudes of 1 A, 2 A and 3 A.

2.4 Position Estimation at Zero Speed

2.4.1 Flow chart for zero speed electrical position estimation

In section 2.3 idealised electromagnetic torques were calculated and illustrated as functions of rotor position. In this section a more detailed discussion of the relationship between electromagnetic torque and position is presented and a flow chart of control options is developed, as illustrated in Fig. 2.7. The flow chart identifies four possible options:

(i) The first option is when the electromagnetic torque is less than the load torque, for all rotor positions. Since the rotor position of the brushless PM machine does not change three shaft torque measurements are obtained and used to estimate the position (stationary); Routine 1.

(ii) The second option is when there is no external shaft load; thus the machine rotor rotates until the electromagnetic torque falls to a zero or null point. Here, the machine rotates and position changes with each phase pair excitation. The measured torque reduces to a null or zero point for each excitation scheme (rotates); Routine 2.

(iii) The third option is when there is an external load that is less than the electromagnetic torque at all times; in this case the electromagnetic torque will

rotate the rotor of the brushless PM machine until the load torque is achieved (rotates); Routine 3.

(iv) The fourth option is when there is an external load that is over a limit defined as the threshold torque, T_{th}, shown in Fig. 2.5. Now the electromagnetic torque will not be able to rotate the rotor at all positions and the rotor angular change will be constrained within a phase-pair excitation window (partial rotation); Routine 4.

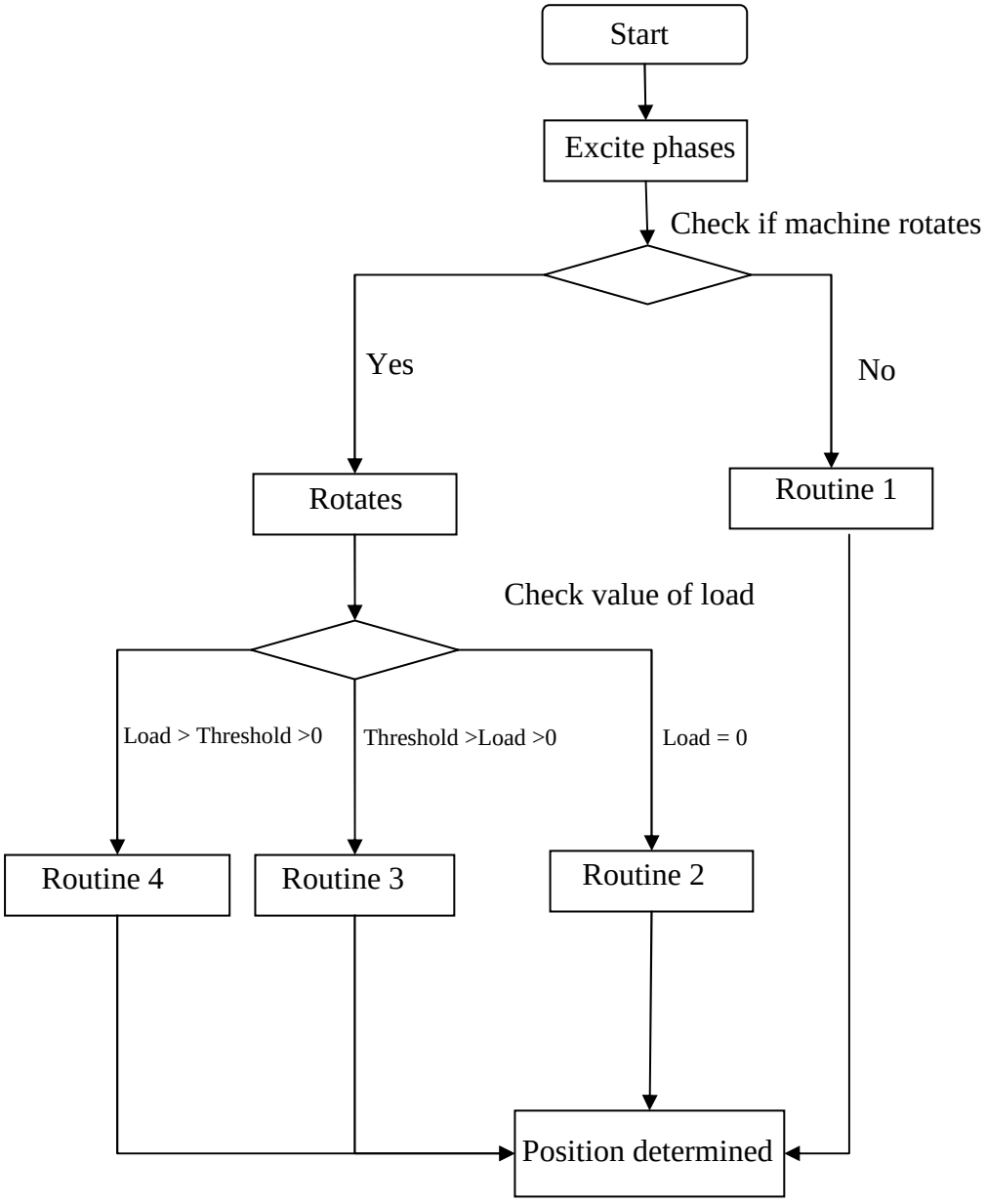

Fig. 2.7 Flow chart illustrating the control options available to determine rotor position.

2.4.2 Routine 1: Electromagnetic torque less than load torque

When two phases of the brushless PM machine are excited with a DC current an electromagnetic torque is generated. If the electromagnetic torque generated is less than the load torque at all positions, the rotor will not rotate and will remain stationary. Thus, the control scheme will excite two phases of the brushless PM machine with DC current, repeating the excitations to cycle through the three possible configurations, i.e. *U-V*, *V-W* and *W-U*. For each excitation shaft torque is measured from which a rotor (sector) and position can be determined.

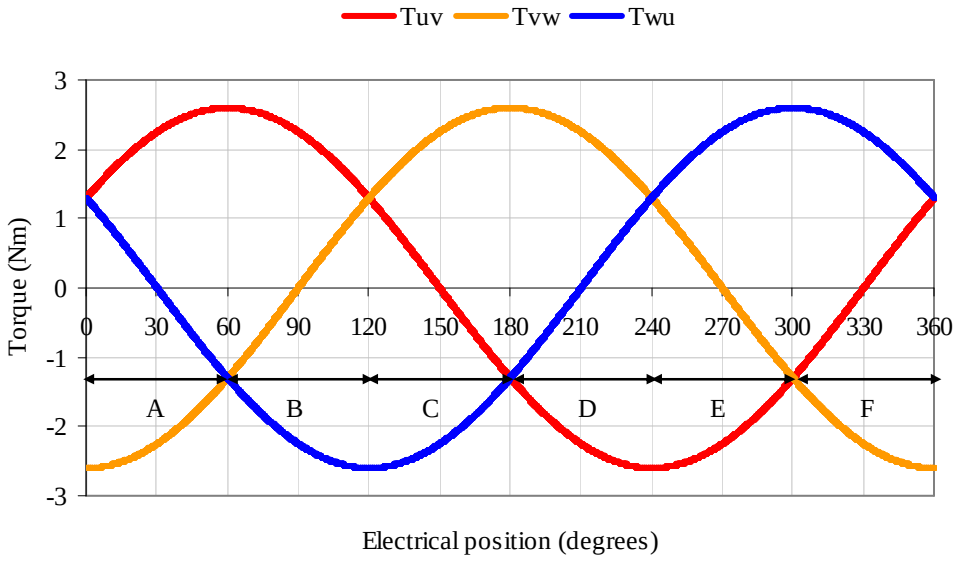

Fig. 2.8 Sectors defined from the three electromagnetic torque calculations for 1A excitation.

Six sectors are defined, *A-F*, as illustrated in Fig. 2.8. The sectors are 60 degrees electrical and determined using simple logic with reference to Fig. 2.8:

Sector *A*:

$$T_{uv} > T_{wu} > T_{vw} \tag{2.23}$$

Sector *B*:

$$T_{uv} > T_{vw} > T_{wu} \tag{2.24}$$

Sector *C*:

$$T_{vw} > T_{uv} > T_{wu} \tag{2.25}$$

Sector *D*:

$$T_{vw} > T_{wu} > T_{uv} \tag{2.26}$$

Sector *E*:

$$T_{wu} > T_{vw} > T_{uv} \tag{2.27}$$

Sector *F*:

$$T_{wu} > T_{uv} > T_{vw} \tag{2.28}$$

There are also the change-over points between sectors can also be determined from a simple logic:

Sector *A* to *B* change-over point:

$$T_{uv} > (T_{wu} = T_{vw}) \tag{2.29}$$

Sector *B* to *C* change-over point:

$$(T_{uv} = T_{vw}) > T_{wu} \tag{2.30}$$

Sector *C* to *D* change-over point:

$$T_{vw} > (T_{uv} = T_{wu}) \tag{2.31}$$

Sector *D* to *E* change-over point:

$$(T_{vw} = T_{wu}) > T_{uv} \tag{2.32}$$

Sector *E* to *F* change-over point:

$$T_{wu} > (T_{vw} = T_{uv}) \tag{2.33}$$

Sector *F* to *A* change-over point:

$$(T_{wu} = T_{uv}) > T_{vw} \tag{2.34}$$

From Fig. 2.8 it can be observed that each sector is 60 degrees electrical and has an angle defined with respect to phase *U* back-EMF, e_u, as detailed in Table 2.1. Applications of the logical tests detailed in (2.23) to (2.34) the rotor position of each sector change over can be determined, as detailed in Table 2.2.

Sectors	Position (electrical degrees)
A	0-60
B	60-120
C	120-180
D	180-240
E	240-300
F	300-360

Table 2.1 Sector angular definition.

Sectors	Position (electrical degrees)
A-B	60
B-C	120
C-D	180
D-E	240
E-F	300
F-A	360 or 0

Table 2.2 Sector change-over angles.

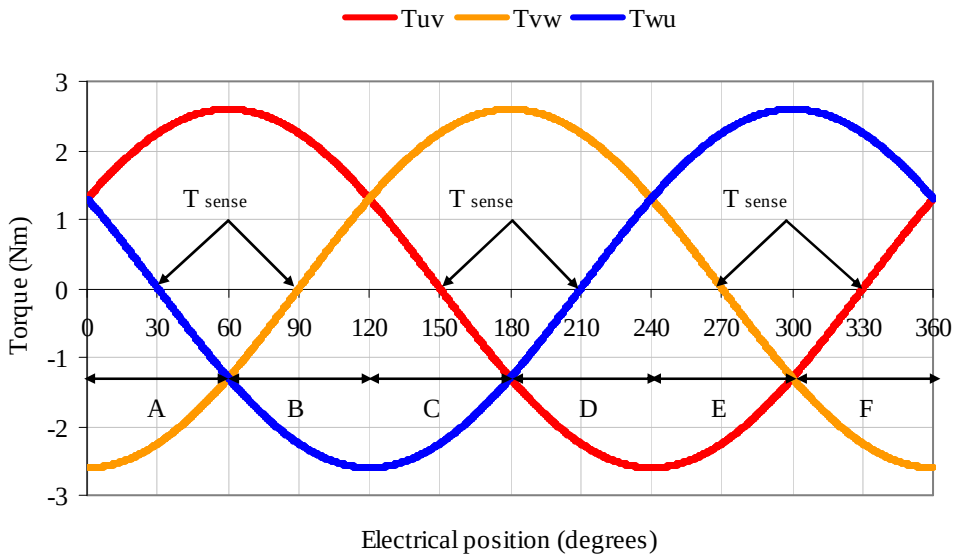

Fig. 2.9 Torque versus angle characteristics, sectors and the T_{sense} calculation for 1 A excitation.

Sectors	Torque sense	Increasing or decreasing
A	T_{wu}	Decreasing
B	T_{vw}	Increasing
C	T_{uv}	Decreasing
D	T_{wu}	Increasing
E	T_{vw}	Decreasing
F	T_{uv}	Increasing

Table 2.3 T_{sense} for each sector.

Thus, after determining the sectors an estimate of the rotor position θ_{es} can be made, for example once the sector is determined electrical position can be estimated by observing the sense of the measured torque signal that crosses zero within a sector and the torque versus angle gradient can be calculated, from which an estimate of actual position is made. Fig. 2.9 illustrates the torque zero crossing points, T_{sense}, and Table 2.3 the rate of change of T_{sense} with position. This methodology can be used for all sectors and generalised via equations (2.35) and (2.36):

If the torque sense is decreasing:

$$\theta_e = \left[\left(\frac{T_{high} - T_{sense}}{T_{high} - T_{low}}\right)(d)\right] + s \tag{2.35}$$

If the torque sense is increasing:

$$\theta_e = \left[\left(\frac{T_{sense} - T_{low}}{T_{high} - T_{low}}\right)(d)\right] + s \tag{2.36}$$

The distance between the sectors, d, and the starting of each sector, s-s_5, is shown in Fig. 2.10.

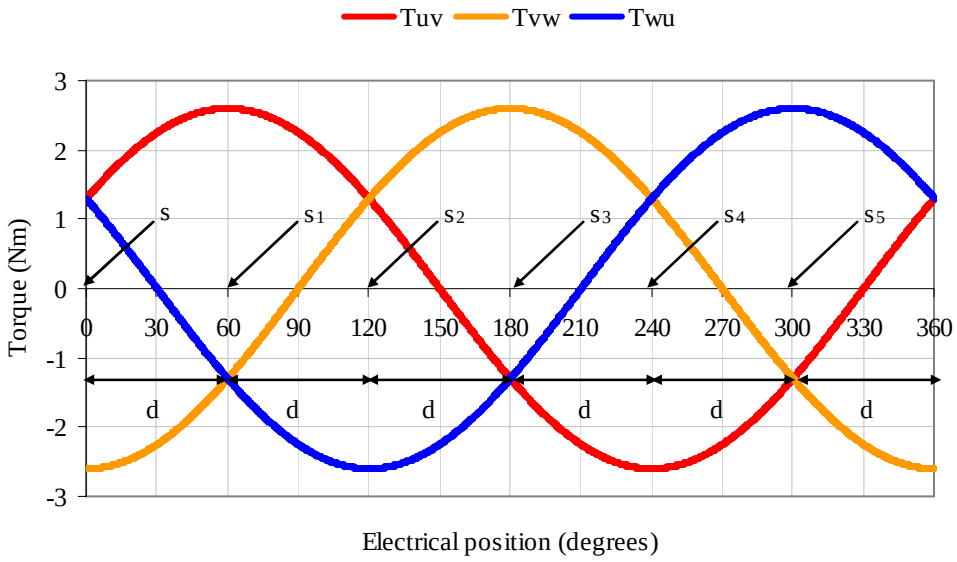

Fig. 2.10 The distances between sectors and the starting point of sector.

Equations (2.37) to (2.48) summarise the calculations for each of the six sectors for a three phase machine. For sector *A* it can be observed from Fig 2.10 that T_{uv} is a higher value and T_{vw} is the lower value, thus T_{wu} is T_{sense} and T_{sense} is as detailed in Table 2.3 is decreasing therefore:

$$\theta_e = \left[\left(\frac{T_{high} - T_{sense}}{T_{high} - T_{low}}\right)(d)\right] + s = \left[\left(\frac{T_{uv} - T_{wu}}{T_{uv} - T_{vw}}\right)(60)\right] + 0 \tag{2.37}$$

For an ideal surface mounted PM machine *d* is always equal to 60 degrees electrical as in the following analysis. However, this value would change if the machine exhibited significant cogging torque or asymmetric saliency. For sector *B*, T_{uv} is the highest and T_{wu} is the lowest value, thus T_{vw} is T_{sense} since T_{sense} is increasing this leads to:

$$\theta_e = \left[\left(\frac{T_{sense} - T_{low}}{T_{high} - T_{low}}\right)(d)\right] + s_1 = \left[\left(\frac{T_{vw} - T_{wu}}{T_{uv} - T_{wu}}\right)(60)\right] + 60 \tag{2.38}$$

For sector C, T_{vw} is the highest and T_{wu} is the lowest value, thus T_{uv} is T_{sense} since T_{sense} is decreasing this leads to:

$$\theta_e = \left[\left(\frac{T_{high} - T_{sense}}{T_{high} - T_{low}}\right)(d)\right] + s_2 = \left[\left(\frac{T_{vw} - T_{uv}}{T_{vw} - T_{wu}}\right)(60)\right] + 120 \tag{2.39}$$

For Sector D, T_{vw} is the highest and T_{uv} is the lowest value, thus T_{wu} is T_{sense} since T_{sense} is increasing this leads to:

$$\theta_e = \left[\left(\frac{T_{sense} - T_{low}}{T_{high} - T_{low}}\right)(d)\right] + s_3 = \left[\left(\frac{T_{wu} - T_{uv}}{T_{vw} - T_{uv}}\right)(60)\right] + 180 \tag{2.40}$$

For sector E, T_{wu} is the highest and T_{uv} is the lowest value, thus T_{vw} is T_{sense} since T_{sense} is decreasing this leads to:

$$\theta_e = \left[\left(\frac{T_{high} - T_{sense}}{T_{high} - T_{low}}\right)(d)\right] + s_4 = \left[\left(\frac{T_{wu} - T_{vw}}{T_{wu} - T_{uv}}\right)(60)\right] + 240 \tag{2.41}$$

For sector F, T_{wu} is the highest and T_{vw} is the lowest value, thus T_{uv} is T_{sense} since T_{sense} is increasing this leads to:

$$\theta = \left[\left(\frac{T_{sense} - T_{low}}{T_{high} - T_{low}}\right)(d)\right] + s_5 = \left[\left(\frac{T_{uv} - T_{vw}}{T_{wu} - T_{vw}}\right)(60)\right] + 300 \tag{2.42}$$

Similarly:

The sector A to B change-over

$$T_{uv} > (T_{wu} = T_{vw}) = 60 \tag{2.43}$$

The sector B to C change-over

$$(T_{uv} = T_{vw}) > T_{wu} = 120 \tag{2.44}$$

The sector C to D change-over

$$T_{vw} > (T_{uv} = T_{wu}) = 180 \tag{2.45}$$

The sector D to E change-over

$$(T_{vw} = T_{wu}) > T_{uv} = 240 \tag{2.46}$$

The sector E to F change-over

$$T_{wu} > (T_{vw} = T_{uv}) = 300 \tag{2.47}$$

The sector F to A change-over

$$(T_{wu} = T_{uv}) > T_{vw} = 360 \tag{2.48}$$

Using equations (2.37) to (2.48) to estimate rotor position when stationary, the estimate of rotor position compared to actual rotor position is shown in Fig. 2.11. The error between the estimated θ_{es} and the actual electrical positions θ_e (in degrees) is determined by:

$$\theta_{error} = \theta_e - \theta_{es} \tag{2.49}$$

The error is illustrated in Fig. 2.12.

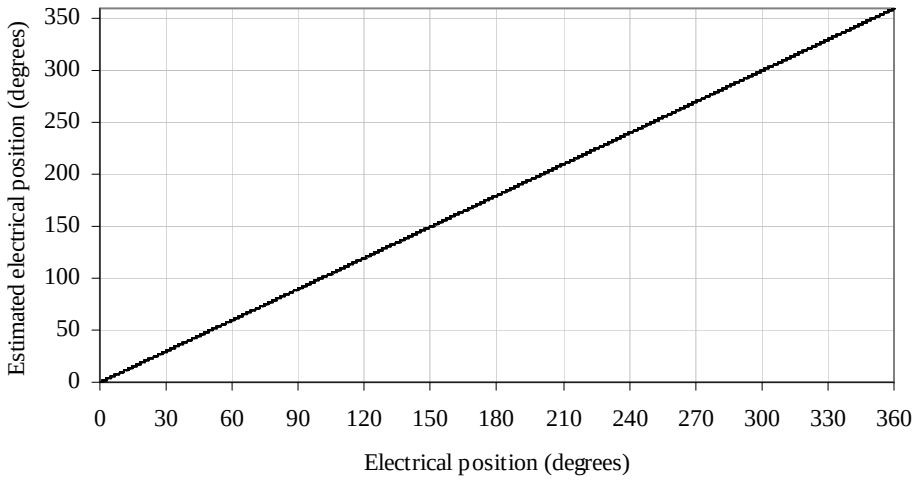

Fig. 2.11 Comparison of estimated versus actual electrical rotor position.

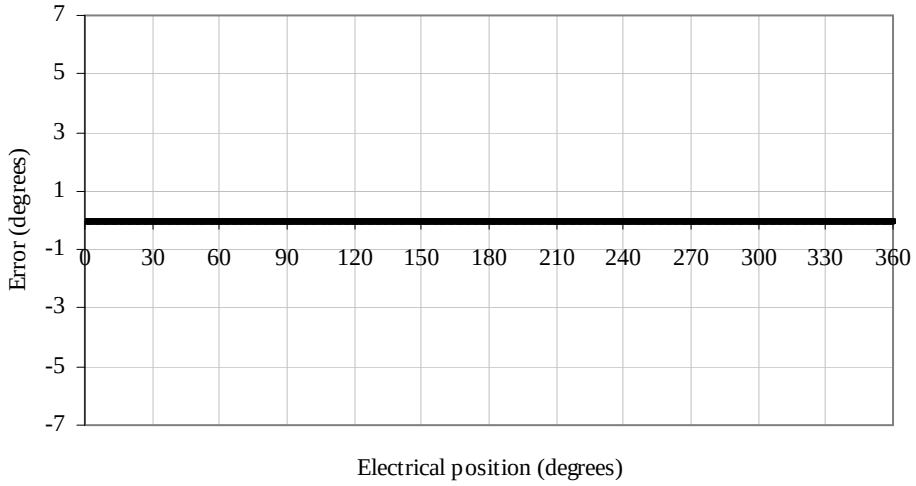

Fig. 2.12 Error between estimated and actual electrical rotor position.

2.4.3 Routine 2: Electromagnetic torque and zero load torque

When the electromagnetic torque is larger than the shaft load torque and there is no external load connected to the machine, the rotor will rotate when two phases of the machine are excited. When the rotor comes to rest the three torque measurements will, ideally, be equal to zero if there is no cogging torque or load perturbations on the system. Referring to Fig. 2.13, if phase *U* and *V* are excited the resultant electromagnetic torque, T_{uv}, will rotate the rotor until it reduces to zero, resulting in the rotor coming to rest at either position A or B.

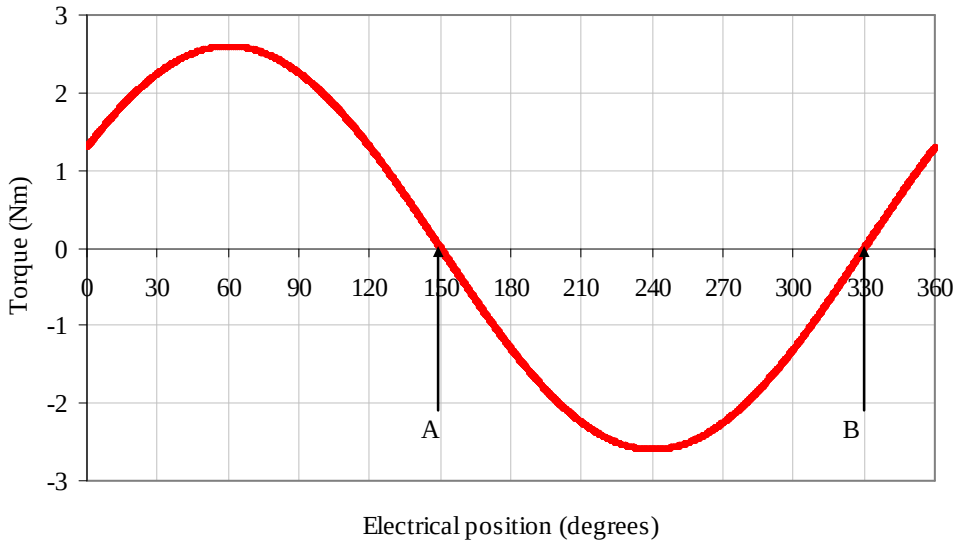

Fig. 2.13 Estimated electrical position at no-load and T_{uv} excited with 1 A.

A second excitation via phases *V* and *W*, will move the rotor from point A to point C if A was the starting point since the torque at that instant is positive. Similarly, it will move from point B to C if B was the start point, since the torque at instant B is negative settling at point C. This can be inferred from Fig. 2.14. A third and final excitation, *W* and *U*, will move the rotor from point C to point D. The sign of the measured torque must be recorded at the instant of the third excitation to determine if the rotor is rotating or not rotating since the torque behaviour during the final excitation must increase than decrease to zero. Thus, measured torque will indicate if the machine rotating is rotating.

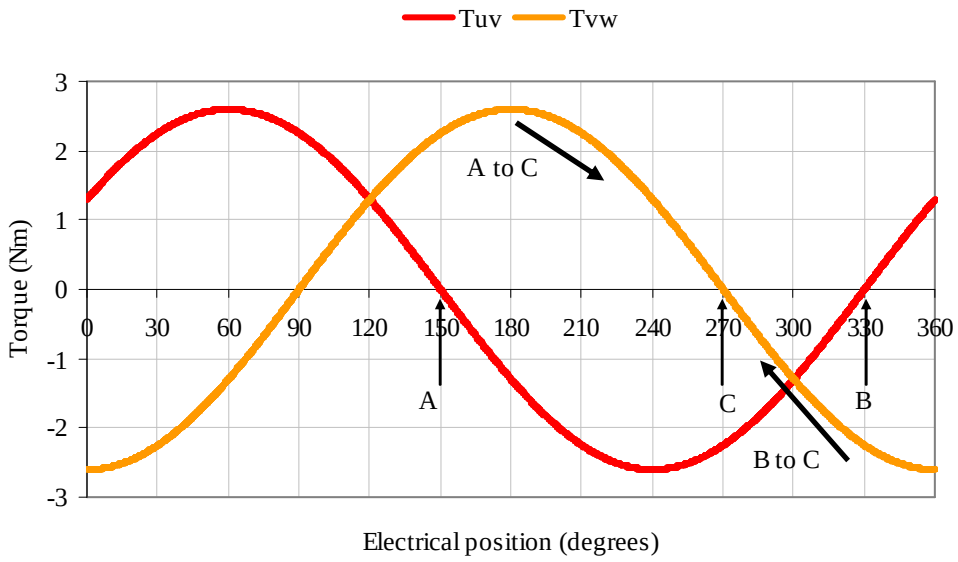

Fig. 2.14 Estimated electrical position no-load and T_{vw} excited with 1 A.

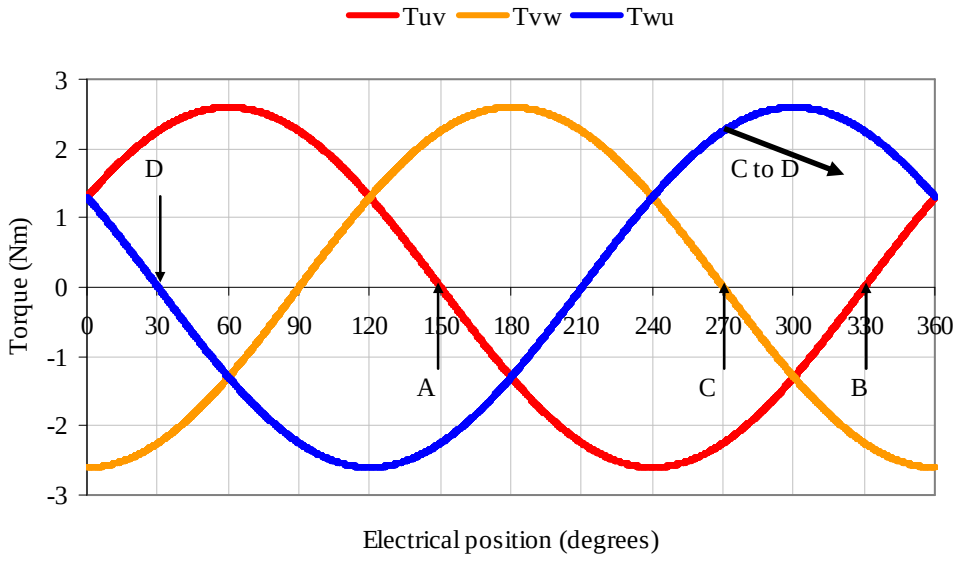

Fig. 2.15 Estimated electrical position no-load and T_{wu} excited with 1 A.

2.4.4 Routine 3: Electromagnetic torque > T_l < T_{th}

Referring again to the flow chart illustrated in Fig. 2.7. If the brushless PM machine electromagnetic torque is larger than the load and the load torque, T_l, is less than the threshold torque on the shaft, the rotor will rotate. If phases *U* and *V* are excited first, the rotor will settle at either point A or B with an offset to no-load position corresponding to the load torque, T_l, as shown in Fig 2.16. To determine the rotor position a second excitation via phases *V* and *W* is performed, thus, the electromagnetic torque will rotate the rotor from point A to point C, Fig. 2.17, or from point B to point C as illustrated in Fig. 2.17.

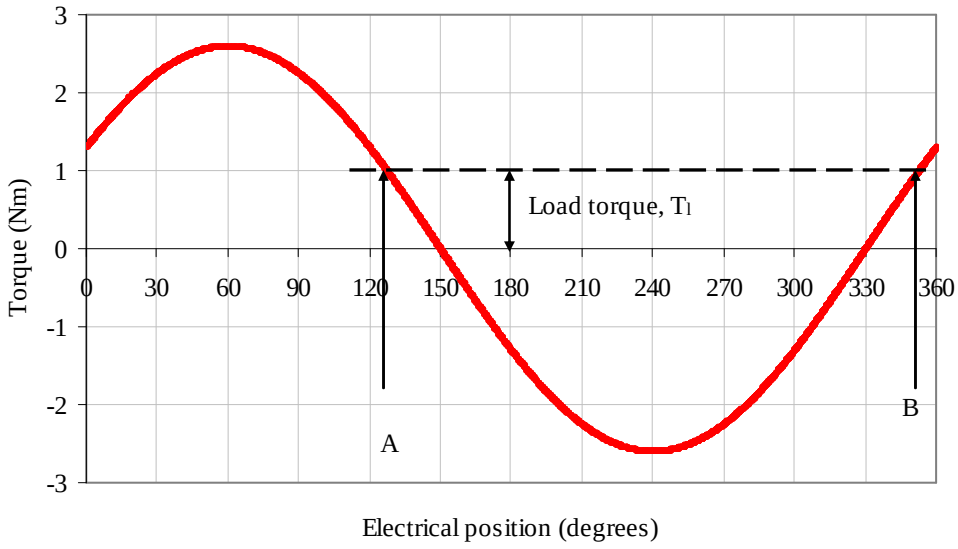

Fig. 2.16 Estimating electrical position when rotor load is less than the threshold load torque and phases *U*-*V* are excited with 1A.

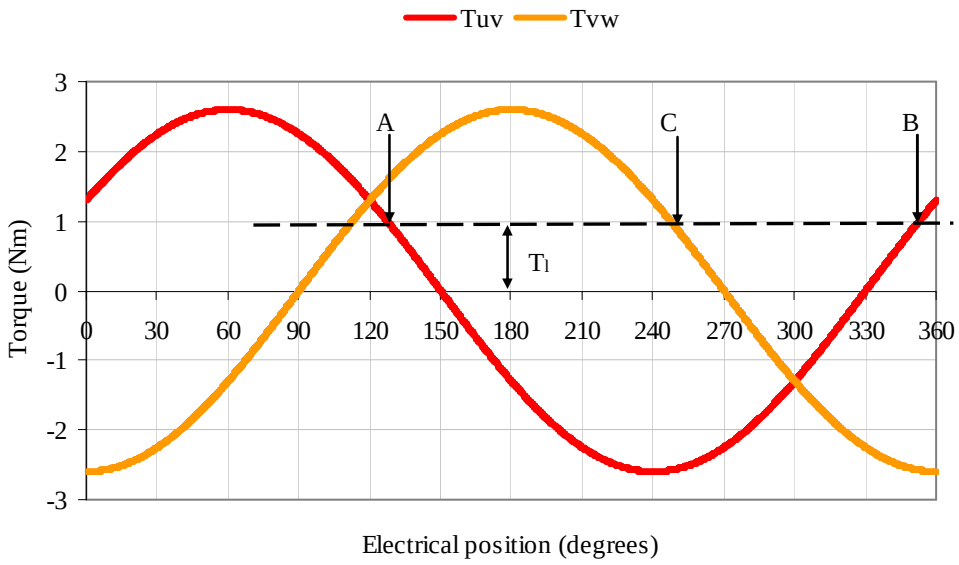

Fig. 2.17 Estimated electrical position when rotor load is less than the threshold load torque and phases *V*-*W* are excited with 1 A.

Finally a final excitation step is made via phases *W* and *U* to determine rotor position the rotor will rotate from point C to point D since the torque at point C due to the *V*-*W* excitation is positive. It is observed here that the torque will initially increase and than decrease until it settles at point D as shown in Fig. 2.18. The rotor position offset can be estimated knowing the maximum excited torque and the measured torque at point D from the following calculation:

$$\theta_{\delta} = \sin^{-1}\left(\frac{T_l}{T_m}\right) \tag{2.50}$$

Where T_l is the load torque and T_m is the maximum torque at 1 A excitation. In the example discussed the load torque = 1 Nm and the maximum excitation torque = 2.6 Nm, thus the estimated position at zero load position is 30 degrees electrical minus the offset which will equal to 7.38 degrees electrical. An important observation here is that as the load torque increases the offset increases. Note, the torque relationship to electrical position of the illustrative machine will be related to the prototype test machine discussed in Chapter 3.

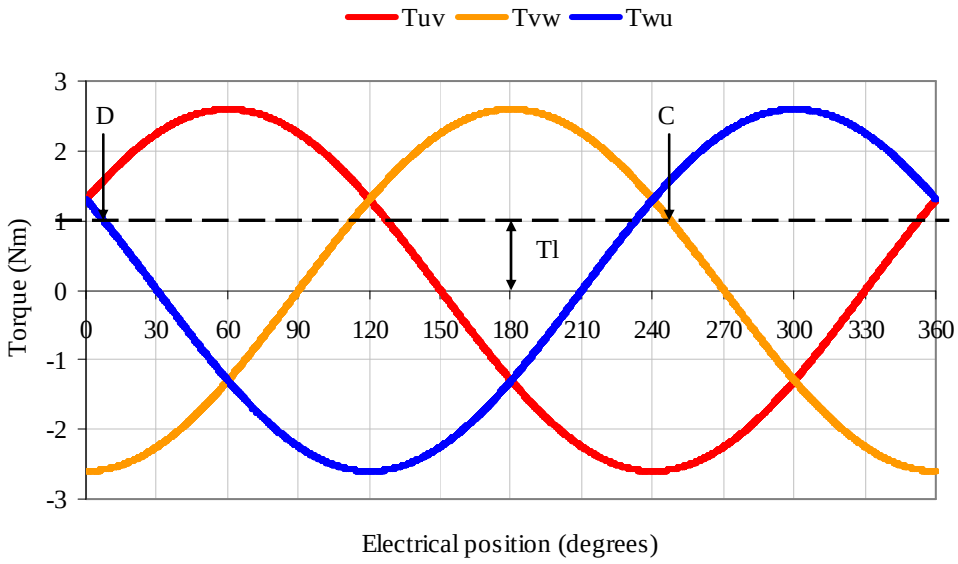

Fig. 2.18 Estimated electrical position when load is less than the threshold load torque and phases *W*-*U* are excited with 1 A.

2.4.5 Routine 4: Electromagnetic torque > T_l > T_{th}

The final case considered is when the electromagnetic torque is larger than the load torque, and the load torque is larger than the threshold torque (T_{th}), as illustrated in Figs. 2.19 to 2.21. In this case, the load torque is sometimes larger than the electromagnetic torque which will lead to the brushless PM machine partially rotating within two sectors. Now the position will vary and there will be three possible final positions.

Case (i): If the initial rotor position is between points A and B then, when exciting phases *U* and *V* the position will move to point B and, when exciting phases *V* and *W*, the position will remain at point B. Finally when exciting the final phases *W* and *U*, the position will move back to point A, as shown in Fig. 2.19.

Case (ii): If the initial rotor position is between points C and D than, when exciting phase *U* and *V*, the rotor will move to point C. Then when exciting phases *V* and *W*, the rotor will return to point D. Finally, when exciting phases *W* and *U*, the position will remain at point D, as shown in Fig. 2.19.

Case (iii): If the initial position is between points E and F then, when exciting phases *U* and *V* the rotor position will move to point E. When exciting phases *V* and *W* the position will remain at point E and finally when exciting the final phases *W* and *U* the rotor will return to point F, as shown in Fig. 2.16.

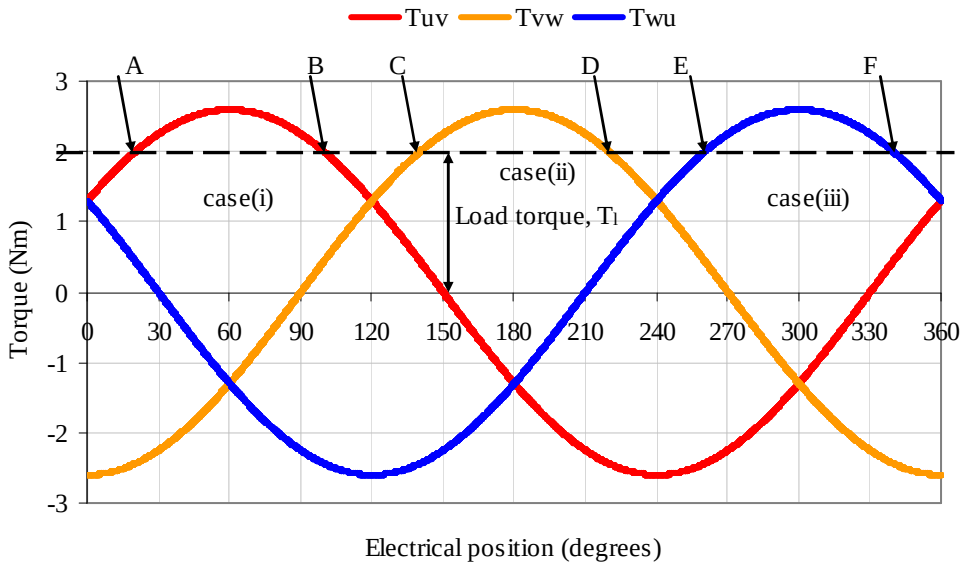

Fig. 2.19 Estimated electrical position when load is greater than T_{th}, Case (i), Case (ii) and Case (iii).

2.4.6 Summary of zero speed position estimation

Given the possibility of accurate measured torque feedback, there are four possible routines to arrive at an estimate of BLPM machine rotor position at zero speed. The first routine was discussed in detail in section 2.4.2 where the electromagnetic torque was always less than the load torque and thus the brushless PM did not rotate on phase excitation. Three torque measurements are taken at three different excitations and used firstly to determine the appropriate sector and than estimate rotor position. The second routine is required when there is no-load torque at all on the system. Thus, for three torque excitations the rotor will rotate and settle at 30 degree electrical increments as discussed in section 2.4.3. The third routine is required when load torque is added to the system and this load torque is less than the threshold torque as defined. Now the electromagnetic torque is always larger than the load torque so at all rotor positions the rotor will rotate as discussed in section 2.4.4. Finally, the fourth routine is when the electromagnetic torque is larger than the load torque, and the load torque is larger than the threshold torque. Here, the

electromagnetic torque will cause partial rotation, i.e. only when the electromagnetic torque is larger than the threshold torque as discussed in section 2.4.5. The most effective routine is to ensure that the electromagnetic torque will not be able to rotate the brushless PM rotor so that it can start from stand-still.

2.5 Brushless PM Control

Basically, two types of control are used to drive brushless PM motors: either brushless DC or brushless AC control. From the control point of view, the difference between the two control schemes is how the currents are generated and their shape, i.e., either rectangular or sinusoidal. In these drive systems, rectangular or sinusoidal reference current waveforms are generated with reference to a rotor position sensor. The advantage of the brushless DC control is its simplicity of implementation requiring, for example, one Hall-effect sensor per machine phase, as opposed to the optical or resolver requirement for brushless AC. The commutation of currents in the phase of a machine should be in phase with the respective phase back-EMF to realise maximum air-gap power production. This necessitates only three discrete sectors for a three phase machine in each electrical cycle generated, as mentioned, via Hall sensors.

The switching strategy for brushless DC drives is explained in detail here, since it underpins the previous start-up routine and subsequent transform to speed control. For maximum air-gap torque per ampere the back EMF voltages and related phase currents are illustrated in Fig. 2.20, showing the back-EMF and 120 degrees electrical current pulse for phase U, V and W. The 120 degree electrical current pulses or commutation events are simple logic developments from the 180 degree electrical, 50:50 mark-space ratio, Hall-effect output signals [15, 116]. The resulting air-gap power for each phase is illustrated in Fig. 2.21. The resultant air-gap which is the sum of all three phase contributions is illustrated in Fig. 2.22. Note, the shape of the phase power waveforms are the same as the phase torque waveforms but scaled by speed and time. These commutation events should be carefully synchronized to the machine back-EMF so that air-gap power is maximised and also the machine ripple is minimised. Fig 2.23 illustrates the impact on air-gap power and torque when the currents are advanced.

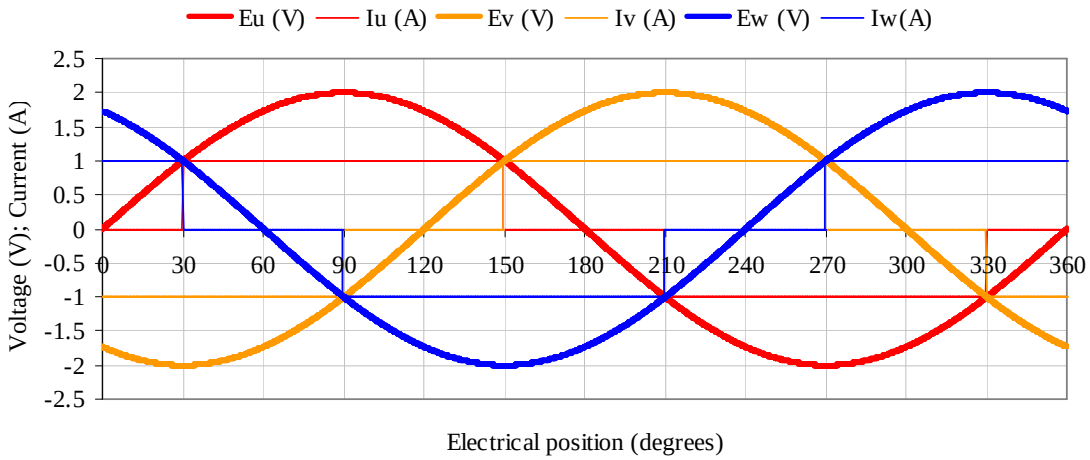

Fig. 2.20 Back-EMFs and associated phase currents.

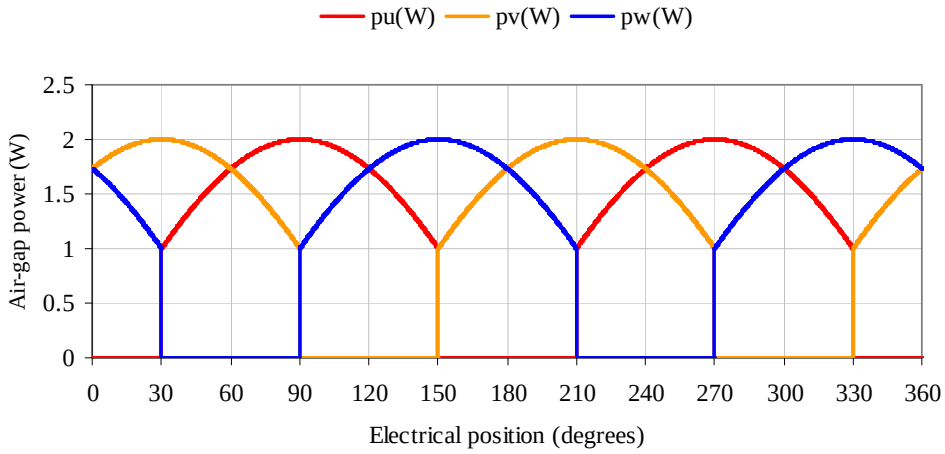

Fig. 2.21 Air-gap powers per phase.

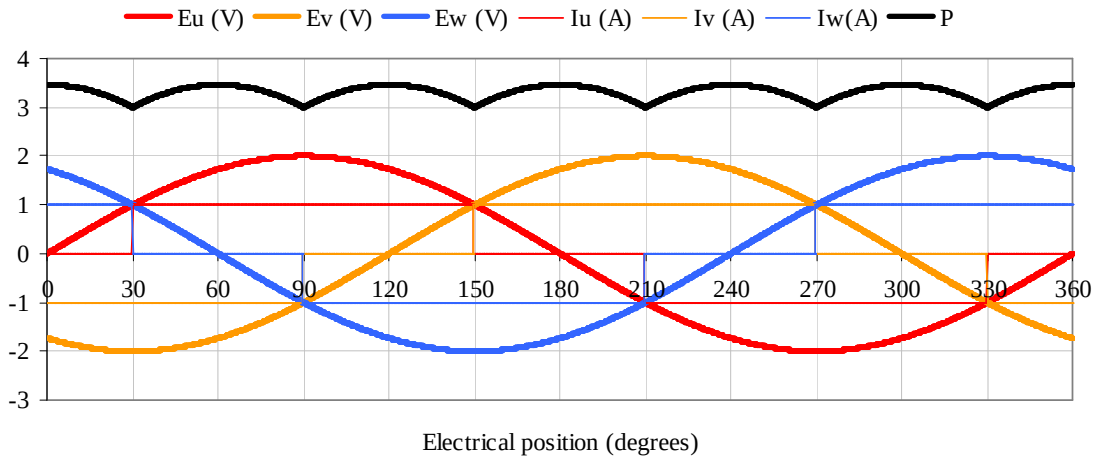

Fig. 2.22 Total air-gap power for phase U, phase V and phaseW.

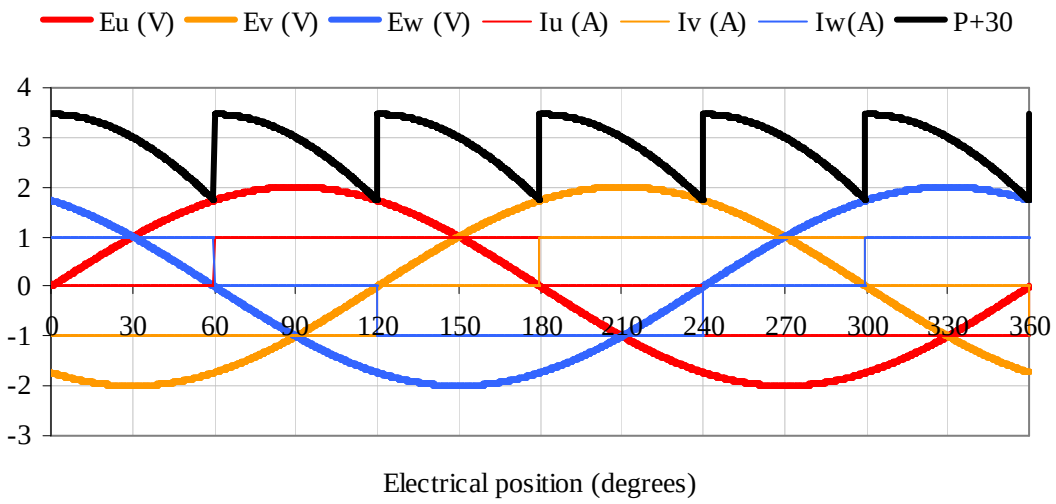

(a) Current advanced by + 30 electrical degrees.

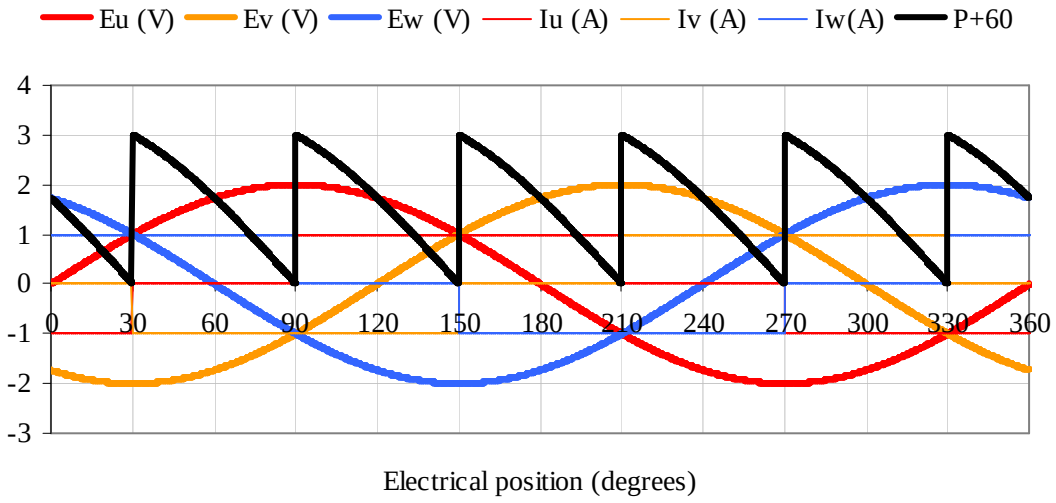

(b) Current advanced by 60 electrical degrees.

Fig. 2.23 Impact on power (torque) ripple due to commutation angle of advance.

2.6 Low Speed Control

2.6.1 Position sensorless (or open-loop) control

When using open-loop 120 degrees electrical or brushless DC control, the BLPM machine will operate synchronously to a certain extent. This means that for a given load, applied voltage and commutation rate, the BLPM machine will maintain open-loop control provided that these three variables do not deviate from the ideal by a significant amount [19, 118]. This technique can exhibit two cases. The first case is when the commutation rate is too slow for at a particular applied voltage. This is referred to as 'over-excited' and will result in the machine accelerating to the next commutation event and then slowing down and waiting for the next commutation. The BLPM machine will be acting like a stepper motor in the extreme case where it snaps to each position until the next commutation occurs. Since the machine is able to accelerate faster then the commutation rate, an excessive current will result in high torques and currents. The second case is when the commutation is too fast for a given voltage this is referred to as 'under-excited'. In this case, the commutation event is early such that the machine cannot accelerate fast enough to catch the next commutation event. Thus, open-loop control of the BLPM machine will be lost and the machine will stall or slow down. Open-loop controller is suitable when the load on the BLPM machine does not change over its operating period.

2.6.2 Position sensorless with measured torque feedback

The disadvantage of open-loop control is that if a sudden load is applied the machine will lose control and may stop rotating, here the use of the measured torque feedback becomes invaluable. Initially the machine is run without load and a table is constructed for each speed and respective terminal voltage. Then the measured torque is fed back to increase or decrease the voltage as the load increases or decreases. This is shown in Fig. 2.24

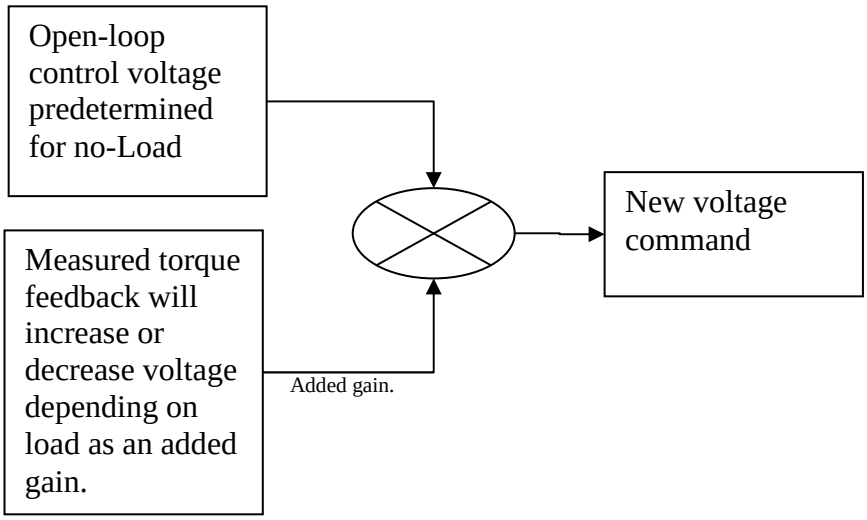

Fig. 2.24 Measured torque feedback block for low speed.

2.7 Summary of BLPM Start-up Routine

This Chapter has investigated and developed a procedure that uses measured torque feedback to estimate zero and low speed position without using other rotor position sensors. The zero speed position estimation has been divided into four routines, of which only three need actual torque measurement. The first routine discussed how the zero speed position can be estimated with the machine stationary. Here, the electromagnetic torque was less than the load torque for all rotor positions. The second routine discussed how the zero speed position can be estimated when the machine is free to rotate but there is no-load connected. The third routine discussed is implemented when the electromagnetic torque is larger than the load torque, and the load torque is less than a threshold torque (as defined in the Chapter). Finally, the fourth routine is implemented when the electromagnetic torque is larger than the load torque, and the load torque is larger than the threshold torque. Routine one is the best between the four routines since it can start the machine from stand-still without rotation. After determining the zero position, low speed control has been discussed to illustrate how at low speed the BLPM can be controlled using measured torque feedback. The idea for start-up and low speed control developed in this chapter will be test validated in Chapter 4.

CHAPTER 3

CHARACTERSATION OF DEVICES

3.1 Introduction

This chapter will characterise the devices used through the thesis. Section 3.2 will describe the position sensor used, which is an optical incremental encoder with 5000 pulses per revolution. Section 3.3 discuses a characterisation of a brushless PM motor. The resistance, inductance and back-EMF are all going to be measured and compared with the manufacturer's supplied data. Section 3.4 will describe the cylindrical SAW torque sensor by examining the display unit, the drift problems and static loading. Then it will be used to measure the cogging torque and the excited torque of the brushless PM machine. Section 3.5 discuses a characterisation of a prototype motor with an integrated SAW torque transducer where the resistance, inductance, back-EMF, cogging torque and torque constant will be characterised.

3.2 Optical Position Sensor

The optical incremental position encoder used is a RI58-Dhollow shaft encoder. The specifications of the position encoder are given in Table 2.1. The pulses per revolution indicate that for every one mechanical revolution 5000 pulses are outputted. The brushless PM motor discussed in Section 3.3 is a three pole-pair machine. That means for the Unimotor in section 3.3 the resolution for one electrical degree is 4 pulses and for the prototype PM machine discussed in Section 3.5 the resolution for one electrical degree is 2 pulses. The speed is limited to 6000 rpm and the temperature should be between -10 to 70 °C.

Attribute Type	Attribute Value	Units
Shaft Type	Standard Incremental	-
Pulse Per Revolution	5000	-
Supply Voltage	5	Vdc
IP Rating Housing	IP65	
Maximum Revolutions	6000	rpm
Operating Temp. Range	-10 to +70	°C

Table 3.1 Position encoder data sheet.

3.3 Unimotor PM Machine Parameters

The data that is supplied by the manufacture's for the unimotor Control Techniques is shown in Table 3.2:

Parameter	Parameter value	Units
Motor voltage	400	V_{pk}
Winding speed	3000	rpm
Incremental encoder	4096	ppr
Stall torque	10.8	Nm
Inertia	15.6	$kgcm^2$
Pole-pair	3	
Stator connection	Star	
Stall current	6.8	A
Rated power	2.83	kW
Resistance line-line	1.72	Ω
Inductance line-line	13.3	mH
Torque constant [k_t]	1.6	Nm/A
Back-EMF constant line-line [k_e]	98	Vrms/krpm

Table 3.2 Unimotor manufacture data.

3.3.1 Resistance measurement

The line-line resistance of the Unimotor brushless PM motor was measured using Ohms law. The measurement of the line-line resistance was measured in the lab by using a muilti meter, a voltage supply and current measurement and an LCR meter. In all the three tests the machine resistance was 2.1 Ω the temperature was 15 centigrade's when the test was conducted. The value obtained is shown in Table 3.3 and compared to the manufacture value.

Product data parameter	Manufacture value	Measured Value	Difference
Resistance line to line	1.72 Ω	2.1 Ω	22% increase

Table 3.3 Measured Line-line resistance of Unimotor.

3.3.2 Back-EMF measurement

The back-EMF line-line voltage is measured by coupling the Unimotor brushless PM motor to another machine, then running the machine at different speeds and measuring the generated open circuit line-line voltage of the PM motor by using a voltage meter [119]. The results of the back-EMF line-line voltage are shown in Table 3.4. These results are plotted in Fig. 3.1. The three back-EMF line-line voltages relative to electrical position are shown in Fig. 3.2 for a steady state speed of 500 rpm.

Speed (rpm)	Back-EMF line-line voltage (Vrms)
20	1.91
50	4.775
100	9.55
200	19.1
500	47.75
1000	95.5
2000	191

Table 3.4 Measured back-EMF line-line voltage of Unimotor.

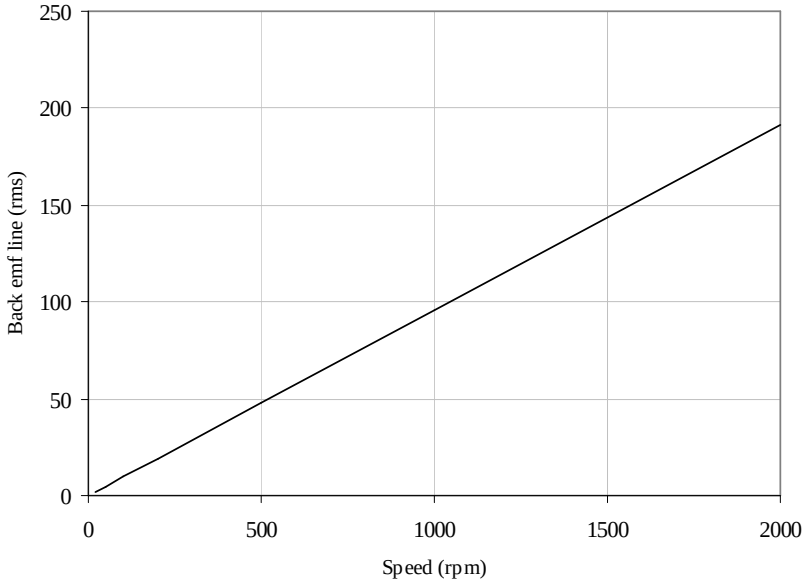

Fig. 3.1 Plot of back-EMF line-line voltage of Unimotor.

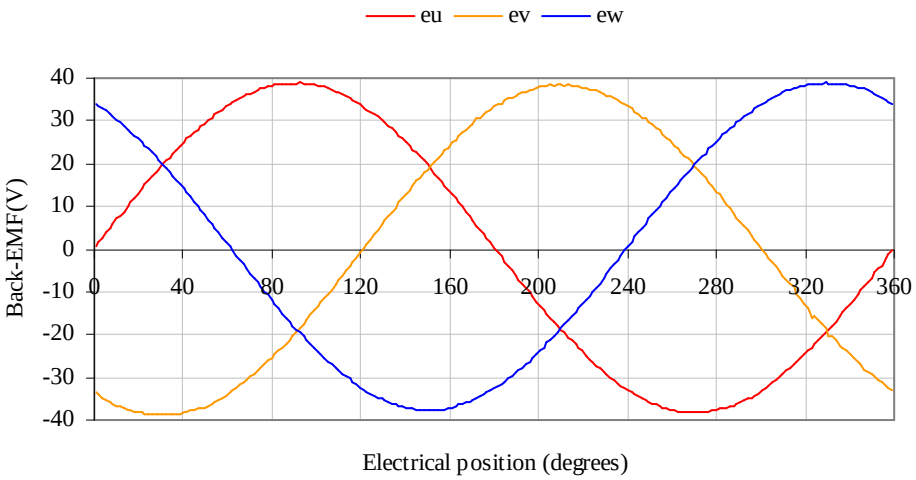

Fig. 3.2 Back-EMF phase voltage measurements at 500 rpm.

The resultant back-EMF in Fig. 3.1 is for the line-line in rms volts whilst in Fig. 3.2 the resultant back-EMF is for the phase voltages.

3.3.3 Inductance measurement

The line-line inductance is measured by rotating the PM machine 360 mechanical degrees and measuring the inductance value on each one electrical degree change. The measurement was done by using DSpace control to monitor the change in the mechanical degrees, electrical degrees and by using an Agilent inductance, capacitance and resistance (LCR) meter. LCR meters measure impedance at spot frequencies. The inductance was first measured to see the effect on inductance as the frequency increased. After 100 kHz the motor winding impedance is capacitive starts to act as a capacitor due the self capacitance as shown in Fig. 3.3.

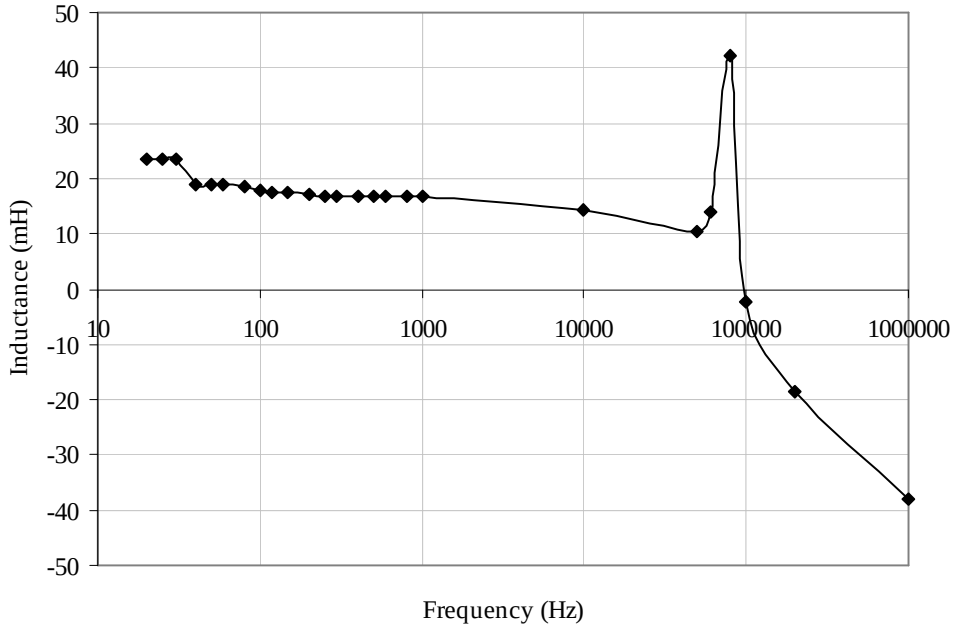

Fig. 3.3 Inductance response as frequency increases of Unimotor.

Fig. 3.4 shows the results for the line-line inductance of the Unimotor at two different frequency measurements which are 20 Hz and 800 Hz. The inductance value that is going to be used for controlling the motor is the measured inductance at 20 Hz shown in Fig. 3.5. The reason for choosing the 20 Hz frequency because the inductance true value is at 0 Hz and the LCR meter can measure inductance from 20 Hz.

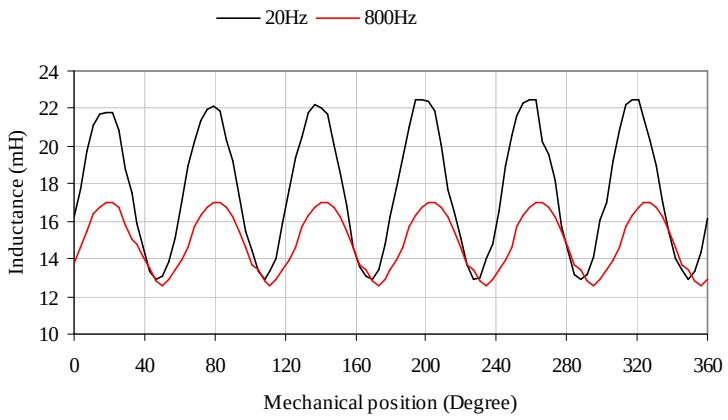

Fig. 3.4 Measured inductance vs. position sweep for two frequencies.

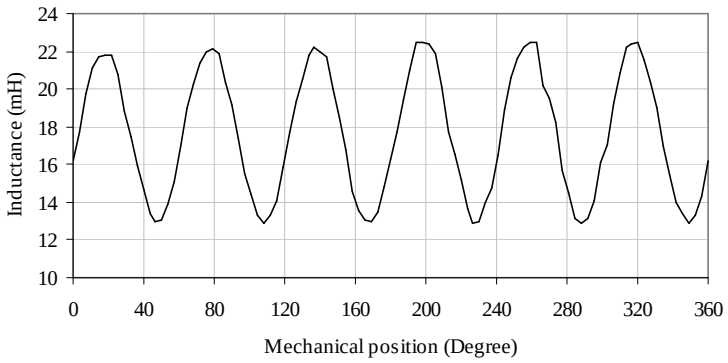

Fig. 3.5 Measured inductance vs. mechanical position.

The measured results are not compatible with the manufacturer's values. When the manufacturer was contacted, they stated that this is a surface mounted PM machine and there should be no more the 10% variation but according to the test done it clearly shows that there was variation of more than 10%. The line-line inductance is related to the rotor reference frame L_d and L_q inductance by [120]:

$$L_{l-l} = L_d + L_q + \left(L_d - L_q\right)\cos\left(2\theta_e + \frac{\pi}{3}\right) \tag{3.1}$$

The Ld and Lq inductances are calculated using the following equations [120]:

$$L_q = \frac{\max(L_{l-l})}{2} \tag{3.2}$$

$$L_d = \frac{\min(L_{l-l})}{2} \tag{3.3}$$

3.4 Characterisation of SAW Torque Transducer

The commercial 20 Nm inline SAW transducer [1-7], Fig. 3.6, used in this work has fixed resonant frequencies determined by the inter digital fingers and explained in appendix A1. The SAW transducer has resonant frequencies at 200 MHz and 201 MHz respectively, resulting in a difference of 1 MHz with a 200 kHz deviation equating to maximum strain in either direction of applied torque. Since the SAW sensors operate at radio frequencies, a simple non-contact coupling can be employed between the rotational devices and stationary processing and by careful design, the influence of external electromagnetic interference can be minimized [5, 6]. The temperature coefficient of the SAW device is <0.01% per °C over the temperature range -10 °C to 50 °C and <0.15% per °C for 50 °C to 125 °C, allowing them to be integrated and accurately used for machine control over typical industrial application temperature ranges. Importantly, for control of electromechanical drive-trains exhibiting significant resonances, the bandwidth of the SAW transducer signal after signal processing is typically >2 kHz [1]. Early transducers were connected via a cable and display unit, as shown in Fig. 3.6 (b), though the latest instrument systems have all processing electronics built inside and are connected via a simple USB link [7].

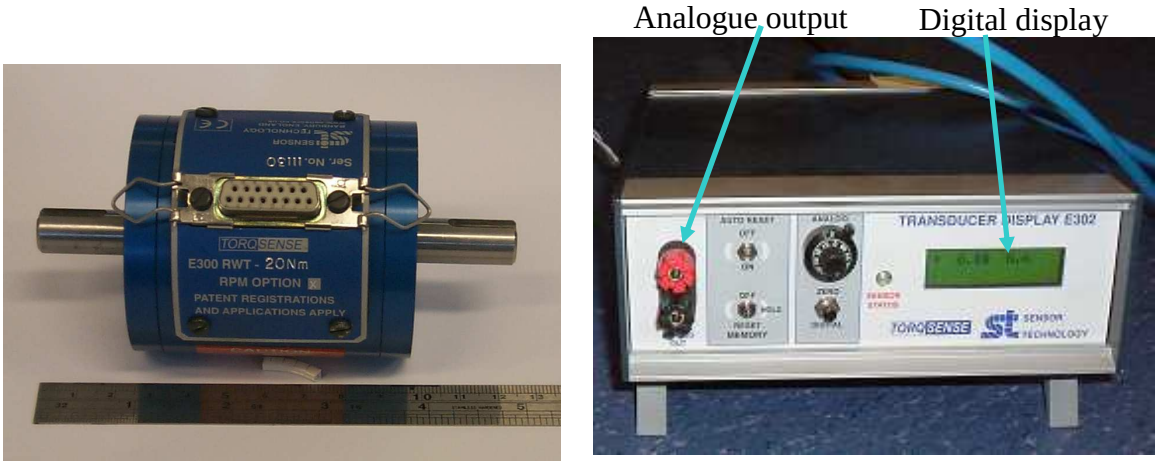

(a) 20 Nm, in-line SAW instrument transducer.

(b) SAW Transducer display unit.

Fig. 3.6 Commercial 20 Nm SAW torque measurement system.

3.4.1 Transducer display unit output

The transducer display analogue output was characterised with the cylindrical 20 Nm torque transducer. Each torque transducer has its own cable connection and its own display. The test was conducted was under no-load and only the analogue output was examined. The first test shown in Fig. 3.7 is for a spectrum analyser from 0 to 60 kHz.

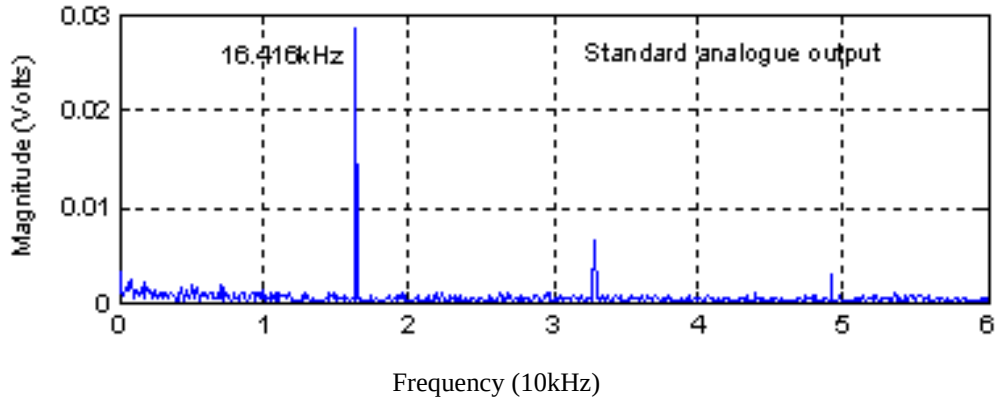

Fig. 3.7 Analogue output of cylindrical torque transducer test one [1].

The test that was done clearly shows there is a 16.5 kHz component and there are two harmonics located at 33 kHz and 49 kHz, respectively. These components are due to reflection modulation at the output stage of the display unit. They are known behaviours of the transducer display [1]. The highest magnitude of the component is 0.03 V and knowing that the max output voltage of the analogue display is 5 V then that will lead to an error of 0.6% of the measured torque. The second test shown in Fig. 3.8 is for a spectrum analyser from 0 MHz to 5 MHz.

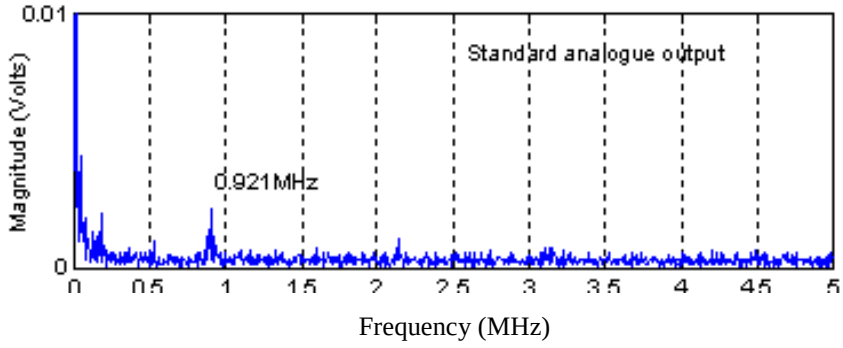

Fig. 3.8 Analogue output of cylindrical torque transducer test two [1].

The second spectrum test clearly shows a component at 0.921 MHz that is nearly equal to 1 MHz . This is due to the SAW resonant frequencies which are 200 MHz and 201 MHz respectively, resulting in a difference of 1 MHz. The magnitude of this frequency is to small, and also will not have much effect on the sensor. The noise components that are shown Fig. 3.7 and Fig. 3.8 are removed in DSpace by adding a digital low pass filter with a cut-off frequency of 2 kHz which was the ideal when test in the lab.

3.4.2 Drift

The display unit when started has to be always calibrated and if left more then 24 hours the anlog output will drift. An example of this is shown in Fig. 3.9. The anlog display was zeroed and the waveform captured, this was repeated 24 hours later. The drift over this period was ≈50 mV or ≈0.2 Nm

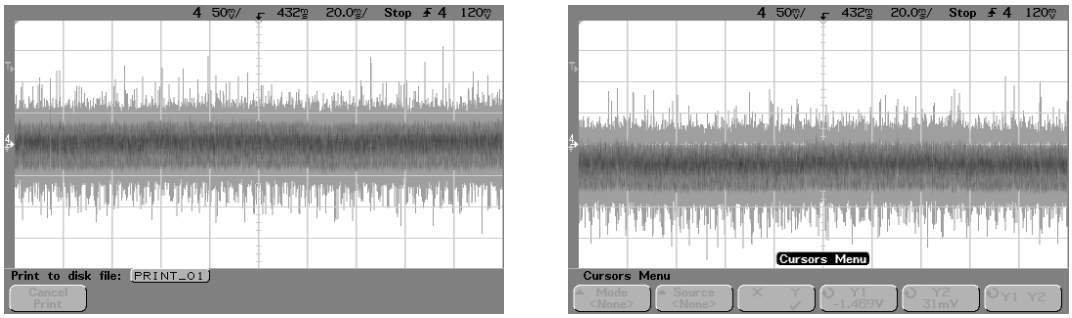

(a) Analogue output when started. (b) Analogue output after 24 hours.

Fig. 3.9 Analogue output drift after 24 hours [1].

3.4.3 Static load

The static load calibration was done before, as in Fig. 3.10. There were two tests performed; the first test is from 0.5 Nm to 5 Nm. The test was carried out by sliding a known mass along length d. The measurements where recorded in Fig. 3.11(a) then a another static load calibration was made for a load from 5 to 35 Nm. This is shown in Fig. 3.11(b). From Fig. 3.11 it can be seen that the analogue output of the display was within 5% from the measured whilst the digital display was inaccurate and was off by 35%. It was also mentioned that in both experiments the steel rod was set at 90° before mass was applied. As a result of the rod bending under full load, slight inaccuracies occurred. The error can be seen in the analogue output of both the graphs in Fig. 3.11, towards the end of the scales the calculated torque is higher than measured.

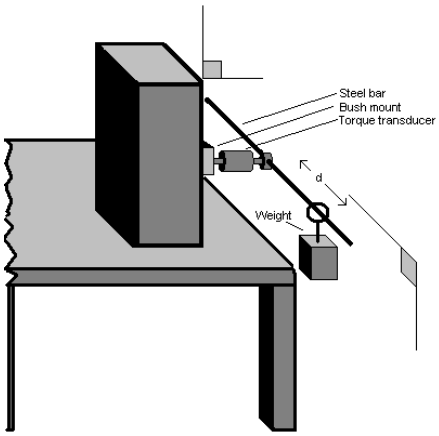

Fig. 3.10 Static loading diagram [1].

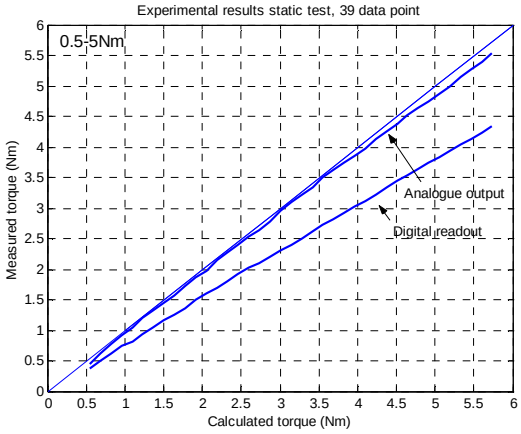

(a) Load from 0.5 to 5 Nm.

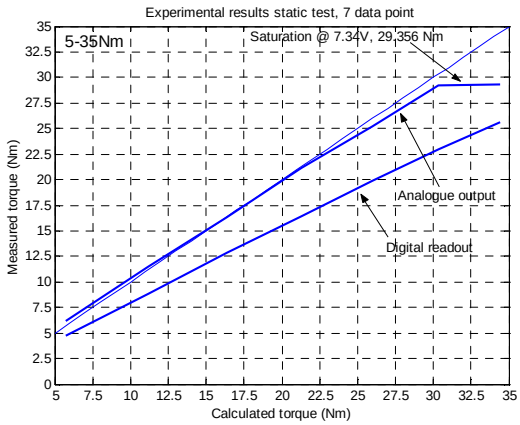

(b) Load from 5 to 35 Nm.

Fig. 3.11 Static load calibrations [1].

3.4.4 Torque measurements

The torque measurement test will examine the torque constant provided by the manufacturer 1.6 Nm/A from Table 3.2 to determine if it is compatible with the SAW torque measurement. The torque constant given by the manufacturer is 1.6 Nm/A, so if there is 1 A excitation, the max resultant torque will be 1.6 Nm. The drive used to drive the motor is shown in Fig. 3.12. The Unimotor under study is shown in Fig 3.13. The SAW sensor is coupled between the two motors, as shown in Fig 3.13. The test was done by rotating the motor at 5 rpm and exciting the Unimotor labelled servoload under study by different current values. The SAW transducer display unit displays the torque measured from the SAW torque sensor and there is an analogue output device which will output -5 to 5 V signal corresponding to the measured shaft torque, since the max measured torque is

20 Nm, the 20 Nm will be equal to 5 V. The experimental results are implemented in 4 steps:

1- Run the motor at 5 rpm speed and measure the torque from Unimotor PM motor with no current excitation. The result is going to be the cogging torque [121, 122] of both machines since the measured torque is the shaft torque. The result of the cogging torque relative to one mechanical position revolution is shown in Fig. 3.14.
2- Run the motor at 5 rpm and measure the torque from Unimotor PM machine with 1 A, 2A and 3A current excitation into two phases. The result of the shaft torque relative to one mechanical position revolution is shown in Fig. 3.15, Fig. 3.16 and Fig. 3.17.

Fig. 3.12 The Unidrive motor drive system [1].

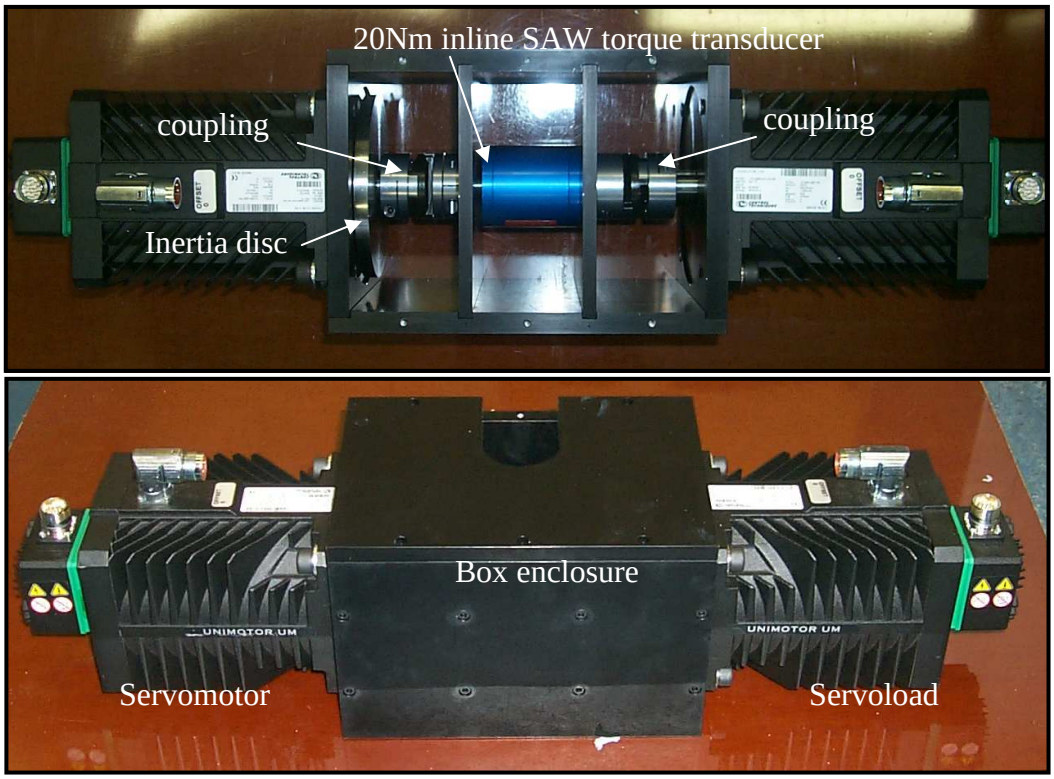

Fig. 3.13 Unimotor and SAW torque sensor coupled [1].

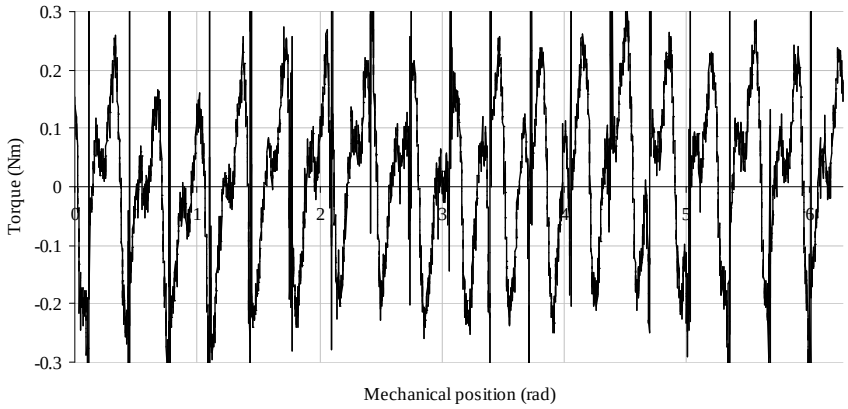

Fig. 3.14 Unimotor measured shaft torque for zero current excitation.

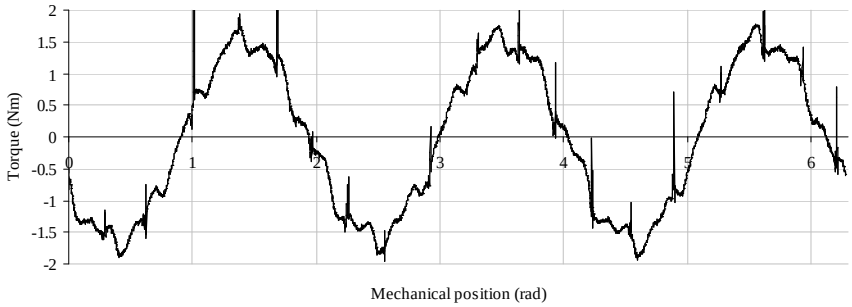

Fig. 3.15 Unimotor measured shaft torque for 1 A excitation.

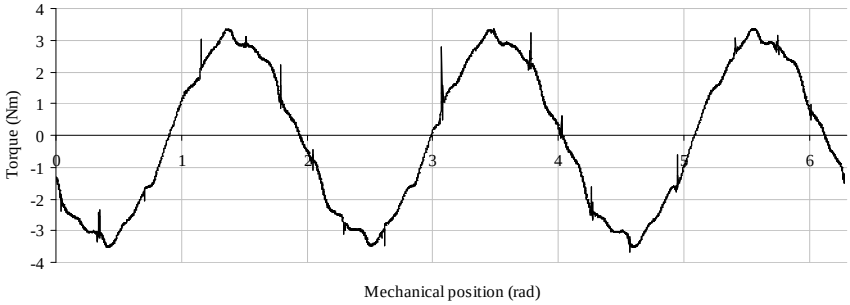

Fig. 3.16 Unimotor measured shaft torque for 2 A excitation.

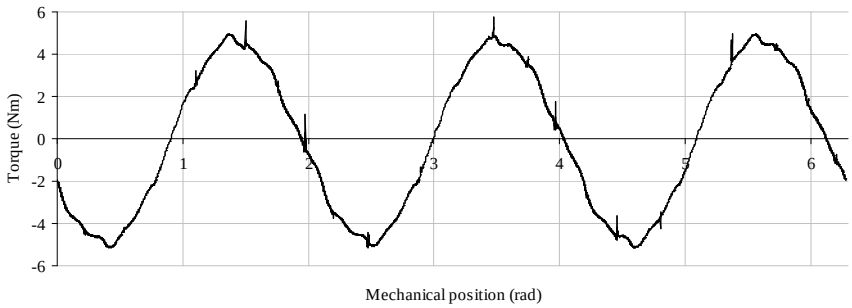

Fig. 3.17 Unimotor measured shaft torque for 3 A excitation.

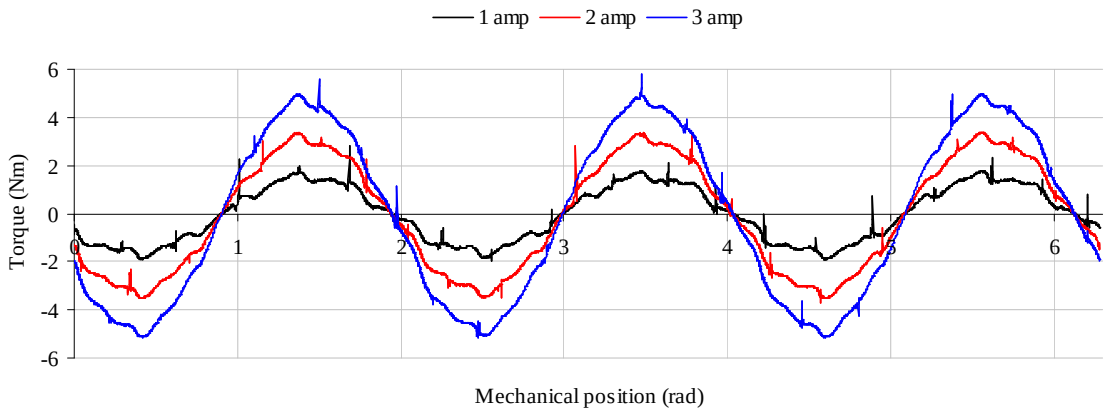

Fig. 3.18 Unimotor measured shaft torques.

The torque measurement that is shown in Fig. 3.14 is the total cogging torque of the two machines since no current was excited and the machine was rotated at 5 rpm. This measurement max value is 0.3 Nm for both machines. This value is also uniform so it does not have any major impact on the rest of the measurements taken. Fig. 3.15 is the torque measurement for a 1 A excitation, the max value is 1.65 Nm. This value is very close to the manufacturer's torque constant. Fig. 3.18 is for all three torque measurements plotted against mechanical position. The max value at position 3.48 mechanical radians on Fig. 3.18 for the 1 A excitation is 1.65 Nm, the 2 A excitation is 3.27 Nm and the 3 A excitation is 4.86 Nm. This clearly shows that a 1 A excitation will generate a electromagnetic torque of 1.65 Nm which is the same with the manufacture torque constant. The spikes are mainly due to the inverter noises. The differences between the manufacture and measured are mainly due the cogging and inertia torque on the system from the two machines.

3.5 Characterisation of Prototype Machine

The prototype machine is a brushless PM machine with an integrated SAW torque sensor transducer, which is shown in Fig. 3.19. Here, two 20 Nm SAW devices and the associated RF module are embedded inside a 2.5 kW, off the shelf, PM machine. The PM machine is modified by altering the rotor shaft and front faceplate design to accommodate the SAW devices and input/output port, as shown in Fig. 3.20. Therefore, the alterations to PM are minimal. The engineering drawings of the PM machine with the SAW torque transducer integration is shown in Fig. 3.21. The following sections will investigate the characterisation of the prototype machine.

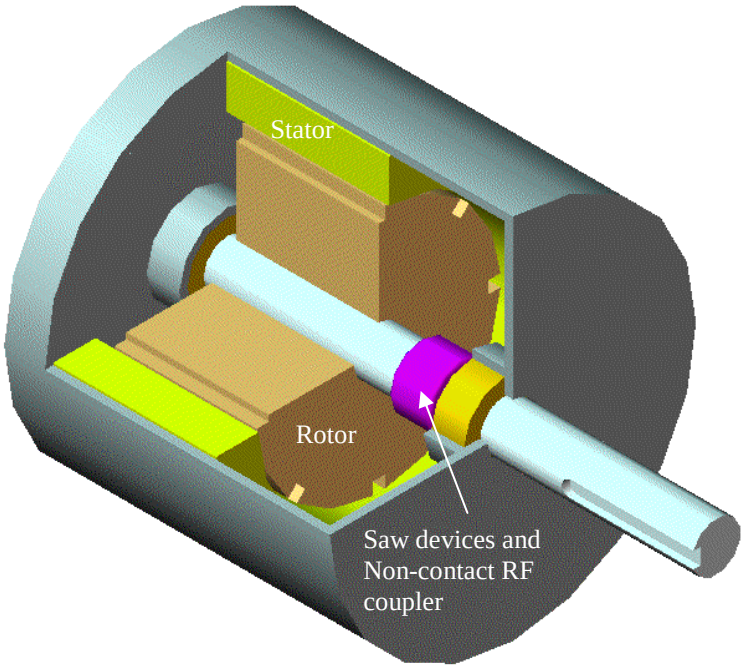

Fig. 3.19 SAW torque sensor inside the prototype PM machine [1].

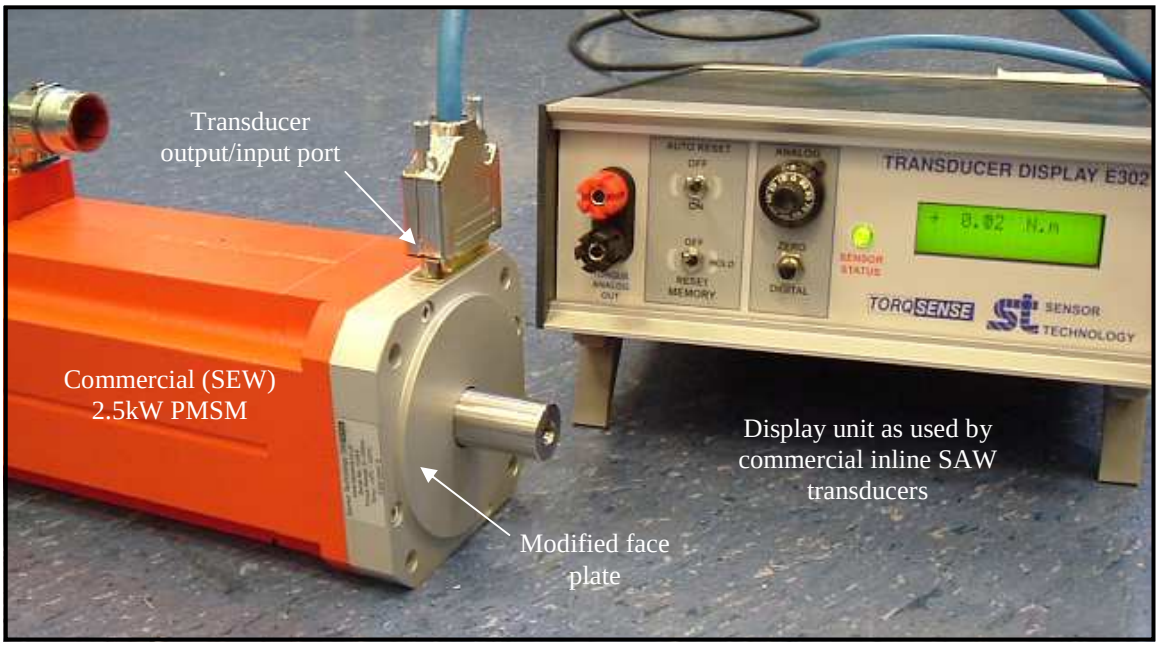

Fig. 3.20 Prototype PM machine with integrated torque transducer [1].

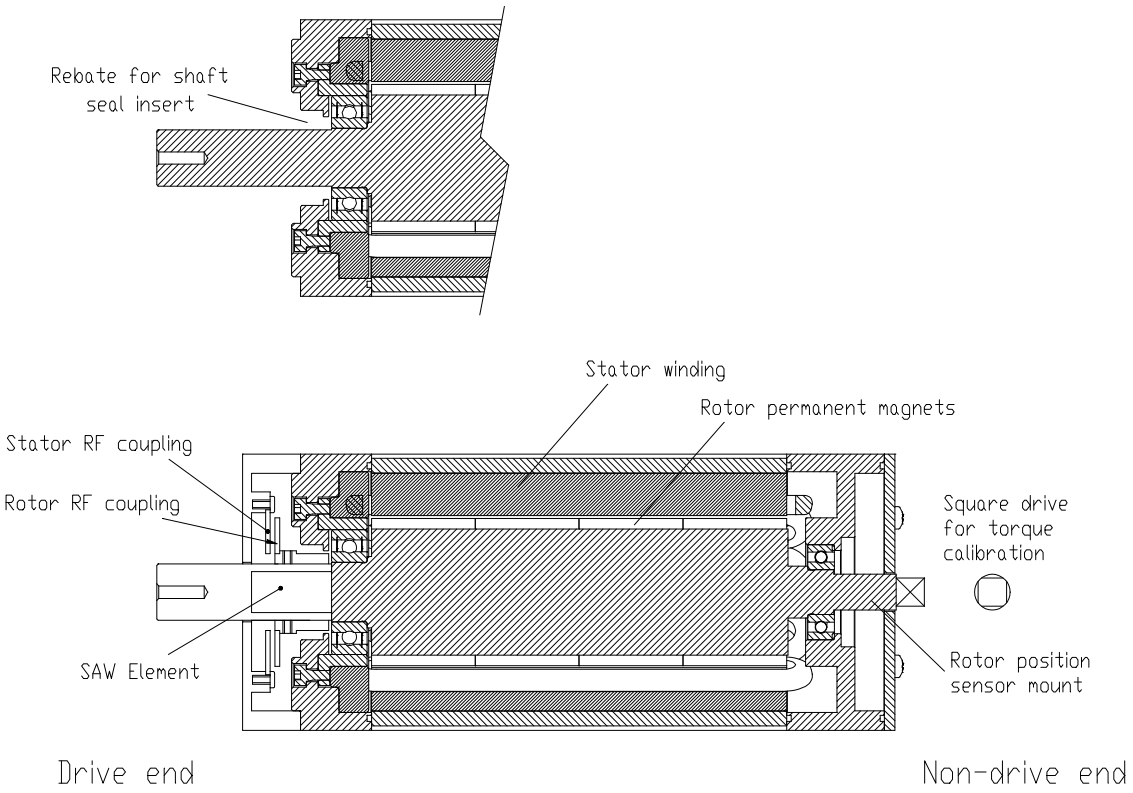

Fig. 3.21 Engineering drawings of the prototype PM [1].

3.5.1 Resistance measurement

The line-line resistance of the prototype brushless PM machine was measured using Ohm's law as shown in Table 3.5. There is no manufacturer's specification for this machine.

Product data parameter	Measured Value
Resistance phase to phase	1.7 Ω

Table 3.5 Measured line-line resistance of prototype PM machine.

3.5.2 Back-EMF measurement

The back-EMF line-line voltage is measured by coupling the prototype PM machine to another machine, then running the machine at different speeds and measuring the generated open circuit line-line voltage of the prototype PM machine by using a voltage meter. The results of the back-EMF line-line voltages are shown in Table 3.6. These results are plotted in Fig. 3.22. The three phase back-EMF voltages relative to position for a 500 rpm are shown in Fig. 3.23.

Speed (rpm)	back-EMF line-line voltage (Vrms)
20	1
50	3.2
100	6.8
200	13.71
500	33.36
1000	67
2000	133.8

Table 3.6 Measured back-EMF line-line voltage.

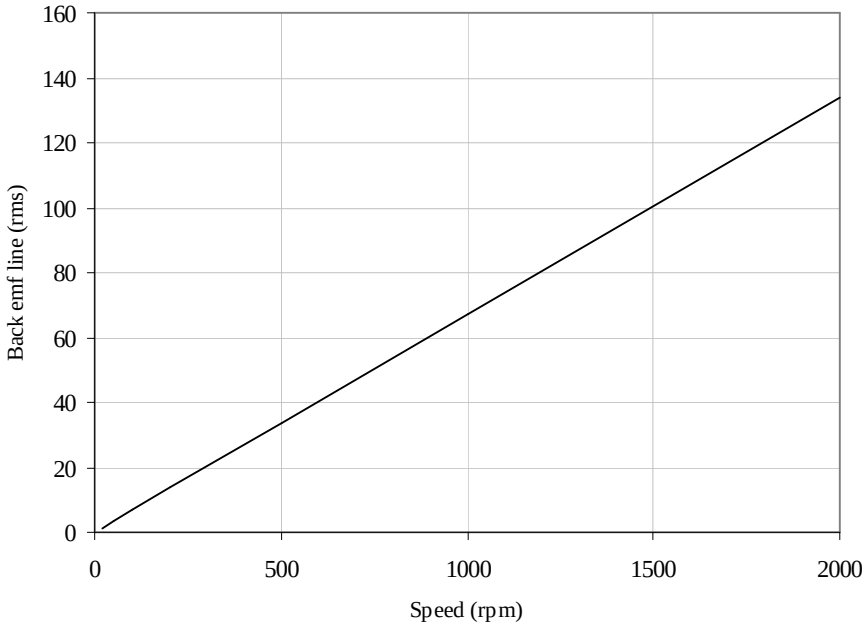

Fig. 3.22 Back-EMF line-line voltage measurements vs. speed.

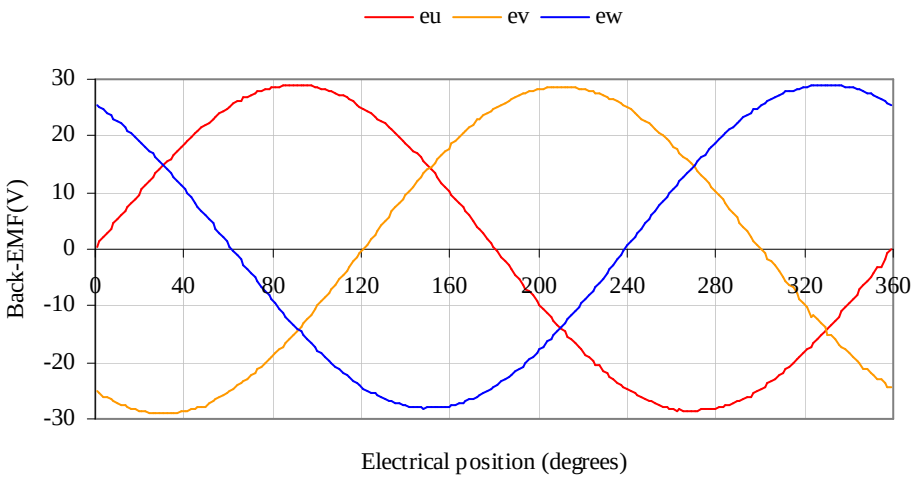

Fig. 3.23 Back-EMF phase voltage vs. electrical position at 500 rpm.

In Fig. 3.22 the resultant back-EMF is for the rms line-line voltage whilst in Fig. 3.23 the resultant back-EMF is for the phase voltage.

3.5.3 Inductance measurement

The line-line inductance is measured by rotating the prototype PM machine 360 mechanical degrees and measuring the inductance values for each electrical degree change. The measurement has been done by using DSpace software to monitor the change in the mechanical and electrical position and by using an Agilent LCR meter. The results of the inductance measurement test done at 20 Hz are plotted in Fig. 3.24.

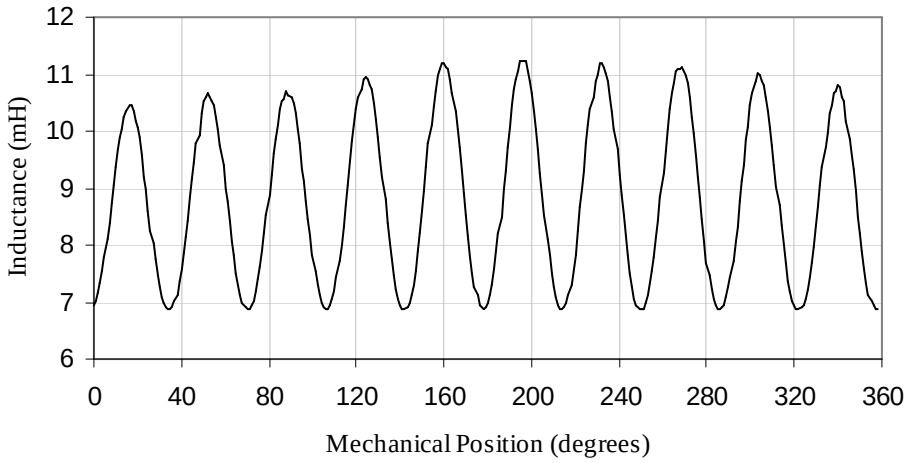

Fig. 3.24 Line-line inductance measurement at 20 Hz.

The measured results of the line-line inductance indicate that they are different magnitudes for different position measurements There are three results that can be made here for the prototype PM machine and they are:

(i) The prototype PM machine is not symmetrical because the magnitudes of the inductance are different.

(ii) The prototype PM machine is salient because it can be observed from Fig. 3.24 that the inductance is changing as position changes.

(iii) The prototype PM machine is a 10-pole machine because it can seen that for one mechanical period there are 10 electrical periods.

The inductance values can be calculated using equations (3.2) and (3.3). The variations in the magnitude could be ignored for simulations and experimental purposes.

3.5.4 Transducer display unit output

The analogue output of the SAW display with no-load for the prototype machine shows there are three frequencies. Fig. 3.25 is showing two periods each period time is 20 ms so the frequency is 50 Hz the amplitude peak is 30 mV equating to 0.6 Nm. This means that an error signal of 0.6% is from the output analogue signal. Fig. 3.26 is a zoom in of period one. It can be seen that there are four periods that are numbered and are repeated. The time of each period is 1 ms so the frequency is 1000 Hz. There is another frequency component which can be seen in Fig 3.27. The time of the period is 52 μs that means the frequency is 19.23 kHz. These noise problems can mostly be filtered out using a digital low-pass filter in DSpace.

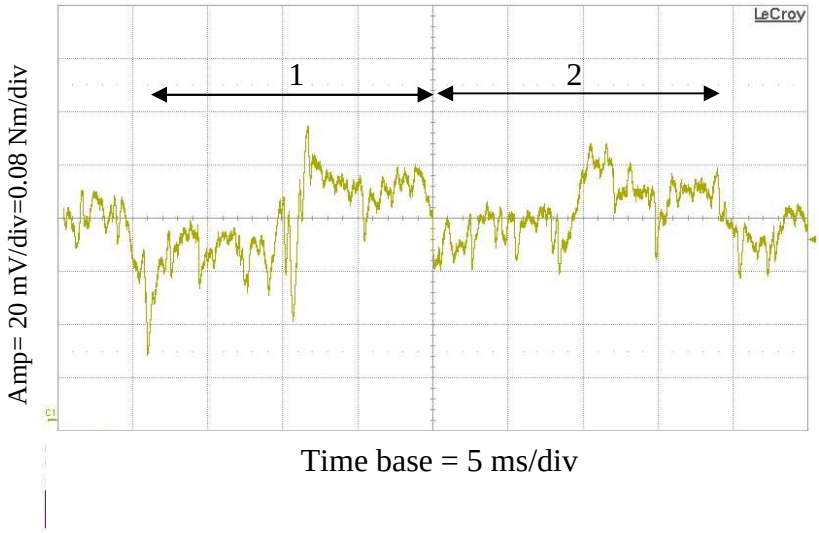

Fig. 3.25 Output of SAW display with two periods.

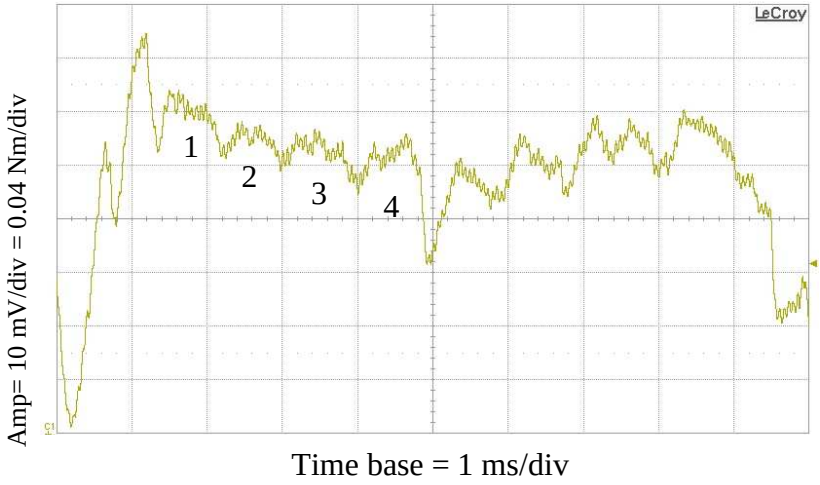

Fig. 3.26 Output of SAW display with four periods.

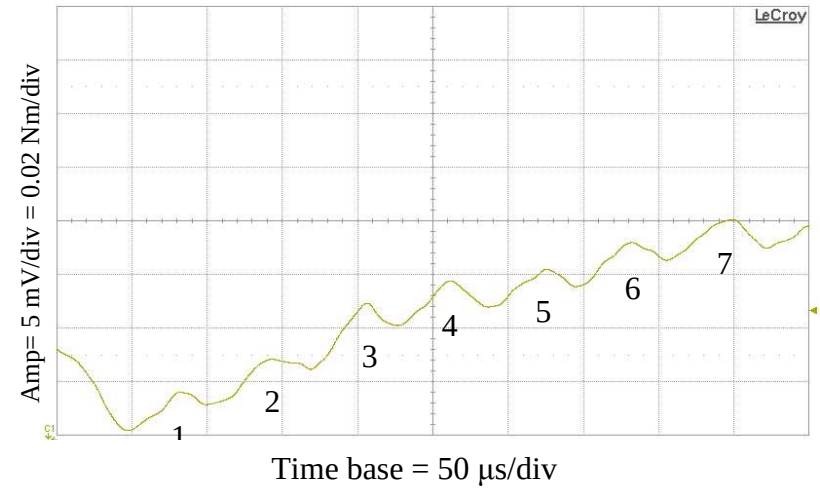

Fig. 3.27 Output of SAW display with seven periods.

3.5.5 Torque measurement

The torque measurement test will examine the torque constant. The torque constant is not given by the manufacturer. The drive used to drive the motor is shown in Fig. 3.28. The prototype machine under study is shown in Fig 3.29. The SAW sensor is integrated in the prototype machine. The test will be done by rotating the motor at 5 rpm and exciting the prototype machine under study by different current levels. The SAW transducer display unit displays the torque measured from the SAW torque sensor and there is an anlog output device which will output -5 to 5 V signal corresponding to the measured shaft torque. Since the max measured torque is 20 Nm, the 20 Nm will be equal to 5 V. The Experimental results are implemented in 4 steps:

(a). Run the motor at 5 rpm and measure the torque from prototype PM machine with no current excitation. The results is going to be the cogging torque of both machines since the measured torque is the shaft torque. The result of the cogging torque relative to one mechanical position revolution is shown in Fig. 3.30.

(b). Run the motor at 5 rpm and measure the torque from prototype PM machine with 1 A, 2 A and 3 A current excitation into two phases. The result of the shaft torque relative to one mechanical position revolution is shown in Fig. 3.31, Fig. 3.32 and Fig. 3.33.

Fig. 3.28 The drive system [1].

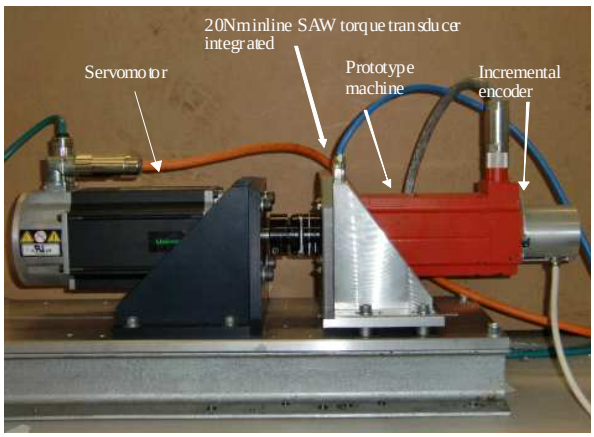

Fig. 3.29 Industrial (left) and prototype (right) servo machines.

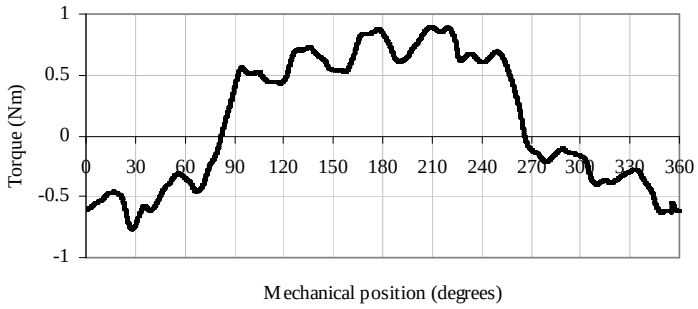

Fig. 3.30 Measured shaft torque for 0 A excitation for prototype PM machine.

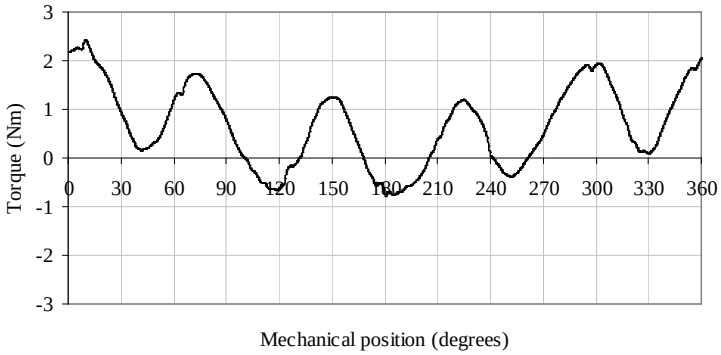

Fig. 3.31 Measured shaft torque for 1 A excitation for prototype PM machine.

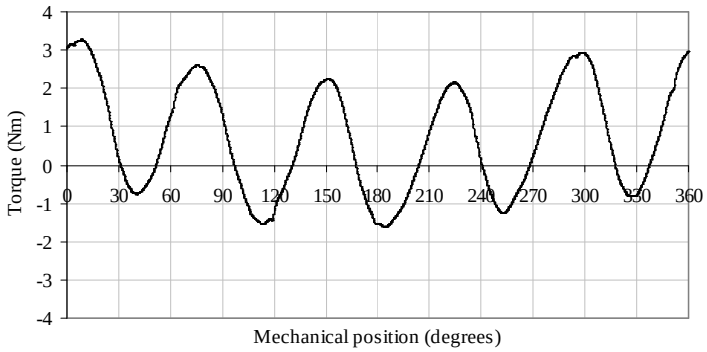

Fig. 3.32 Measured shaft torque for 2 A excitation for prototype PM machine.

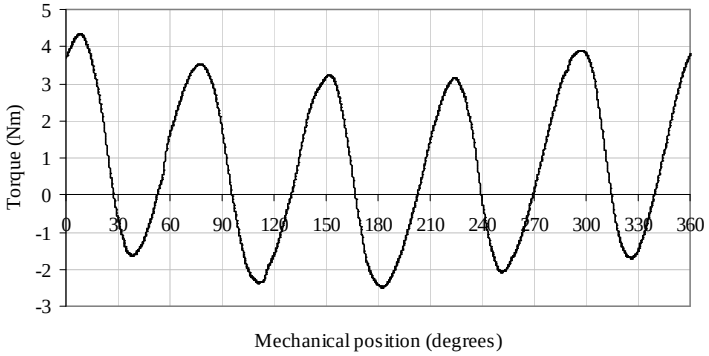

Fig. 3.33 Measured shaft torque for 3 A excitation for prototype PM machine.

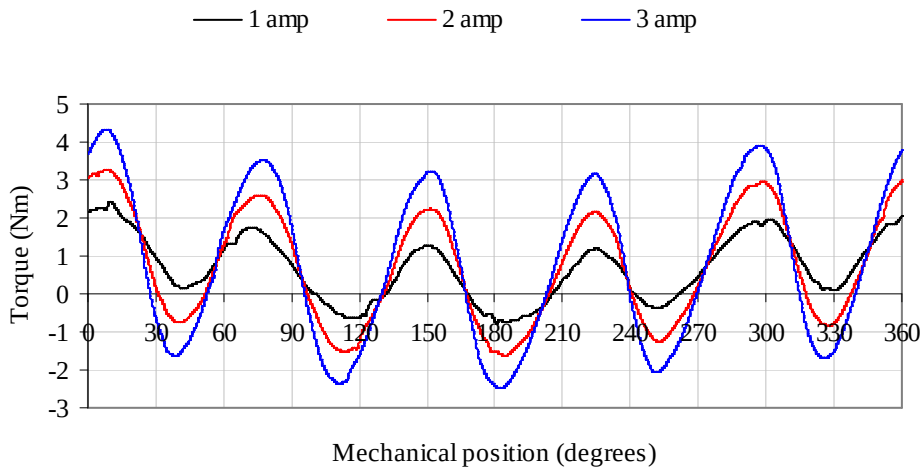

Fig. 3.34 Measured shaft torques excitation for prototype PM machine.

The torque measurement that is shown in Fig. 3.30 is the total cogging torque of the two machines since no current was excited and the machine was rotated at 5 rpm. This measurement max value is 0.8 Nm for both machines. This value is relatively big and not uniform so it does have a major impact on the rest of the measurements taken. Fig. 3.35 is the torque measurement for a 1 A excitation after subtracting the cogging torque Fig. 3.30 that was in the system. The torque constant shown is 1 Nm, as in Fig. 3.35. Fig. 3.34 is for all three torque measurements plotted against mechanical position. From Fig. 3.34 the max shaft torque value at position 153.38 mechanical degrees for 1 A excitation is 1.21 Nm and for the 2 A excitation the torque measured 2.2 Nm and for the 3 A excitation the torque measured 3.18 Nm. By subtracting the 2 A excitation from the 1 A excitation the resultant torque is 1 Nm.

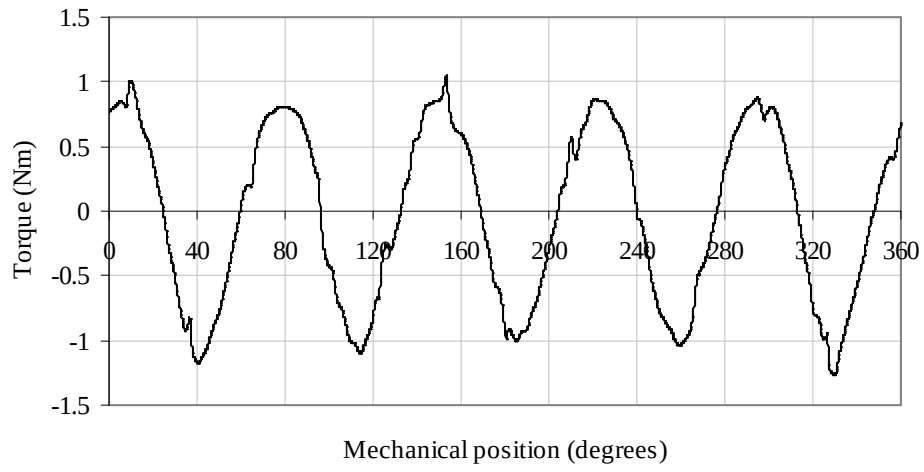

Fig. 3.35 Measured shaft torque without cogging torque

3.5.6 Torque response time

It is very difficult to know the response time of the SAW torque sensor since there is load on the system all the time. An experiment here is shown to see how fast the response for the measured torque is to the current excitation. The rotor was locked and a current was excited through phases *U* and *V* and the measured shaft torque was observed. Then another current excitation was applied through phase *V* and *W*. Fig 3.36 shows the current steps. Fig. 3.37 shows the time where the current excitations are changed from phases *U* and *V* to *V* and *W* at approximately t= 1.2 s. Fig. 3.38 shows the response time of the measured torque was measured. From Fig. 3.37 the current excitation through phases *V* and *W* start at 1.1995 s. In Fig. 3.38 it can be seen that the torque start to pick the response at 1.201 s. There was a delay of 1.5 ms. One reason for this delay is that there is a digital low-pass filter with a 2 kHz cut off frequency filtering the torque output.

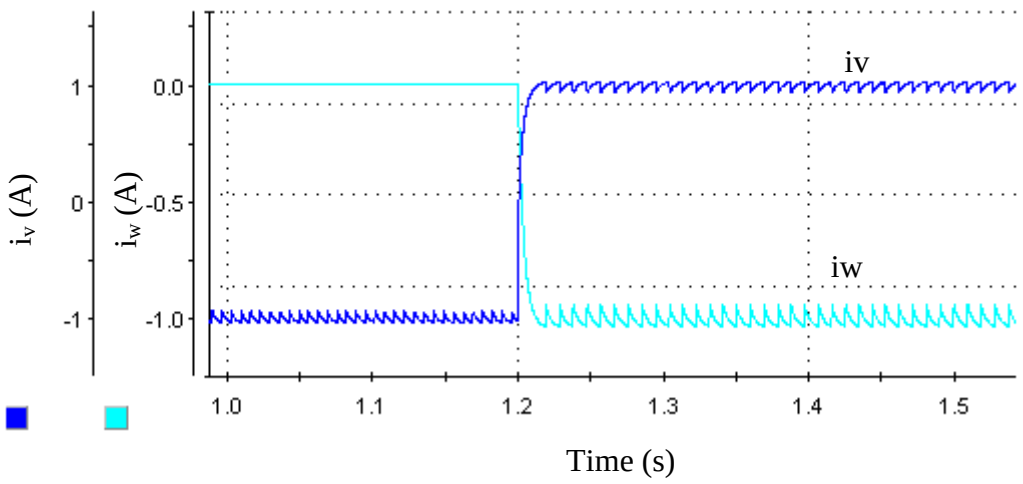

Fig. 3.36 Current observation for a 1 A excitation.

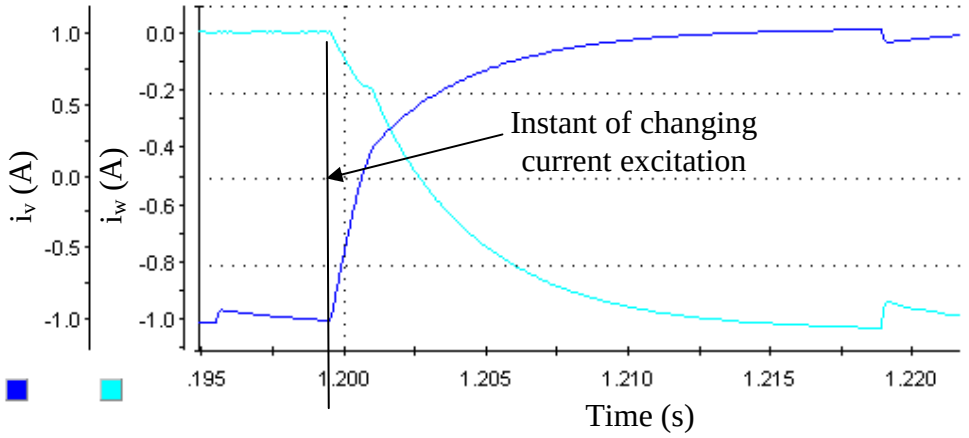

Fig. 3.37 Current observation for a 1 A excitation zoomed in.

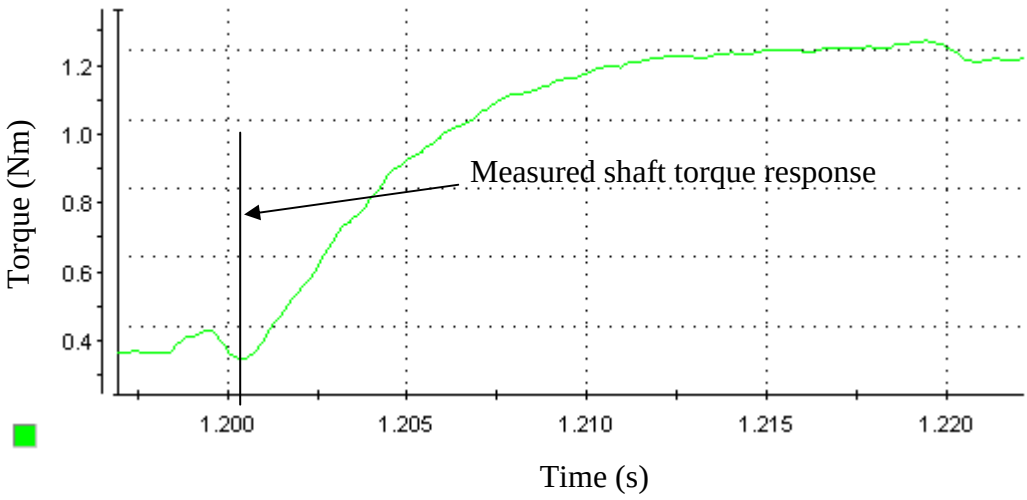

Fig. 3.38 Response time of the measured torque.

3.5.7 DSpace system

The start-up routine proposed in Chapter 2 will be implemented via a DSpace controlled drive system comprising of a commercial brushless PM machine, the Unimotor coupled directly to a prototype brushless PM machine, as illustrated by the test facility schematic of Fig. 3.39 and by the rig photography gallery of Fig. 3.40. The current and voltage instrumentation, full-bridge power electronic inverter, gate drive circuitry, filters and protections are discussed in detail in Appendix A3. An overview of the DSpace machine control platform developed as part of this research study is also discussed in Appendix A3.

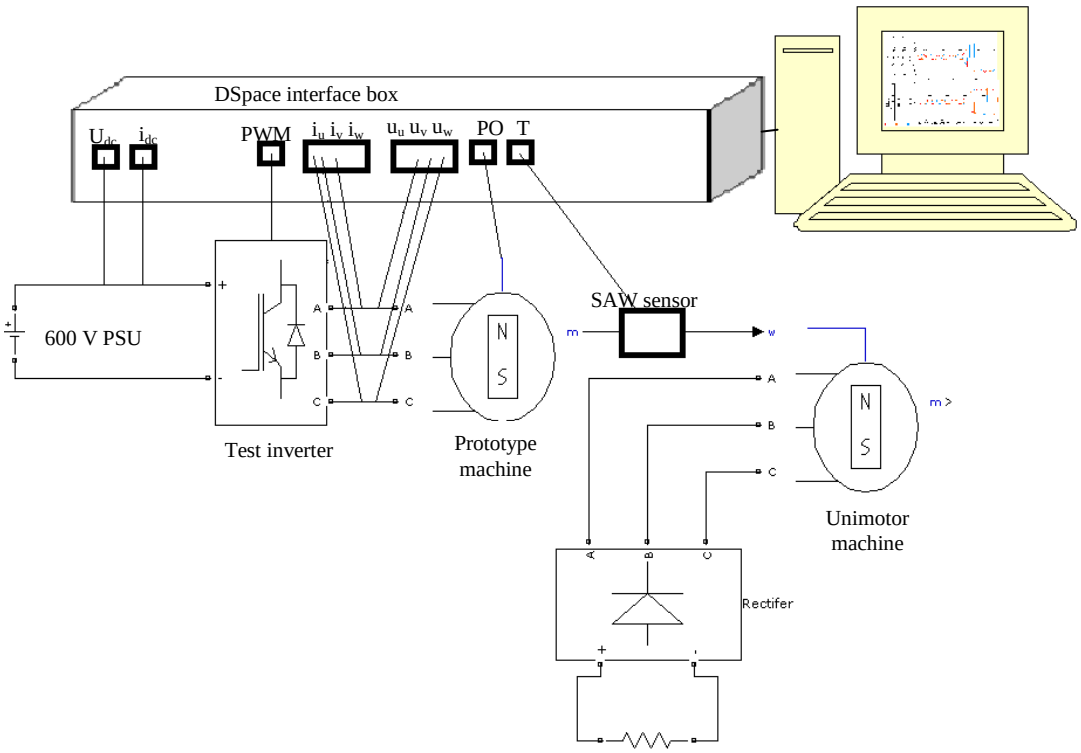

Fig. 3.39 Test rig schematic.

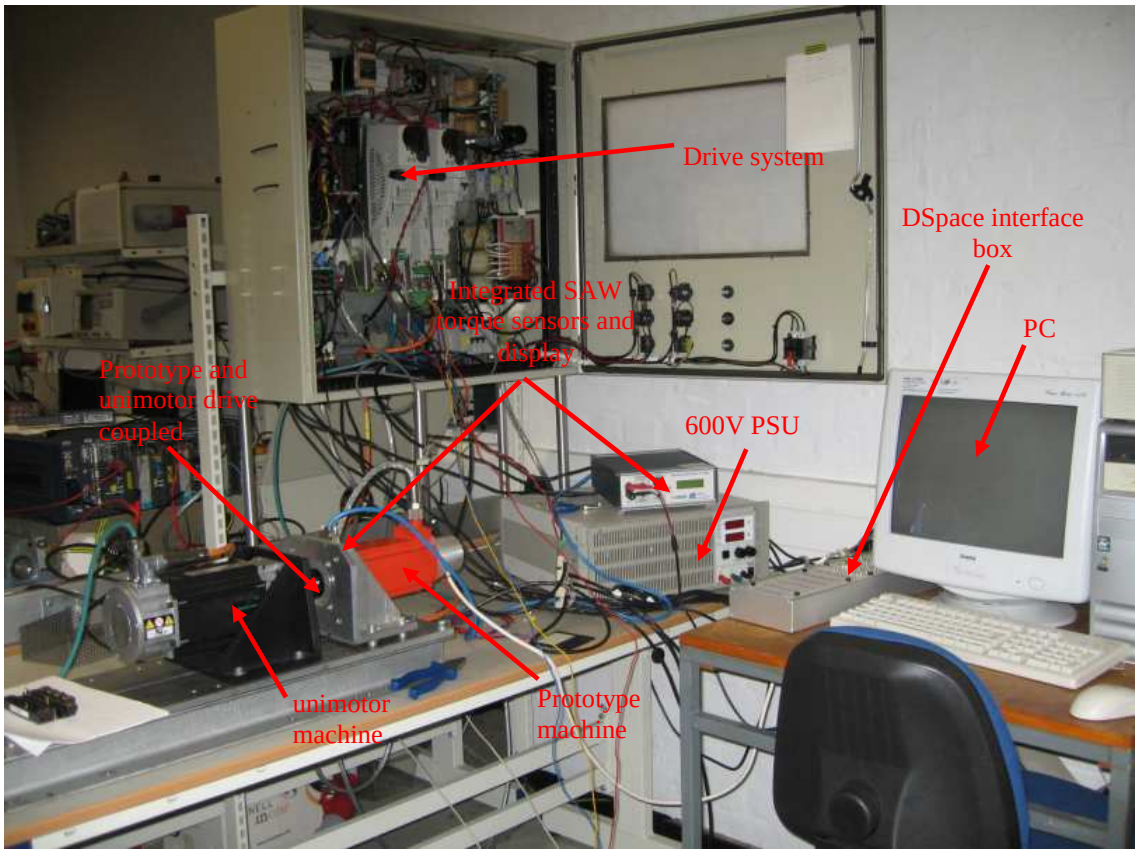

(a) Complete test rig

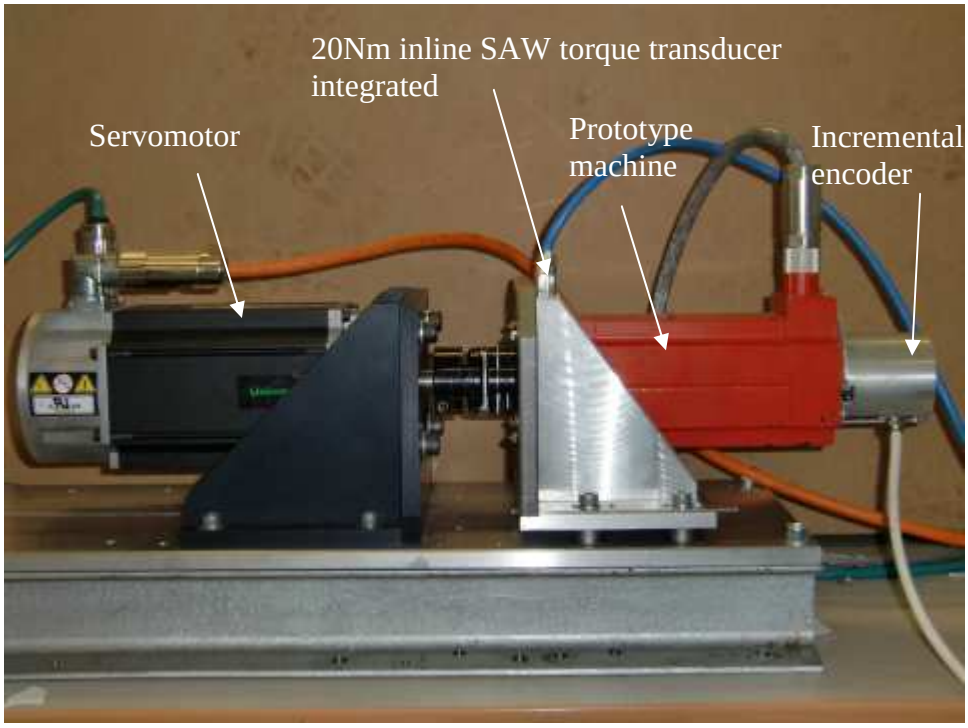

(b) Mechanical system overview.

Fig. 3.40 Experimental rig facility.

3.6 Summary

This chapter characterised a position sensor then investigated the parameters of Unimotor brushless PM machine, then characterised the cylindrical torque transducer and finally characterised the prototypes brushless PM machine with the integrated torque transducer. The Unimotor manufacturer's parameters that were examined are the resistance, the inductance, the back-EMF and the torque constant. The resistance was 22% increased due to rated temperature. The inductance was different since it was stated that the unimotor is a surface mounted PM machine and the saliency should be between 11.97 to 14.63 mH. The manufacturer quoted the inductance is 13.3 +-10% while when using an LCR meter clearly showed the inductance was 13.5 to 22 mH, which is not as the manufacturer gave but it clearly shows that it's a 6-pole machine. The back-EMF given by the manufacturer was 98 Vrms whilst the measured back-EMF test was 95 Vrms, which are very close to each other. The torque constant that was given by the manufacturer was 1.6 Nm/A while when investigated by using the SAW torque sensor and the results of the torque sensor was 1.65 Nm/A but that could be due to load in the system such as the cogging torque. The second characterisation was for the cylindrical torque SAW sensor. There was drift where the torque is offset after a certain time. This can be taken care off by zeroing the display and adjusting the offsets before an experiment started. There was noise in the system but the max amplitude was 30 mV which will contribute 0.6% error. The torque sensors static test showed that there was a 5% error between actual and measured torque and this also can be taken care off as by offset. The prototype brushless PM machine was investigated. There was no manufacturer's data given for it. The resistance test was concluded to know the value of the resistance. The inductance was measured. It was noticed that the measured inductance had different amplitudes, which means that the machine is an asymmetric machine. The back-EMF test was done and the back-EMF line voltage was measured at 1000 rpm and is equal to 67 Vrms. The torque constant was also obtained and was shown to be equal to 1 Nm/A. The integrated SAW sensor was also analysed. There was noise which causes 0.6% error. There was a load in the shaft with no excitation which could be due to misalignment. The torque excitation was shown for three level of excitation and the magnitudes increased linearly. The excited torque when subtracted from the non excited torque in the system outputs a better waveform. There was a delay of 1.5 ms mainly due to the digital low-pass filter.

CHAPTER 4

EXPERIMENTAL VALDITION FOR START-UP ROUTINE

4.1 Introduction

Chapter 2 discussed the theory and procedures of a zero and low speed start-up routine for control of a BLPM machine without a rotor position sensor both without and with measured torque feedback. This Chapter will discus the torque characterisation of the Unimotor and Prototype machine and then the practical implementation of the routines using the test facility described in Chapter 3. Results are presented to validate the theoretical routines derived in Chapter 2.

4.2 Unimotor PM Machine

4.2.1 Introduction and cogging torque

The Unimtor brushless PM characterisation and control was discussed in Chapter 3 and Appendix A.3 in terms of the machine electrical terminal parameters. Here, the machine cogging torque and its impact on the start-up routine are discussed in greater detail. Cogging torque is the torque due to the interaction between the rotor PM and stator slots of a PM machine. It is also known as detent or rotor current torque and is an undesirable torque component for machine operation, since, it is essentially a torque disturbance to the control systems dynamics. The cogging torque of the Unimotor machine under

investigation was measured using the in-line SAW torque transducer discussed in Chapter 3. The Unimotor machine was rotated at low speed of 5 rpm by a second Unimotor machine and the Control Techniques inverter systems illustrated in Fig. 3.12. Thus, the shaft torque is measured and transferred to DSpace using the analogue output of the torque sensor display, shown in Fig. 3.6. The measured cogging torque results are illustrated in Fig. 4.1.

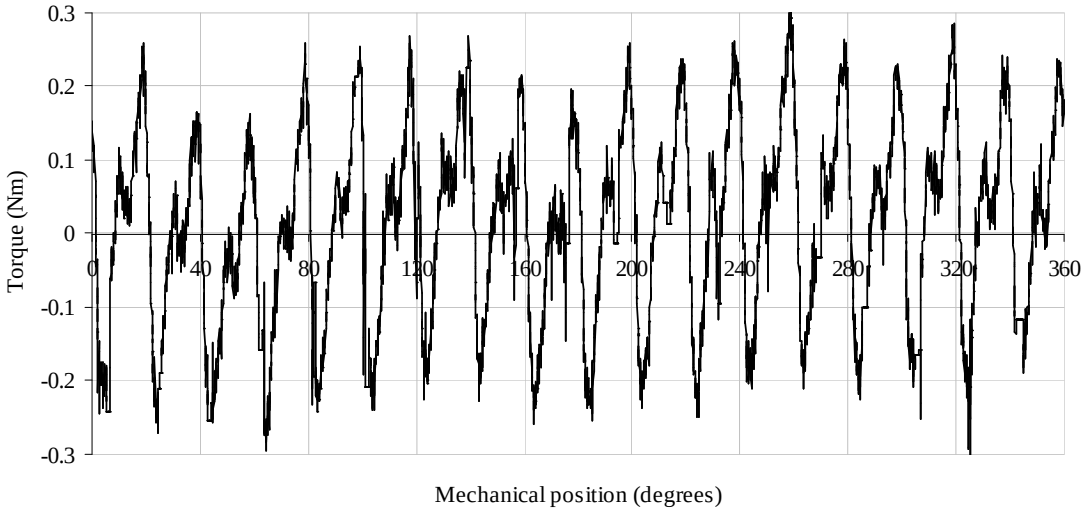

Fig. 4.1 Unimotor cogging torque measurements per mechanical revolution.

4.2.2 Electromagnetic torque

As shown in Chapter 3 the Unimotor machine has a sinusoidal back-EMF, and the machine cogging torque is relatively small when compared to the electromagnetic torque. Hence, the analysis of Chapter 2 should be straight forward to validate. To this end, the back-to-back Unimotor test rig with in-line torque transducer, Fig. 3.13, was used. The test procedure is similar to that in Chapter 2, but rather than calculating torque, the torque will be directly measured via the in-line SAW torque transducer and read into DSpace. The three steps for characterisation are:

(a). Phases *U*-*V* of one Unimotor are excited with 3 A DC and the second Unimotor used to drive the system at very low speed (5 rpm). The rotor position is measured using the optical encoder that is also aligned to phase *U* back-EMF.

(b). Similarly, phases *V*-*W* are then excited with 3A DC and the Unimotor driven at very low speed (5 rpm) for one mechanical revolution. The shaft torque and position are measured and read into DSpace.

(c). Finally, phases *W-U* are excited with 3A DC and the Unimotor driven at 5 rpm for one mechanical revolution. Shaft torque and position are read into DSpace.. The shaft torque measurements for the three tests are plotted in Fig. 4.2 for one mechanical revolution, showing an essentially balanced set of results.

A comparison of the wave shape of the calculated electromagnetic torques in Chapter 2 for an illustrative machine and the experimental results in Fig. 4.3 for one electrical period show good agreement. The perturbations in the torque waveforms of Fig. 4.3(b) arise from the cogging and reluctance torque previously discussed.

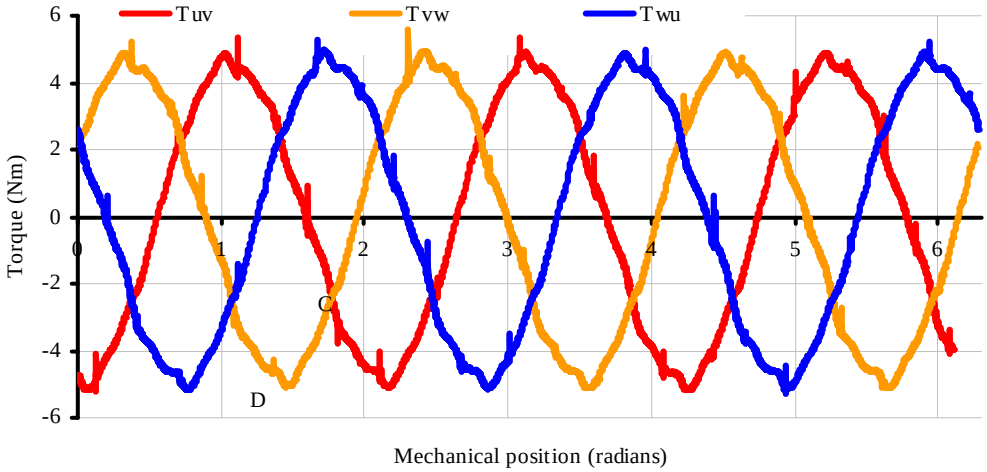

Fig. 4.2 Torques due to line-to-line current excitation of 3 A, one graph for comparison.

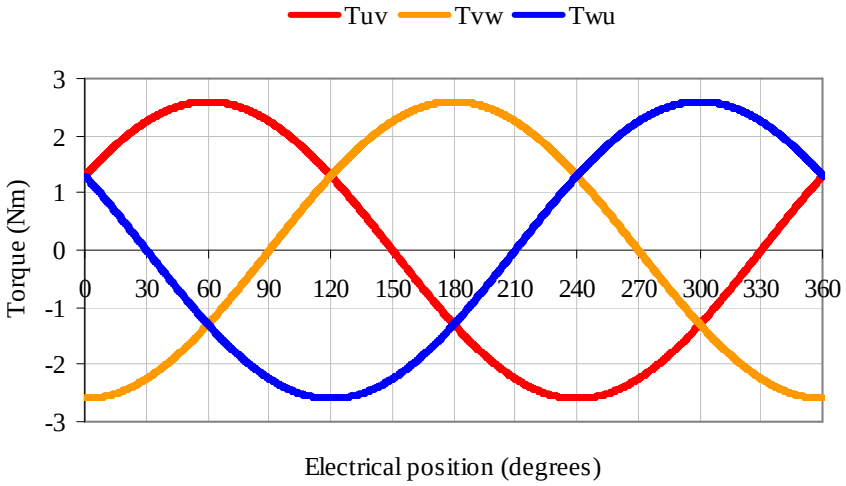

(a) Calculated.

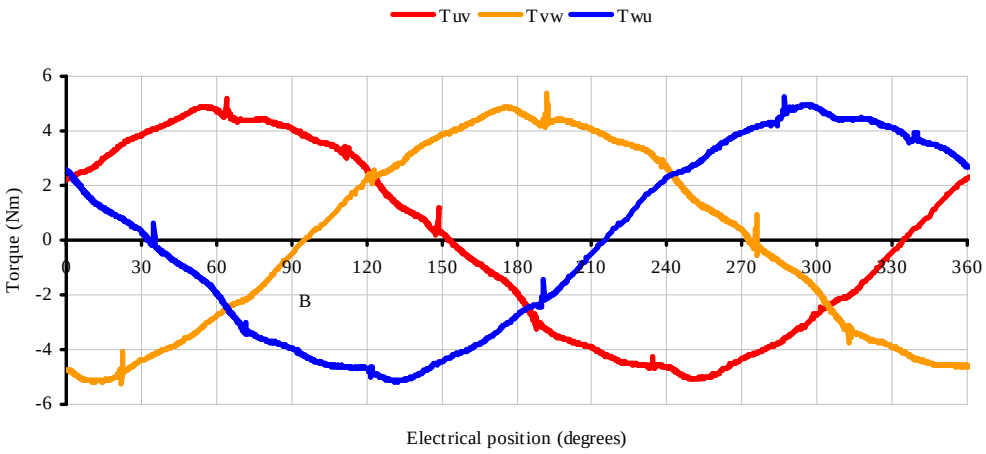

(b) Experimental.

Fig. 4.3 Comparison of calculated and experimental results of electromagnetic torques T_{uv}, T_{vw} and T_{wu} for 3 A current excitation.

4.2.3 Routine 1: Electromagnetic torque less than load torque

The start-up routines are now demonstrated using measured data as input. Considering routine 1, and a rotor at an initial position as illustrated in Fig. 4.4. Three torque measurements for a 3 A excitation are taken at points A, B and C. The torque measurement at point A is equal to 0.99 Nm due to the *U-V* excitation current. However, for this value of torque the rotor could be at position A or A', shown in Fig. 4.4. The torque measurement at B is equal to 3.16 Nm which is due to *V-W* excitation current and the torque measurement at C is equal to -4.96 Nm which due to the *W-U* excitation current. Equation (2.23)-(2.28) are used to determine the sector, which from (2.25) is sector C in this case. Then equations (2.37)-(2.42) are used. In this case equation (2.39) is the appropriate choice, leading to the following:

$$\theta = \left[\left(\frac{T_{high} - T_{sense}}{T_{high} - T_{low}}\right)(d)\right] + s = \left[\left(\frac{T_{vw} - T_{uv}}{T_{vw} - T_{wu}}\right)(60)\right] + 120 = \left[\left(\frac{3.16 - 0.99}{3.16 + 4.96}\right)(60)\right] + 120 = 136 \qquad (4.1)$$

Comparing the rotor position angle calculated via (4.1) using measured torque as input data, to that measured via an incremental optical encoder shows good agreement, i.e. 136 to 137 degrees electrical respectively, which is within 0.6%.

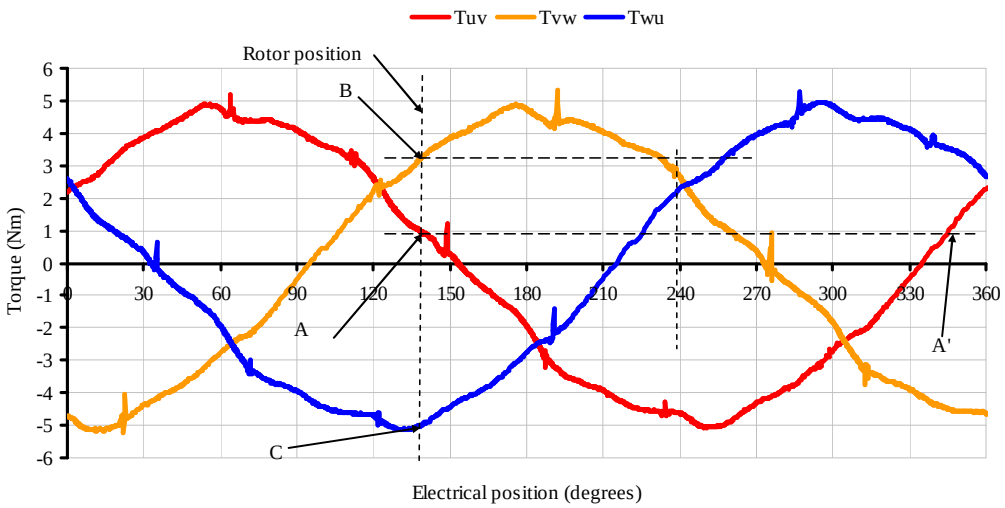

Fig. 4.4 Example of routine 1 electromagnetic torque less than load torque for Unimotor.

4.2.4 Routine 2: Electromagnetic torque and zero load torque

Referring to Chapter 2, here in routine 2, the Unimotor electromagnetic torque is larger than the shaft load torque there is no external load connected to the machine, the rotor will ideally rotate when two phases of the machine. When the rotor comes to rest the three torque measurements will, ideally, be equal to zero if there is no cogging torque or load perturbations on the system. Referring to Fig. 4.5, if phase *U-V* are excited excited with 3 A the resultant electromagnetic torque, T_{uv}, will rotate the rotor until it reduces to zero, resulting in the rotor coming to rest at either position A or B. A second excitation via phases *V-W* excited with 3 A will move the rotor from point A to point C if A was the starting point since the torque at that instant is positive. Similarly, it will move from point B to C if B was the start point, since the torque at instant B is negative settling at point C. A third and final excitation excited with 3 A, *W-U*, will move the rotor from point C to point D which is at 30 degrees electrical.

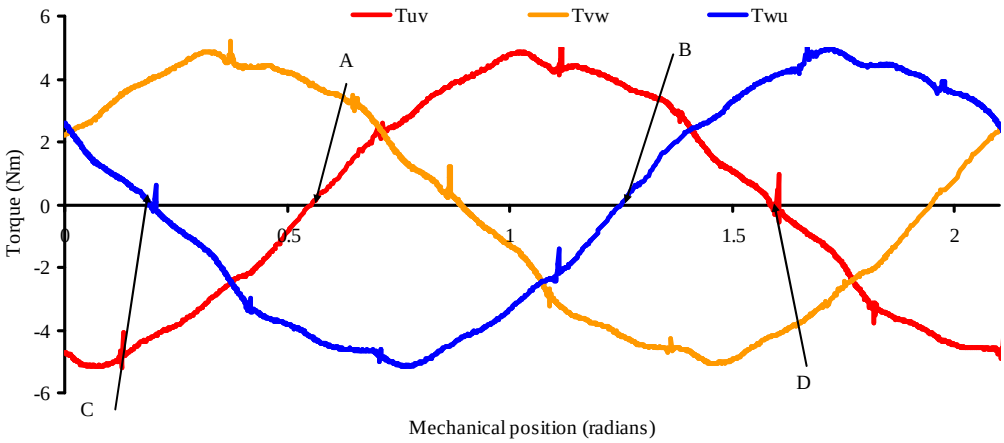

Fig. 4.5 Example of routine 2 electromagnetic torque and zero load torque for Unimotor.

4.2.5 Routine 3: Electromagnetic torque $> T_l < T_{th}$

If the Unimotor machine electromagnetic torque is larger than the load torque, T_l, and is less than the threshold torque, T_{th}, on the shaft, the rotor will rotate. If phases *U*-*V* are excited first, the rotor will settle at either point A or B with an offset to the no-load position corresponding to the load torque, T_l, of 1.9 Nm in this case, as illustrated in Fig 4.6. To determine the rotor position a second excitation via phases *V*-*W* is performed, thus, the electromagnetic torque will rotate the rotor from point A to point C or from point B to point C as illustrated in Fig. 4.6. Finally an excitation step is made via phases *W*-*U* to determine rotor position the rotor will rotate from point C to point D since the torque at point C due to the W-*U* excitation is positive. The excitation current, I, is 3A and the machine torque constant, K_t, is 1.67 Nm/A, hence the maximum torque for this current should be 5.01 Nm. The three torque measurements should be under the threshold torque, T_{th}, which is calculated as (4.2):

$$T_{th} = IK_t \sin(120) = 3*1.67*0.86603 = 4.33879 Nm \tag{4.2}$$

The three excitation torques that rotate the rotor to position D are equal to the load torque of 1.9 Nm, which is less than threshold torque. The rotor position offset can be estimated knowing the maximum excited torque and the measured torque at point D from the solution of (4.3):

$$offset = \sin^{-1}\left(\frac{T_l}{T_m}\right) = \sin^{-1}\left(\frac{1.9}{5.01}\right) = 22.28^o \, electrical \tag{4.3}$$

The electrical position at point D of Fig 4.7, will then be equal to:

$$D = 30 - 22.28 = 7.7^o \, electrical \tag{4.4}$$

The actual measured position at D is 6.4 degrees electrical which is 0.36% error in degrees electrical.

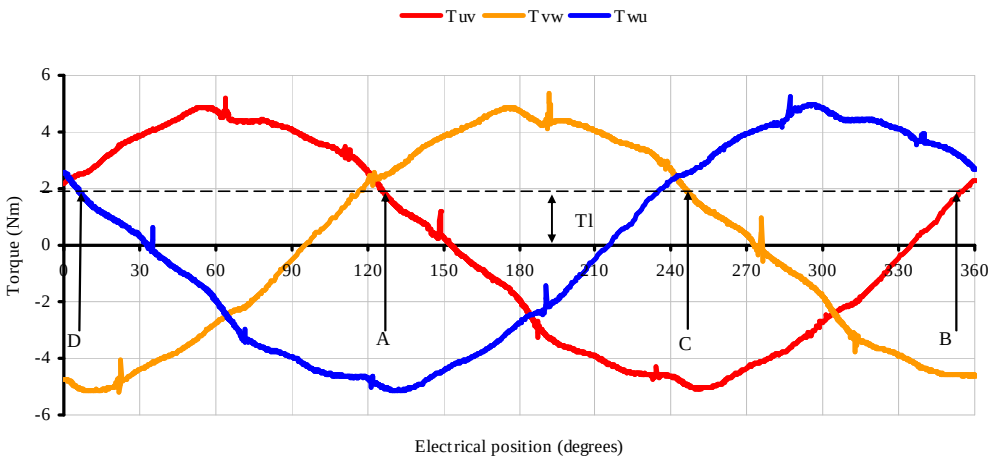

Fig. 4.6 Example of routine 3 electromagnetic torque $> T_l < T_{th}$ for Unimotor.

4.2.6 Routine 4: Electromagnetic torque > T_l > T_{th}

The final case considered is when the electromagnetic torque is larger than the load torque, and the load torque is larger than the threshold torque (T_{th}), as illustrated in Fig. 4.7. In this case, the load torque is sometimes larger than the electromagnetic torque which will lead to the Unimotor machine partially rotating within two sectors. Now the position will vary and there will be three possible final position solutions.

Case (i): If the initial rotor position is between points A and B and the excited current is 3 A then, when exciting phases *U* and *V* the position will move to point B and, when exciting phases V and W, the position will remain at point B. Finally when exciting the final phases *W* and *U*, the position will move back to point A, as shown in Fig. 4.7.

Case (ii): If the initial rotor position is between points C and D then, when exciting phase *U* and *V*, the rotor will move to point C. Then when exciting phases *V* and *W*, the rotor will return to point D. Finally, when exciting phases *W* and *U*, the position will remain at point D, as shown in Fig. 4.7.

Case (iii): If the initial position is between points E and F then, when exciting phases *U* and *V* the rotor position will move to point E. When exciting phases *V* and *W* the position will remain at point E and finally when exciting the final phases *W* and *U* the rotor will return to point F, as shown in Fig. 4.7.

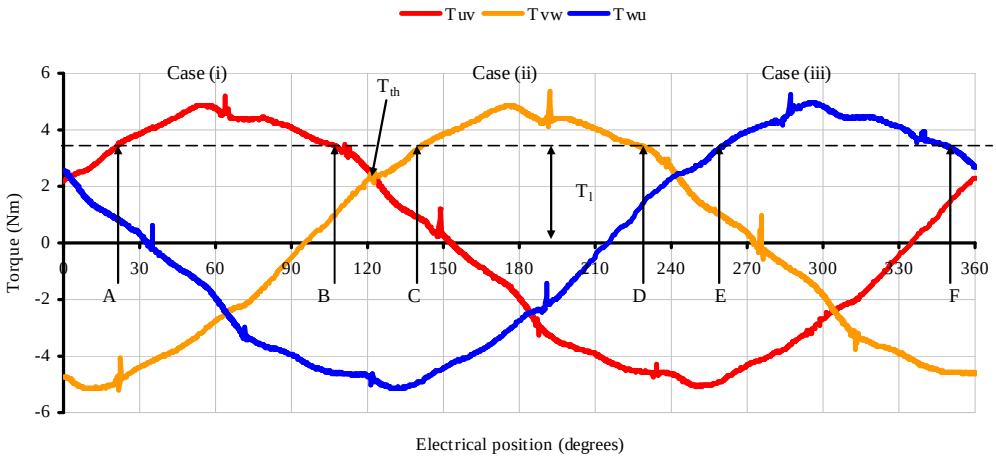

Fig. 4.7 Example of routine 4 electromagnetic torque > T_l>T_{th}, cases(i), (ii), and (iii) for Unimotor.

4.2.7 Summary

The four routines that were developed in Chapter 2 to estimate rotor position have been tested by application to the Unimotor machine. The tests were carried out using an inline cylindrical instrument SAW torque sensor coupled between two similar Unimotors as discussed in Chapter 3. The results of the measured and estimated torques are very similar with good accuracies. The next evaluation is to use the technique on the prototype machine with integrated torque sensor.

4.3 Prototype PM Machine

The prototype brushless PM characterisation presented in section 3.5.5 had a noticeable difference between the prototype and Unimotor machines is the level of cogging torque between the two topologies, being much higher for the prototype machine. During early tests it became apparent that this was a significant problem and hence further detailed characterisation of the no-load cogging torque had to be undertaken.

4.3.1 Cogging torque analysis

The cogging torque of the prototype machine was measured using the integrated SAW torque sensors. The prototype machine was rotated at a very slow speed (5 rpm) by using the in-line connected Unimotor, as illustrated in Fig. 3.29 the experimental test facility. The shaft torque at low speed is measured and transferred to DSpace using the analogue output of the torque sensor display, as shown in Fig. 3.20. The measured cogging torque for one complete rotor revolution is shown in Fig. 4.8. Since there is no electrical magnetic design information for either machine the cause of these perturbations can only be speculative. If is clear from the near static test (5 rpm) that the prototype machine or internal torque sensing system, has a once per mechanical revolution cyclic load. This is probably due to a mis-alignment problem or an internal problem within the motor. However, this 1-per revolution cyclic load is found to be repeatable and hence, since it could be characterised, was treated as an external load disturbance.

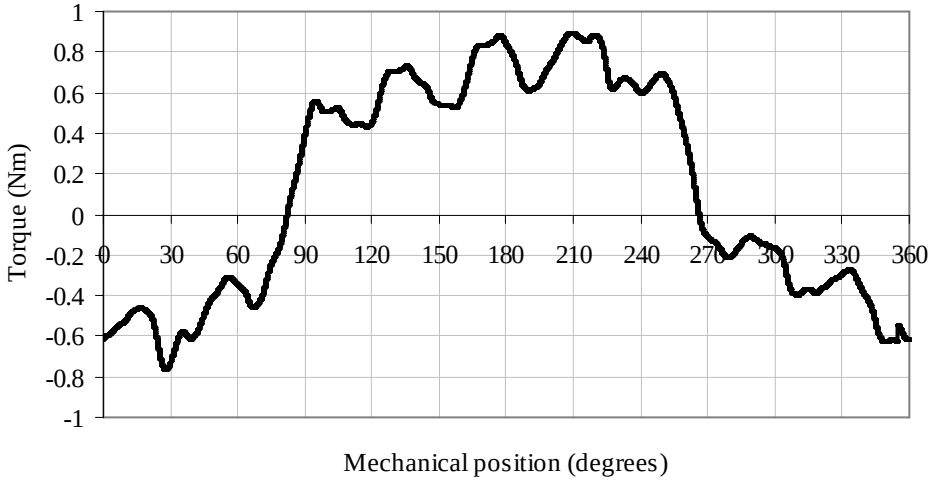

Fig. 4.8 Prototype machine cogging torque for one mechanical revolution.

4.3.2 Electromagnetic torque analysis

The prototype machine electromagnetic torque profile is characterised. In a similar manner to that taken the Unimotor machine the characterisation steps are:

(i) The prototype machine phases *U*-*V* are excited with 1 A dc while being rotated at low speed (5 rpm). The position and shaft torque are measured and recorded via DSpace. The torque for phase *U*-*V* excitation, T_{uv}. The no-load cogging torque, T_{cog}, is also plotted for reference. It is noted that the 1-per revolution cyclic load simply off-sets the electromagnetic torque and can thus be accounted for once characterised.

(ii) Machine phases *V*-*W* are then excited with 1 A dc with the rotor driven at low speed (5 rpm). Shaft torque and rotor position for one mechanical revolution. are recorded into DSpace.

(iii) Finally, phases *W*-*U* excited with 1A dc and the rotor driven at low speed (5 rpm). Shaft torque and position for one mechanical revolution are recorded via DSpace.

Shaft torques for the three excitation options and the no-load cogging torque are plotted in Fig. 4.9 for one mechanical revolution for comparison. Simply subtracting the cogging and 1-per revolution cyclic load yields the excitation torque due to the relevant phase excitation, as illustrated in Fig. 4.10. The system cogging and 1-per revolution cyclic torques are undesirable and can be taken account of by either subtracting from the total measured torques or storing the in the start-up procedure and treating the data as an external torque disturbance.

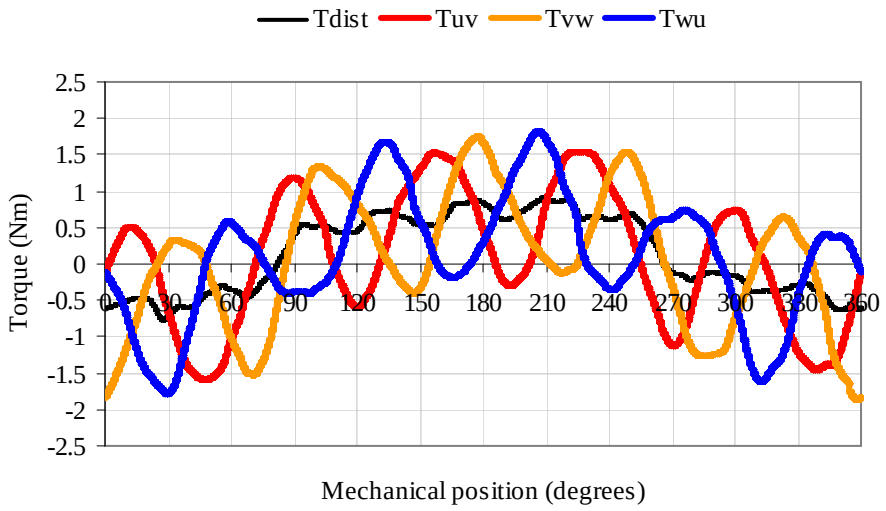

Fig. 4.9 Measured shaft torque for the three excitation options and no-load cogging torque.

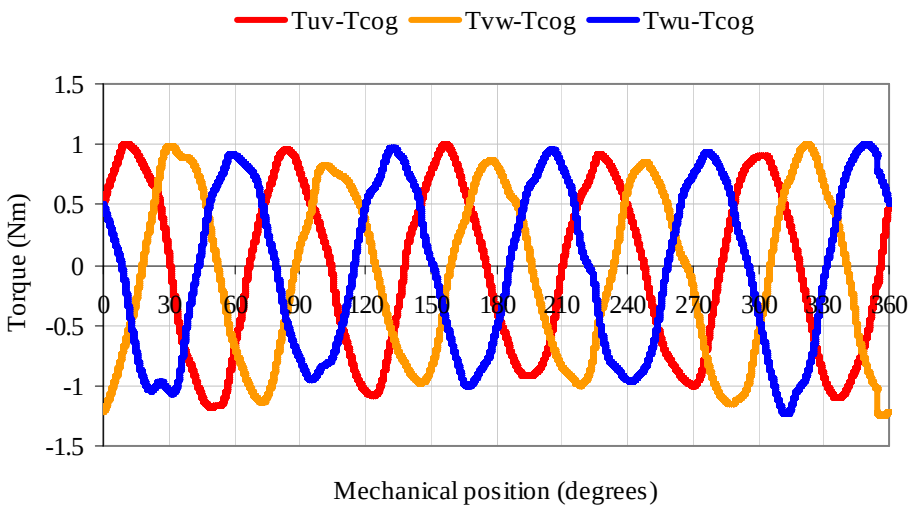

Fig. 4.10 Measured shaft torque for the three phase excitations options minus cogging and disturbance torques.

4.3.3 Routine 1: Electromagnetic torque less than load torque

Taking the cogging and 1-per revolution cyclic load torques into account when analysing the measured shaft torques for a 1 A excitation, the start-up procedures discussed in Chapter 2 were applied to the prototype machine. From here on the machine cogging and 1-per revolution cyclic torques will be simply referred to as the disturbance load torques, T_{dist}. Recalling that routine 1 is when the prototype machine does not rotate when excited, thus the load torque is greater then the electromagnetic torque, as illustrated in Fig. 4.11 for one electrical period. The data can be used to determine the sectors, as per the theory of Chapter 2, but with an offset due to the disturbance load torques. The same rules for deriving the sector can be applied here, although there are some minor offsets that due to the disturbance torques and measurement accuracies. Taking these into account, the sector angles are defined shown in Table 4.1 and the sector change-over angles in Table 4.2.

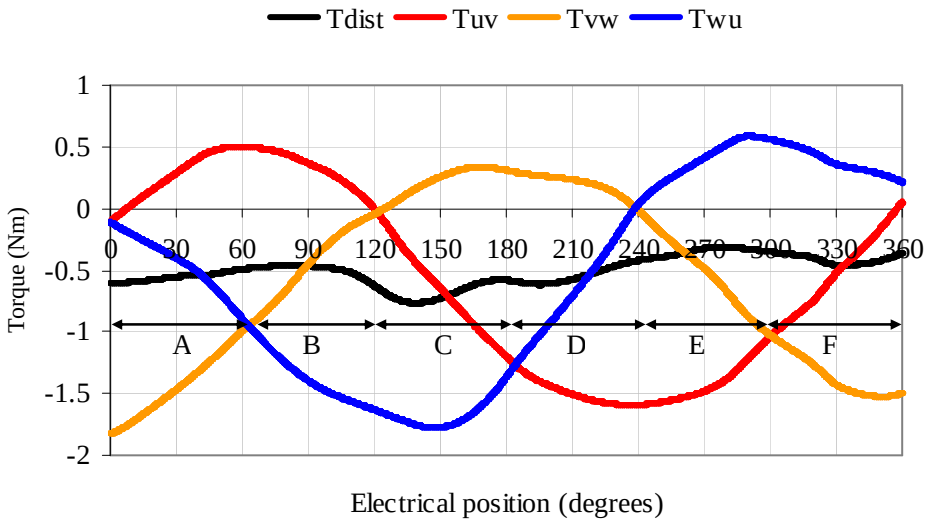

Fig. 4.11 Sector determination for prototype machine

Sector	Electrical position (degrees)
A	0-60
B	60-121
C	121-182
D	182-239
E	239-300
F	300-360

Table 4.1 Sector angular definition for prototype machine.

Sector	Electrical position (degrees)
A-B	60
B-C	121
C-D	184
D-E	239
E-F	300
F-A	360 or 0

Table 4.2 Sector change-over angles for sector for prototype machine.

Although there are disturbance torques, the rules used in the theory of Chapter 2 to determine the sector and position can be employed here. An example, one random electrical position will be chosen.

The three torque measurements are taken as per routine. For example T_{uv} = 0.694 Nm; T_{vw} = -1.182 Nm and T_{wu} = 0.037 Nm, as illustrated in Fig. 4.12. Using equation (2.27) sector A is identified and the angular position calculated as:

$$\theta_e = \left[\left(\frac{T_{high} - T_{sense}}{T_{high} - T_{low}}\right)(d)\right] + s = \left[\left(\frac{T_{uv} - T_{wu}}{T_{uv} - T_{vw}}\right)(60)\right] + 0 = \left[\left(\frac{0.694 - 0.037}{0.694 + 1.182}\right)(60)\right] + 0 = 21 \qquad (4.6)$$

Measured electrical position for this estimate is 19.98 degrees so the positional error is 0.27%. Using the full set of measured torque data, electrical position is estimated for one electrical period via the procedures and equations in Chapter 2. The results are plotted versus actual measured electrical position, as illustrated 4.13, showing very good agreement the error in measured and predicted rotor position is illustrated in Fig. 4.14, Showing maximum deviation of +6.8 to -4.2 degrees electrical.

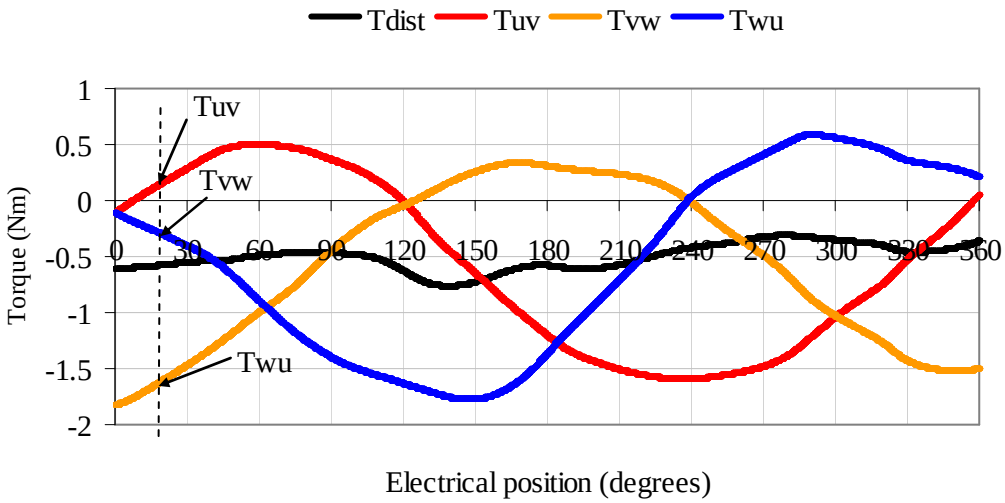

Fig. 4.12 Example of routine 1 electromagnetic torque less than load torque for Prototype machine.

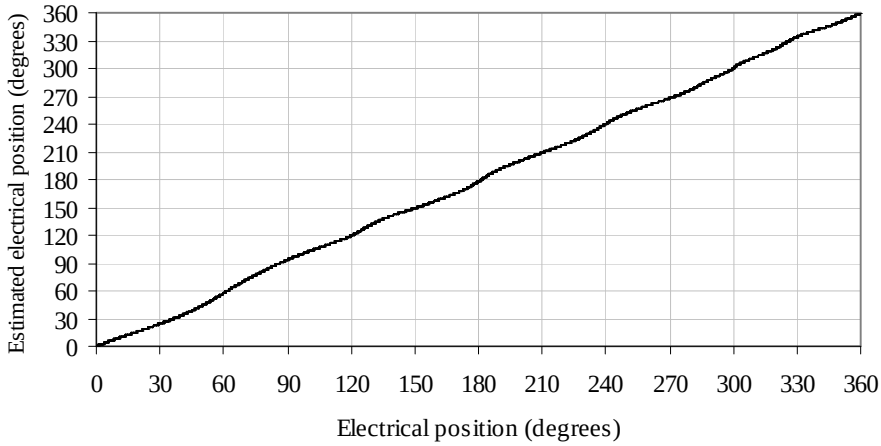

Fig. 4.13 Comparison of estimated and measured rotor electrical position for the prototype machine.

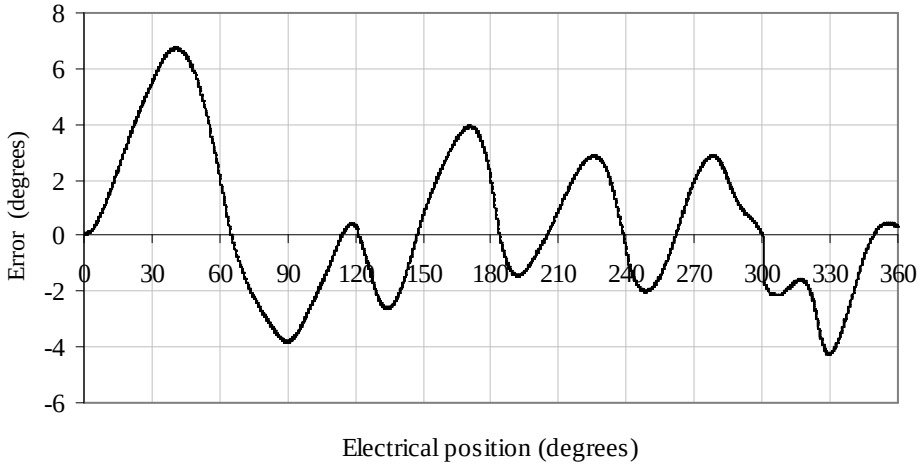

Fig. 4.14 Variation of error between estimated and measured with electrical position.

Fig. 4.15 illustrates the DSpace PC interface displays as the controller works through the example start-up procedure, showing the measured shaft torque versus time for the *U-V*, *V-W* and *W-U* excitations (a) and the measured and calculated position and final values of T_{uv}, T_{vw} and T_{wv} (b).

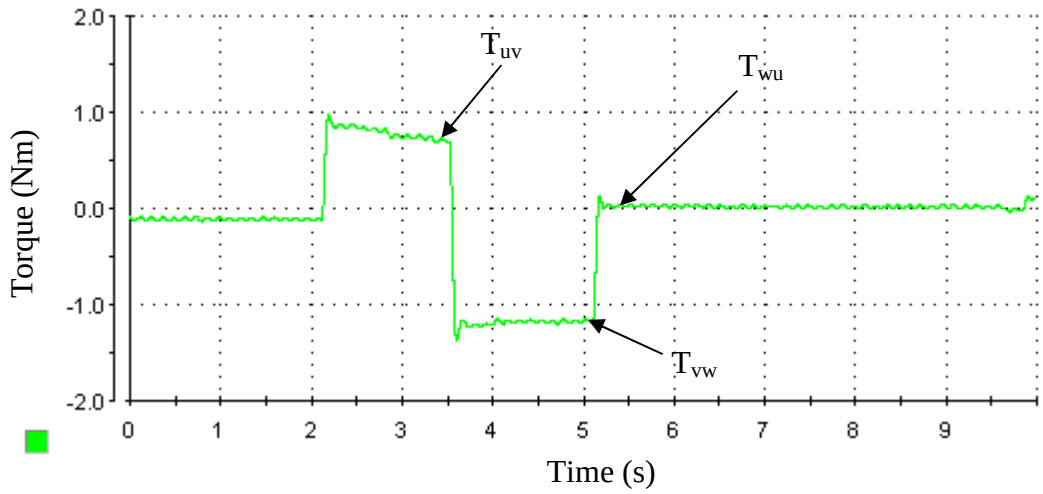

(a) Measured shaft torque versus time.

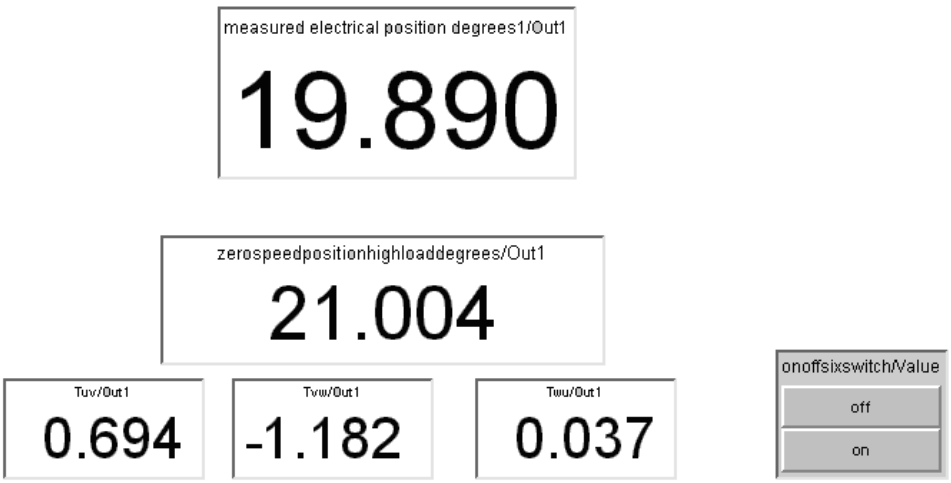

(b) Measured and estimated position and the three excitations torques, T_{uv}, T_{vw}, T_{wu}.

Fig. 4.15 DSpace screen presentation of start-up routine results.

4.3.4 Routine 2: Electromagnetic torque and zero load torque

If the prototype machine electromagnetic torque is larger then the load and disturbance torques the machine rotor will rotate. However, unlike the Unimotor machine, the disturbance torques cannot be ignored and will hence be the reference torque. Again, illustrating the procedure by way of an example the first electrical period is shown in Fig. 4.16 can be observed from Fig. 4.16, if the first 1 A excitation, the *U-V* phase the rotor rotates to point A or point B. then second excitation, *V-W*, will then move the rotor to point C whether it is at point A or B. The last excitation, *W-U*, moves the rotor from point C to D.

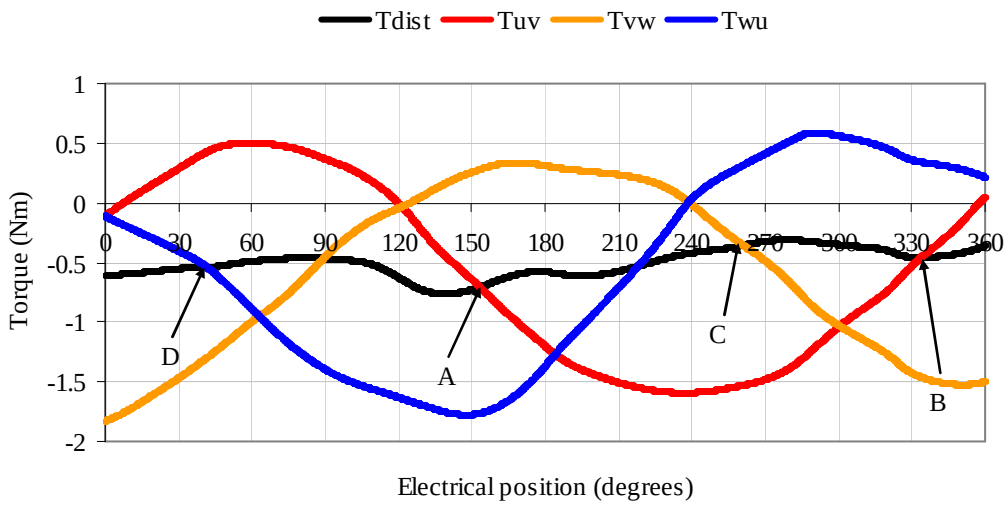

Fig. 4.16 Example of routine 2 electromagnetic torque and zero load torque for prototype machine.

The zero load torque results are shown here for two cases; case one when the position moves to point A after the *U-V* excitation, then it moves from A to B after the *V-W* excitation and finally it moves from point B to point D, as shown in Fig. 4.17. The corresponding measured torque is shown in Fig. 4.18.

The second case *U-V* is when the position moves to point B after the *U-V* excitation. It then moves from B to C after the *V-W* excitation, finally it moves from point C to point D after the *W-U* excitation, as shown in Fig. 4.19. The corresponding measured torque is also shown in Fig. 4.20.

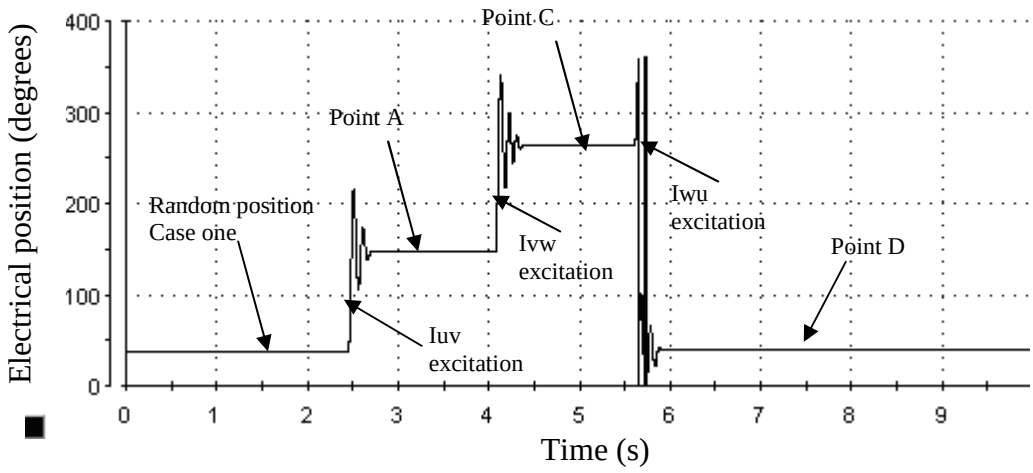

Fig. 4.17 Measured electrical position due to three current excitations case one.

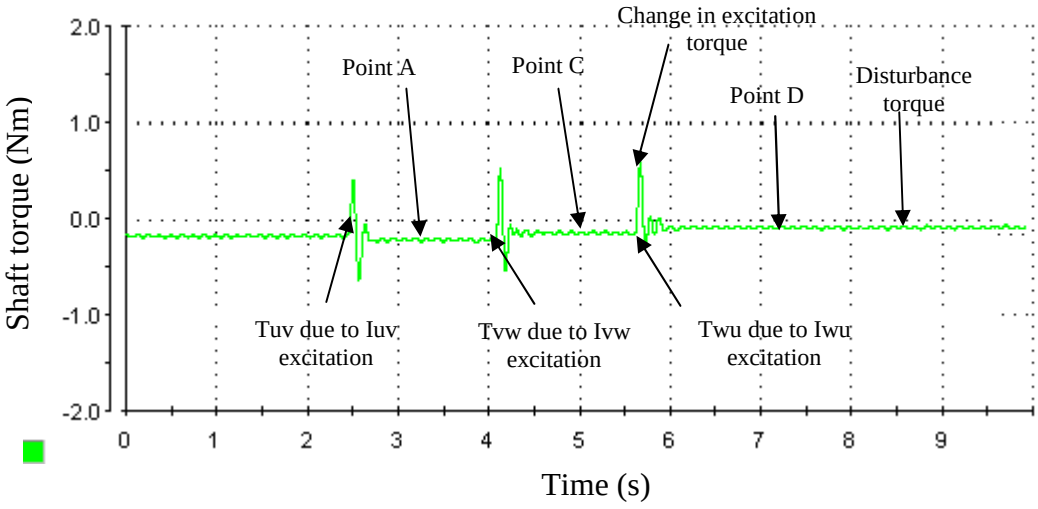

Fig. 4.18 Measured shaft torque due to three current excitation case one.

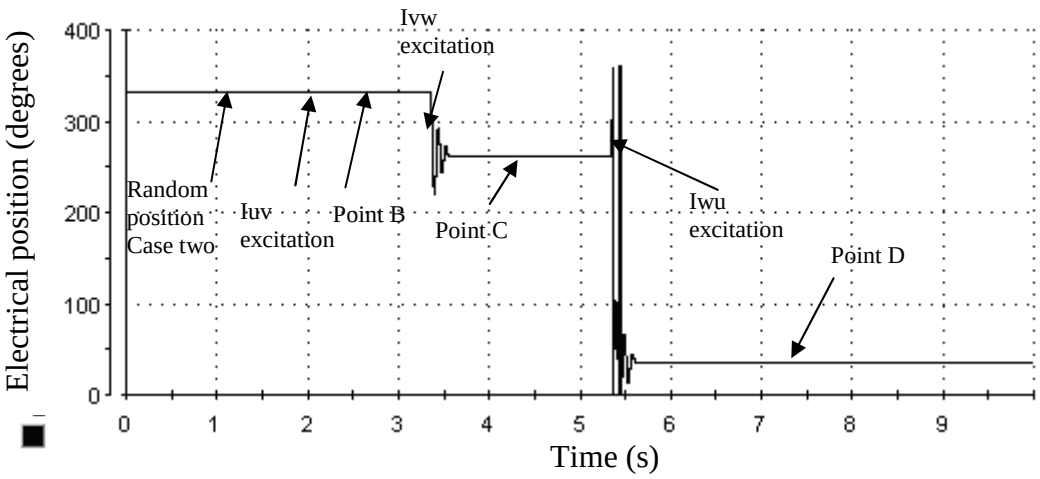

Fig. 4.19 Measured electrical position due to three current excitations case two.

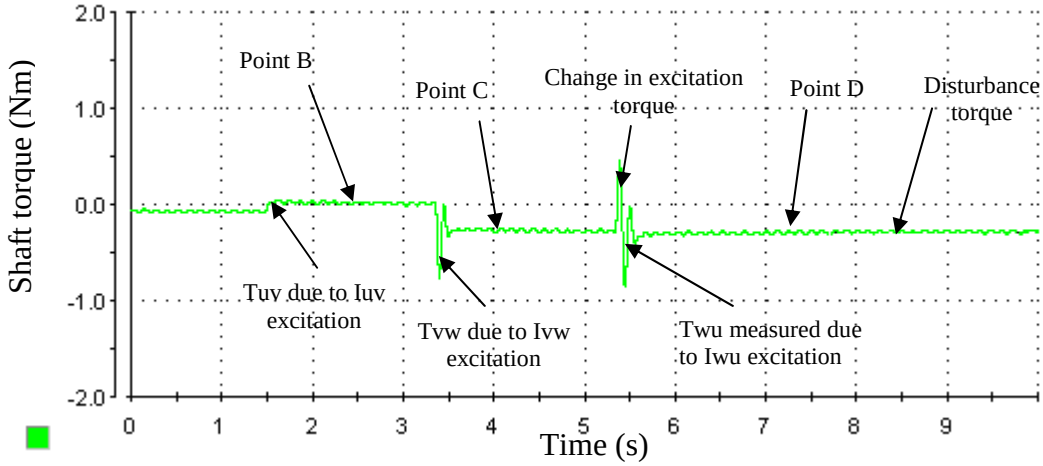

Fig. 4.20 Measured shaft torque due to three current excitation case two.

4.3.5 Routine 3: Electromagnetic torque > T_l < T_{th}

When the prototype PM machine electromagnetic torque is larger then the load torque the rotor will rotate an example electrical period is shown in Fig. 4.21 showing load and disturbance torques. Considering the electrical period shown in Fig. 4.21, when phase, *U-V* are excited with 1 A current the rotor will either move to point A or point B. The second excitation, *V-W*, will move either point A to C and or point B to C. The last excitation, *W-U*, moved point C moves to D.

Two cases will be given as examples of DSpace outputs; firstly a light load shown in Figs. 4.22 and 4.23, than a doubling of the load toques as shown in Figs. 4.24 and 4.25 in both cases the initial position is 79 electrical degrees. For the lightly loaded case, the rotor position moves to point A after the *U-V* excitation; it then moves from A to C during *V-W* excitation; and finally it moves from point C to point D during the *W-U* exaltation, as shown in Fig. 4.22, the corresponding measured torque is shown in Fig. 4.23. The end torque value is equal to 0.2 Nm.

The second case is when load torque is increased to 0.4 Nm. It can be seen in Fig. 4.24 that the start position of 79 electrical degrees was chosen randomly. The rotor moves position to point A during the *U-V* excitation, then it moves from A to C during the *V-W* excitation, and finally it moves from point C to point D during the *W-U* excitation as shown in Figs. 4.24 and 4.25. The corresponding measured torque is shown in Fig. 4.25. The end torque value is equal to 0.4 Nm. The results corresponding well to the theory Chapter 2, provided that the load torque is lower then the threshold torque.

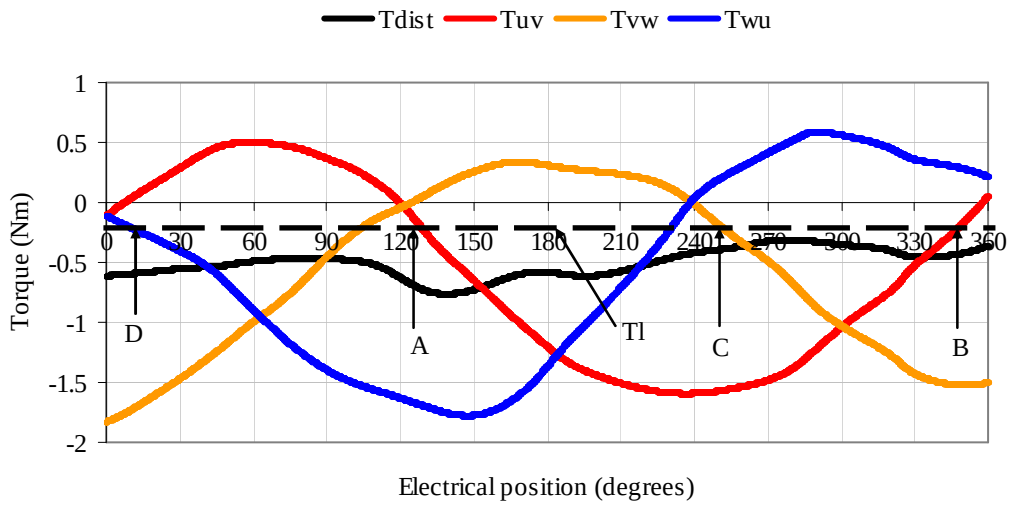

Fig. 4.21 Example of routine 3 electromagnetic torque > T_l<T_{th} for prototype machine.

.

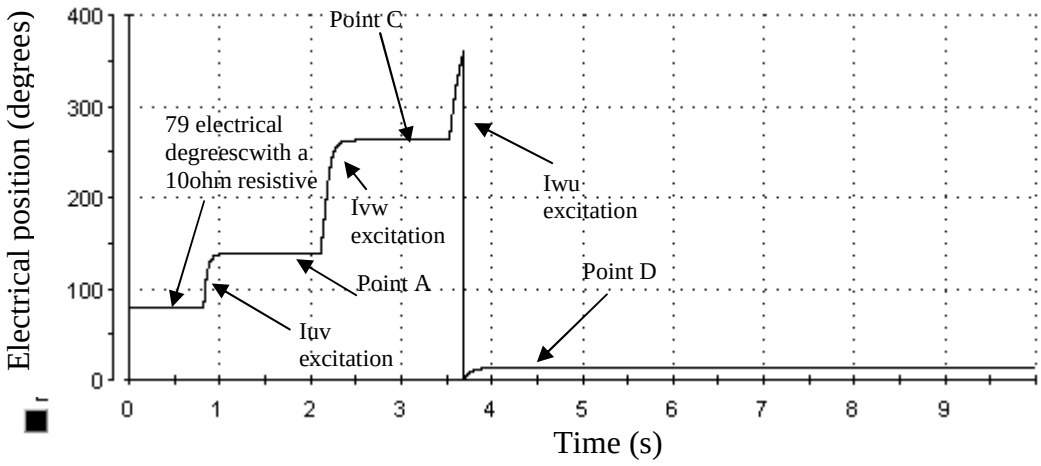

Fig. 4.22 Measured electrical position during three current excitation sequences for case one, with a load of 0.2 Nm.

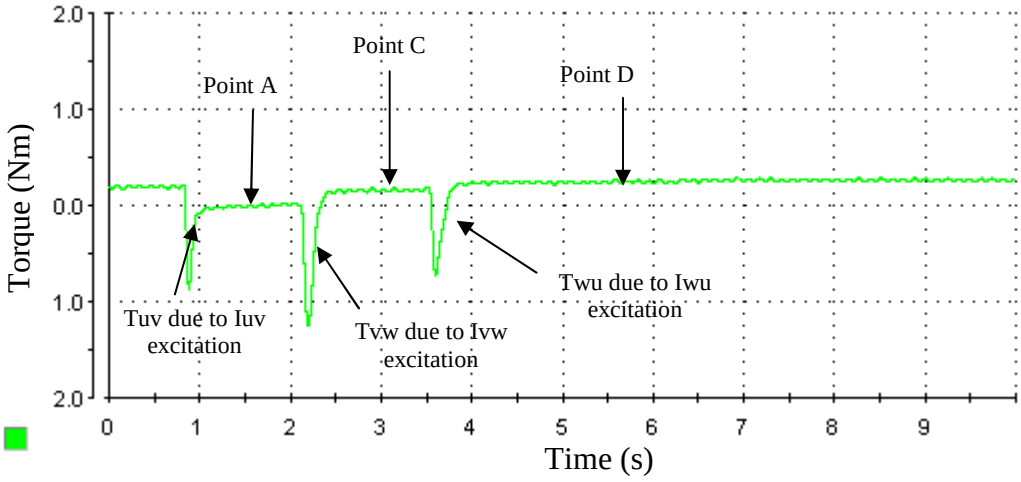

Fig. 4.23 Measured shaft torque during three current excitation sequences for case one, with a load of 0.2 Nm.

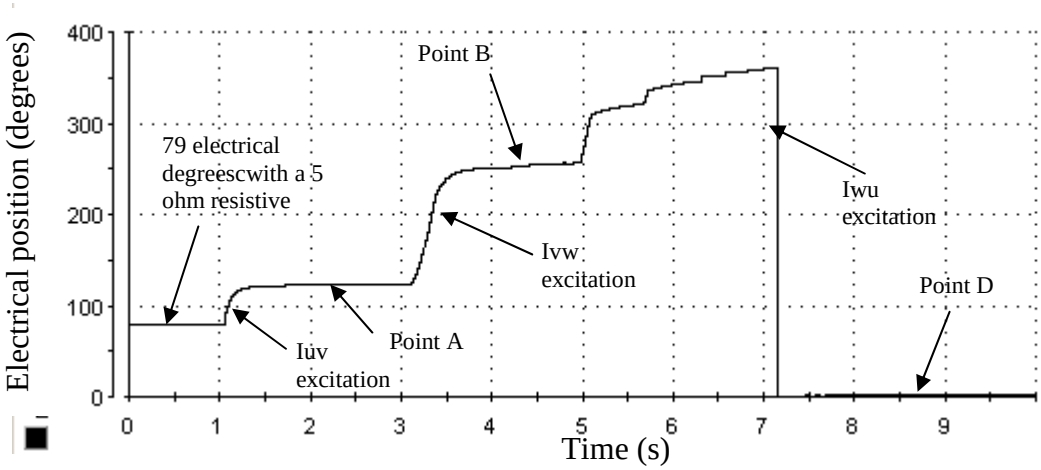

Fig. 4.24 Measured electrical position during three current excitation sequences for case two, with a load of 0.4 Nm.

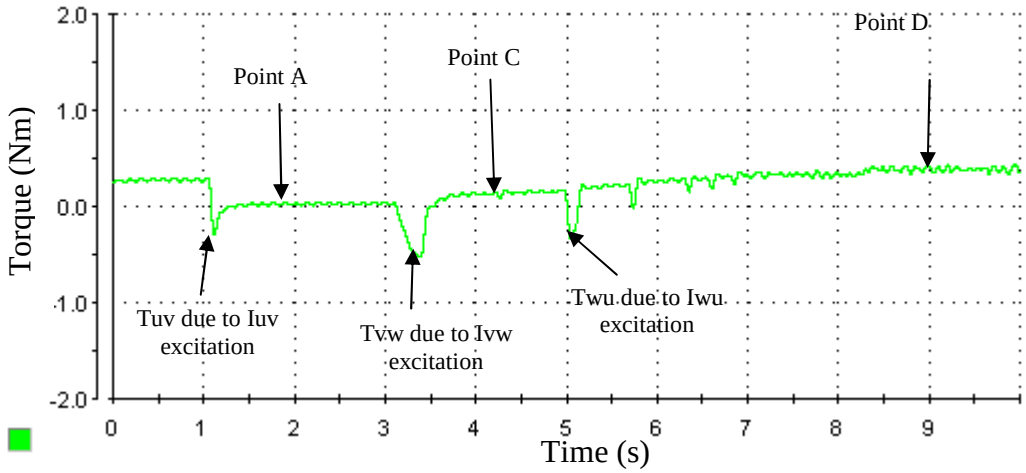

Fig. 4.25 Measured shaft torque during three current excitation sequences for case two, with a load of 0.4 Nm.

4.3.6 Routine 4: Electromagnetic torque > T_l > T_{th}

When the prototype PM machine electromagnetic torque is larger then the load torque, and the load torque is larger then the threshold load torque the rotor rotates. An electrical period is illustrated in Fig.4.26 with $T_l > T_{th}$. The initial rotor position is at 79 electrical degrees, which is point A. When phases *U-V* is excited with 1 A current a positive torque is produced. Since this torque is larger than the load torque, the rotor will move to point C, then phase *V-W* are excited. Although the excitation torque for phase *V-W* is larger than the load, the torque is less than the threshold torque rotor will remain at point C. Finally, when phases *W-U* are excited the excitation torque for phases *W-U* it will move the rotor to point B this is shown in Fig. 4.26. Only one case (i) is shown in Fig 4.28. The rotor position changes due to the three 1 A excitation, the torque corresponding measurements are shown in Fig. 4.28. The rotor position is between point B and C, these results can be easily shown for the other two cases.

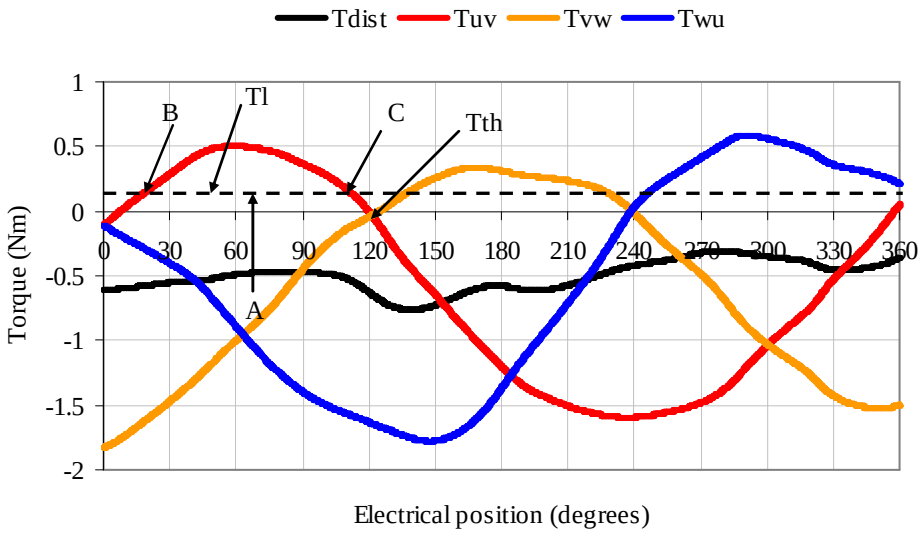

Fig. 4.26 Example of routine 4 electromagnetic torque > $T_l > T_{th}$, cases(i), for prototype machine.

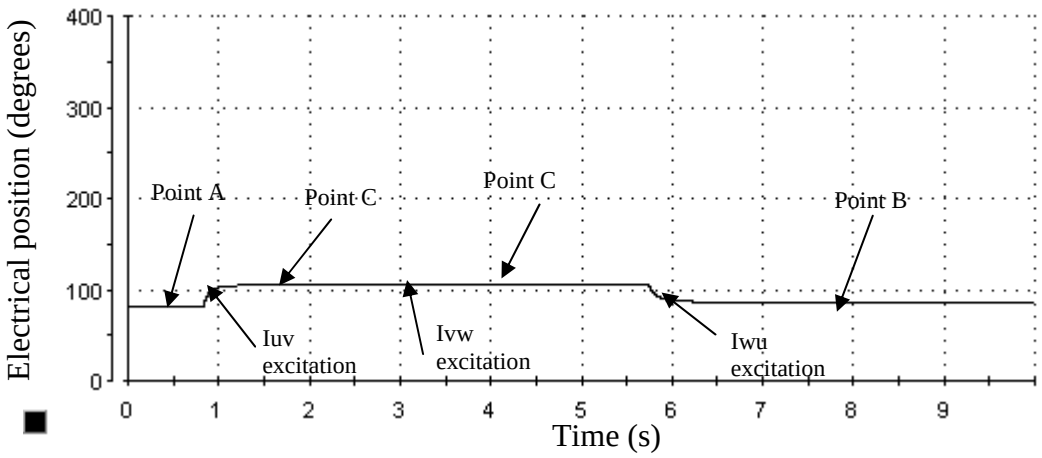

Fig. 4.27 Measured electrical position due to three current excitation sequences with load torque higher then the threshold torque.

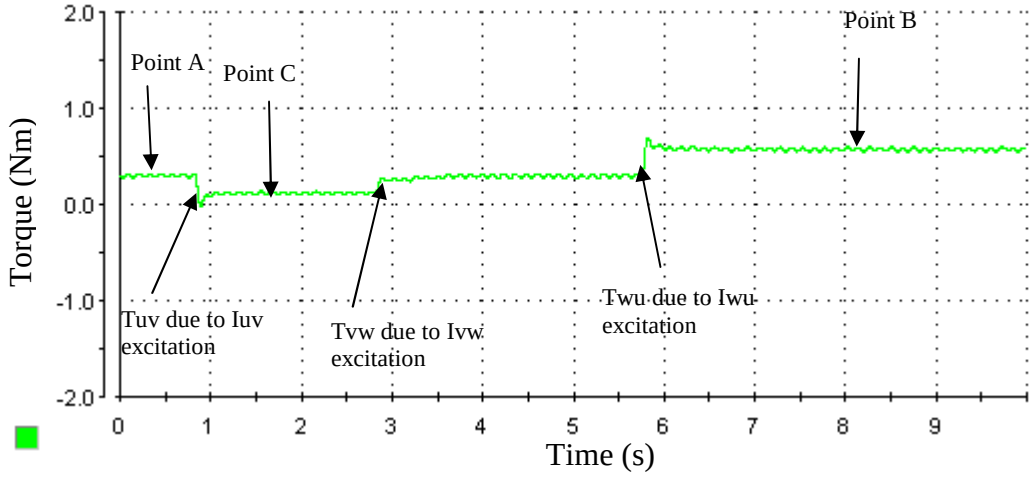

Fig. 4.28 Measured shaft torque during three current excitation sequences with load torque higher then the threshold torque.

4.3.7 Zero speed position estimation summary

This Chapter has so far discussed zero speed position estimation using measured torque feedback, presenting four routines to satisfy the four shaft load torque options. The best routine is when rotor position is determined when stationary via three small currents exciting phases *U-V*, *V-W* and *W-U* in sequence, that are not of high enough value to rotate the rotor. However, the controller can account for all four routines. The benefit of zero speed position is that the initial position can be estimated and input to the machine control, so from the first excitation only positive torque is generated and the controller does not generate negative torque. If a negative torque is produced as illustrated in Fig. 4.29 then rotor direction and will reverse, as illustrated in Fig. 4.30. However, if the initial position is calculated then the torque produced will be positive and the speed response not reversed. Measured torque, electrical and mechanical position, and derivative of the torque due to the initial position estimation, are illustrated in Fig 4.30, to compare alongside the rotor speed profile of Fig. 4.30. The code for the start-up procedure routines are created in DSpace. Similarly, Figs. 4.31 illustrates dynamic measured torque, electrical and mechanical position, and derivative of the measured torque du to initial position estimation, while Fig. 4.32 illustrates rotor speed response due to positive torque production.

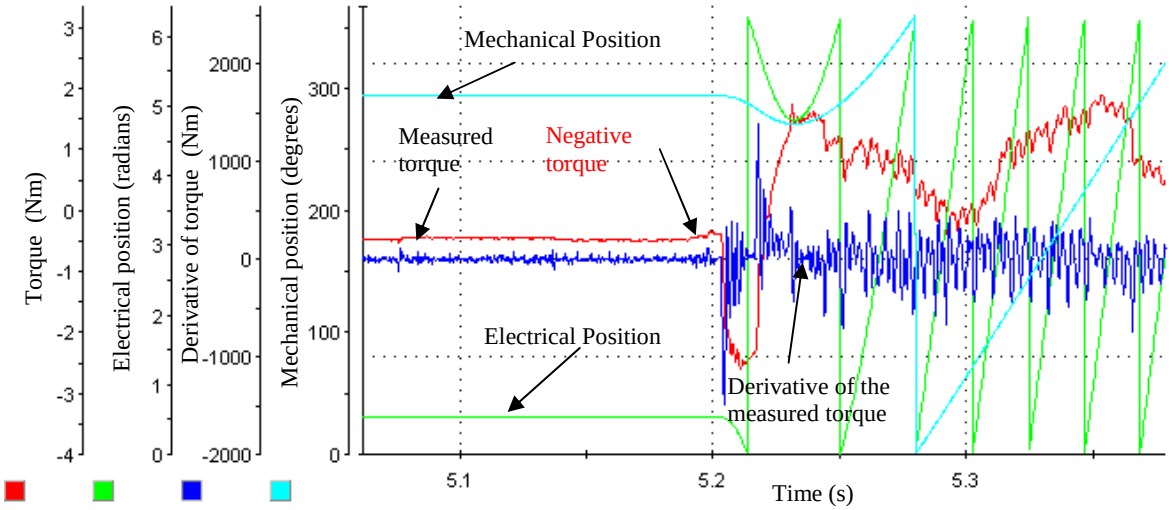

Fig. 4.29 System response to no initial position estimation.

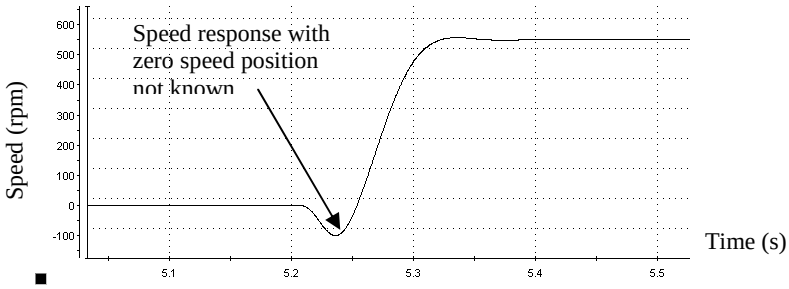

Fig. 4.30 Speed response due to negative torque production.

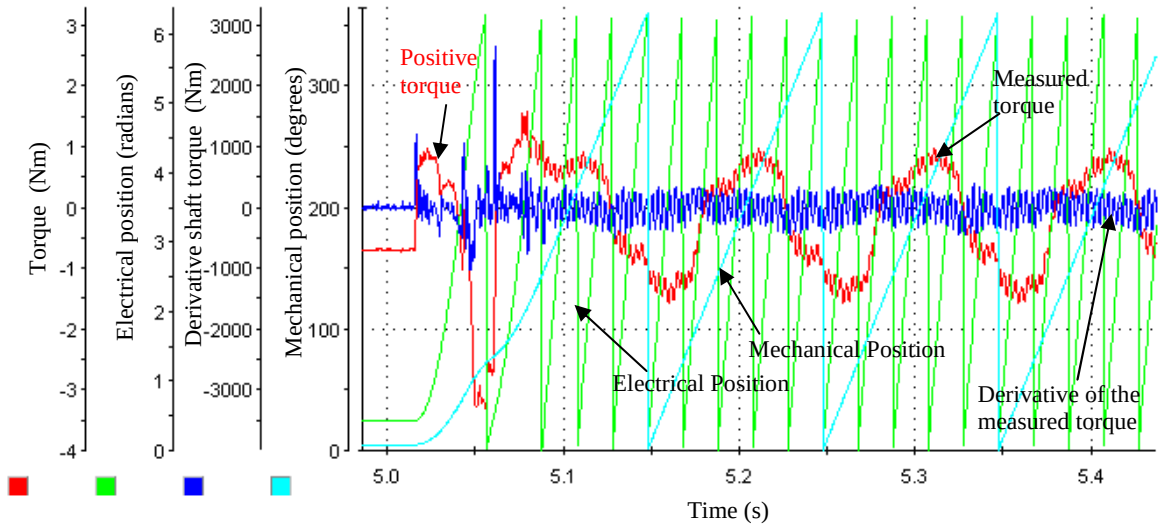

Fig. 4.31 System response due to initial position estimation.

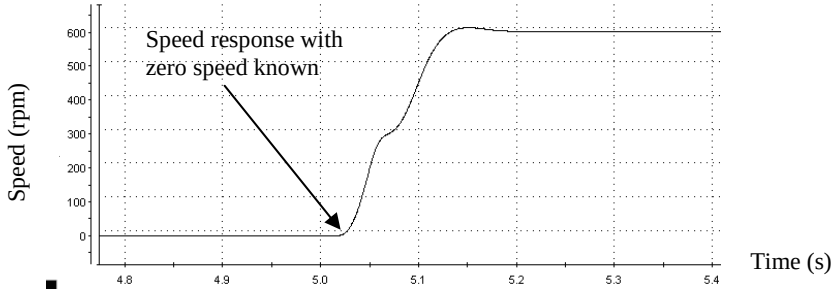

Fig. 4.32 Speed response due to positive torque.

4.4 Low Speed Control of Prototype PM Machine

4.4.1 Position sensorless (or open-loop) control

There are several techniques to control the PM machine at low speed as discussed in Chapter 1 and 2. The technique discussed here is open-loop control. Brushless DC control will operate synchronously to a certain extent but is highly sensitive to load and speed perturbations and will stalling should the control equilibrium be disturbed. This means that for a given load, applied voltage, and commutation rate the machine will rotate on open-loop control provided that these three variables do not deviate from the ideal by a significant amount. The ideal is determined by the machine back-EMF voltage and the torque constant. Loss of control manifests itself in two cases:

- when the commutation rate is too slow for the applied voltage, i.e. the machine is overexcited. This will result in the machine will accelerating to the next commutation event too quickly and then slowing down to wait until for the next commutation event. The PM machine will be acting like a stepper motor in the extreme case, where it snaps to each position until the next commutation occurs. Since the machine is able to accelerate faster then the commutation rate, an excessive current will occur, as shown in Fig. 4.33 where the torque clearly is oscillatory, and in Fig. 4.34 where the phase current values are excessive. The speed is 150 rpm and there is no load.
- when the commutation rate is too fast for a given voltage, i.e. under excitation. If the commutation arrives too early that the machine cannot accelerate fast enough to catch the next commutation event, the open-loop control will be lost and the machine stalls abruptly. The open-loop loss of control looks like a discontinuity in the machine response which makes control difficult. The torque response is shown in Fig. 4.35 and the current response in Fig. 4.36. The speed is 150 rpm and there is no load.

An alternative to over- or under-excited is to adjust the commutation rate until self-locking open-loop control is achieved, as illustrated in Fig. 4.37 showing the torque response, in Fig. 4.38 showing the current response. This open-loop controller is achieved when the load on the motor does not change over a commutation period, then the response curve of the machine speed relative to the applied voltage is linear. The main issue here is that the load should be constant. Open-loop control therefore ensures that pulse width modulation (PWM) is linearly proportional to the effective voltage. To summarise, this form of open-

loop control can be achieved at low speed, but if the load is dynamic is applied then the technique will be highly unstable. The open-loop control as discussed in Chapter 2 requires knowledge of the line voltage for each speed, as shown in Fig. 4.39 for the prototype machine. The speed is 150 rpm and there is no load.

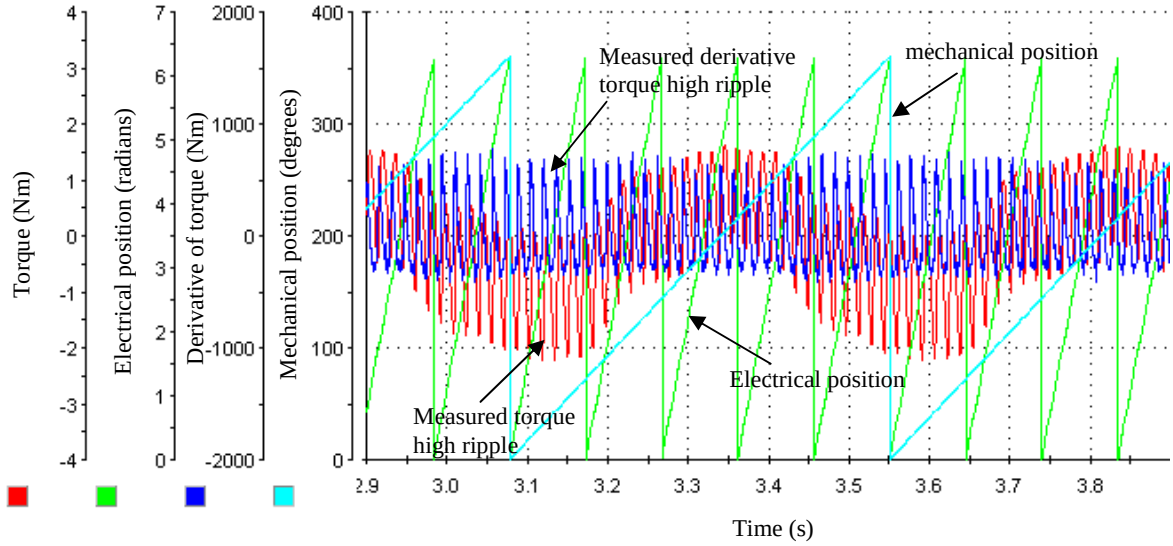

Fig. 4.33 Over-excitation of the prototype machine (acting like a stepper motor).

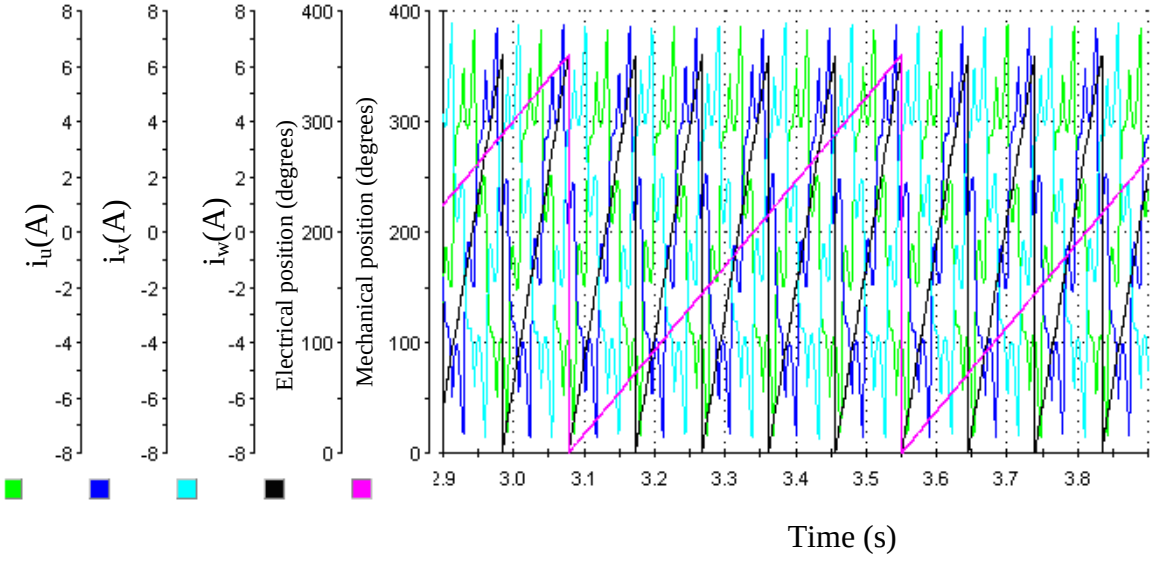

Fig. 4.34 High phase currents due to over-excitation.

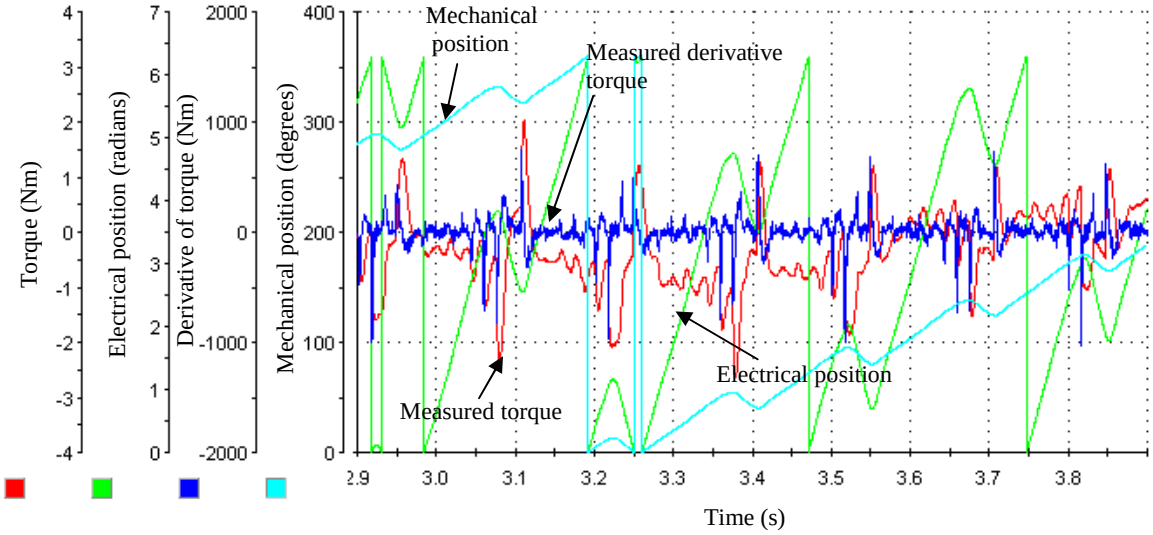

Fig. 4.35 Machine measured torque when control is lost due to under-excitation.

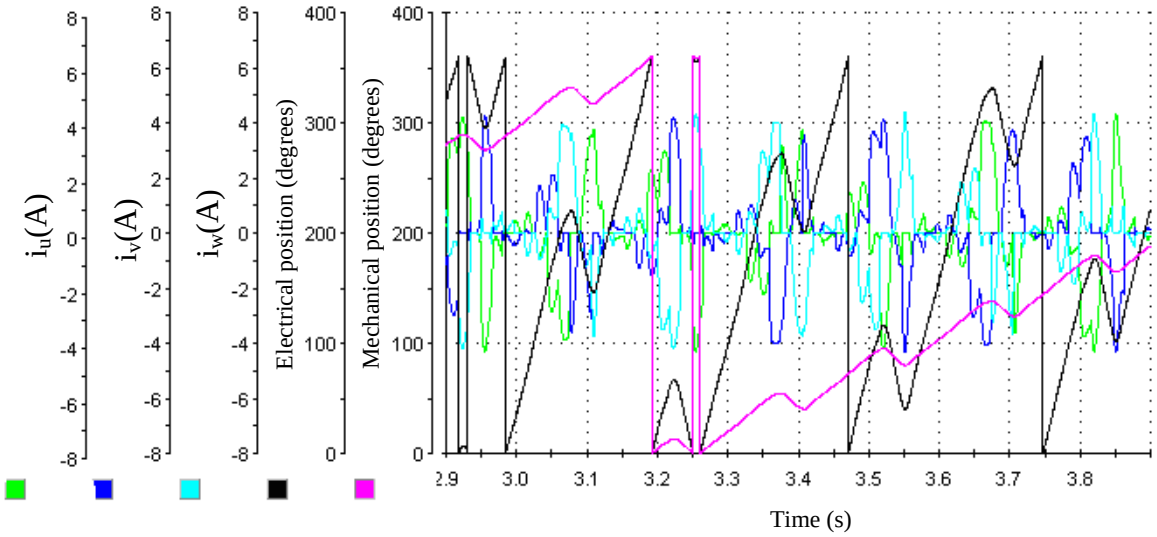

Fig. 4.36 Current response during under-excited event.

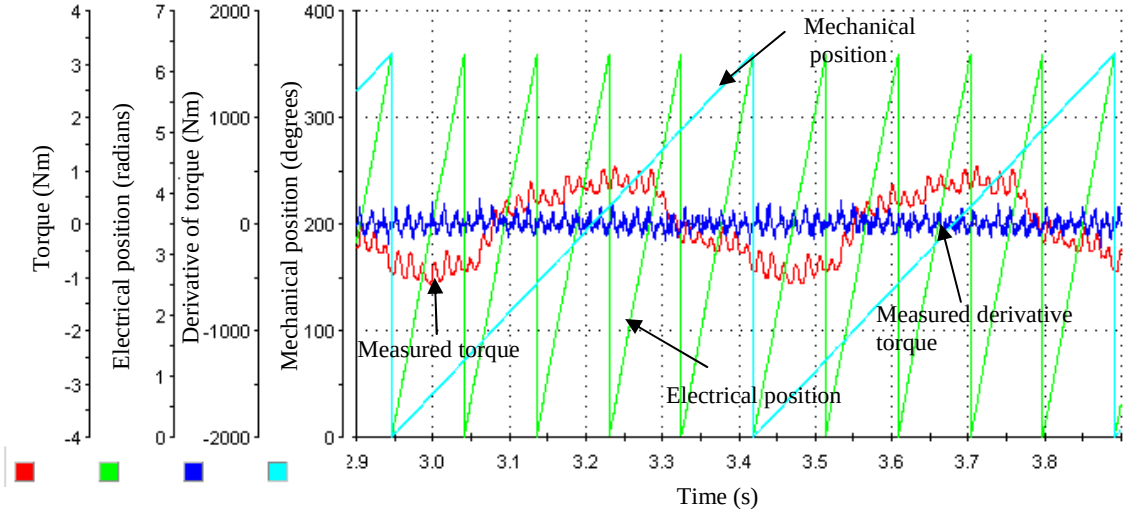

Fig. 4.37 Measured shaft torque of machine ideal response.

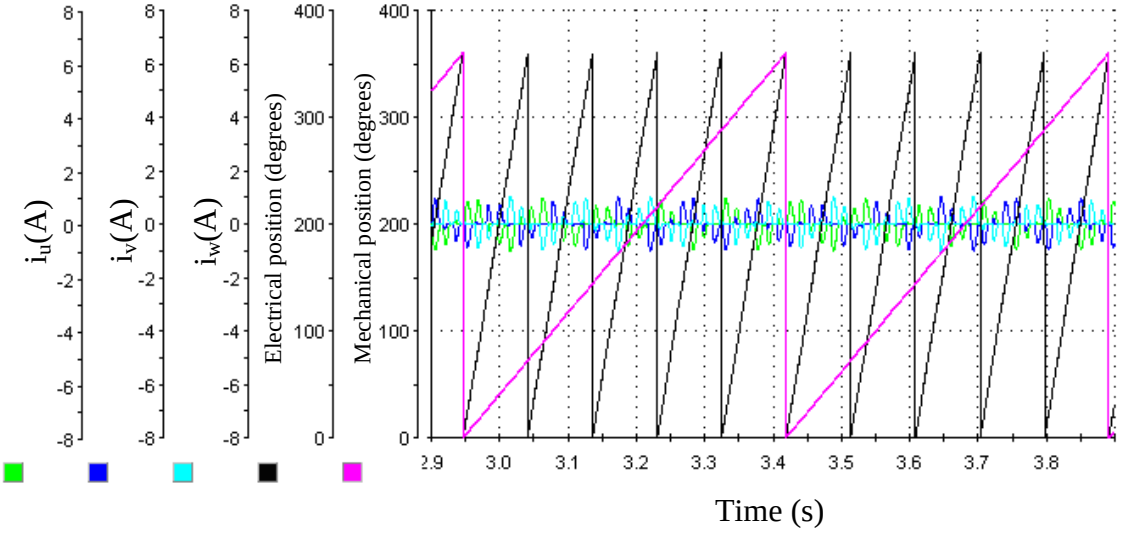

Fig. 4.38 Current waveform during response ideal response.

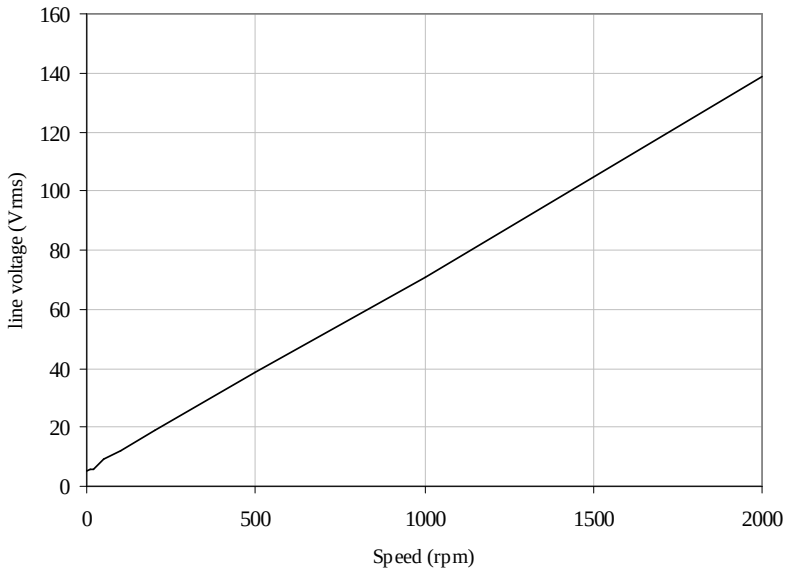

Fig. 4.39 Machine line voltage versus speed for prototype machine.

4.4.2 Position sensorless with measured torque feedback

The open-loop control discussed in section 4.4.1 is simple and easy to implement, but practically useless in applications having dynamic torque and speed perturbations. However, the open-loop control scheme is worthy of consideration if augmented via an additional control function, hence becoming closed-loop control using measured torque feedback. The machine was initially excited without load and a table is constructed for each speed and PWM cycle as discussed in section 4.4.1. Then, the measured torque feedback is used as a gain to increase or decrease the PWM duty as the load increases or decreases. Then from Fig. 4.39 the voltage is known for no-load condition so when load is added the torque feedback voltage is summed with the no-load voltage to the new voltage command which corresponds to a new PWM duty cycle as discussed in Chapter 2 and appendix (A3). In Fig. 4.40 the machine speed is shown for no-load operation. Phase current and torque measurements are illustrated in Figs. 4.41 and 4.42 respectively. When load is added of 2 Nm the control increases the PWM demand to compensate for the load, the speed response is shown in Fig. 4.43. The torque and current responses are shown in Figs. 4.44 and 4.45 respectively. After the machine exceeds threshold speed in the prototype machine is equal to 150 rpm, another sensorless control is used which will be discussed in Chapter 5.

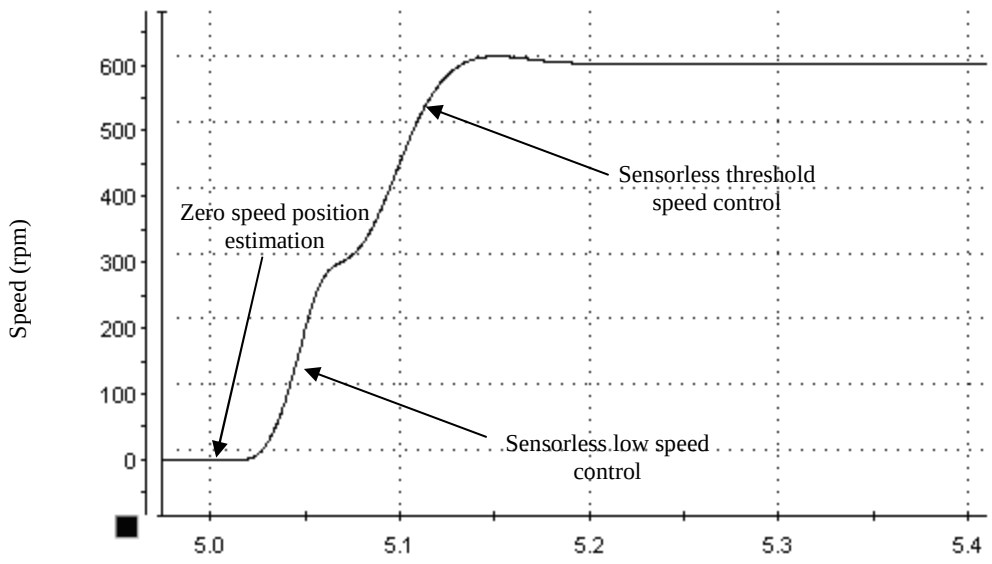

Fig. 4.40 No-load speed response.

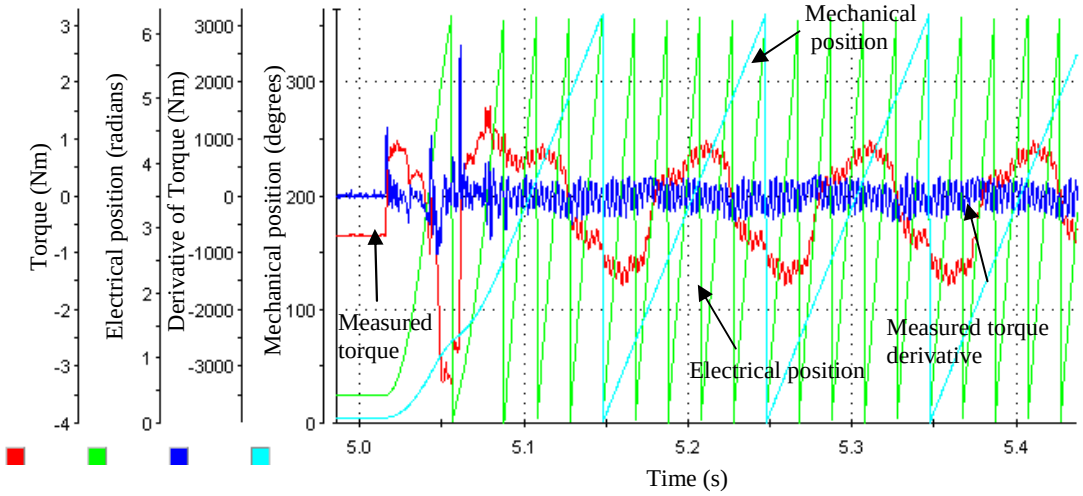

Fig. 4.41 No-load torque response.

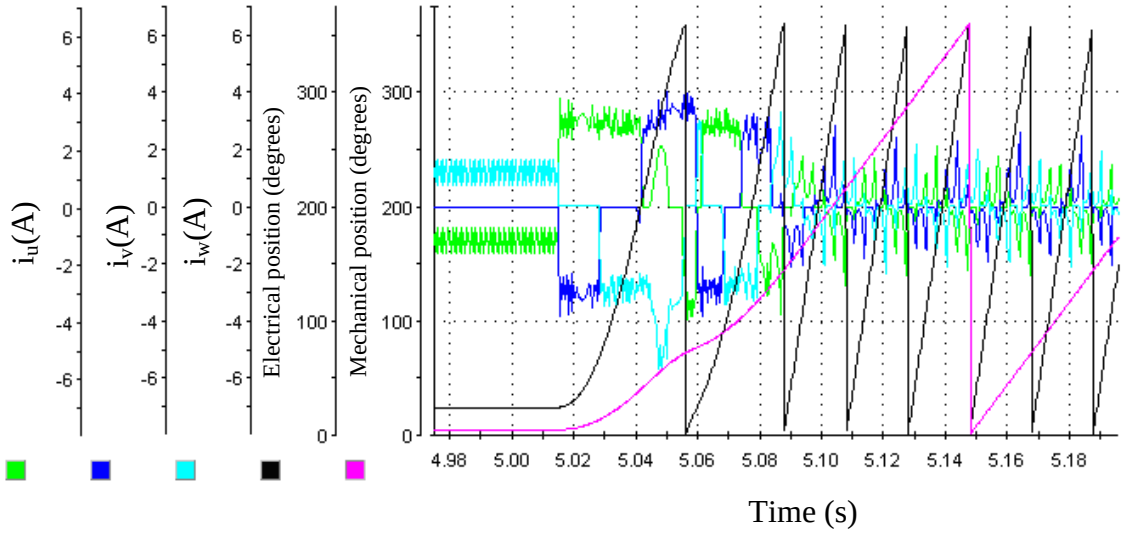

Fig. 4.42 No-load current response.

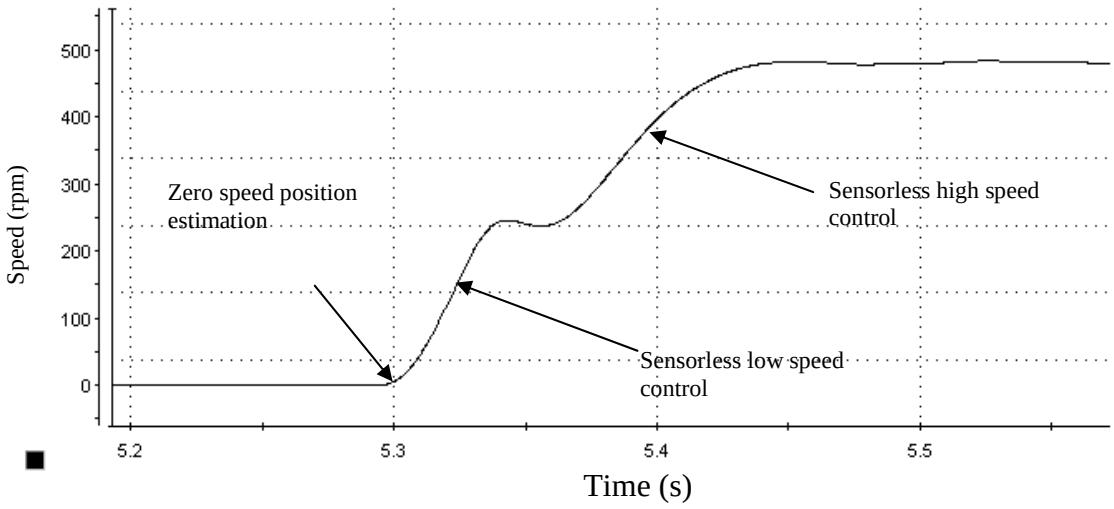

Fig. 4.43 Load speed response.

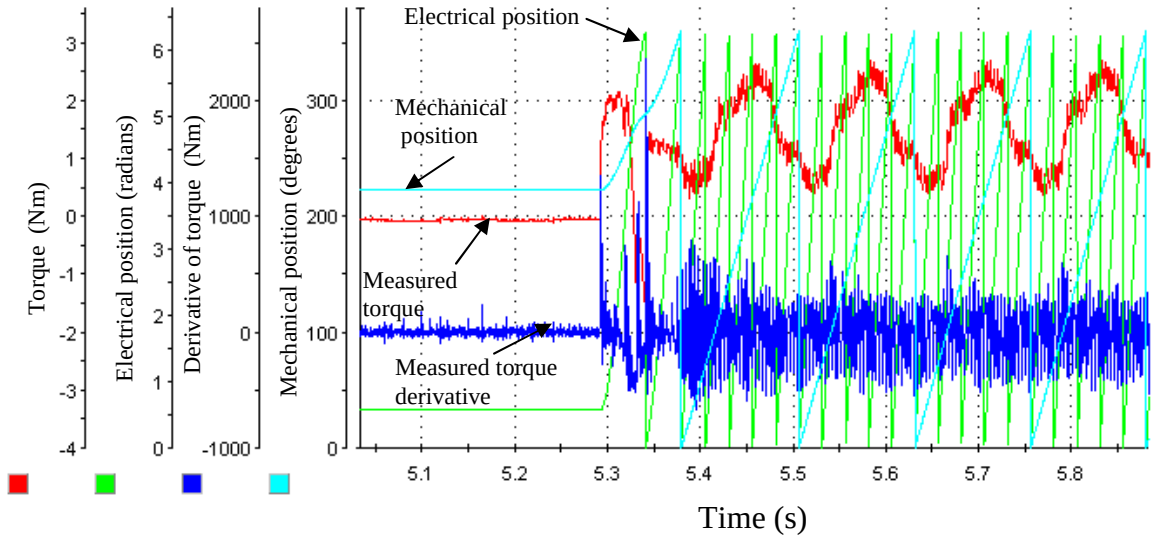

Fig. 4.44 Load torque response.

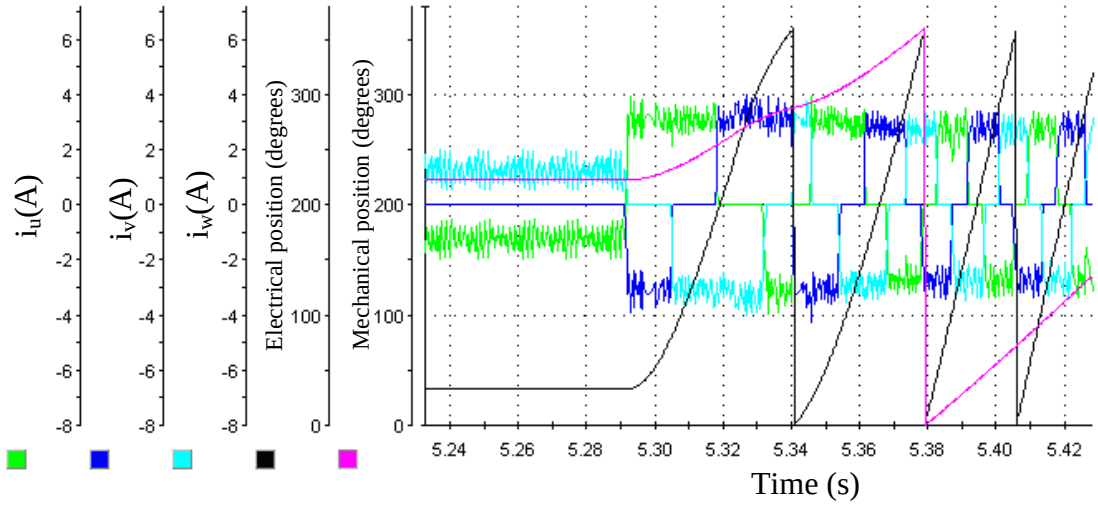

Fig. 4.45 Load current response.

4.5 Summary

Chapter 4 has discussed the experimental implementation of the start-up procedure developed in Chapter 2. The torque start-up using for the Unimotor PM machine was then discussed and shown to similar to the idealised machine model discussed in Chapter 2, due to the high quality of manufacture of this machine. The prototype machine was then investigated and the no-load torque characterised. It was noted that there was a load on the system that may have been caused by an internal-misalignment. This was considered as a disturbance torque on the system. The zero speed estimation procedure was implemented to control the prototype machine via DSpace. The first routine showed the zero position estimation error was within 1% when implemented via DSpace. Then the second routine settled to around 30 electrical degrees. The third routine settled between 0 and 30 electrical degrees as the load increased the position offset toward 0 electrical degrees. The fourth routine predicted the position between two sectors.

Low speed control was investigated firstly by implementing open-loop brushless DC and then using measured torque feedback to make it closed-loop resulting in improved control of the machine at low speed. With the procedures developed machine control can be realised from zero and low speed with all load conditions by using measured torque feedback.

CHAPTER 5

FLUX-LINKAGE ESTIMATION USING MEASURED TORQUE FEEDBACK

5.1 Introduction

In chapter 2 a theory for zero and low speed control without the use of measured position was described. Chapter 4 implemented the zero and low speed control procedures for different loads. Chapter 5 now discuses the use of flux estimators to control speed over a predetermined threshold speed which, for the system studied in this thesis is between 150-300 rpm. The flux estimation technique can be divided into two types :

- Open-loop flux-linkage estimation without feedback, but by direct flux estimation. The open loop flux estimation was used firstly with a pure integrator to estimate the flux as in [1], but the pure integrator had drift and initial value problems. The integration drift is a problem when using (1.7) and (1.8), but by using a low pass filter it is reduced [30].
- Closed-loop flux-linkage estimation is when the torque is calculated to compensate for position offsets. This method is implemented in two ways: one with a full electro-mechanical model where torque is calculated as in [38], and the three phase currents are measured to estimate flux. Torque is then calculated from measured currents and estimated flux. The second method is when the flux-linkage is calculated from the measured current and voltages, a look-up table of flux-linkage / position and current characteristics is used to estimate current and position. This chapter will discuses a flux estimator closed loop with measured torque feedback rather then a table or a electro-mechanical model.

5.2 Flux-Linkage Estimator

5.2.1 Introduction

Is this section a simple position sensorless control system is described to control the phase angles of the stator currents to maintain maximum torque per stator ampere over a wide range of speed and torque. The flux position is estimated from the measured current and voltages which are then manipulated and used to control the switching angle of the power electronics inverter and here the stator currents. Many types of flux observer have been discussed in papers and books [30-38]. In general, the steady-state first derivative of the angle gives the speed. However, in the transient state, the stator flux-linkage space vector moves relative to the rotor to produce a new torque level and that influences speed. This effect can be neglected if the rate-of-change of the electromagnetic torque is limited. The angle between the stator flux-linkage, $\psi_{s,}$ and stator current, $I_{s,}$ is 90 electrical degrees, to produce max torque per current excitation as shown in Fig. 5.1. This concept will be used to control the prototype brushless PM machines above threshold speed which is (150-300) typically the reason for choosing such speed to calculate the flux-linkage at lower speeds the back-EMF voltage is very low and the resistance voltage drop becomes dominant. Choosing the threshold speed depends on the speed where it can be calculated in the prototype machine it 150 rpm.

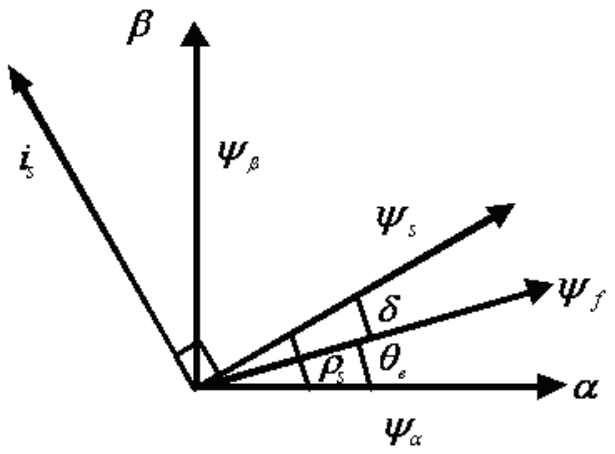

Fig. 5.1 Stator current and flux-linkage phase diagram.

5.2.2 Flux-linkage estimator equations

The stator current space vector in the stationary reference frame fixed to the stator can be expressed as [36]:

$$\begin{bmatrix} i_\alpha \\ i_\beta \\ i_\gamma \end{bmatrix} = \sqrt{\frac{2}{3}} \begin{bmatrix} 1 & \frac{-1}{2} & \frac{-1}{2} \\ 0 & \frac{\sqrt{3}}{2} & \frac{-\sqrt{3}}{2} \\ \frac{1}{\sqrt{2}} & \frac{1}{\sqrt{2}} & \frac{1}{\sqrt{2}} \end{bmatrix} \begin{bmatrix} i_u \\ i_v \\ i_w \end{bmatrix} \tag{5.1}$$

The following alpha and beta axis currents in the stator reference frame can be expressed as a real and imaginary current as:

$$i_s = i_\alpha + j i_\beta \tag{5.2}$$

The alpha and beta axis currents can be obtained from the measured stator current by:

$$i_\alpha = \sqrt{\frac{2}{3}} \left(i_u - \frac{1}{2} i_v - \frac{1}{2} i_w \right) \tag{5.3}$$

$$i_\beta = \sqrt{\frac{2}{3}} \left(\frac{\sqrt{3}}{2} i_v - \frac{\sqrt{3}}{2} i_w \right) \tag{5.4}$$

For a balanced machine and supply conditions:

$$i_u + i_v + i_w = 0 \tag{5.5}$$

Thus by considering (5.5), (5.3) and (5.4) can be written as (5.6) and (5.7) respectively:

$$i_\alpha = \sqrt{\frac{2}{3}} \left(i_u - \frac{1}{2}(-i_u - i_w) - \frac{1}{2} i_w \right) = \sqrt{\frac{2}{3}} \left(\frac{3}{2} i_u \right) = \sqrt{\frac{3}{2}} i_u \tag{5.6}$$

$$i_\beta = \sqrt{\frac{2}{3}} \left(\frac{\sqrt{3}}{2} i_v - \frac{\sqrt{3}}{2} i_w \right) = \frac{1}{\sqrt{2}} (i_v - i_w) = \frac{1}{\sqrt{2}} \left(i_v - (-i_u - i_v) \right) = \frac{1}{\sqrt{2}} (i_u + 2 i_v) \tag{5.7}$$

The stator voltages can be defined similarly; thus the alpha and beta stator voltages in the stationary reference frame are:

$$u_s = u_\alpha + ju_\beta \tag{5.8}$$

$$u_\alpha = \sqrt{\frac{2}{3}}\left(u_u - \frac{1}{2}(-u_u - u_w) - \frac{1}{2}u_w\right) = \sqrt{\frac{2}{3}}\left(\frac{3}{2}u_u\right) = \sqrt{\frac{3}{2}}u_u \tag{5.9}$$

$$u_\beta = \sqrt{\frac{2}{3}}\left(\frac{\sqrt{3}}{2}u_v - \frac{\sqrt{3}}{2}u_w\right) = \sqrt{\frac{2}{3}}\frac{\sqrt{3}}{2}(u_v - u_w) = \frac{1}{\sqrt{2}}(u_v - u_w) \tag{5.10}$$

These can be obtained from the measured line voltages by (5.11) – (5.13):

$$u_{uv} = u_u - u_v \tag{5.11}$$

$$u_{vw} = u_v - u_w \tag{5.12}$$

$$u_{wu} = u_w - u_u \tag{5.13}$$

For a balanced machine and supply conditions:

$$0 = u_u + u_v + u_w \tag{5.14}$$

By considering (5.9)-(5.14) the alpha and beta voltages can be written as (5.15) and (5.16) respectively:

$$u_\alpha = \sqrt{\frac{3}{2}}\frac{1}{3}(u_{uv} - u_{wu}) \tag{5.15}$$

$$u_\beta = -\frac{1}{\sqrt{2}}(u_{wu} + u_{uv}) \tag{5.16}$$

The stator flux vector can be obtained by integration of the terminal voltages minus the stator Ohmic drop as:

$$\psi_l = \int u_l - R_s i_s dt \tag{5.17}$$

By considering the alpha and beta axis current (5.2) and alpha and beta axis voltages (5.8), The alpha and beta axis stator flux-linkage components are obtained:

$$\psi_s = \psi_\alpha + j\psi_\beta \tag{5.18}$$

Thus, the following alpha and beta axis stator flux-linkage components in the stator reference frame are obtained:

$$\psi_\alpha = \int u_\alpha - R_s i_\alpha dt \tag{5.19}$$

$$\psi_\beta = \int u_\beta - R_s i_\beta dt \tag{5.20}$$

The angle of the stator flux-linkage space vector which shown in Fig 5.1 can be obtained from the two-axis stator flux-linkage component as:

$$\rho_s = \tan^{-1}\left(\frac{\psi_\beta}{\psi_\alpha}\right) \tag{5.21}$$

The performance of the flux-linkage position estimator in (5.21) depends on the accuracy of the integration technique used and also the accuracy of the monitored voltages and currents. The integration becomes problematic at low frequencies where the stator voltage values are very small and are dominated by the resistor voltage drops. The errors associated with the monitored voltages and currents are:

- phase shift due to the voltage sensor used,
- offset in the measurement systems,
- quantization error in the digital system,
- and magnitude errors because of the conversion factors.

The resistance value must be accurately measured for accurate flux-linkage estimation. The analogue integrators cause the system to drift which causes a large error of the position of the stator flux-linkage. An incorrect flux angle will cause phase modulation in the control of the phase currents at fundamental frequency. This will produce unwanted fundamental frequency oscillations in the electromagnetic torque of the machine [14]. This flux-linkage estimator is known as an open-loop estimator, a DSpace schematic of which is shown in Fig. 5.2.

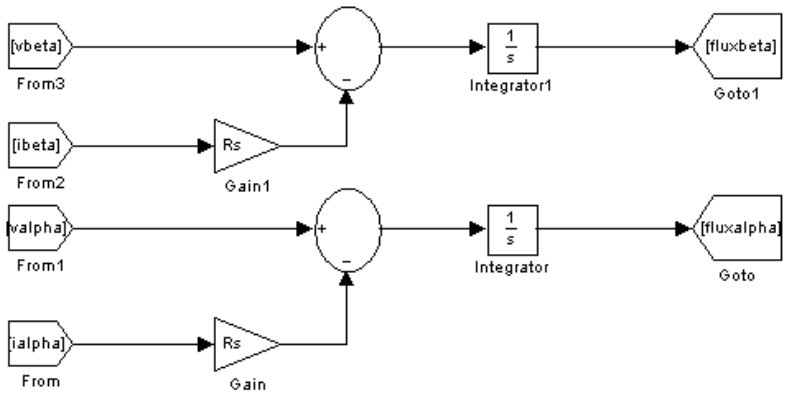

Fig. 5.2 Open-loop flux-linkage estimator.

Another method is where the stator flux-linkage can be estimated using a low pass filter instead of a pure integrator, in this case the 1/s integrator is replaced with (T/s+T) where T is a suitable time constant [14], as illustrated in Fig. 5.3. This is the method that will be used to control the prototype brushless PM after the threshold speed is reached. The constant chosen for this machine is 0.001 s based on a trial and error method.

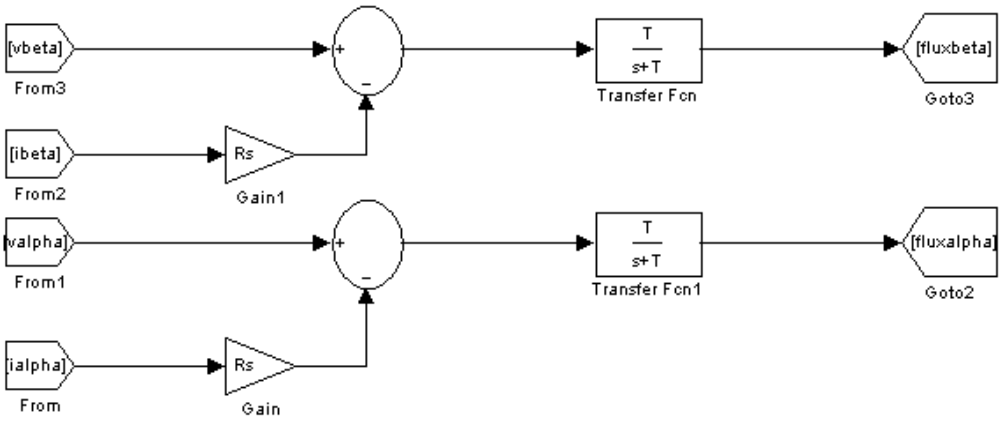

Fig. 5.3 Low pass flux-linkage estimator.

From the α and β stator flux-linkage and stator current components, the electromagnetic torque can be calculated as [106]:

$$T = \frac{3}{2} P\left(\psi_\alpha i_\beta - \psi_\beta i_\alpha\right) \tag{5.22}$$

where *P* is the machine pole-pair number. An alternative equation for the electromagnetic torque is also given by [106]:

$$T_e = \frac{3p\psi_s}{4L_\alpha L_\beta}[2\psi_{ff} L_\beta \sin(\delta) - \psi_s (L_\beta - L_\alpha)\sin 2\delta] \tag{5.23}$$

The rotor position, θ_e required to estimate the speed is then computed as the difference between the stator flux-linkage angle ρ_s and the load-angle [106, 123] as:

$$\theta_e = \rho_s - \delta \tag{5.24}$$

Finally the rotor electrical speed can be calculated by differentiating the rotor position:

$$\omega_e = \frac{d\theta_e}{dt} \tag{5.25}$$

The load-angle can be estimated from load torque, where the load torque is estimated using equations (5.23). However, it is very difficult to estimate the load-angle since machine parameters may change. In Chapter 1 another method was reviewed that used a look-up table, but also this method has errors due to machine parameters changes [16]. Here in Chapter 5 the measured shaft torque to estimate the load-angle and account for the offset problem due to load torque.

5.3 Simulation of Low pass Flux-Linkage Estimator

The performance of the low pass flux-linkage shown in Fig. 5.3, estimator was investigated using Matlab/Simulink. The back EMF is calculated using (5.26)-(5.28). The prototype machine was rotated at low speed using the start-up technique of Chapter 2 and 4 until the motor reached the threshold speed where the flux-linkage technique can be used to estimate position and this is 150 rpm for the prototype machine. For the simulation study the machine was accelerated from 0 to 1000 rpm and low pass filter shown in Fig. 5.3 used to estimate the position.

$$e_u = k_e w_e \sin(\theta_e) \tag{5.26}$$

$$e_v = k_e w_e \sin(\theta_e + \frac{2\pi}{3}) \tag{5.27}$$

$$e_w = k_e w_e \sin(\theta_e - \frac{2\pi}{3}) \tag{5.28}$$

5.3.1 Low pass flux-linkage estimator at no-load

The Brushless PM machine starts from stand-still and is accelerated to 1000 rpm with no-load this is shown in Fig. 5.4. The electromagnetic torque, phase current, back-EMF, and estimated position for no-load are shown in Fig. 5.5 to Fig. 5.7.

Fig. 5.5 shows the simulated electromagnetic torque response. The start-up torque from 0 to 0.01 s is to start the machine and get the speed accelerated from 0 to 1000rpm. Then there is small amount of torque that is required to overcome the friction losses.

Fig. 5.6 shows the current and the back-EMF for phase U. The start-up current which is from 0 to 0.01 s is to accelerate the machine from 0 to 1000 rpm. Then there is a small amount of current which supplies the no-load torque. Fig. 5.7 show simulated electrical positions and flux-linkage estimated position, the flux-linkage cannot estimate position at zero and low speed so it will be used only for speeds higher the threshold speed. Fig. 5.8 shows the measured and estimated electrical positions zoomed in to show that the estimated algorithm is performing well at over threshold speed.

To summarise, the position estimation at no-load using the low pass filter estimator performance is very good because the there is no offset due to load. If load is added then either a look-up table should be used to compensate for the load angle difference or an estimate of load angle from the flux and current could be used. In the next section load is going to be added without compensation from a look-up table or an estimate, and the measured and estimated position are going to be compared.

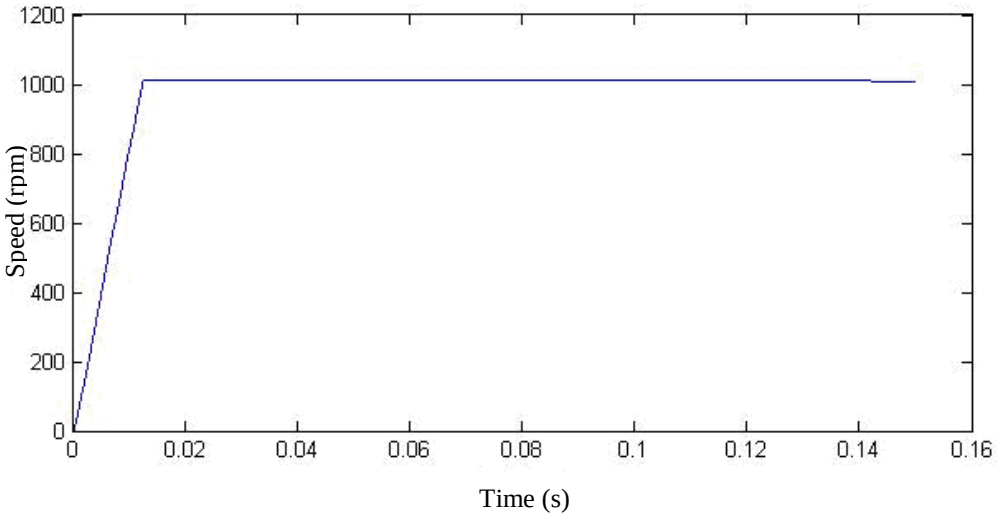

Fig. 5.4 Simulated speed response with no-load.

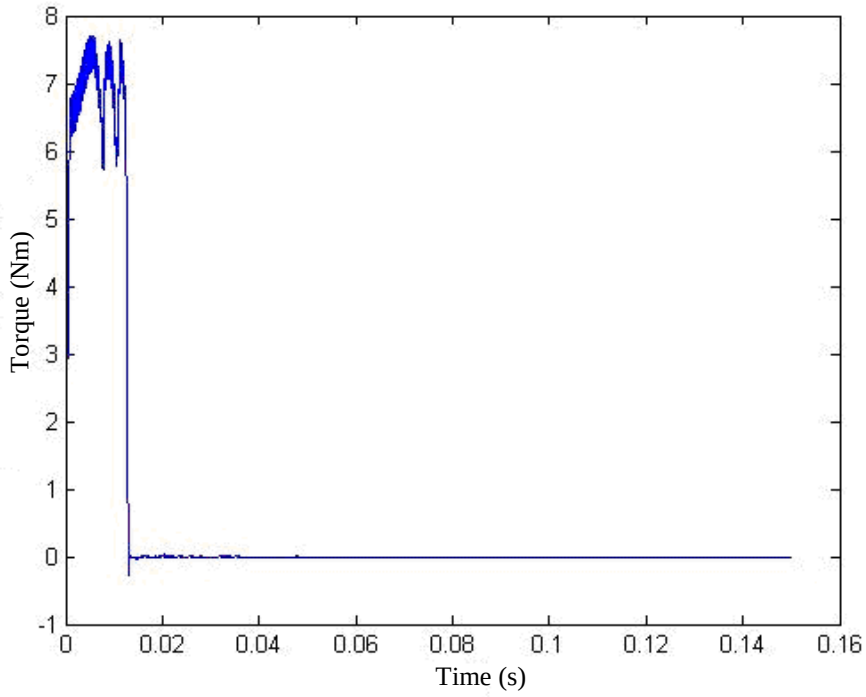

Fig. 5.5 Simulated electromagnetic torque response with no-load.

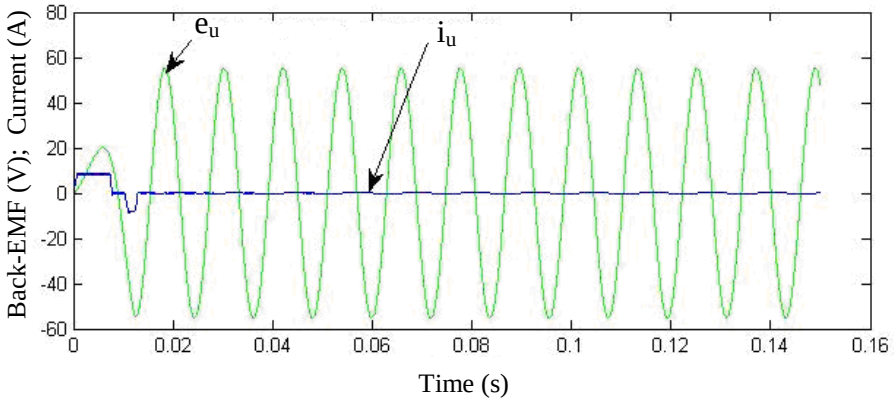

Fig. 5.6 Simulated phase u current and back-EMF with no-load.

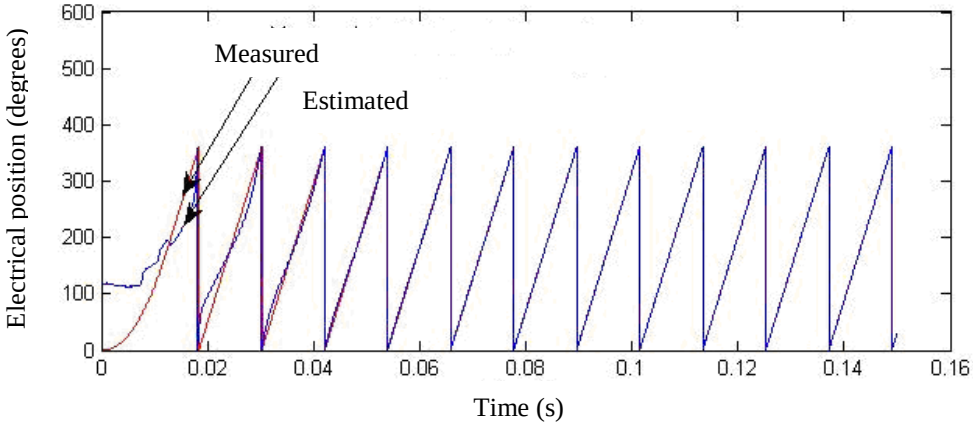

Fig. 5.7 Simulated measured and estimated electrical position with no-load.

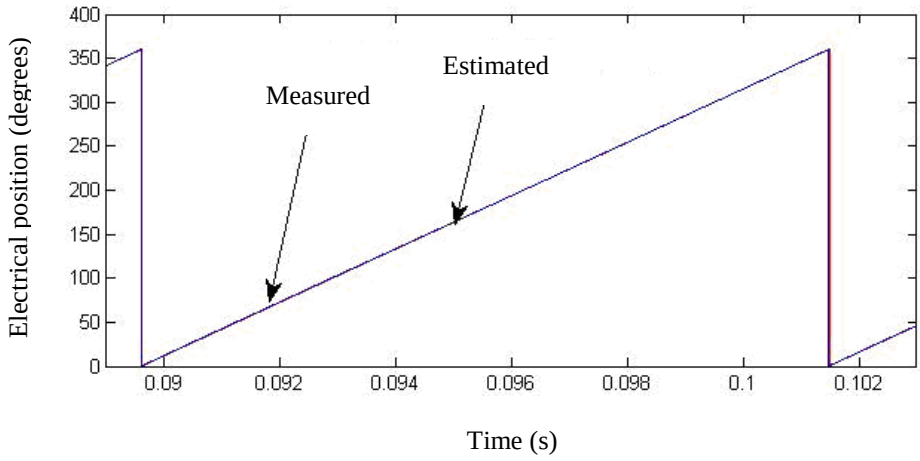

Fig. 5.8 Simulated measured and estimated electrical position with no-load.

5.3.2 Low pass flux-linkage estimator at load

The brushless PM machine starts from stand-still and is accelerated to 1000 rpm with load, as shown in Fig. 5.9. The electromagnetic torque, phase current, back-EMF and estimated position are shown in Figs. 5.10 to Fig. 5.12 respectively.

Fig. 5.11 shows the current and the back-EMF for phase *U*. The start-up current from 0 to 0.01 s is that required to accelerate the machine and load systems from 0 to 1000 rpm. There after, the current supplies the steady load. Fig. 5.12 shows the estimated and measured electrical position. There is an offset between the estimated and measured position that can be shown in further detail in Fig. 5.13 which is a zoom of Fig. 5.12 to show the offset detail. To summarise, the performance when there is no-load the low pass filter estimator performance is very good because there is no offset due to load. But as load of 7 Nm is inserted a offset angle occurs. This angle is usually estimated from the measured current and voltages but changes in machine parameters, due to temperature for example, can changes cause an error to the estimation.

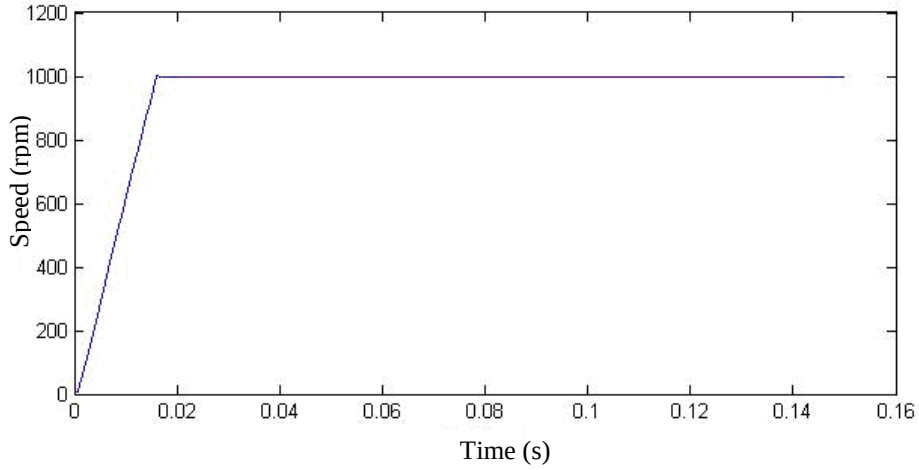

Fig. 5.9 Simulated speed response with load.

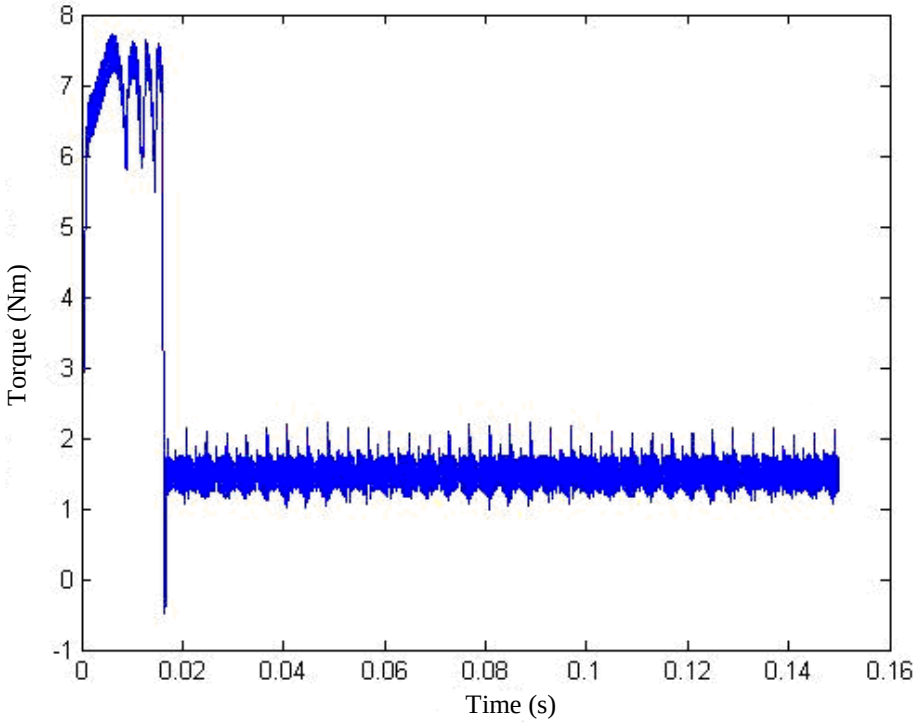

Fig. 5.10 Simulated electromagnetic torque response with 7 Nm load.

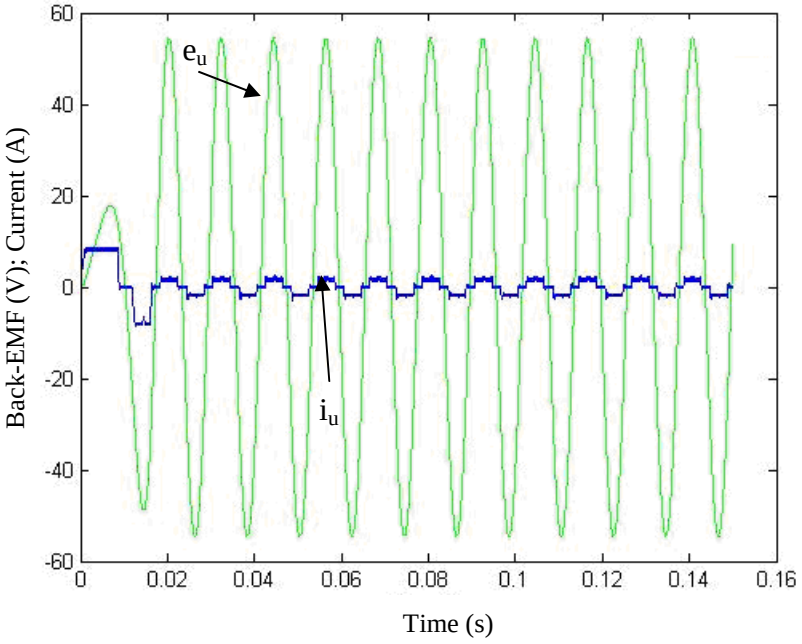

Fig. 5.11 Simulated phase u current and back-EMF with 7 Nm load.

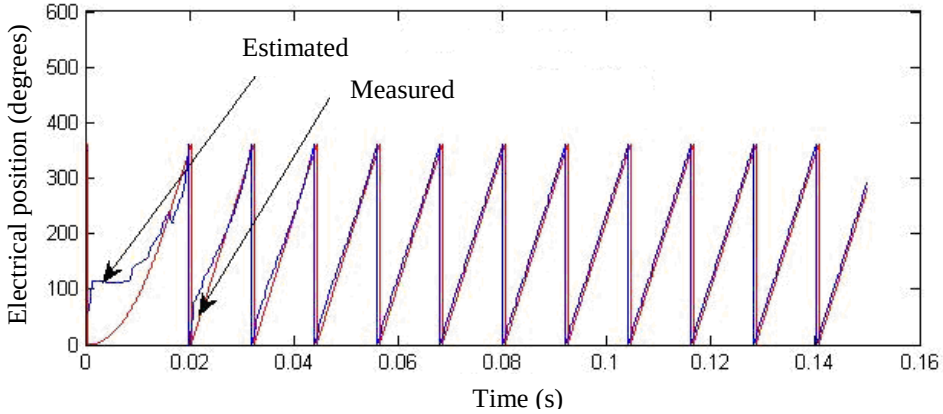

Fig. 5.12 Simulated measured and estimated electrical position with load.

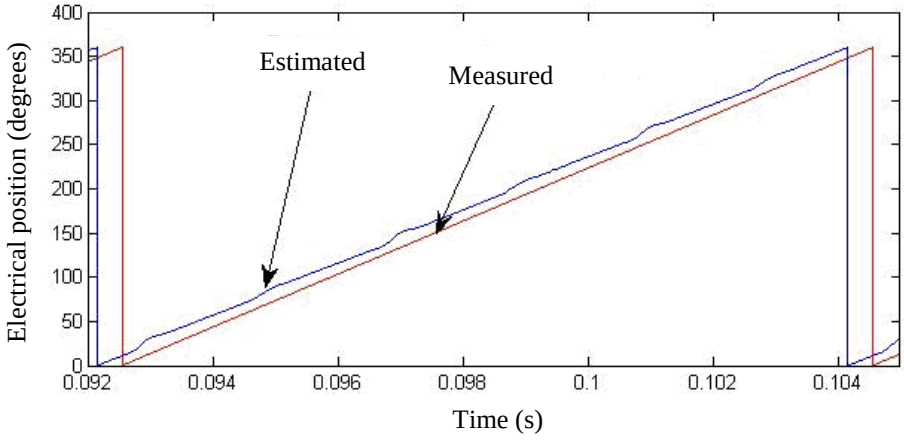

Fig. 5.13 Simulated measured and estimated electrical position with load.

5.3.3 Low pass flux-linkage estimator at load using measured torque feedback

The flux-linkage estimator performance works well for a fixed load. However, when the load is changing dynamically, the load angle will change. The error in position due to a sudden load change will cause an offset between the measured position and estimated position. From Fig. 5.13 the error between the measured and estimated electrical position can be calculated, as shown in Fig. 5.14. The flux-linkage position relative to rotor electrical position is calculated as (5.24). The load angle can be calculated from the measured torque as the torque constant is known. Using measured torque feedback to calculate the load angle and thus account for load offset, this is shown in Fig. 5.15 and Fig. 5.16 for a load of 7 Nm and a speed of 1000 rpm.

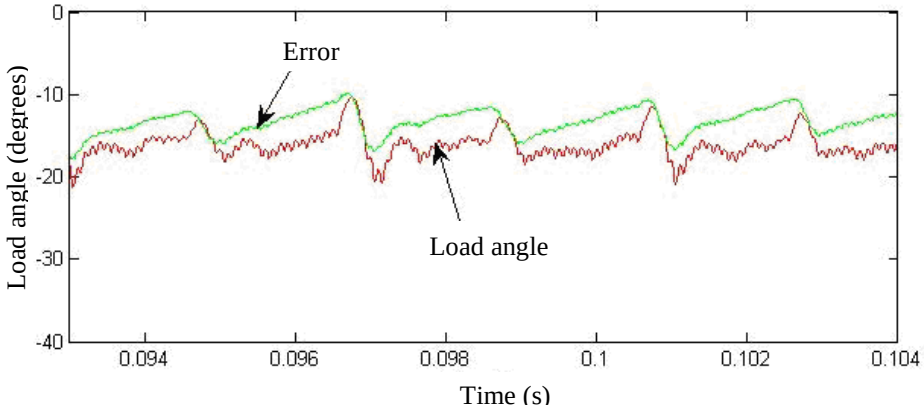

Fig. 5.14 Simulated load angle and error between measured and estimated electrical positions.

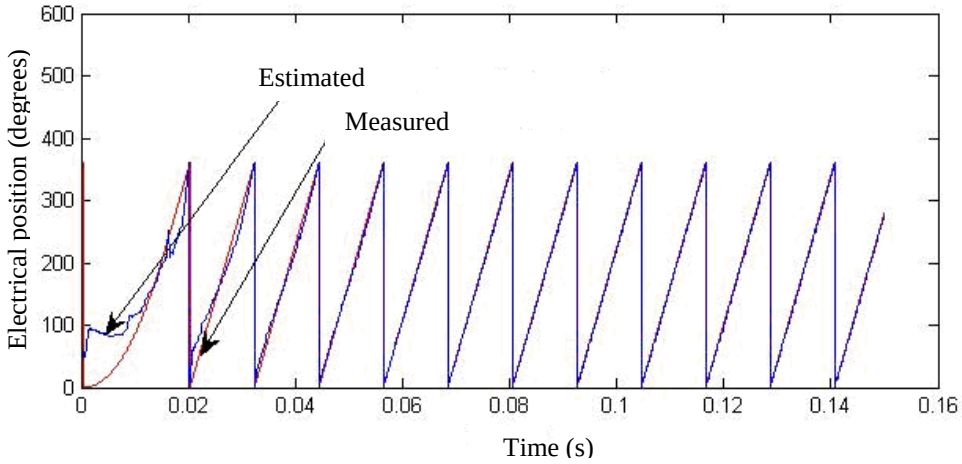

Fig. 5.15 Simulated estimated and measured electrical position with torque feedback.

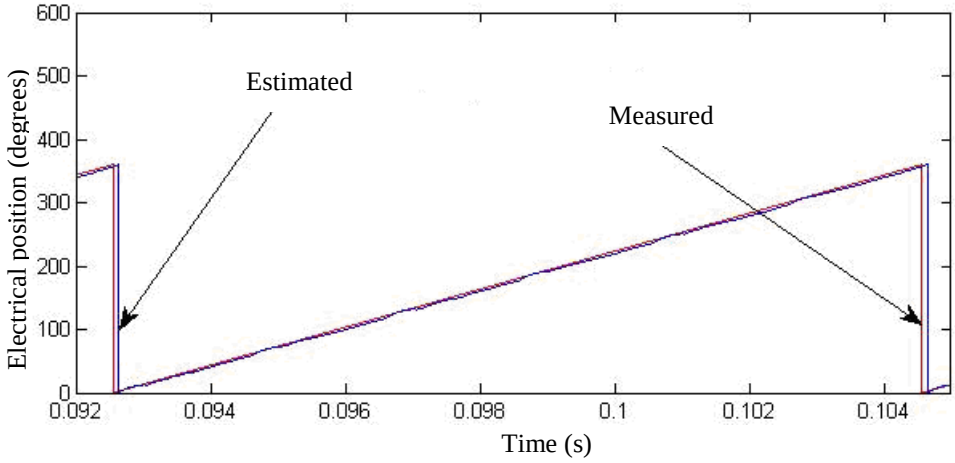

Fig. 5.16 Estimated and measured electrical position with torque feedback.

5.4 Experimental Results of Low pass Flux-Linkage Estimator

5.4.1 Flux-linkage estimation with and without measured torque feedback

Firstly the start-up routine discussed in chapter 2 and 4 is used to bring the machine up to threshold speed (150 rpm) then the flux estimation technique is used for estimating position from 150-1000 rpm. When there is no-load and the speed is at 1000 rpm the measured torque is shown in Fig. 5.17 relative to the measured mechanical and electrical position it can be seen that the load is varying from 1.0 to -1.0 Nm due to the mis-aliment problem discussed throughout the Chapters.

The estimated position using flux estimation technique with no-load is shown without and with measured torque feedback in Fig. 5.18. The error between the measured and estimated position with no-load is shown in Fig. 5.19, where it can be seen that the error when no measured torque feedback is used is 0.15 electrical radians which is an angular error of 2.4%, while when using the measured torque feedback is 0.08 electrical radians which is an angular error of 1.2%.

The second test is attaching a 1.25 Nm load to the machine. The measured torque, electrical and mechanical positions are shown in Fig. 5.20. The estimated position using flux estimation technique with 1.25 Nm load is shown in Fig. 5.21. The error between the measured and estimated position is shown in Fig. 5.22 where it can be seen that the error when no measured torque feedback is used is 0.22 electrical radians which is an angular error of 3.5 %, while when using the measured torque feedback is 0.18 electrical radians which is an angular error of 2.8%.

The third test is attaching a 2 Nm load to the machine. The measured torque, electrical and mechanical position is shown in Fig. 5.23. The estimated position using flux estimation technique with a 2 Nm load is shown in Fig. 5.24. The error between the measured and estimated position is shown in Fig. 5.25 where it can be seen that the error when no measured torque feedback is used is 0.26 electrical radians which is an angular error of 4.1%, while when using the measured torque feedback is 0.18 electrical radians which is an angular error of 2.8%.

The fourth test is attaching a 3 Nm to the machine. The measured torque, electrical and mechanical positions are shown in Fig. 5.26 and Fig. 5.27. The estimated position using flux estimation technique with a 3 Nm load attached is shown in Fig. 5.28, where it can be seen that the error when no measured torque feedback is used is 0.33 electrical radians

which is an angular error of 5.25 %, while when using the measured torque feedback is 0.15 electrical radians which is an angular error of 2.3%.

The fifth test is attaching a 5 Nm load to the machine. The measured torque, electrical and mechanical positions are shown in Fig. 5.29 and Fig. 5.30. The estimated position using flux estimation technique with a 5 Nm load attached is shown in Fig. 5.31, where it can be seen that the error when no measured torque feedback is used is 0.44 electrical radians which is an angular error of 7%, while when using the measured torque feedback is 0.14 electrical radians which is an angular error of 2.2%.

From the results presented and summarised in Table 5.1, it can be seen that as load increased the error between the measured and estimated electrical position, for example at 5 Nm the error was 0.44 electrical radians which is equal to 25 electrical degrees, causing a large torque ripple. However, when measured torque feedback is implemented the angular error was reduced to 0.15 radians and as the torque response is much improved.

Load (Nm)	electrical position error without measured torque feedback (radians)	electrical position error with measured torque feedback (radians)
No-load	0.15	0.08
1.25	0.22	0.18
2	0.26	0.18
3	0.33	0.15
5	0.44	0.14

Table 5.1 Error of load offset angle from measured electrical position.

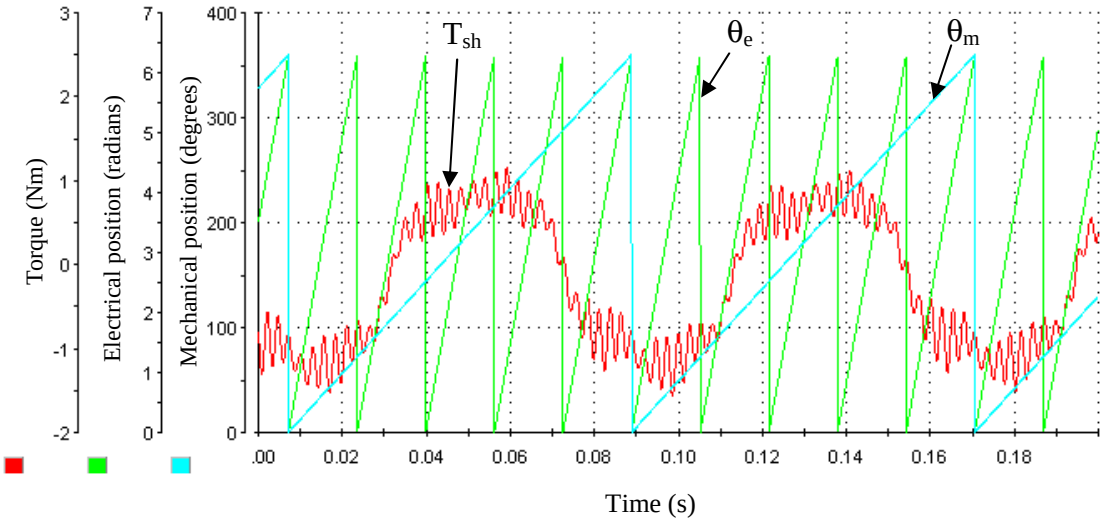

Fig. 5.17 Measured torque, electrical and mechanical positions with no-load.

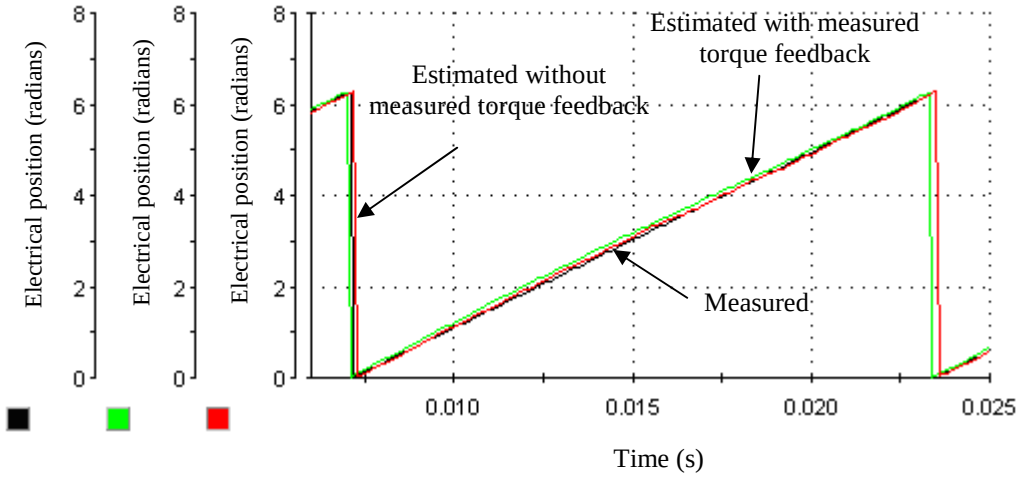

Fig. 5.18 Measured and estimated electrical positions with no-load.

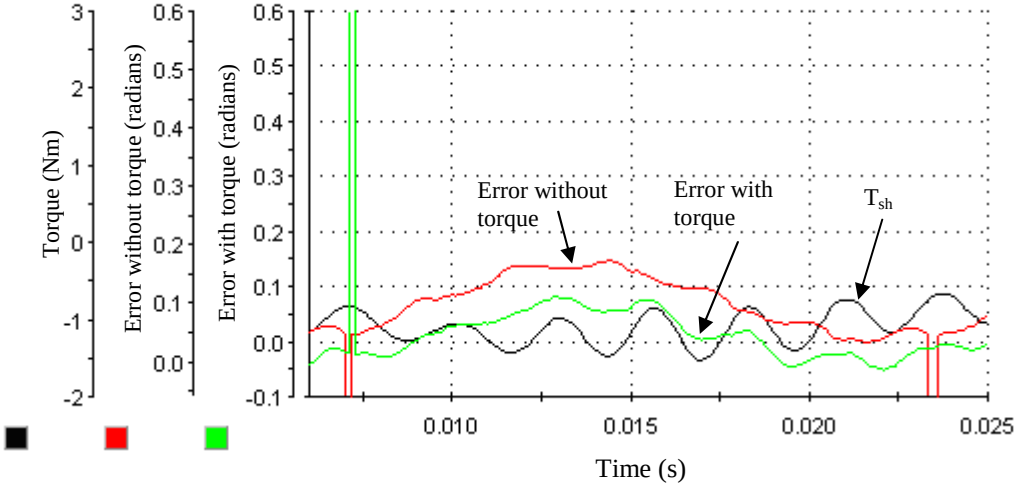

Fig. 5.19 Error of measured and estimated electrical position with no-load.

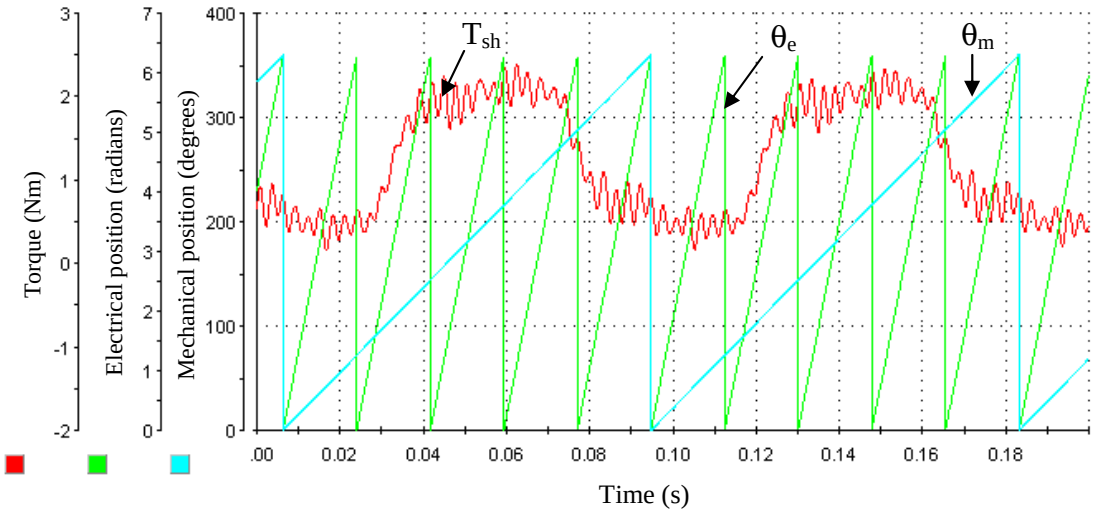

Fig. 5.20 Measured torque, electrical and mechanical positions with 1.25 Nm load.

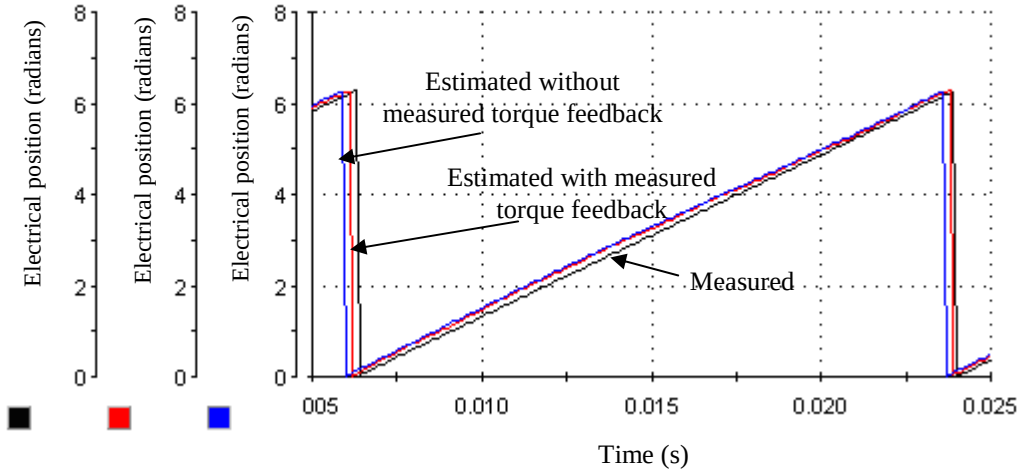

Fig. 5.21 Measured and estimated electrical position with 1.25 Nm load.

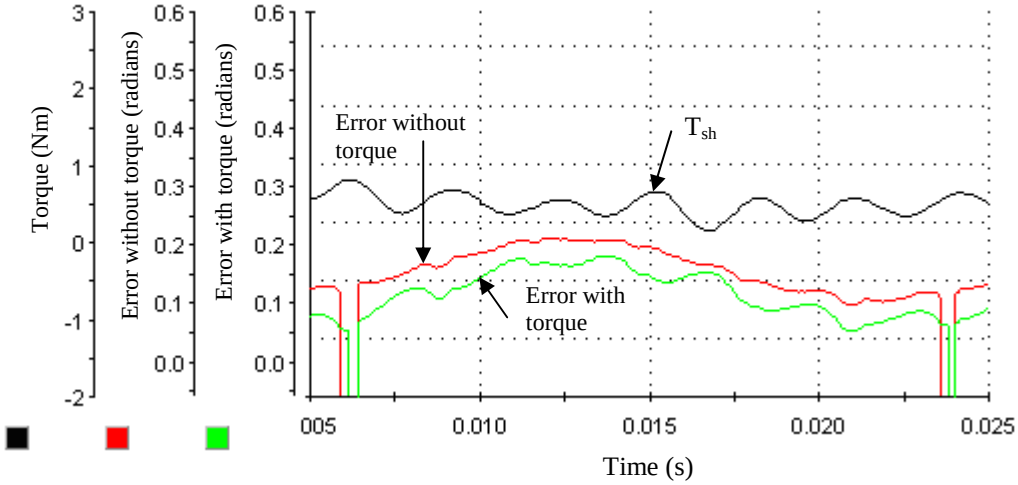

Fig. 5.22 Error of measured and estimated electrical positions with 1.25 Nm load.

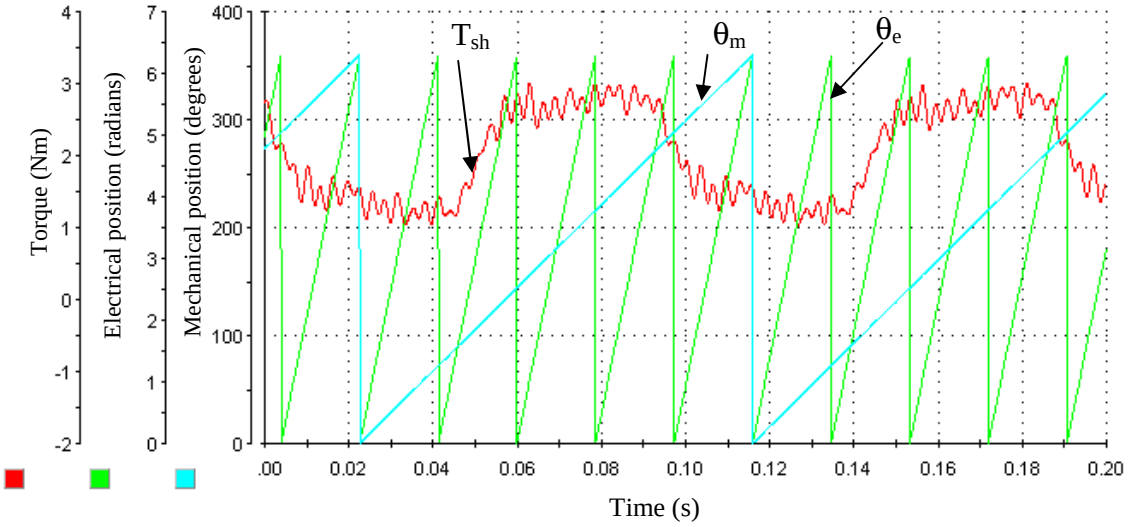

Fig. 5.23 Measured torque, electrical and mechanical position with 2 Nm load.

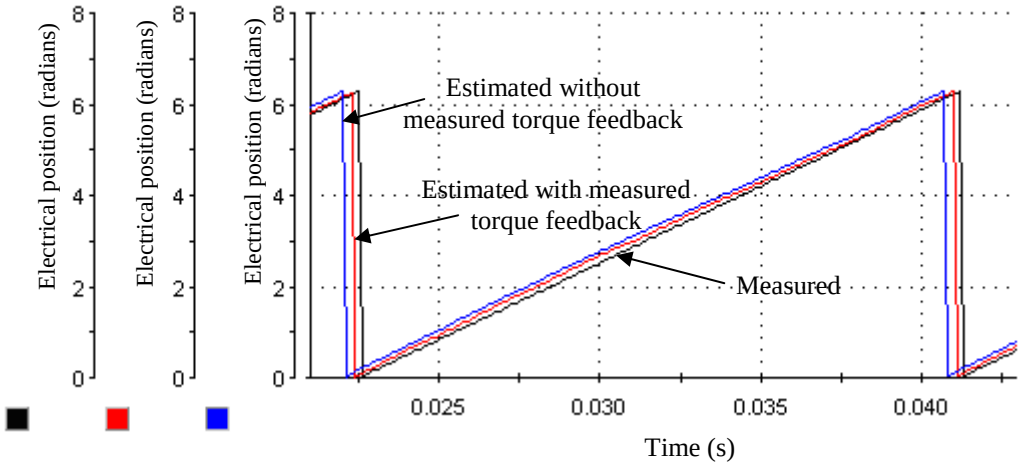

Fig. 5.24 Measured and estimated electrical positions with 2 Nm load.

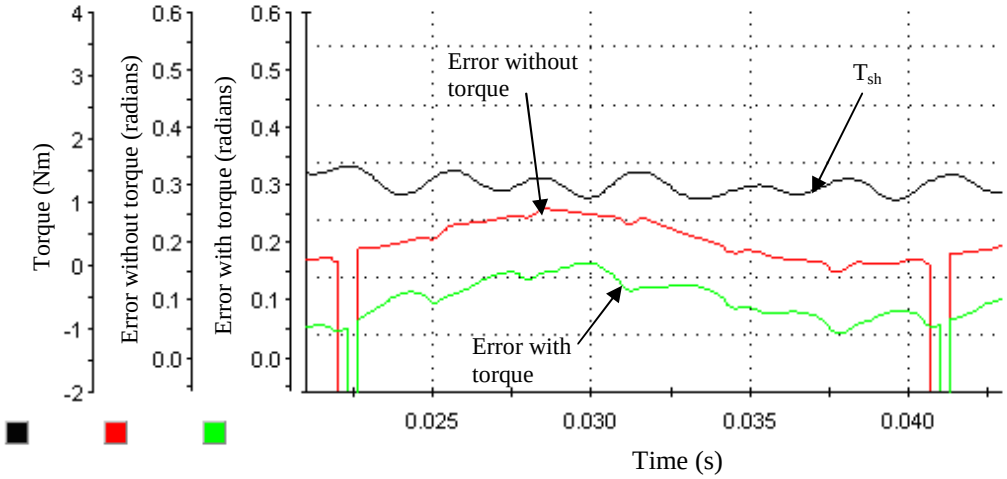

Fig. 5.25 Error of measured and estimated electrical position with 2 Nm load.

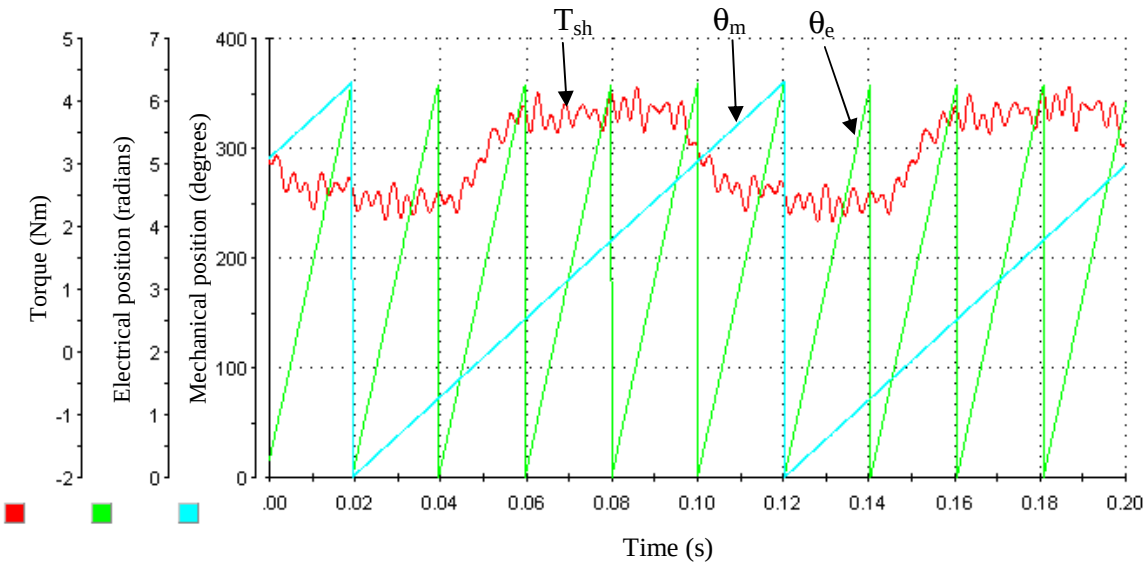

Fig. 5.26 Measured torque, electrical and mechanical position with 3 Nm load.

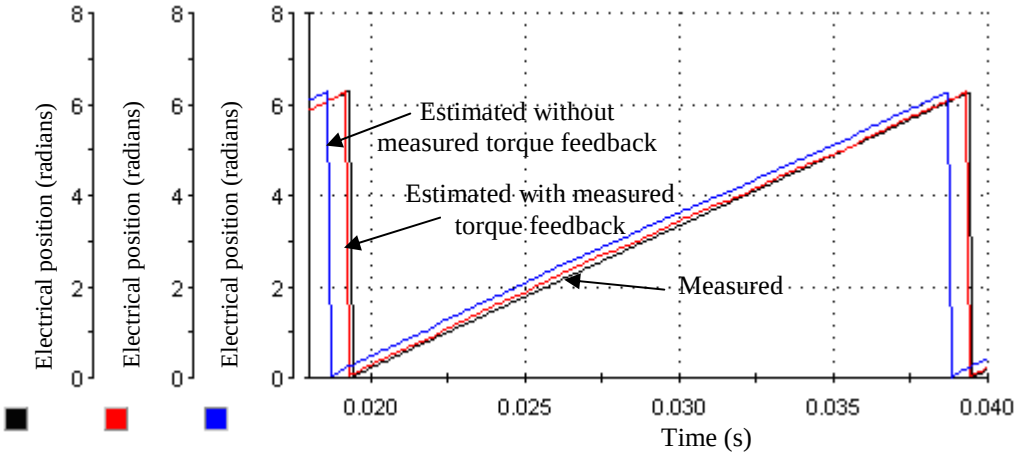

Fig. 5.27 Measured and estimated electrical positions with 3 Nm load.

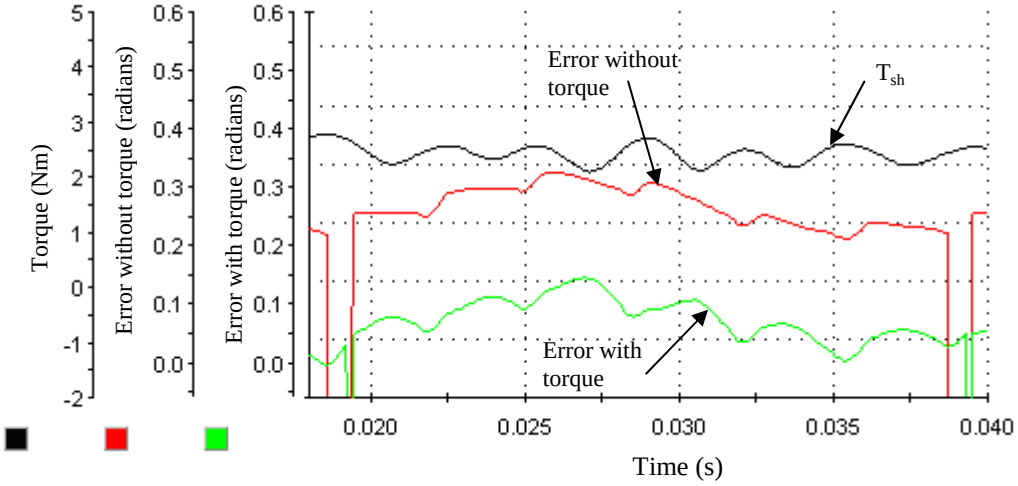

Fig. 5.28 Error of measured electrical and estimated electrical position with 3 Nm load.

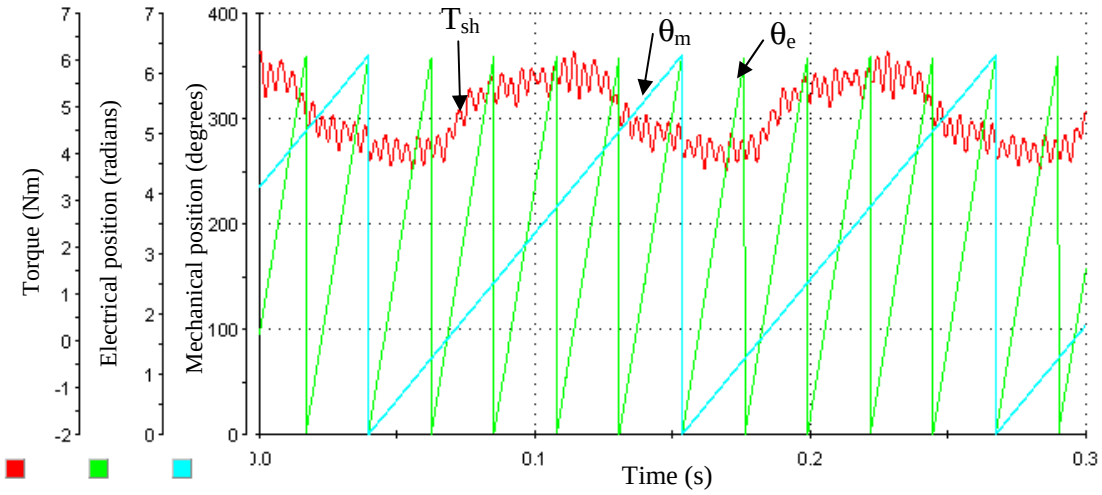

Fig. 5.29 Measured torque, electrical and mechanical position with 5 Nm load.

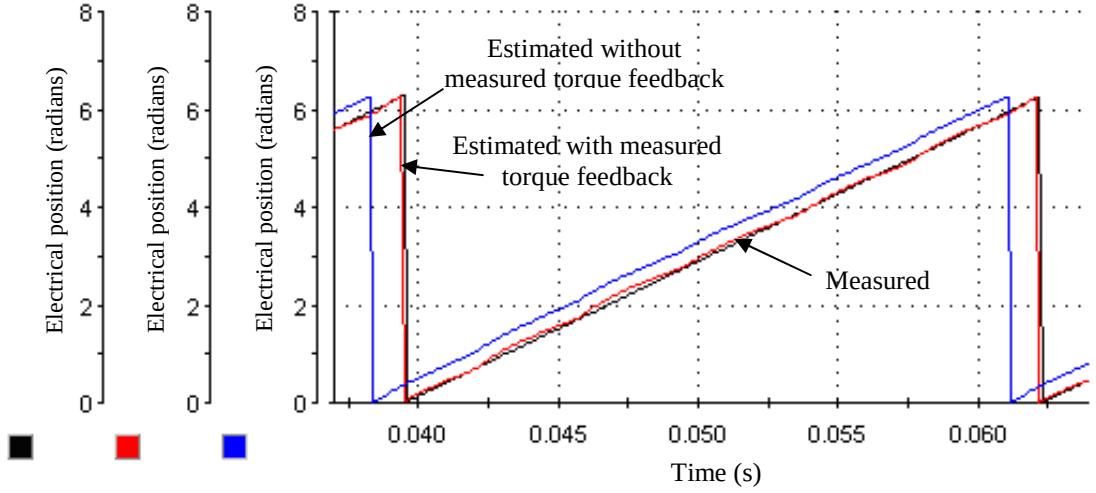

Fig. 5.30 Measured and estimated electrical positions with 5 Nm load.

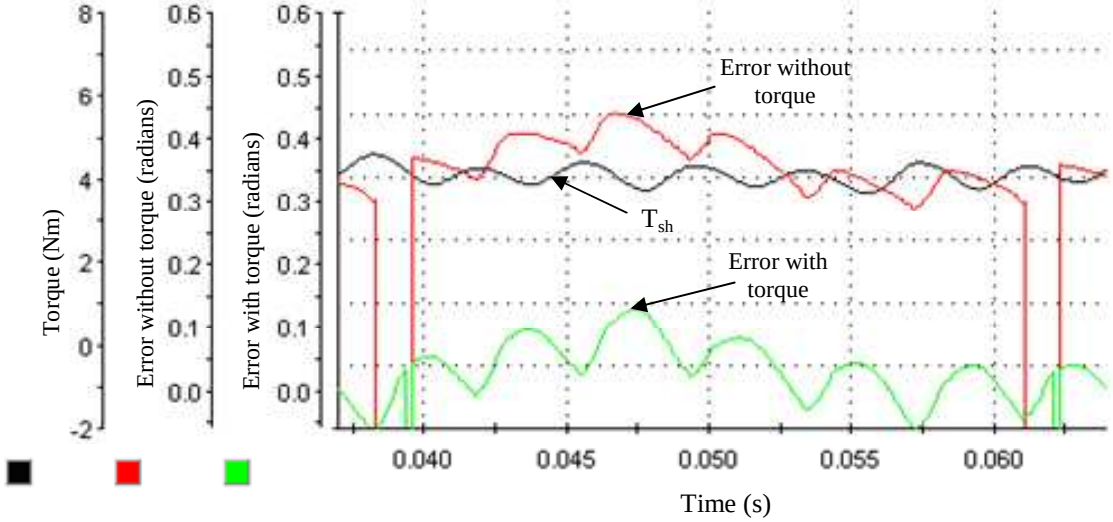

Fig. 5.31 Error of measured and estimated electrical position with 5 Nm load.

5.5 Number of Sensors

The systems described in this thesis so far needs at least 3 current and 3 voltage sensors, and a torque measurement device. The torque system described is a low cost system in mass production a SAW torque transducer cost $10 US [7]. The current and voltage sensors cost more than the torque sensor. Further cost reduction is possible for the system described by lowering the number current and voltage of sensors.

5.5.1 Single DC current sensor technique

The inverter used consists of six IGBT switches. The main application is motor control, thus information of the phase currents are very important for control protection against possible fault conditions like short circuit. The inverter typically has three phase current sensors and one DC link current sensor to have full information of the system. However, this approach is not economical so the three phase currents can be reconstructed by one single current measured in the drive system DC link [124-126].

The commutation sequence for a typical 3-phase BLDC motor is UV-UW-VW-VU-WU-WV and repeats from there on. Each phase is active for 120 electrical degrees. At any given time/step or commutation interval, there are only two phases active or conducting. The third phase is inactive or floating. This control technique has a built in dead-time and ensures that the two switches in the same phase-leg are not active at the same time. The switch control signal is applied to the upper and lower devices to control the current and voltage. There are two cases here that will be investigated for one sequence.

Case one: over-modulated is when two switches are conducting but there is no pulse width modulation (PWM), i.e. so-called over-modulated operation, phase UV sequence will be analysed, referring to Fig. 5.32, current flows from positive DC through the upper-side of the inverter bridge, U, to the machine winding across phases A and B, then passes through the low side of the bridge VV and to the negative DC. The arrows indicate the direction of current flow. In this case, the current through phase U is equal to the current through phase VV and equal the DC link current, prior to the main DC link capacitor: so by knowing that switch U is on and switch VV is on, then the phase current can be identified and set equal to the DC link current.

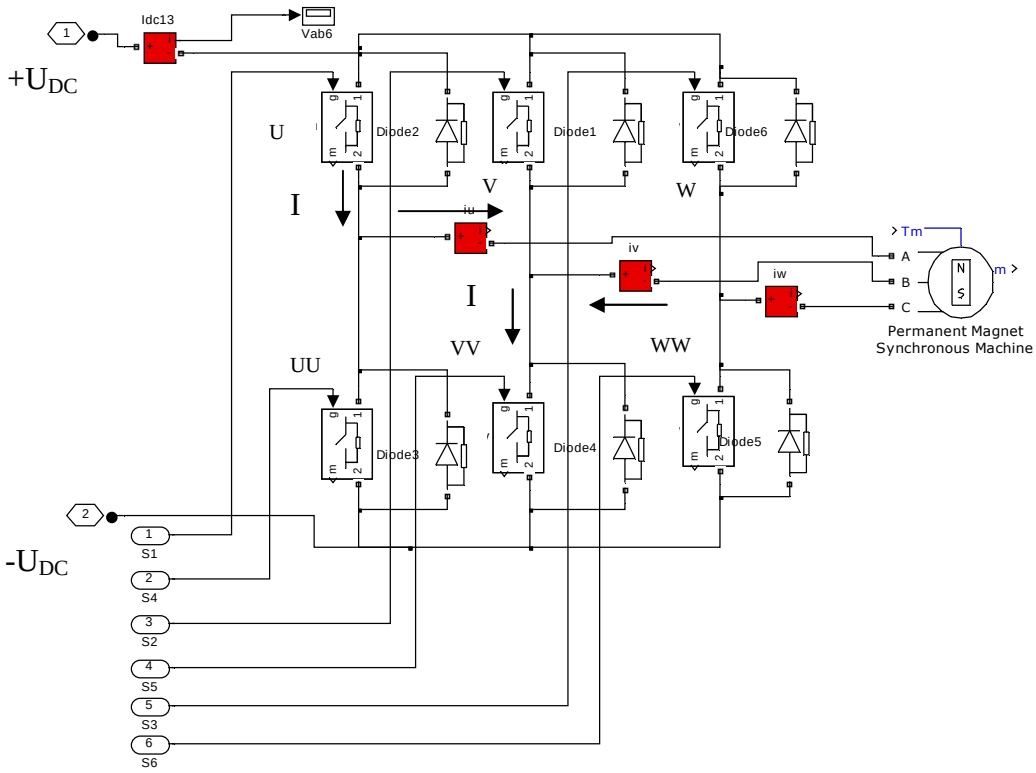

Fig. 5.32 Case one: UV excitation showing current direction.

Case two: PWM controlled considers the same two switches as in Case one, but the modulation index is less 1. The PWM will switch according to the current control set point, but the commutation sequence remains unchanged. When the PWM events open the main power switching devices current still flows due to the stored energy in the machine inductance. The current path is via the bridge diodes. The current will flow back to the supply, as shown in Fig. 5.33. In this case the current in the DC link will equal the inverse current. Tables 5.2 and 5.3 are derived from Case one and Case two for all switches the Tables equate the DC current to the phase current during the six commutation steps.

Three phase inverters used for machine control normally implement complete information about the three phase currents and the DC link current, to control the machine and also to protect against damaging over currents. The phase currents can be reconstructed from the current information in the DC link current and the system proposed the use one DC current measurement to control the machine.

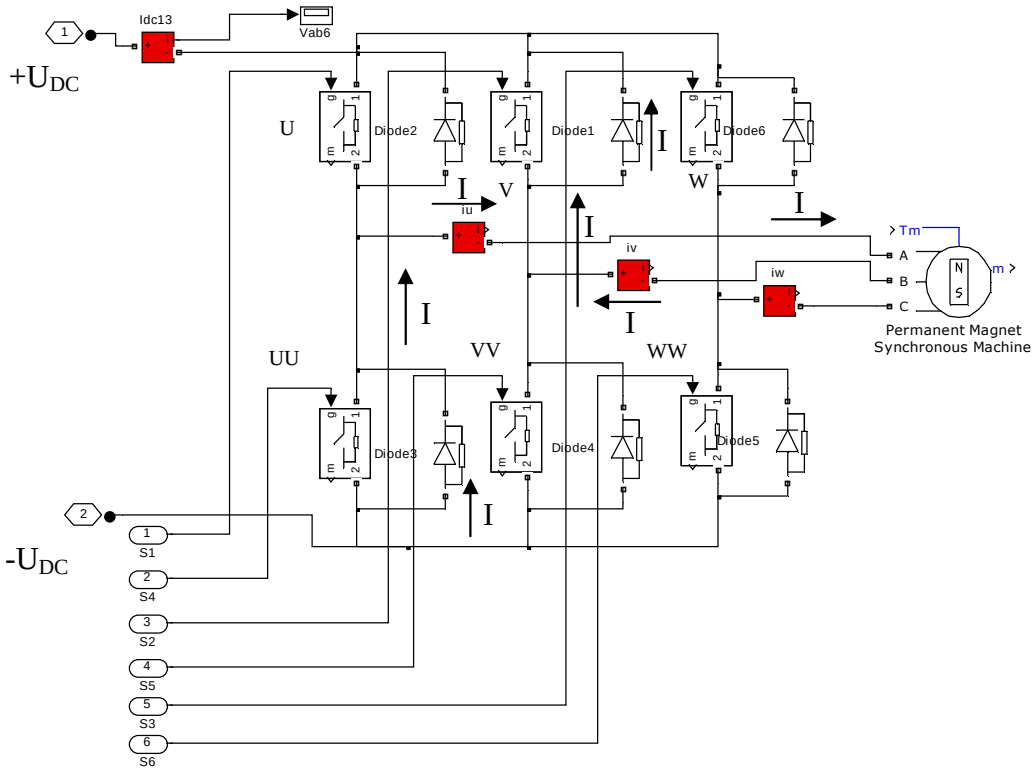

Fig. 5.33 Case two: UV excitation with two switches off, showing current direction.

5.5.2 Single DC voltage sensor technique

Estimation of the stator flux requires three stator terminal voltages sensors. However, the DC link voltage and the switching states of the six power devices of the inverter can be used to reconstruct the three terminals voltages [14]. The switching sequences are for brushless DC control. Fig. 5.47 and examining the voltage states when phase U and V are switched on, it can be seen from Kirchhoff voltage law that the DC link voltage can be equated to the phase voltage as:

$$u_u = \frac{1}{2}u_{DC} \tag{5.31}$$

$$u_v = -\frac{1}{2}u_{DC} \tag{5.32}$$

Tables 5.4 can be constructed if all switches sequences are considered.

Commutation sequence	i_u	i_v	i_w	Rotor position (degrees electrical)
UV	i_{DC}	$-i_{DC}$	0	30-90
UW	i_{DC}	0	$-i_{DC}$	90-150
VW	0	i_{DC}	$-i_{DC}$	150-210
VU	$-i_{DC}$	i_{DC}	0	210-270
WU	$-i_{DC}$	0	i_{DC}	270-330
WV	0	$-i_{DC}$	i_{DC}	330-30

Table 5.2 Relationship between DC-link and phase currents Case one.

Commutation sequence	i_u	i_v	i_w	Rotor position (degrees electrical)
UV	$-i_{DC}$	i_{DC}	0	30-90
UW	$-i_{DC}$	0	i_{DC}	90-150
VW	0	$-i_{DC}$	$-i_{DC}$	150-210
VU	i_{DC}	$-i_{DC}$	0	210-270
WU	i_{DC}	0	$-i_{DC}$	270-330
WV	0	i_{DC}	$-i_{DC}$	330-30

Table 5.3 Relationship between DC-link and phase currents Case two.

Commutation sequence	v_u	v_v	v_w	Rotor position (degrees electrical)
UV	$0.5V_{dc}$	$-0.5V_{dc}$	0	30-90
UW	$0.5V_{dc}$	0	$-0.5V_{dc}$	90-150
VW	0	$0.5V_{dc}$	$-0.5V_{dc}$	150-210
VU	$-0.5V_{dc}$	$0.5V_{dc}$	0	210-270
WU	$-0.5V_{dc}$	0	$0.5V_{dc}$	270-330
WV	0	$-0.5V_{dc}$	$0.5V_{dc}$	330-30

Table 5.4 Relationship between DC-link and phase voltages.

5.5.3 Experimental results

The relationship of the DC current and switches sequence to the three phase currents is shown here via experimental results for the reduced sensor method. Fig. 5.34 shows the measured mechanical position, electrical position, and measured torque for a step change in load torque from 0 to 2 Nm at 0.53s. Fig. 5.35 shows the measured electrical position compared with (i) electrical position estimated using three current, three voltage sensors and one SAW torque sensor and (ii) only one DC current, one DC voltage sensor and one SAW torque sensor.

Fig. 5.36 illustrates the three measured phase currents during the transient response. The measured DC current is shown in Fig. 5.37. The estimated three phase currents, from the measured DC current, is shown in Fig. 5.38. The DC current when there is no-load goes slightly negative due to the reversal diodes in the power inverter. The estimated three currents from the DC current are delayed due to the low pass filtering of the signal. Fig. 5.36 illustrates the three measured phase voltages during the transient response which at speed 1000 rpm a load was added of 3 Nm, the estimated three phase voltages are shown in Fig. 5.39. There is a delay of 5 ms between the measured and estimated voltages due to the low pass filter.

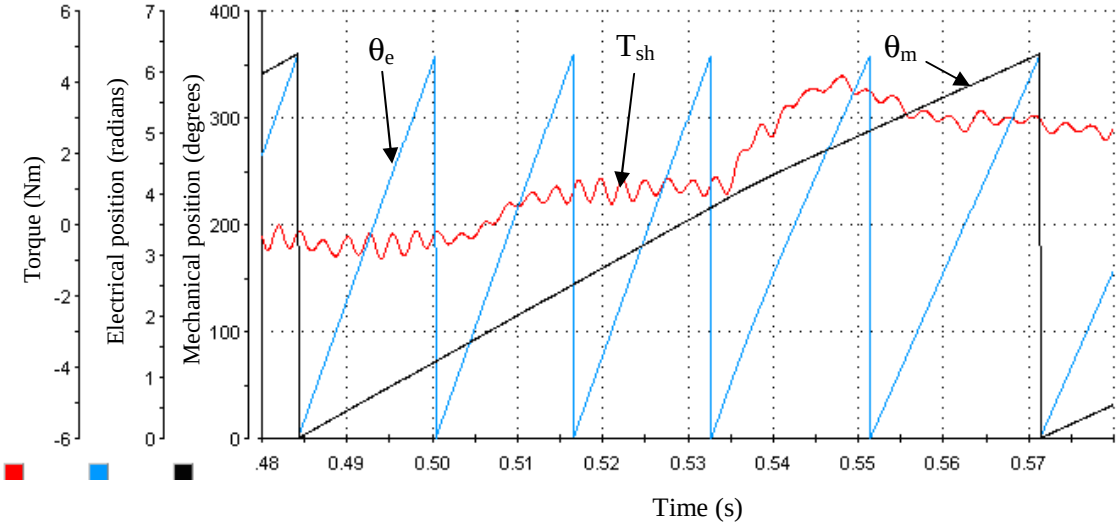

Fig. 5.34 Measured torque, mechanical and electrical positions during step load of 3 Nm at speed of 1000rpm.

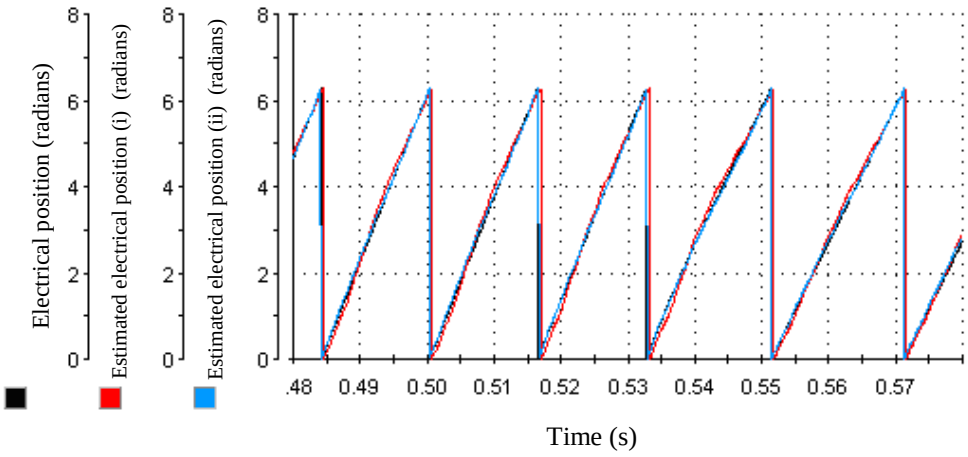

Fig. 5.35 Estimated electrical position with reduced sensors.

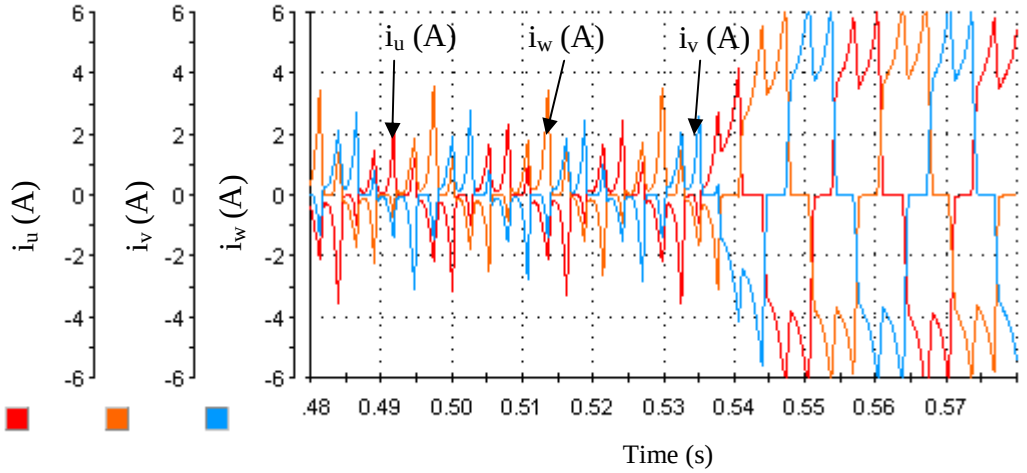

Fig. 5.36 Measured three phase current during transient response.

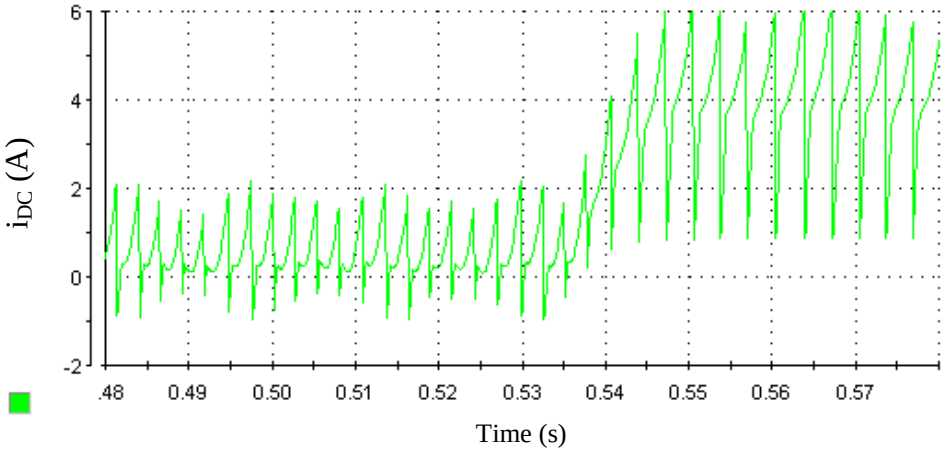

Fig. 5.37 Measured DC current during transient response.

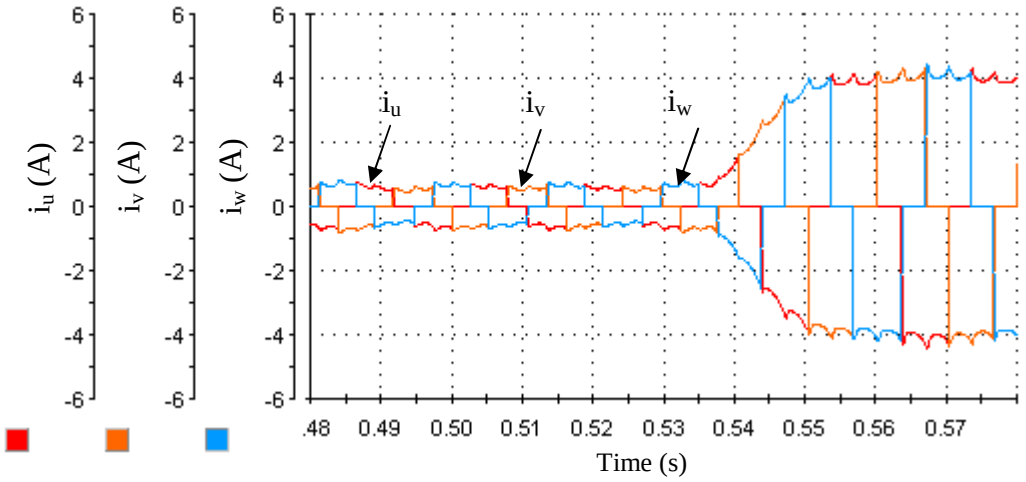

Fig. 5.38 Generated three phase currents during transient response from the DC current.

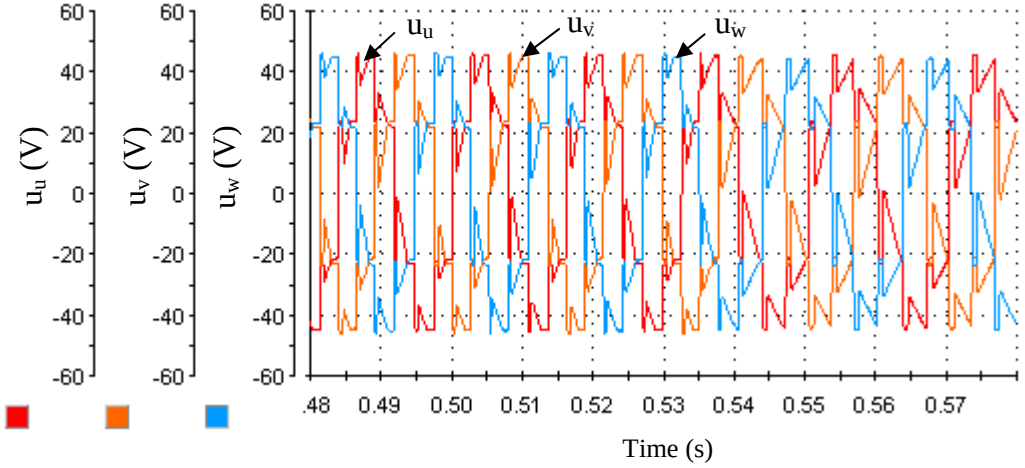

Fig. 5.39 Measured three phase voltages during transient response.

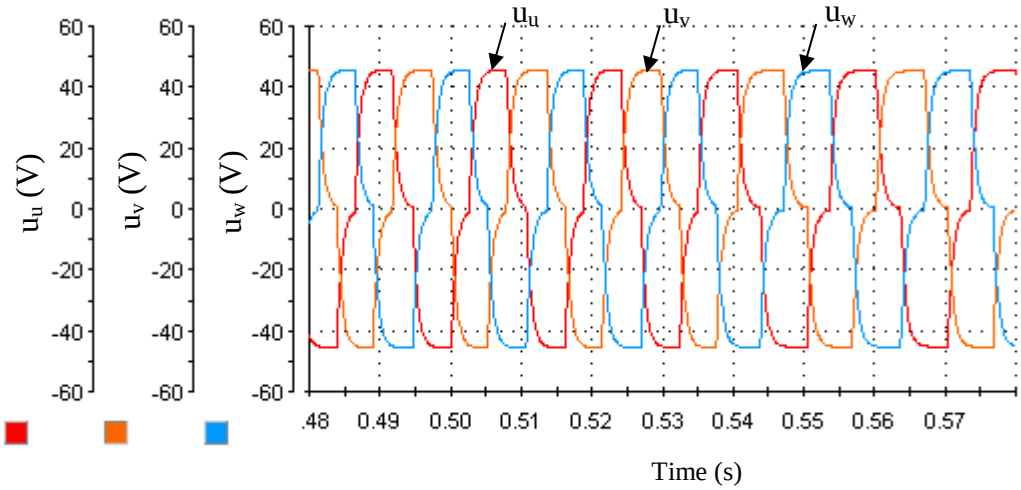

Fig. 5.40 Generated three phase currents during transient response from the DC current.

5.6 Summary

This Chapter discussed a simple rotor position sensorless control technique that is employed above the threshold speed of 150 rpm. When the machine exceeds the threshold speed a flux estimation technique is enabled to estimate the position. Firstly, the flux estimation is discussed, and then simulated. The standard flux estimation worked for no-load and could not work for varying loads. Here, the load angle effect on position was shown in simulation then it has been illustrated in test rig. This was further shown in simulation that by adding load, the load angle got larger. When using the measured torque feedback the position error was improved.

The second part of this Chapter was validation of the simulation study via experimental results. Firstly, the electrical position with no-load was estimated, then the test repeated for increasing load. Five different load conditions without measured torque feedback were considered. The position estimation error increased for increasing load. Measured torque feedback was used to measure the load angle and the same five cases were repeated with measured torque feedback. In all of the five load conditions with measured torque feedback, a reduced error (within 2% error) was measured.

Then the last two sections of this Chapter focused on reducing the number of sensors in a BLDC machine drive-system. Then experimental results were presented showing control of the machine using one DC link current and one DC link voltage sensor and an integrated SAW torque transducer.

CHAPTER 6

CONCLUSIONS AND FUTURE WORK

6.1 Review of Presented Work

This Chapter concludes the work presented in this thesis. To begin with this section summarises the work discussed in Chapters 1-5, with Section 6.2 describing the conclusions drawn from this work. Section 6.3 outlines the novelty of the work carried out and lists the publications that have been a direct result of this work.

- Chapter 1, this Chapter discussed the BLPM drive systems, the BLPM drive systems require rotor position (angle) feedback to effectively control phase current and optimise torque per ampere. The position feedback schemes reported in the literature are summarized in the flowchart illustrated in Fig. 1.23. Sensorless control strategies for the BLPM machines are generally based on calculating position from the machine parameters, via measurement of terminal voltages and currents. All of the main sensorless control strategies for detecting rotor position have been reviewed in this Chapter, as presented in Table 1.1. The table left-hand column links to the relevant references in the right-hand column. The compilation of this table was undertaken to try to collect the main techniques, the applicable drive systems (BLDC or AC), the existence of experimental validation and an audit of the required sensors into one overview. The table is not claimed to be exhaustive, but serves to highlight prior research effort with that of the research reported in this thesis. Position sensors such as absolute or incremental encoders, or resolvers and there associated circuitry have disadvantages in that they contain delicate parts that makes them sensitive to

mechanical abuse and temperature. Oil, dirt or dust can harm or contaminate the encoder disk. Gratings, may also be broken by shock loads or sustained vibrations. The LED and photo detectors are also sensitive to mechanical and electrical disturbances. Brushless resolvers are relatively robust, but the associated resolver-to-digit converter electronics is complex and generally a high cost components in the drive system. The main issue with back-EMF detection schemes is that they do not work at zero and low speeds, they require at least three voltage and two current sensors and a comparator circuit to sense the neutral voltage, or free wheeling diode circuit which necessitates additional isolated power supplies. These techniques are sensitive to speed and load changes which can cause instabilities. There is also is a delay between actual and estimated positions which must be predetermined. In the flux-linkage estimation methods the main disadvantages are used: the machine parameters, hence sensitivity to parameter variations due to temperature load (saturation) etc. These estimation techniques require two current and two voltage sensors. The load torque must be estimated by a look-up table or torque estimation technique to estimate the load angle offset. Moreover, zero and low speed operation is not possible. The disadvantage of observers is that they do not work at zero and low speed. The common problem for all observers is that if the currents and voltages are DC there will not be enough information for position estimation. The need for a detailed electrical model of the machine so that the error signal can be constructed from the measured and estimated states leads to increased computation requirements. The machine electrical parameters, the inductance, resistance and back-EMF coefficient are required, but load torque information is also necessary to consider the steady state error due to parameter perturbations. A loss of the observer stability will results in erratic and possibly destructive machine operation. The variation in inductance and machine modifications techniques are similar since they require machines to be specifically designed or modified to exhibit saliency. The main advantage of this method is that position can be estimated at zero and low speed. However, inductance variation for rotor position estimation is complicated: in a surface mounted magnet machine since there is no saliency so any variation of winding inductances with rotor position arises from magnetic saturation, the back-EMF dominates the rate-of-change in the current, the variation of incremental inductances with rotor position undergoes two cycles per electrical cycle causing an ambiguity in sensed position, the distortion due to the nonlinearities of the inverter, and due to load offsets and noise caused by signal injection. Other techniques such as fuzzy logic and neural networks have similar issues to observers techniques. The

unique topology of the matrix converter provides additional advantages over a two-level inverter in that it is capable of applying smaller input voltages to the machine when the position measurement is needed at low speed, but not at zero speed. Finally, direct torque control is similar to closed-loop flux-estimator schemes. Sensorless position techniques behave poorly, if at all, at zero and low speeds (0-300rpm) and load torque must be estimated to know the load angle offset. In all the position sensorless techniques researched [18-110], at least two current and one voltage sensor are required to establish closed-loop control and for estimation of position.

- Chapter 2, This Chapter has investigated and developed a procedure that uses measured torque feedback to estimate zero and low speed position without using other rotor position sensors. The zero speed position estimation has been divided into four routines, of which only three need actual torque measurement. The first routine discussed how the zero speed position can be estimated with the machine stationary. Here, the electromagnetic torque was less than the load torque for all rotor positions. The second routine discussed how the zero speed position can be estimated when the machine is free to rotate but there is no-load connected. The third routine discussed is implemented when the electromagnetic torque is larger than the load torque, and the load torque is less than a threshold torque (as defined in the Chapter). Finally, the fourth routine is implemented when the electromagnetic torque is larger than the load torque, and the load torque is larger than the threshold torque. Routine one is the best between the four routines since it can start the machine from stand-still without rotation. After determining the zero position, low speed control has been discussed to illustrate how at low speed the BLPM can be controlled using measured torque feedback.

- Chapter 3, This chapter characterised a position sensor then investigated the parameters of Unimotor brushless PM machine, then characterised the cylindrical torque transducer and finally characterised the prototypes brushless PM machine with the integrated torque transducer. The Unimotor manufacturer's parameters that were examined are the resistance, the inductance, the back-EMF and the torque constant. The resistance was 22% increased due to rated temperature. The inductance was different since it was stated that the unimotor is a surface mounted PM machine and the saliency should be between 11.97 to 14.63 mH. The manufacturer quoted the inductance is 13.3 +-10% while when using an LCR meter clearly showed the

inductance was 13.5 to 22 mH, which is not as the manufacturer gave but it clearly shows that it's a 6-pole machine. The back-EMF given by the manufacturer was 98 V_{rms} whilst the measured back-EMF test was 95 V_{rms}, which are very close to each other. The torque constant that was given by the manufacturer was 1.6 Nm/A while when investigated by using the SAW torque sensor and the results of the torque sensor was 1.65 Nm/A but that could be due to load in the system such as the cogging torque. The second characterisation was for the cylindrical torque SAW sensor. There was drift where the torque is offset after a certain time. This can be taken care off by zeroing the display and adjusting the offsets before an experiment started. There was noise in the system but the max amplitude was 30 mV which will contribute 0.6% error. The torque sensors static test showed that there was a 5% error between actual and measured torque and this also can be taken care off as by offset. The prototype brushless PM machine was investigated. There was no manufacturer's data given for it. The resistance test was concluded to know the value of the resistance. The inductance was measured. It was noticed that the measured inductance had different amplitudes, which means that the machine is an asymmetric machine. The back-EMF test was done and the back-EMF line voltage was measured at 1000 rpm and is equal to 67 V_{rms}. The torque constant was also obtained and was shown to be equal to 1 Nm/A. The integrated SAW sensor was also analysed. There was noise which causes 0.6% error. There was a load in the shaft with no excitation which could be due to misalignment. The torque excitation was shown for three level of excitation and the magnitudes increased linearly. The excited torque when subtracted from the non excited torque in the system outputs a better waveform. There was a delay of 1.5 ms mainly due to the digital low-pass filter.

- Chapter 4 has discussed the experimental implementation of the start-up procedure developed in Chapter 2. The torque start-up using for the Unimotor PM machine was then discussed and shown to similar to the idealised machine model discussed in Chapter 2, due to the high quality of manufacture of this machine. The prototype machine was then investigated and the no-load torque characterised. It was noted that there was a load on the system that may have been caused by an internal-misalignment. This was considered as a disturbance torque on the system. The zero speed estimation procedure was implemented to control the prototype machine via DSpace. The first routine showed the zero position estimation error was within 1% when implemented via DSpace. Then the second routine settled to around 30 electrical degrees. The third routine settled between 0 and 30 electrical degrees as the load increased the position

offset toward 0 electrical degrees. The fourth routine predicted the position between two sectors.

Low speed control was investigated firstly by implementing open-loop brushless DC and then using measured torque feedback to make it closed-loop resulting in improved control of the machine at low speed. With the procedures developed machine control can be realised from zero and low speed with all load conditions by using measured torque feedback.

- Chapter 5, This Chapter discussed a simple rotor position sensorless control technique that is employed above the threshold speed of 150 rpm. When the machine exceeds the threshold speed a flux estimation technique is enabled to estimate the position. Firstly, the flux estimation is discussed, and then simulated. The standard flux estimation worked for no-load and could not work for varying loads. Here, the load angle effect on position was shown in simulation then it has been illustrated in test rig. This was further shown in simulation that by adding load, the load angle got larger. When using the measured torque feedback the position error was improved.

  The second part of this Chapter was validation of the simulation study via experimental results. Firstly, the electrical position with no-load was estimated, then the test repeated for increasing load. Five different load conditions without measured torque feedback were considered. The position estimation error increased for increasing load. Measured torque feedback was used to measure the load angle and the same five cases were repeated with measured torque feedback. In all of the five load conditions with measured torque feedback, a reduced error (within 2% error) was measured.

  Then the last two sections of this Chapter focused on reducing the number of sensors in a BLDC machine drive-system. Then experimental results were presented showing control of the machine using one DC link current and one DC link voltage sensor and an integrated SAW torque transducer.

6.2 Future Work

This research could pave the way for further research in this area ways:

6.2.1 Challenges in measured torque feedback control

The SAW torque transducer has drift and noise problems which contributed 0.6 Nm error. This error is due to the amplifier system as discussed in the thesis. The system can be further enhanced if these drift and noise problems can be reduced. One option would be to test the new SAW torque transducer which requires only a USB wire without the need for the display unit and according to the manufacture exhibits lower noise and has no drift problems. If this is the case it will be interesting to develop a full torque observer, as ideally if the machine is excited knowing the zero speed position a positive torque will be generated, the torque will increase until a certain position then decrease, at that instant the next switch should change. The noise and drift problems on the torque signal has prevented such an observer being designed.

6.2.2 Applications to other machines

The application of the SAW torque transducer was investigated in this work on a three phase BLPM. Industry is now focusing on multi phase BLPM machines which can loose a phase and still can be controlled. It will be interesting to investigate the performance of the SAW torque sensor with a multi phase machine. Another area where the SAW sensor based control could be used would be in the control of switched reluctance machines.

6.2.3 Reduced sensors implementation

The system noise due to using one DC current and one DC voltage sensor can be reduced if the whole system is built in one package. The interesting part here is that the DC current sensor should be positioned between the inverter switches and the DC capacitor, taking up space, however the distance between the switches and the capacitors should be minimized to reduced sensor noise. Implementing the reduced sensor control is challenging as system noise and control performance need to be carefully examined.

6.3 Area of Novelty and Publications

The following aspects of the work presented in this thesis are novel:

- The use of measured torque feedback to control the BLPM machine drive without a position sensor at zero speed to high speed.
- There are only four possible zero speed position estimation for all load condition, routine one electromagnetic torque less the load torque does not rotate, routine two electromagnetic torque larger then load torque and there is no-load (rotate), routine three electromagnetic torque larger then load torque and there is load that is less then threshold torque (rotate), routine four electromagnetic torque larger then load torque and there is load that is larger then threshold torque (partial rotate).
- Low speed control using measured torque feedback at different load conditions.
- Flux-linkage position estimation using measured torque feedback using three current and three voltage sensors then reducing the number of sensors to one DC current and one DC voltage sensor.

The following publications have resulted from the work presented in this thesis, to-date:

- F. Alrifai, N. Schofield, “Control of PM Machines with Non-contact Measured Torque Feedback,” 14th International Conference EPE-PEMC 2010, pp. 1-6, September 2010.

- F. Alrifai and N. Schofield, “Control of brushless PM machines using measured torque feedback,” International Symposium on Power Electronics Electrical Drives Automation and Motion (SPEEDAM2010), Vol., No., pp. 996-1001, June 2010.

- E. Peralta-Sanchez, F. Alrifai and N. Schofield, “Direct Torque Control of permanent magnet motors using a single current sensor,” IEEE International Conference on Electric Machines and Drives Conference, IEMDC '09., pp. 89-94, 3-6 May 2009.

REFERENCES

[1] T.M. O'Sullivan, "Enhanced performance of servo-drive systems by shaft-torque feedback," Ph.D thesis in the Department of Electronic and Electrical Engineering, The University of Sheffield, January 2005.

[2] T.M. O'Sullivan and N. Schofield, "Simulation and experimental validation of induction machine dynamics driving multi-inertial loads," International Journal of Applied Electromagnetic and Mechanics, Vol. 19, pp. 231-236, 2004.

[3] T.M. O'Sullivan and N. Schofield, "Improved performance of motor-drive systems by SAW shaft torque feedback," Journal of the Institute of Measurement and Control, Vol. 37/9, pp. 276-282, 2004.

[4] T.M. O'Sullivan and N. Schofield, "High-performance control of dual-inertia servo-drive systems using low-cost integrated SAW torque transducers," IEEE Industrial Electronics, Vol. 53, Issue 4, pp. 1226-1237, June 2006.

[5] A. Lonsdale, "Dynamic rotary torque measurement using surface acoustic waves," Sensors Magazine, Vol. 18, pp. 51-56, October 2001.

[6] A. Pohl and F. Seifert, "Wirelessly Interrogable Surface Acoustic Wave Sensors for vehicular applications," IEEE Transaction on Instrumentation and Measurement, Vol. 46, pp. 1031-1038, August 1997.

[7] Sensor Technology Ltd, Torque Transducers, website reference: www.sensors.co.uk, last accessed June 2010.

[8] Richard Crowder, "Electric drives and electromechanical system," Book, Elsever, Oxford OX2 8DP, ISBN: 0750657578, 2006.

[9] "Things you need to know about sizing and applying Resolvers," Motion System Design, website site reference: www.motionsystemdesgin.com, last accessed March 2009.

[10] "What is a resolver?," Advanced Micro Control, website site reference: http://www.amci.com/tutorials/tutorials-what-is-resolver.asp, last accessed October 2010.

[11] T. Katagiri, T. Momose and H. Mizumoto, "An integrated single-output signal encoder for both multi-turn absolute encoder use and incremental encoder use," Conference Record of the IEEE Industry Applications Society Annual Meeting, Vol. 1, No. 1, pp. 347-351, 2-6 Oct. 1994.

[12] J. Christensen, "Selecting optical encoders," Motion System Design, website reference: www.motionsystemdesign.com, last accessed June 2006.

[13] J. R. Frus and B. C. Kua, "Closed-loop control of step motors using waveform detection," Proc. Int. Conf. Stepping Motors and Systems, Leeds, U.K., pp. 77-84, 1976.

[14] Peter Vas, "Sensorless Vector and direct torque control," Book, Oxford science publications, Oxford OX2 6DP, ISBN: 019858564651, 1998.

[15] C. Pepin, "Hall sensors on the move," motion system design, website site reference: www.motionsystemdesign.com , last accessed September 2009.

[16] P.P. Acarnley and J.F. Watson, "Review of position-sensorless operation of brushless permanent-magnet machines," IEEE Transactions on Industrial Electronics, Vol. 53, No. 2, pp. 352- 362, April 2006.

[17] P. Pillay, R. Krishnan, "Application characteristics of permanent magnet synchronous and brushless DC motors for servo drives," IEEE Transactions on Industry Application, Vol. 27, No. 5, pp. 986-996, Oct. 1991.

[18] K. Iizuka, H. Uzuhashi, M. Kano, T. Tsunehiro Endo and K. Mohri, "Microcomputer Control for Sensorless Brushless Motor," IEEE Transactions on Industry Applications, , Vol. IA-21, No. 3, pp. 595-601, May 1985.

[19] S. Jianwen, D. Nolan, M. Teissier and D. Swanson, “A novel microcontroller-based sensorless brushless DC (BLDC) motor drive for automotive fuel pumps,” IEEE Transactions on Industry Applications, Vol. 39, No. 6, pp. 1734- 1740, Dec. 2003.

[20] Y. Amano, T. Tsuji, A. Takahashi, S. Ouchi, K. Hamatsu and M. Iijima, “A sensorless drive system for brushless DC motors using a digital phase-locked loop,” Electr. Eng. Jpn., Vol. 142, No. 1, pp. 57 - 66, 2003.

[21] P. Ching-Tsai and E. Fang , “A Phase-Locked-Loop-Assisted Internal Model Adjustable-Speed Controller for BLDC Motors,” IEEE Transactions on Industrial Electronics, Vol. 55, No. 9, pp. 3415-3425, Sept. 2008.

[22] P. Ferrais, A. Vagati, and F. Villata, “P.M. brushless motor drives: a self commutation system without rotor-position sensor,” Proceeding of the ninth annual symposium on incremental motion control systems and devices, Vol. 1, No. 1, pp. 305-312, June 1980.

[23] M. Nagata and S. Yanase, “Control apparatus for brushless motor,” US Patent Number: 4641066, February 1987.

[24] J.C Moreira , “Indirect sensing for rotor flux position of permanent magnet AC motors operating over a wide speed range,” IEEE Transactions on Industry Applications, Vol. 32, No. 6, pp. 1394-1401, Dec. 1996.

[25] J.X. Shen, Z.Q. Zhu and D. Howe, “Sensorless flux-weakening control of permanentmagnet brushless machines using third-harmonic back-EMF,” IEEE International Electric Machines and Drives Conference IEMDC'03., Vol. 2, 1229- 1235, June 2003.

[26] T.M. Jahns, R.C. Becerra and M. Ehsani, “Integrated current regulation for a brushless ECM drive,” IEEE Transactions on Power Electronics, Vol. 6, No. 1, pp. 118-126, Jan. 1991.

[27] R.C. Becerra, T.M. Jahns and M. Ehsani, “Four-quadrant sensorless brushless ECM drive,” Sixth Annual Conference Proceedings on Applied Power Electronics Conference and Exposition APEC '91, pp. 202-209, March 1991.

[28] S. Ogasawara and H. Akagi, “An approach to position sensorless drive for brushless DC motors ,” IEEE Transactions on Industry Applications, Vol. 27, No. 5, pp. 928-933, Oct. 1991.

[29] O. Shinkawa, K. Tabata, A. Uetake, T. Shimoda, S. Ogasawara and H. Akagi, “Wide speed operation of a sensorless brushless DC motor having an interior permanent magnet rotor,” Conference Record of the Power Conversion Conference, Vol. 1, No. 2, pp. 364-370, April 1993.

[30] R. Wu and G.R. Slemon, “A permanent magnet motor drive without a shaft sensor,” IEEE Transactions on Industry Applications, Vol. 27, No. 5, pp. 1005-1011, Oct. 1991.

[31] L. Tian-Hua and C. Chien-Ping, “Adaptive control for a sensorless permanent-magnet synchronous motor drive,” IEEE Transactions on Aerospace and Electronic Systems , Vol. 30, No. 3, pp. 900-909, Jul. 1994.

[32] L. Tian-Hua and C. Chien-Ping, “Controller design for a sensorless permanent-magnet synchronous drive system,” IEE Proceedings on Electric Power Applications, Vol. 140, No. 6, pp. 369-378, Nov. 1993.

[33] M. Naidu and B.K Bose, “Rotor position estimation scheme of a permanent magnet synchronous machine for high performance variable speed drive,” Conference Record of the 1992 IEEE on Industry Applications Society Annual Meeting, Vol. 1, No. 3, pp. 48-53, Oct. 1992.

[34] D. Montesinos, S. Galceran, F. Blaabjerg, A. Sudria and O. Gomis, “Sensorless control of PM synchronous motors and brushless DC motors - an overview and evaluation,” European Conference on Power Electronics and Applications, Vol. 1, No. 1, Oct. 2005.

[35] J. Hu and B. Wu, “New integration algorithms for estimating motor flux over a wide speed range,” , IEEE Transactions on Power Electronics, Vol. 13, No. 5, pp. 969-977, Sep. 1998.

[36] N. Ertugrul and P. Acarnley, “A new algorithm for sensorless operation of permanent magnet motors,” IEEE Transactions on Industry Applications, Vol. 30, No. 1, pp. 126-133, Feb. 1994.

[37] C. D. French and P. Acarnley, “Control of permanent magnet motor drives using a new position estimation technique,” IEEE Transactions on Industry Applications, Vol. 32, No. 5, 1996.

[38] S. Ichikawa, Z. Chen, M. Tomita, S. Doki and S. Okuma, “Sensorless controls of salient-pole permanent magnet synchronous motors using extended electromotive force models,” Electr. Eng. Jpn., Vol. 146, No. 3, 2004.

[39] Z. Chen, M. Tomita, S. Doki and S. Okuma, “An extended electromotive force model for sensorless control of interior permanent-magnet synchronous motors,” IEEE Transactions on Industrial Electronics, Vol. 50, No. 2, pp. 288- 295, Apr. 2003.

[40] S. Morimoto, K. Kawamoto and Y. Takeda, “Position and speed sensorless control for IPMSM based on estimation of position error,” Electr. Eng. Jpn., Vol. 144, No. 2, 2003.

[41] N. Matsui, T. Takeshita and K. Yasuda, “A new sensorless drive of brushless DC motor,” Proceedings of Power Electronics and Motion Control, Vol. 1, pp. 430-435, 1992.

[42] N. Matsui and M. Shigyo, “Brushless DC motor control without position and speed sensors,” IEEE Transactions on Industry Applications, Vol. 28, pp. 120-127, 1992.

[43] N. Matsui, “Sensorless PM brushless DC motor drives,” IEEE Transactions on Industrial Electronics, Vol. 43, pp. 300-308, 1996.

[44] A. Consoli, S. Musumeci, A. Raciti and A. Testa, “Sensorless vector and speed control of brushless motor drives,” IEEE Transactions on Industrial Electronics, Vol. 41, No. 1, pp. 91-96, Feb. 1994.

[45] R.B. Sepe and J.H. Lang, “Real-time observer-based (adaptive) control of a permanent-magnet synchronous motor without mechanical sensors,” IEEE Transactions on Industry Applications, Vol. 28, No. 6, pp.1345-1352, Dec. 1992.

[46] L. Sicot, S. Siala, K. Debusschere and C. Bergmann, “Brushless DC motor control without mechanical sensors,” 27th Annual IEEE Power Electronics Specialists Conference, Vol. 1, pp. 375-380, Jun.1996.

[47] K. Joohn-Sheok and S. Seung-Ki, “High performance PMSM drives without rotational position sensors using reduced order observer,” The IEEE Industry Applications Conference, Vol. 1, No. 8, pp. 75-82, Oct. 1995.

[48] J. Solsona, MI Valla and C. Muravchik, “A nonlinear reduced order observer for permanent magnet synchronous motors,” IEEE Transactions on Industrial Electronics , Vol. 43, No. 4, pp. 492-497, Aug. 1996.

[49] J. Hu, D.M. Dawson and K. Anderson, “Position control of a brushless DC motor without velocity measurements,” IEE Proceedings on Electric Power Applications, Vol. 142, No. 2, pp. 113-122, Mar. 1995.

[50] T. Senjyu and K. Uezato, “Adjustable speed control of brushless DC motors without position and speed sensors,” International IEEE/IAS Conference on Industrial Automation and Control: Emerging Technologies, pp. 160-164, May 1995.

[51] T. Senjyu, M. Tomita, S. Doki and S. Okuma, “Sensorless vector control of brushless DC motors using disturbance observer,” 26th Annual IEEE Power Electronics Specialists Conference PESC '95, Vol.2, No.1, pp. 772-777, 18-22 Jun. 1995.

[52] T.F. Chan, W. Wang and P. Borsje, Y.K Wong and S.L. Ho, “Sensorless permanent-magnet synchronous motor drive using a reduced-order rotor flux observer,” IET Electric Power Applications, Vol. 2, No. 2, pp. 88-98, March 2008.

[53] T. Furuhashi, S. Sangwongwanich and S. Okuma, “A position-and-velocity sensorless control for brushless DC motors using an adaptive sliding mode observer,” IEEE Transactions on Industrial Electronics, Vol. 39, No. 2, pp. 89-95, Apr. 1992.

[54] Z.M.A. Peixo, S.A. Freitas, P.F. Seixas, B.R. Menezes, P.C. Cortizo and W.S. Lacerda, “Application of sliding mode observer for induced e.m.f., position and speed estimation of permanent magnet motors,” Proceedings of 1995 International Conference on Power Electronics and Drive Systems, Vol. 2, No. 1, pp. 599-604, Feb. 1995.

[55] H. Jun, Z. Dongqi, L. Yongdong and G. Jingde, “Application of sliding observer to sensorless permanent magnet synchronous motor drive system,” 25th Annual IEEE Power Electronics Specialists Conference, Vol. 1, pp. 532-536, June 1994.

[56] Y. Zhang and V. Utkin, “Sliding mode observers for electric machines-an overview,” 28th Annual Conference of IECON 02, Vol. 3, pp. 1842-1847, 2002.

[57] L. Changsheng and M. Elbuluk, “A sliding mode observer for sensorless control of permanent magnet synchronous motors,” Conference Record of the 2001 IEEE in Industry Applications, Vol. 1, pp. 1273-1278, 2001.

[58] S. Chi, Z. Zhang and L. Xu, “Sliding-Mode Sensorless Control of Direct-Drive PM Synchronous Motors for Washing Machine Applications,” IEEE Transactions on Industry Applications, Vol. 45, No. 2, pp. 582-590, March 2009.

[59] K. Young-Seok, A. Jun-Young, Y. Wan-Sik and C. Kyu-Min, “A speed sensorless vector control for brushless DC motor using binary observer,” proceedings of the 1996 IEEE IECON 22nd International Conference on Industrial Electronics, Control, and Instrumentation, Vol. 3, pp. 1746-1751, Aug. 1996.

[60] X. Xiao, C. Chen and M. Zhang, “Dynamic Permanent Magnet Flux Estimation of Permanent Magnet Synchronous Machines,” IEEE Transactions on Applied Superconductivity, Vol. 20, No. 3, pp. 1085-1088, June 2010.

[61] M. Schroedl , “Operation of the permanent magnet synchronous machine without a mechanical sensor,” Fourth International Conference on Power Electronics and Variable-Speed Drives, Vol. 1, No. 5, pp. 51-56, July 1990.

[62] Z. Peroutka, V. Smidl, V. and D. Vosmik, “Challenges and limits of extended Kalman Filter based sensorless control of permanent magnet synchronous machine drives,” 13th European Conference on Power Electronics and Applications, Vol. 1, No. 8, pp. 1-11, Sept. 2009.

[63] F. Parasiliti, R. Petrella and M, Tursini ,“Sensorless speed control of a PM synchronous motor based on sliding mode observer and extended Kalman filter,” Thirty-Sixth IAS Annual Meeting. Conference Record of the 2001 IEEE Industry Applications Conference, Vol. 1, No. 3, pp. 533-540, Oct. 2001.

[64] S. Ostlund and M. Brokemper, “Sensorless rotor position detection from zero to rated speed for an integrated PM synchronous motor drive,” IEEE Transactions on Industrial Applications, Vol. 32, No. 5, 1996.

[65] J.-I. Ha, K. Ide, T. Sawa and S.-K. Sul, “Sensorless rotor position estimation of an interior permanent-magnet motor from initial states,” IEEE Transactions on Industrial Applications, Vol. 39, No. 3, 2003.

[66] G. H. Jang, J. H. Park and J. H. Chang, “Position detection and start-up algorithm of a rotor in a sensorless BLDC motor utilising inductance variation,” Power Applications Proceeding. Inst. Elect. Eng., Vol. 149, No. 2, 2002.

[67] M. Tursini, R. Petrella and F. Parasiliti, “Initial rotor position estimation method for pm motors,” Transactions on Industrial Applications, Vol. 39, No. 6, 2003.

[68] S. Nakashima, Y. Inagakiand and I. Miki, “Sensorless initial rotor position estimation of surface permanent-magnet synchronous motor,” IEEE Transactions on Industrial Applications, Vol. 36, No. 6, 2000.

[69] R Raute, C. Caruana, J. Cilia, C.S. Staines and M. Sumner, “A zero speed operation sensorless PMSM drive without additional test signal injection,” 2007 European Conference on Power Electronics and Applications, Vol. 3, No. 2, pp. 1-10, Sept. 2007.

[70] D. Salt, D. Drury and D. Holliday, “Compensation of nonlinear distortion effects for signal injection based sensorless control,” 5th IET International Conference on Power Electronics, Machines and Drives (PEMD 2010), Vol. 1, No. 1, pp. 1-6, 19-21 April2010.

[71] A.S. Budden, R. Wrobel, D. Holliday, P.H. Mellor and P. Sangha, “Sensorless Control of Permanent Magnet Machine Drives for Aerospace Applications,” International Conference on Power Electronics and Drives Systems, Vol. 1, No. 8, pp. 372- 377, Jan. 2006.

[72] G. El-Murr, D. Giaouris and J.W. Finch, “Online cross-coupling and self incremental inductances determination of salient Permanent Magnet Synchronous Machines,” 5th IET International Conference on Power Electronics, Machines and Drives (PEMD 2010), , Vol. 1, No. 2, pp. 1-4, April 2010.

[73] J.M. Guerrero, M. Leetmaa, F. Briz, A. Zamarron and R.D. Lorenz, “Inverter nonlinearity effects in high frequency signal injection-based, sensorless control methods,” 38th IAS Annual Meeting Conference Record of the Industry Applications Conference, Vol. 2, pp. 1157- 1164, Oct. 2003.

[74] R. Leidhold and P. Mutschler, “Sensorless position estimation by using the high frequency zero-sequence generated by the inverter,” 35th Annual Conference of IEEE Industrial Electronics, Vol. 1, No. 5, pp. 1282-1287, Nov. 2009.

[75] M. Tomita, M. Satoh, H. Yamaguchi, S. Dokia and S. Okuma, “ Sensorless Estimation of Rotor Position of Cylindrical Brushless DC Motors Using Eddy Current,” 4th International Workshop on Advanced Motion Control Proceedings, Vol. 1, pp. 24-28, 1996.

[76] M. Tomita, S. Doki, H. Yamaguchi and S. Okuma, “A sensorless estimation of rotor position of cylindrical brushless DC motors using eddy current,” Proceedings of the 1996 IEEE IECON 22nd International Conference on Industrial Electronics, Control, and Instrumentation, Vol. 3, pp. 1723-1728, Aug. 1996.

[77] N. Bianchi, S. Bolognani and A. Faggion, “Rotor design arrangement of SPM motors for the sensorless control at low speed and standstill,” 14th International Conference EPE-PEMC 2010, Sep. 2010.

[78] T.A. Nondahl, C. Ray and P.B. Schmidt, “A permanent magnet rotor containing an electrical winding to improve detection of motor angular position,” The 1998 IEEE Industry Applications Conference, Vol. 1, No. 5, pp. 359-363, Oct. 1998.

[79] T.A. Nondahl, C. Ray, P.B. Schmidt and M.L. Gasperi , “A permanent-magnet rotor containing an electrical winding to improve detection of rotor angular position,” IEEE Transactions on Industry Applications, Vol. 35, No. 4, pp. 819-824, Aug. 1999.

[80] H. Ohta, I. Masukane and K. Matsuse, “Rotor pole discrimination and simple starting method of new single phase PM motor without position sensor,” International Power Electronics and motion control conference, Vol. 2, pp. 616–621, 2000.

[81] H. Ohta, R. Tsuchimoto, T. Sato, H.Kubota, K. Matsuse and Y. Kawase, "Distinguishing method of the magnetic polarity at standstill mode on PM motor using the partial magnetic saturation of stator core," in Proc. JIASC 1999, Vol. 1, pp. 105–108, 1999.

[82] I. Masukane, T. Baba, K. Matsuse, H. Ohta and K. Obayashi, "Characteristics of the permanent magnet motor with closed slot core for position sensorless drive," in Proc. JIASC 2001, Vol. 1, pp. 215–218, 2001.

[83] T. Baba, I. Masukane, K. Matsuse, H. Ohta and K. Obayasi, "Characteristics and analysis of the permanent magnet synchronous motor with closed slot stator core for position sensorless drive," in Proc. PCCO, Vol. 1, pp. 265–269, 2002.

[84] K. Matsuse, T. Baba, I. Masukane, H. Ohta and R. Tsuchimoto, "Position-sensorless starting method and driving characteristics of closed-slot small permanent-magnet motor," IEEE Transactions on Industrial Applications ,Vol. 39, No. 2, pp. 451 - 456, 2003.

[85] D.E. Hesmondhalgh, D. Tipping and M. Amrani, "A new magnetic rotor position sensing unit for brushless DC motors," International Conference on Electrical Machines, pp. 99-104, September 1988.

[86] D.E. Hesmondhalgh, D. Tipping and M. Amrani, "Performance and design of an electromagnetic sensor for brushless DC motors," IEE Proceedings on Electric Power Applications, Vol. 137, No. 3, pp. 174-183, May 1990.

[87] H.A. Toliyat, L. Hao, D.S. Shet and T.A. Nondahl, "Position-sensorless control of surface-mount permanent-magnet AC (PMAC) motors at low speeds," IEEE Transactions on Industrial Electronics, Vol. 49, No. 1, pp. 157-164, Feb. 2002.

[88] H. Fengtai and T. Dapeng, "A neural network approach to position sensorless control of brushless DC motors," Proceedings of the 1996 IEEE 22nd International Conference on Industrial Electronics, Control, and Instrumentation, IECON, Vol. 2, No. 5, pp. 1167-1170, Aug. 1996.

[89] T.D. Batzel and K.Y. Lee, “An approach to sensorless operation of the permanent-magnet synchronous motor using diagonally recurrent neural networks,” IEEE Transactions on Energy Conversion, Vol. 18, No. 1, pp. 100-106, Mar. 2003.

[90] G. Hai-Jiao, S. Sagawa, T. Watanabe and O. Ichinokura, “Sensorless driving method of permanent-magnet synchronous motors based on neural networks,” IEEE Transactions on Magnetics, Vol. 39, No. 5, pp. 3247- 3249, Sept. 2003.

[91] H. Le-huy and M. Hamdi, “Control of a direct-drive DC Motor by Fuzzy Logic,” Industry Applications Society Annual Meeting Conference, pp. 732-738, October 1993.

[92] M. Hamdi, G. Lachiver and M. Ghribi, M., “A sensorless control scheme based on fuzzy logic for AC servo drives using a permanent-magnet synchronous motor,” Canadian Conference on Electrical and Computer Engineering, Vol. 1, No. 4, pp. 306-309, Sep.1995.

[93] S.M.M. Mirtalaei, J.S. Moghani, K. Malekian and B. Abdi, “A novel sensorless control strategy for BLDC motor drives using a fuzzy logic-based neural network observer,” International Symposium on Power Electronics, Electrical Drives, Automation and Motion, SPEEDAM 2008, Vol. 1, No. 4, pp. 1491-1496, June 2008.

[94] P.S. Frederiksen, J. Birk and F. Blaabjerg, “Comparison of two, energy optimizing techniques for PM-machines,” 20th International Conference on Industrial Electronics, Control and Instrumentation, IECON '94, Vol.1, No.5, pp. 32-37, Sep. 1994.

[95] P.W. Wheeler, J. Rodriguez, J.C. Clare, L. Empringham and A. Weinstein, “Matrix converters: a technology review,” IEEE Transactions on Industrial Electronics, Vol. 49, No. 2, pp. 276-288, Apr. 2002.

[96] D. Casadei, G. Serra, A. Tani and L. Zarri, “Matrix converter modulation strategies: a new general approach based on space-vector representation of the switch state,” IEEE Transactions on Industrial Electronics, Vol. 49, No. 2, pp. 370-381, Apr. 2002.

[97] Q. Gao, G.M. Asher and M. Sumner, “Zero speed position estimation of a matrix converter fed AC PM machine using PWM excitation,” Power Electronics and Motion Control Conference, pp. 2261-2268, Sept. 2008.

[98] A. Arias, L. Empringham, G.M. Asher, P.W. Wheeler, M. Bland, M. Apap, M. Sumner and J.C. Clare, “Elimination of Waveform Distortions in Matrix Converters Using a New Dual Compensation Method,” IEEE Transactions on Industrial Electronics, Vol. 54, No. 4, pp. 2079-2087, Aug. 2007.

[99] L. Helle, K.B. Larsen, A.H. Orgensen, S. Munk-Nielsen and F. Blaabjerg, “Evaluation of modulation schemes for three-phase to three-phase matrix converters,” IEEE Transactions on Industrial Electronics, Vol. 51, No. 1, pp. 158- 171, Feb. 2004.

[100] G. Qiang, G.M. Asher, M. Sumner and L. Empringham, “Position Estimation of a Matrix-Converter-Fed AC PM Machine From Zero to High Speed Using PWM Excitation,” IEEE Transactions on Industrial Electronics, Vol. 56, No. 6, pp. 2030-2038, June 2009.

[101] J.P. Johnson, M. Ehsani and Y. Guzelgunler, “Review of sensorless methods for brushless DC,” Thirty-Fourth IAS Annual Meeting. Conference Record of the 1999 IEEE on Industry Applications Conference, Vol. 1, pp. 143-150, 1999.

[102] T. Senjyu and K. Uezato, “Adjustable Speed Control of Brushless D C Motors without Position and Speed Sensors,” Proc. on Industrial Applications and Control: Emerging Technologies, pp. 160-164, 1995.

[103] J. Hu, D. Zhu, Y. Li, and J. Gao, “Application of Sliding Observer to Sensdess Permanent Magnet Synchronous Motor Drive System,” Power Electronics Specialists Conference, Vol. I, pp. 532-536, 1994.

[104] P. Min-Ho and L. Hong-Hee, “Sensorless vector control of permanent magnet synchronous motor using adaptive identification,” 15th Annual Conference of IEEE Industrial Electronics Society, IECON '89, Vol. 1, No. 1, pp. 209-214, Nov. 1989.

[105] I. Takahashi and T. Noguchi, “A new quick-response and high-efficiency control strategy of an induction motor,” IEEE Transactions on Industry Applications, Vol. IA-22, pp. 820-827, 1986.

[106] L. Zhong, M.F. Rahman, W.Y. Hu and K.W. Lim, “Analysis of direct torque control in permanent magnet synchronous motor drives,” IEEE Transactions on Power Electronics, Vol. 12, No. 3, pp. 528-536, May 1997.

[107] T. Lixin, Z. Limin, M.F. Rahman and Y. Hu, “A novel direct torque controlled interior permanent magnet synchronous machine drive with low ripple in flux and torque and fixed switching frequency,” IEEE Transactions on Power Electronics, Vol. 19, No. 2, pp. 346- 354, March 2004.

[108] X. Zhuang and M.F. Rahman, “An Adaptive Sliding Stator Flux Observer for a Direct-Torque-Controlled IPM Synchronous Motor Drive,” IEEE Transactions on Industrial Electronics, Vol. 54, No. 5, pp. 2398-2406, Oct. 2007.

[109] G. Foo and M.F. Rahman, “Sensorless Direct Torque and Flux-Controlled IPM Synchronous Motor Drive at Very Low Speed Without Signal Injection,” IEEE Transactions on Industrial Electronics, Vol. 57, No. 1, pp. 395-403, Jan. 2010.

[110] G. Foo and M.F. Rahman, “Direct Torque Control of an IPM-Synchronous Motor Drive at Very Low Speed Using a Sliding-Mode Stator Flux Observer,” IEEE Transactions on Power Electronics, Vol. 25, No. 4, pp. 933-942, April 2010.

[111] F. Alrifai and N. Schofield, “Control of brushless PM machines using measured torque feedback,” International Symposium on Power Electronics Electrical Drives Automation and Motion (SPEEDAM2010), pp. 996-1001, 14-16 June 2010.

[112] F. Alrifai, N. Schofield, “Control of PM Machines with Non-contact Measured Torque Feedback,” 14th International Conference EPE-PEMC 2010, Sep. 2010.

[113] E. Peralta-Sanchez, F. Alrifai and N. Schofield, “Direct Torque Control of permanent magnet motors using a single current sensor,” IEEE International Conference on Electric Machines and Drives Conference, IEMDC '09, pp. 89-94, May 2009.

[114] R. Krishnan, “PM Synchronous and Brushless DC Motor Drives,” Book, Taylor and Francis Group, NW, Suit 300, ISBN:978082475384, 2010.

[115] P. Krause, “Analysis of electric machinery and drive systems,” Book, John Wiley & Sons, ISBN: 9812531505, 2002.

[116] E. Ramsden, “Hall-Effect Sensors Theory and Applications,” Book, Elsevier, ISBN: 978-0-7506-7934-3, 2006.

[117] JMD Murphy and FG Turnbull, “Power electronic control of AC motors,” Pergamon Press, ISBN: 0080226833, 1988.

[118] R. Krishnan and R. Ghosh, “Starting algorithm and performance of a PM DC brushless motor drive system with no position sensor,”20th Annual IEEE Power Electronics Specialists Conference, PESC '89, Vol. 2, No. 1, pp. 815-821, Jun. 1989.

[119] W.L. Soong, “PM Machines: Parameter Measurement and Performance Prediction,” Power Engineering Briefing Note Series, May. 2008.

[120] D. Grenier, L.-A. Dessaint, O. Akhrif, Y. Bonnassieux and B. LePioufle, “Experimental Nonlinear Torque Control of a Permanent Magnet Synchronous Motor Using Saliency,” IEEE Transactions on Industrial Electronics, Vol. 44, No. 5, pp. 680-687, October 1997.

[121] R. Deodhar, D. Staton, T. Jahns and T.J.E. Miller, “Prediction of cogging torque using the flux-MMF diagram technique,” IEEE Transactions on Industry Applications, Vol. 32, pp. 569-576, Jun. 1996.

[122] D.M. Ionel, M. Popescu, M. McGilp, T.J.E Miller, S. Dellinger and A.O. Smith Corp, “Assessment of torque components in brushless permanent-magnet machines through numerical analysis of the electromagnetic field, ” IEEE Transactions on Industry Applications, Vol. 41, pp. 1149- 1158, Oct. 2005.

[123] A. Consoli, S. Musumeci, A. Raciti and A.Testa, “Sensorless vector and speed control of brushless motor drives,” IEEE Transactions on Industrial Electronics, Vol. 41, No. 1, pp. 91-96, Feb. 1994.

[124] S. Joong-Ho and C. Ick, “Commutation torque ripple reduction in brushless DC motor drives using a single DC current sensor, ” IEEE Transactions on Power Electronics, Vol. 19, No. 2, pp. 312- 319, March 2004.

[125] H. Jung-Ik, “Current Prediction in Vector-Controlled PWM Inverters Using Single DC-Link Current Sensor,” IEEE Transactions on Industrial Electronics, Vol. 57, No. 2, pp. 716-726, Feb. 2010.

[126] F. Blaabjerg, J.K. Pedersen, U. Jaeger and P. Thoegersen, “Single current sensor technique in the DC link of three-phase PWM-VS inverters: a review and a novel solution,” IEEE Transactions on Industry Applications, Vol. 33, No. 5, pp. 1241-1253, Oct. 1997.

APPENDIX A1

SURFACE ACOUSTIC WAVES TORQUE MEASUREMENT SYSTEM

A1.1 Rayleigh Waves

Surface acoustic waves are also known as Rayleigh waves, named after Lord Rayleigh an English scientist born in 1885. Lord Rayleigh demonstrated theoretically that waves could be propagated over the plane boundary between a linearly elastic half space and a vacuum, where the amplitude decays exponentially with depth. The theory was implemented around 1930, where Voltmer and White, of the University of California, generated such waves, which are more commonly known referred to as Surface Acoustic Waves (SAW) or Rayleigh waves, on the free surface of an isotropic, elastic substrate, namely quartz. The influence of the material properties of the surface layer of a sample on the velocity and attenuations of surface acoustic waves permits the latter to be used for the assessment of residual stress in the surface layer, as well as the thermal and mechanical properties of the surface layer of the sample [5].

A1.2 SAW Torque Transducer

The SAW transducer is shown schematically in Fig. A1.1. The SAW's are produced by metallic film transducers on the surface of a piezoelectric material. An alternating voltage applied to the transducer produces waves. The wave period is determined by the interdigital configuration, thus the wave frequencies can be physically set to a given

frequency. When stress is applied to the SAW device, strain is induced, which can be either a state of tension or compression. The strain will change the spacing of the interdigital elements and hence the operating frequency changes. For example, if an excitation frequency is set to 500 MHz and 1Nm of tension applied, the excitation frequency will decrease; conversely an revisable compressive stain will increase the frequency by the same amount. The quality factor of the transducer is high; therefore, by measuring the impedance, a tracking oscillator can be controlled [5].

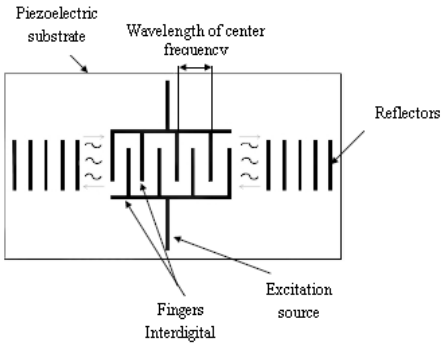

Fig. A1.1 Outline of SAW transducer [5].

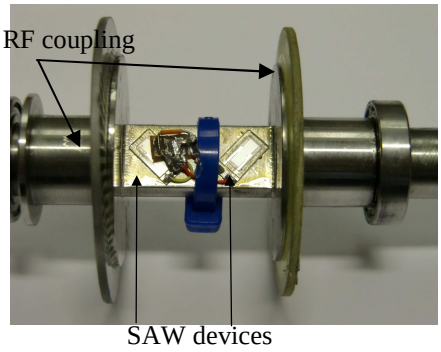

Fig. A1.2 Two SAW transducers each with there own antenna.

The measurement of torque with SAW sensors in general is based on bending, stretching, or compressing of the sensor substrate. So a typical SAW torque transducer contains two SAW elements that are used in a half bridge configuration, one positioned so as to be sensitive to the principle compressive stain and the other poisoned to observe the principle tensile strain. Note that in the absence of bending moments and axial forces, the principle stress planes lie perpendicular to one another and at 45 degrees to the plane about which the tensional moment is applied. The two SAW transducers and their associated antenna are illustrated in Fig. A1.2. The two frequencies produced by the SAW elements are mixed together to produce difference and sum signals. The difference signal is a measure of induced strain and hence, from the knowledge of the material properties and governing equations, torque is implied. The sum signal is a measure of the shaft temperature [5]. The primary frequency of oscillations can be chosen to lie between 100-1000MHz with the difference frequency varying up to 1.0 MHz. The two combined SAW elements result in a transducer having the following specifications:

Resolution: 1 part in 10^6

Linearity: 0.1%

Bandwidth: 1MHz

APPENDIX 2

ROTOR POSITION SENSORS

A2.1 Introduction

Brushless PM drive systems require precise rotor position information feedback to optimise dynamic performance. The drive system performance thus depends on the static and dynamic characteristics of the rotor position transducer that is selected. When drive system measured quantities are rapidly changing, the dynamic relationship between the input and output of the measurement system have to be considered, particularly when discrete sampling is involved. In contrast, the measured parameters may change slowly in some applications and signal drift may become problematic, hence the static performance should also be considered. The selection of a suitable rotor position transducer should consider the following assessments [8]:

(i) Accuracy: a measure of how the output of the transducer relates to the true value at the input.

(ii) Dead-band: the largest change in input to which the transducer will fail to respond, usually caused by mechanical effects such friction, gears.

(iii) Drift: the variation in the transducer output which is not caused by a change at the input.

(iv) Linearity: a measure of the consistency of the input-to-output ratio over the useful measurement range of the transducer.

(v) Resolution: the smallest change in the input that can be detected.

(vi) Repeatability: a measure of the closeness with which a group of output values agree for a constant input.

A2.2 Resolvers

Resolvers are electromechanical transducers that in conjunction with appropriate electronics convert rotor shaft angle into an absolute analogue position signal [9]. The device is illustrated in Fig. A2.1 showing a mechanical cross-section view (a) and simplified electrical circuit representation (b). As the relative position of the static and rotating coils change, the resolver output varies as the sine of either electrical or mechanical angle. Connection to the rotating coil is made by either brushes or slip rings, or more usually via inductive coupling. The inductive (brushless) resolvers offer up to 10 times the life of brushed types and are insensitive to vibration and dirt. The stator consists of two output windings spaced apart by 90 degrees electrical and the primary of a rotary transformer [10]. The rotor carries the secondary of the rotary transformer that is used to excite the main rotor coil, as shown in Fig. A2.1 (b).

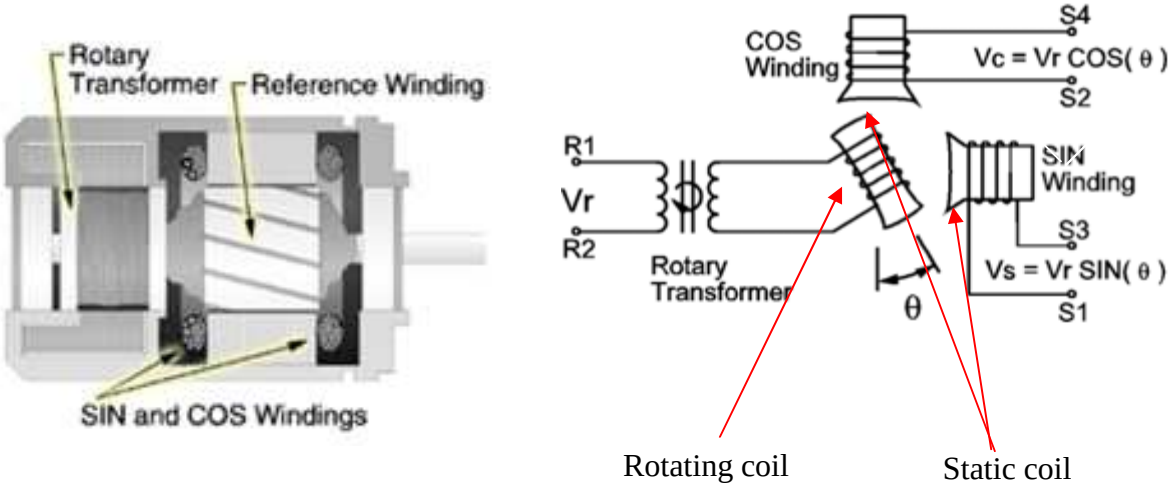

(a) Mechanical cross-section view. (b) Simplified electrical circuit representation.

Fig. A2.1 Resolver-electromechanical position transducer [10].

In general [10], the static rotor transducer winding is excited by an AC Reference Voltage (Vr) of typically 5 kHz. The induced voltages in the SIN and COS windings are equal to the value of the Reference Voltage multiplied by the SIN or COS of the angle of the input shaft from a fixed zero point. Thus, the resolver provides two voltages whose ratio represents the absolute position of the input shaft, i.e:

$$\tan\theta_r = \frac{\sin\theta_r}{\cos\theta_r} \tag{A2.1}$$

where θ_r is the rotor shaft angle. Because the ratio of the SIN and COS voltages is considered, any changes in the resolvers' characteristics, such as those caused by aging or a change in temperature, are ignored. An additional advantage of the SIN / COS ratio is that the shaft angle is absolute. Even if the shaft is rotated with power removed, the resolver will report its new position value when power is restored. In the selection of a resolver, two major parameters need to be considered: the resolution and the accuracy, both static and dynamic. The major disadvantage of resolvers is the need for interfacing electronics. The resolver analog output to digital conversion also adds complexity.

A2.3 Optical Encoders

Optical encoders can take one of two forms:

- incremental and
- absolute.

Each of theses types of encoder consists of three main parts, as illustrated in Fig. A2.2, that is:

(i) an optical receiver,

(ii) a light source,

(iii) and a code wheel

The receiver is normally a phototransistor or diode which responds to the light intensity received from a local light source [11]. The light source can be either a filament bulb but more usually a solid state light emitting diode. The different kinds of optical encoders are characterized by the information contained on the code wheel and by how it is interpreted by an external control system as illustrated in Fig. A2.3. Showing the construction on an incremental encoder (a). The encoder code wheel has a single track of equally sized, opaque and translucent slots. As the wheel rotates, an equal work-space digital signal is produced with a frequency proportional to the speed of rotation. The incremental encoder is essentially a pulse generator, signalling on each increment of motion. There are mainly two kinds of incremental encoders either rotary incremental encoder which gives pulses

per revolution, or linear encoders which returns data in pulses per inch or millimetre. The incremental encoder keeps no record of its actual position, thus a one per revolution index pulse is also included. Incremental encoders produce square-wave pulse trains. They typically have two output channels (A and B) offset from each other by half a pulse width (90 degrees) to provide information on direction of rotation, as shown in Fig. A2.4. When the machines rotates clock-wise then channel A will lead channel B, else if the machine rotates counter-clock wise, channel A will lag channel B.

If absolute rotor position is required from the sensor, a number of discrete discs, associated LEDS and sensors are required as illustrated in Fig. A2.3 (b). The absolute encoder usually implements binary or gray code, with one bit per track. The gray code is preferred because only one bit changes between any positioned state, as detailed in Table A2.1. The encoder disks are costly, hence, absolute devices tend to be more expensive than incremental.

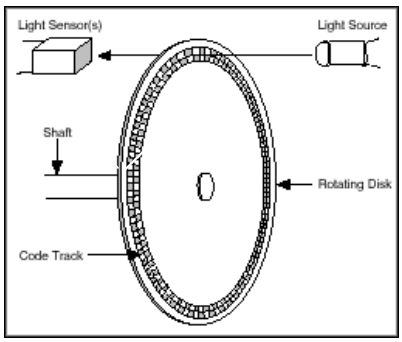

Fig. A2.2 Main components of incremental and absolute encoder [11].

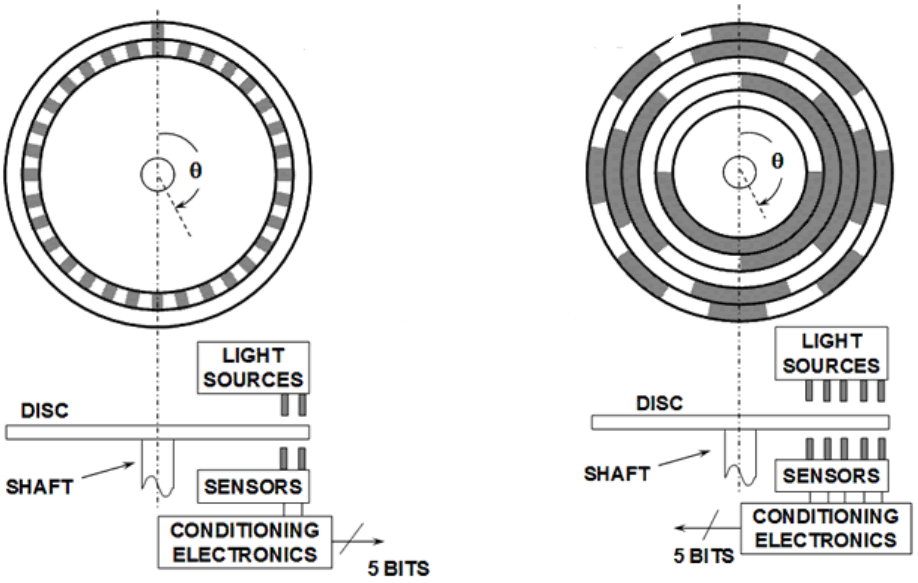

(a) Incremental. (b) Absolute.

Fig. A.2.3 Incremental and absolute encoder disk schemes [12].

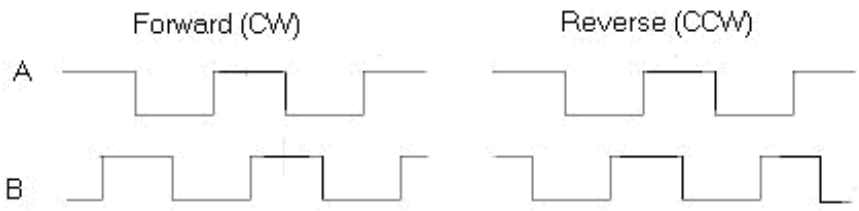

A

B

Fig. A2.4 Incremental encoders A and B pulses [12].

Decimal code	Binary code	Gray code
0	0000	0000
1	0001	0001
2	0010	0011
3	0011	0010
4	0100	0110
5	0101	0111
6	0110	0101
7	0111	0100
8	1000	1100
9	1001	1101
10	1010	1111
11	1011	1110
12	1100	1010
13	1101	1011
14	1110	1001
15	1111	1000

Table A2.1 Binary and Gray code as used in absolute optical encoders [12].

APPENDIX A3

EXPERIMENTAL VALIDITION HARDWARE AND DSPACE SYSTEM

A3.1 Introduction

The start-up routine proposed in Chapter 2 is implemented via a DSpace controlled drive system comprising of a commercial brushless PM machine, the Unimotor coupled directly to a prototype brushless PM machine, as illustrated by the test facility schematic of Fig. 3.39 and by the rig photography gallery of Fig. 3.40. The current and voltage instrumentation, full-bridge power electronic inverter, gate drive circuitry, filters and protections are discussed here for completeness. An overview is also given of the DSpace machine control platform developed as part of this research study.

A3.2 Current sensors

There are four current sensors in the system, they are used to monitor the currents through the three phases and also monitor the dc current. The current transducer used here is Hall current sensor which is LA 55-P from LEM, the data sheet is in the appendix. Since the current that is going to be measured is usually under 25A. Then the measuring resistance is going to be selected to be 160 ohm for maximum accuracy. The output of the current sensors will be a voltage which be filtered through a low pass filter with a cut off frequency of 2 kHz. the chosen low pass cut off frequency was choose because the inverter PWM carrier frequency at 10 kHz and the operating frequency is very low so that the delay and magnitude effect cause by the low filter does not effect the measurement. The current sensors diagram and how they are attached to the inverter is shown in Fig. A3.1. The

current sensor is shown in Fig. A3.2, and shown in the real system used as in Fig A3.3. The output of the low pass filter is connected to a DSpace system. The DSpace system converts the current to it real value and accounts for all offset and magnitude changes needed and then used as feedback this is shown in Fig. A3.4. The system only needs one DC current to control the three phase current this will be explained in detail in chapter 5.

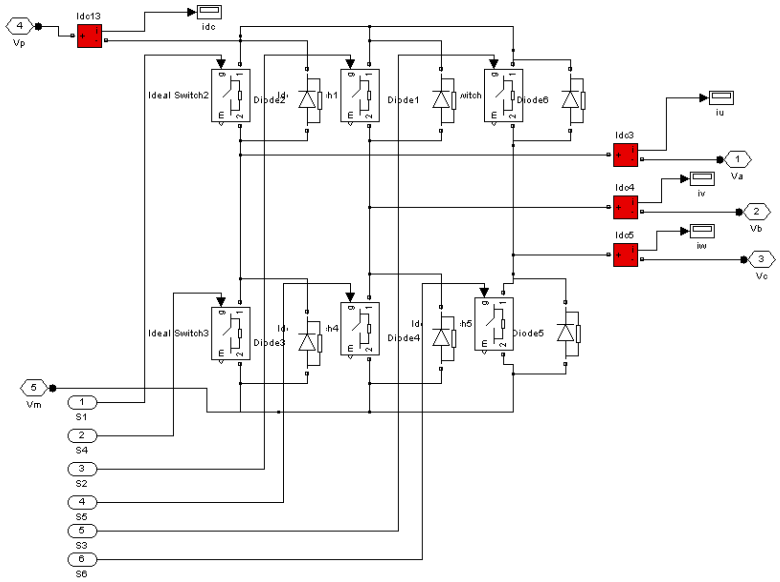

Fig. A3.1 Current sensors schematic on the inverter.

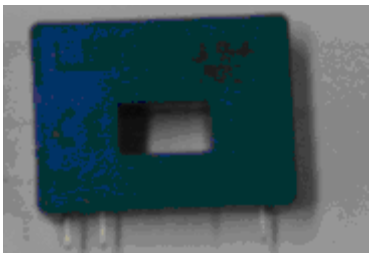

Fig. A3.2 Current sensor.

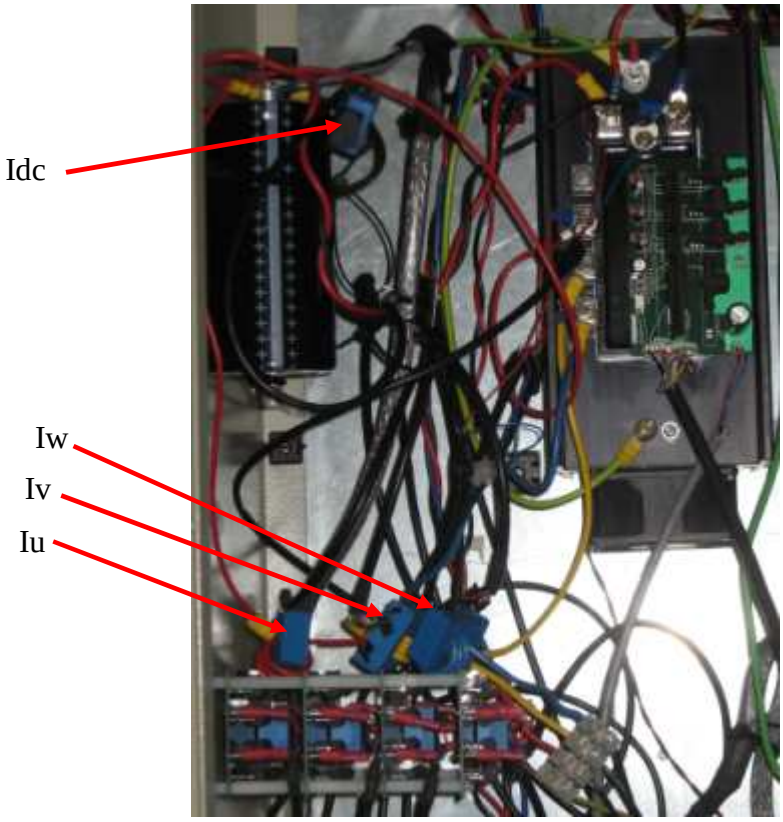

Fig. A3.3 Current sensors attached to real inverter.

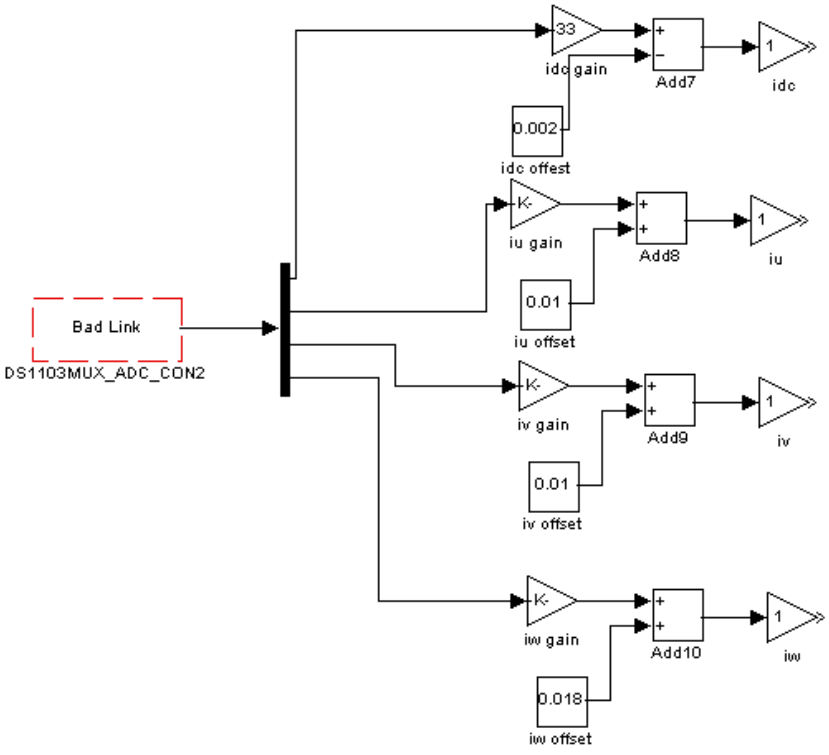

Fig. A3.4 Current sensors in DSpace code.

A3.3 Voltage sensors

The voltage sensors used are made by LEM there known as the voltage transducers LV 25-1000. The voltage maximum that is going to be used in the experiment is going to be within +-1000 volts. For maximum accuracy the resistance will be chosen to be 320 ohms from the data sheet. There are four voltage sensors that are going to be used in the experiment to measure the three phase voltage and also the DC voltage. The diagram of how these voltages are going to be inserted with respect to the inverter is shown in Fig. A3.5. The voltage sensor that is used in the system is shown in Fig. A3.6. The voltage sensors are shown in the experimental rig as in Fig. A3.7. The output of the voltage sensors is connected to a low pass filter with a cut off frequency of 2 kHz. The offset and amplitude is adjusted in accordingly is DSpace as shown in Fig. A3.8.

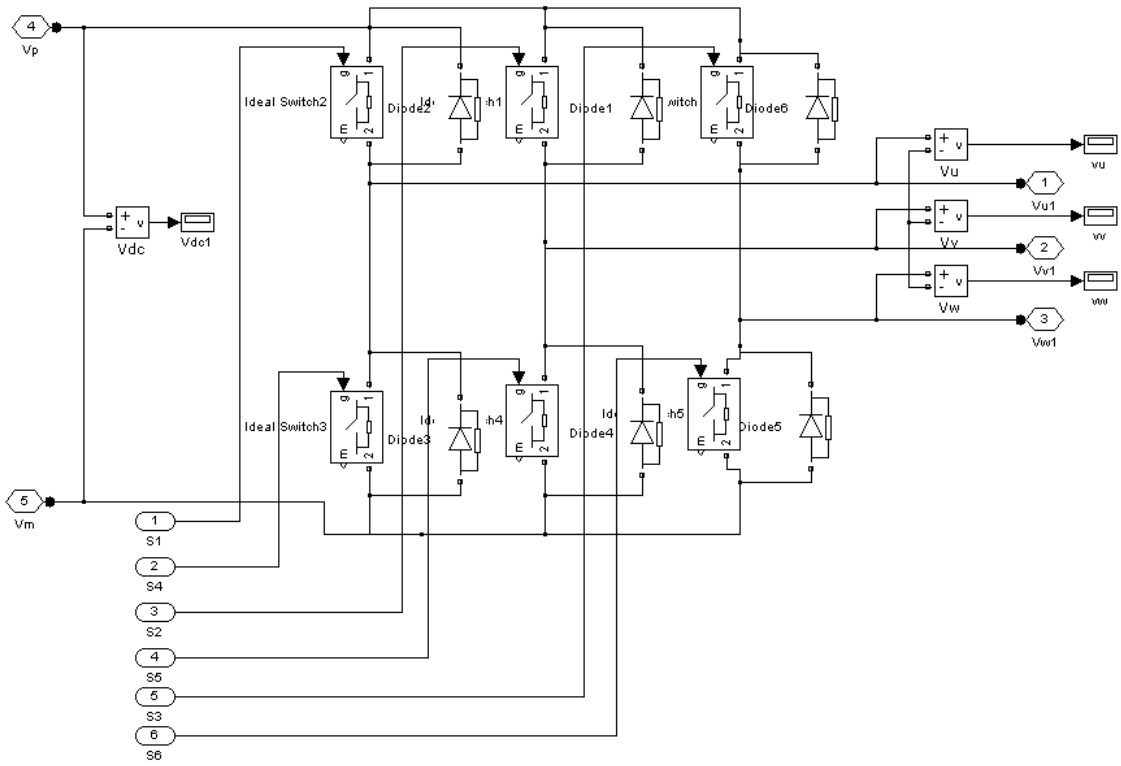

Fig. A3.5 Voltage sensor schematic on the inverter.

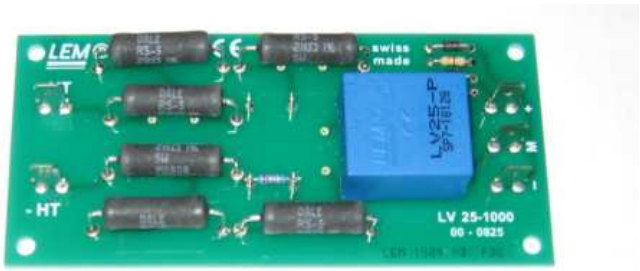

Fig. A3.6 Voltage sensor board.

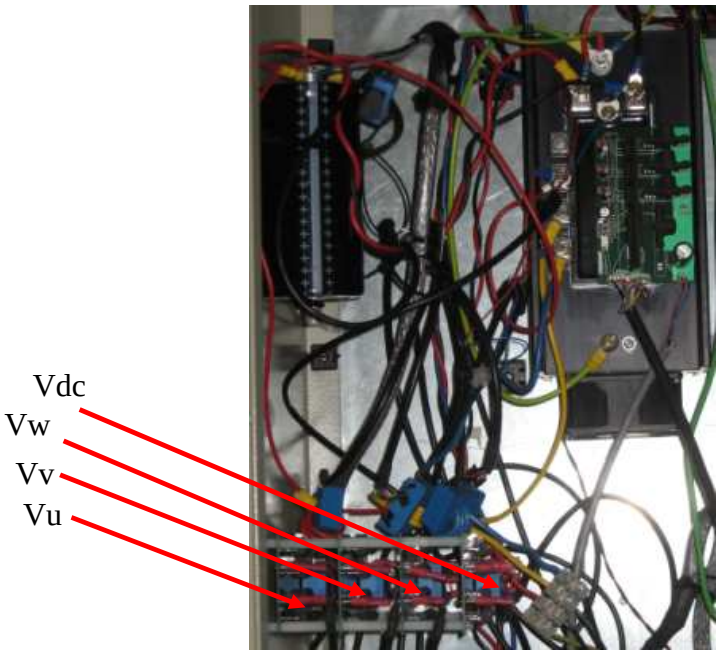

Fig. A3.7 Voltage sensors attached to real inverter.

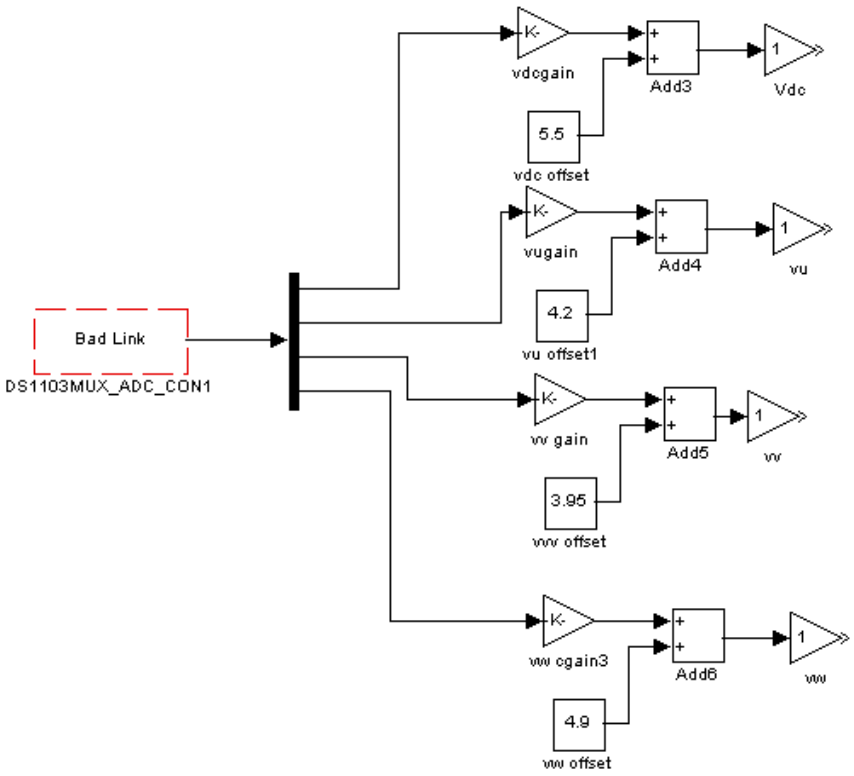

Fig. A3.8 Voltage sensors in DSpace code.

A3.4 Low-pass filter circuit

The printed circuit made to deliver the measured currents and voltages values to DSpace is explained here. The circuit consists of a measured resistance given in the data sheet that is used to receive the out current of the current sensor and the voltage sensor respectively. The best value for the resistance to be used for the application here is 160 and 320 ohms for the current and voltage sensors. The low pass filter is used to take out the high frequency the value chosen for the cut off frequency is 2 kHz many test have made using different cut off frequency until this value was choose since the fundamental frequency used is very low, the delay, and amplitude effect are very small and compensated in DSpace. The measuring resistance and low pass circuit diagram is shown in Fig. A3.9 in PCB format. The measuring resistance and low pass circuit after it built is shown Fig. A3.10 and is shown in the experimental rig as in Fig. A3.11.

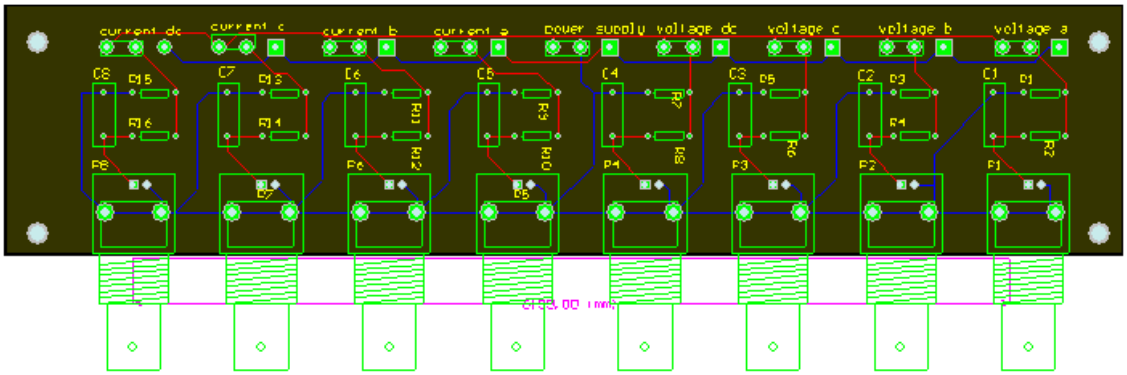

Fig. A3.9 Low-pass filter and measuring resistance circuit in PCB.

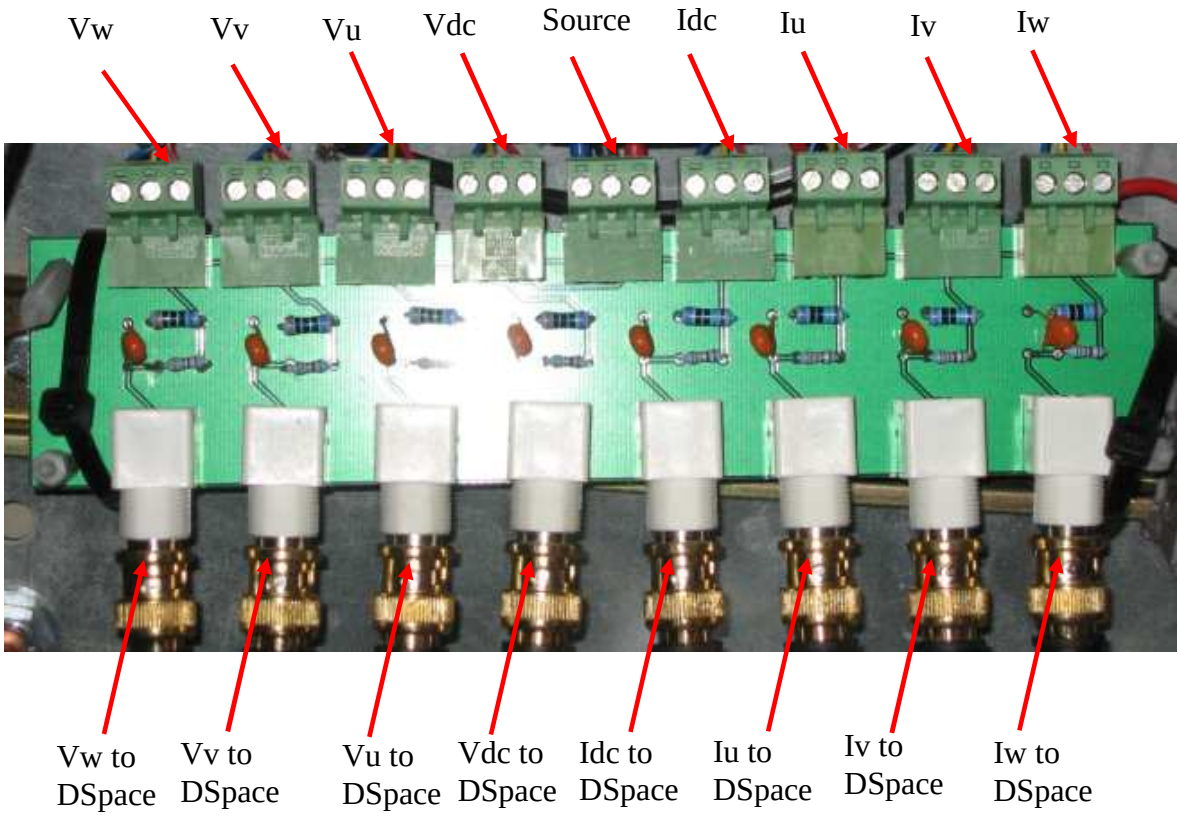

Fig. A3.10 Low-pass filter and measuring resistance circuit after being built.

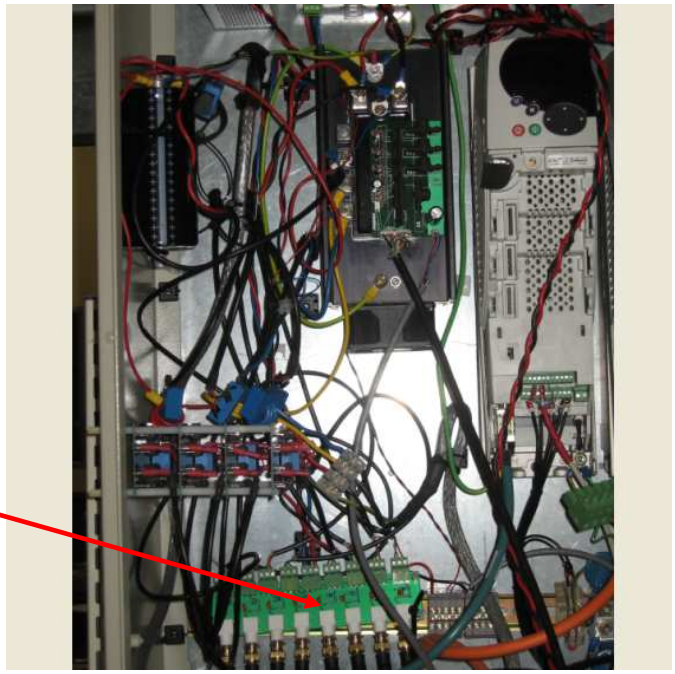

Fig. A3.11 Low pass filter and measuring resistance circuit in the rig.

A3.5 IGBT inverter circuits

The inverter used is a BP7B is shown in Fig. A3.12. it is an isolated interface circuit for six and seven pack low and medium power L-series intelligent power modules (IPMs). It consists of a VLA606-01R which is opto-interface for isolation of control signals and also isolates the power supply for the IPMs built in gate drive and protection circuits. The isolation helps to directly connect the IPM to the logic level control it shown in Fig. A3.13. The IPMs part number PM25RLA120 has a built in gate drive and a protection circuit, the PM25RLA120 has a common control ground for all three low sides IGBT. This permits the use of a single low side supply so that only four isolated supplies are required this is shown in Fig. A3.14. The VLA106-24151 and VLA106-24154 are isolated dc-dc converter which operate from a single 24 V dc supply and produces an isolated 15 V dc output and provides up 100 mA for control power and 300mA respectively, it also uses a transformer to provide 2500VRMS isolation between the primary and secondary, the VLA106-24151 is show in Fig. A3.15.

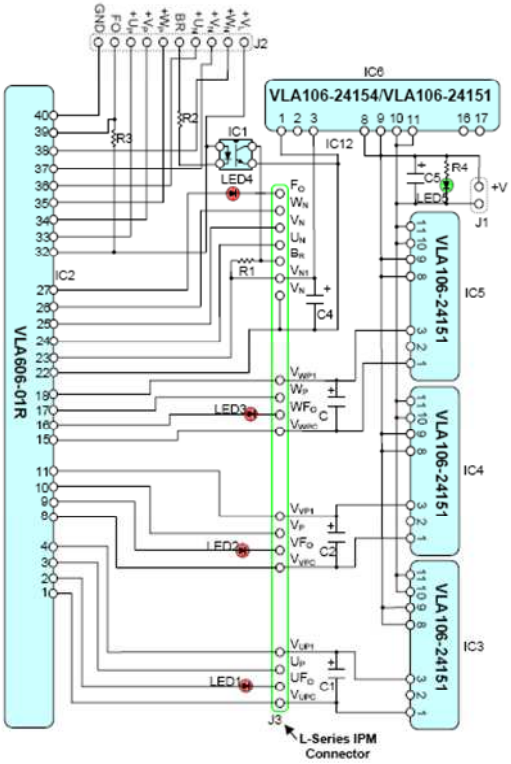

Fig. A3.12 BP7B circuit diagram.

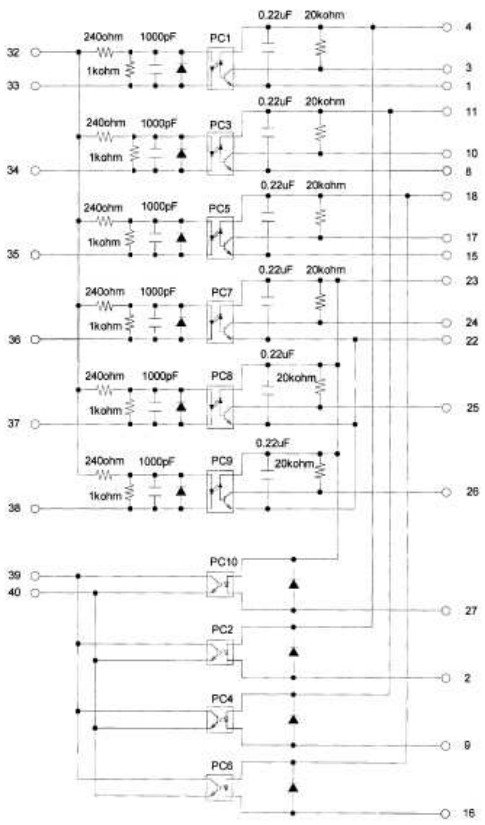

Fig. A3.13 VLA606-01R circuit diagram (optical coupler).

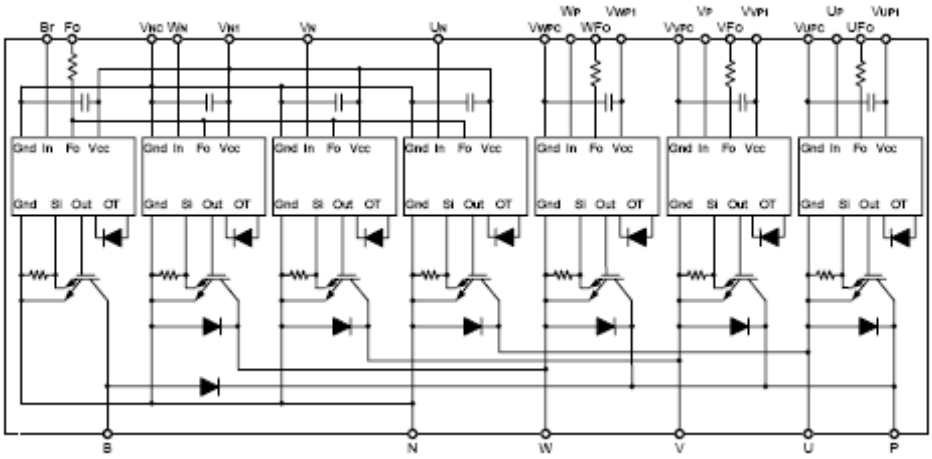

Fig. A3.14 PM25RLA120 IPMs circuit diagram (IGBT).

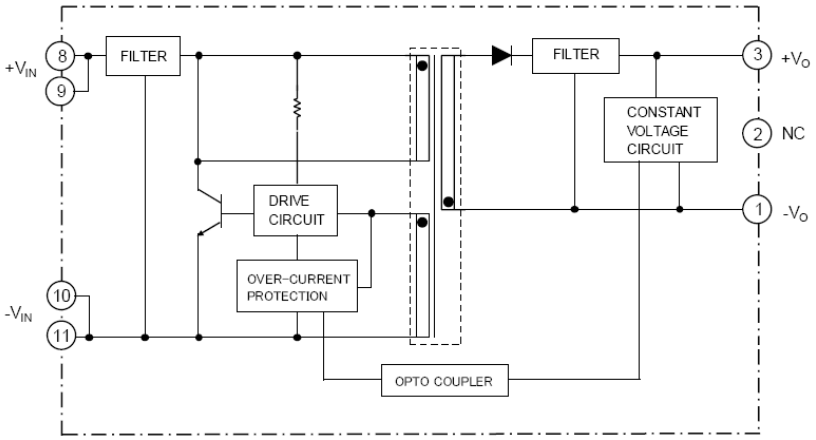

Fig. A3.15 VLA106-24151 circuit diagram (DC-DC).

The circuit uses the VLA606-01R to transfer logic level control signals between the system controller and the IPMs. The internal optocouplers provide galvanic isolation to completely separate the controllers from the high voltage in the power circuit. The VLA606-01R also provides isolated control power supplies to power the IPMs built in gate drive and protection circuits. From Fig. A3.12 the six main IGBT on/off control signals are transferred to the IPMs through VLA606-01R. The input control signal is inverted by the VLA606-01R so that leads that an on signal is generated by low pin ground and off signal is generated by an on 5 volts input signal. The input signal from the control is inputted from pins 33-38 (Up, Vp,Wp, Un, Vn, Wn) and outputted from pins 24-26 Wn, Vn, Un for the low side and the high side are 17, 9, 3,Wp, Vp, Up. Isolated control power for the IPM is supplied by VLA106-24151 (IC3, IC4, IC5, IC6). Each power supply is decoupled at the IPM's pins with a low impedance electrolytic capacitor (C1-C4). These capacitors must be low impedance/high ripple current types because they are required to supply the high current gate drive pulses to the IPM's internal gate driving circuits. The DC to DC converters are powered from a single 24VDC supply connected at CN3. The 24VDC supply is decoupled by the electrolytic capacitor C5 to maintain a stable well filtered source for the DC to DC converters. The current draw on the 24V supply will range from about 75mA to 200mA depending on the module being driven and switching frequency. A power indicator consisting of an LED (LED5) in series with current limiting resistor (R4) is provided to show that the 24VDC supply is present. A typical controller interface for the BP7B can be shown as on signal (IPM control input low) is generated by pulling the respective control input low (GND) using a CMOS buffer capable of sinking at least 16mA (74HC04 or similar) shown in Fig A3.16.

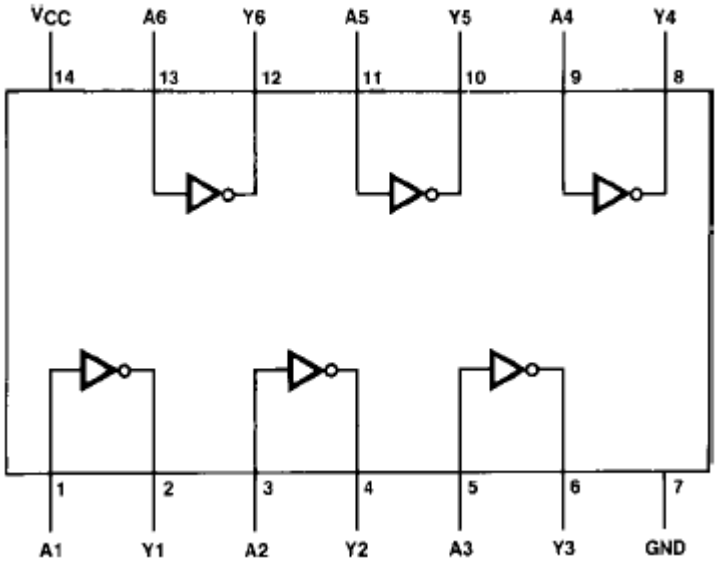

Fig. A3.16 74hc04 buffer circuit (for sinking current).

In the off state the buffer should actively pull the control input high to maintain good noise immunity. Open collector drive that allows the control input to float will degrade common mode noise immunity and is therefore not recommended. If the IPM's built in protection is activated it will immediately shut down the gate drive to the affected IGBT and pull the associated FO pin low. This causes the VLA606 to pull the fault feedback signal (Pin 9 of J2) low. When a fault is detected by the IPM a fault signal with a minimum duration of 1ms is produced. Any signal on the fault line that is significantly shorter than 1ms can not be a legitimate fault and should be ignored by the controller. An active fault signal indicates that severe conditions have caused the IPM's self protection to operate. The fault feedback signal should be used by the system controller to stop the operation of the circuit until the cause of the fault is identified and corrected. Repetitive fault operations may result in damage to the IPM. The BP7B circuit is shown in Fig. A3.17; the IGBT used is PM25RLA120 IPMs is shown in Fig. A3.18 and the CMOS buffer between DSpace and the BP7B circuit is shown in Fig. A3.19. The whole system is shown in Fig A3.20. The DSpace block used to communicate with the BP7B through CMOS buffer is shown in Fig. A3.21.

Fig. A3.17 BP7B circuit diagram.

Fig. A3.18 PM25RLA120 circuit diagram.

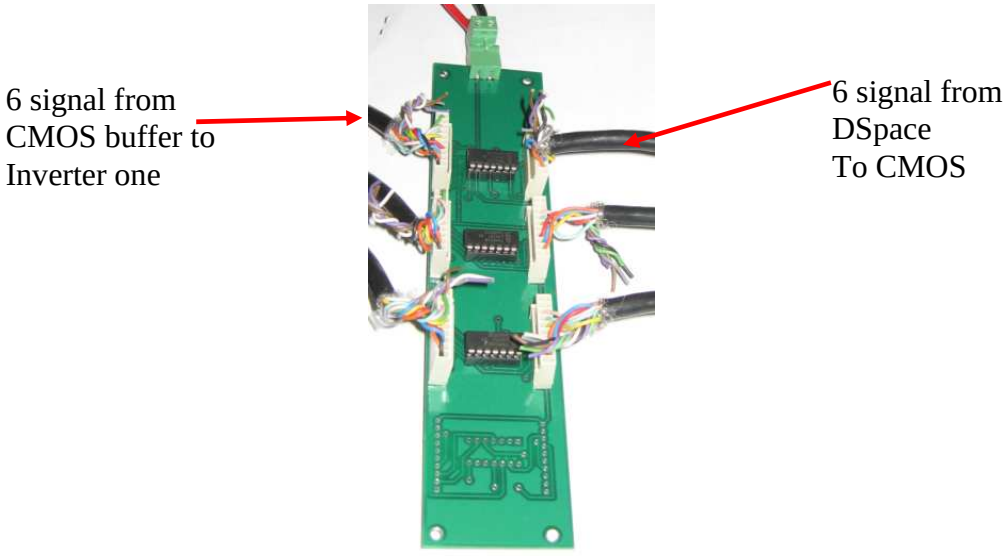

Fig. A3.19 CMOS buffer circuit.

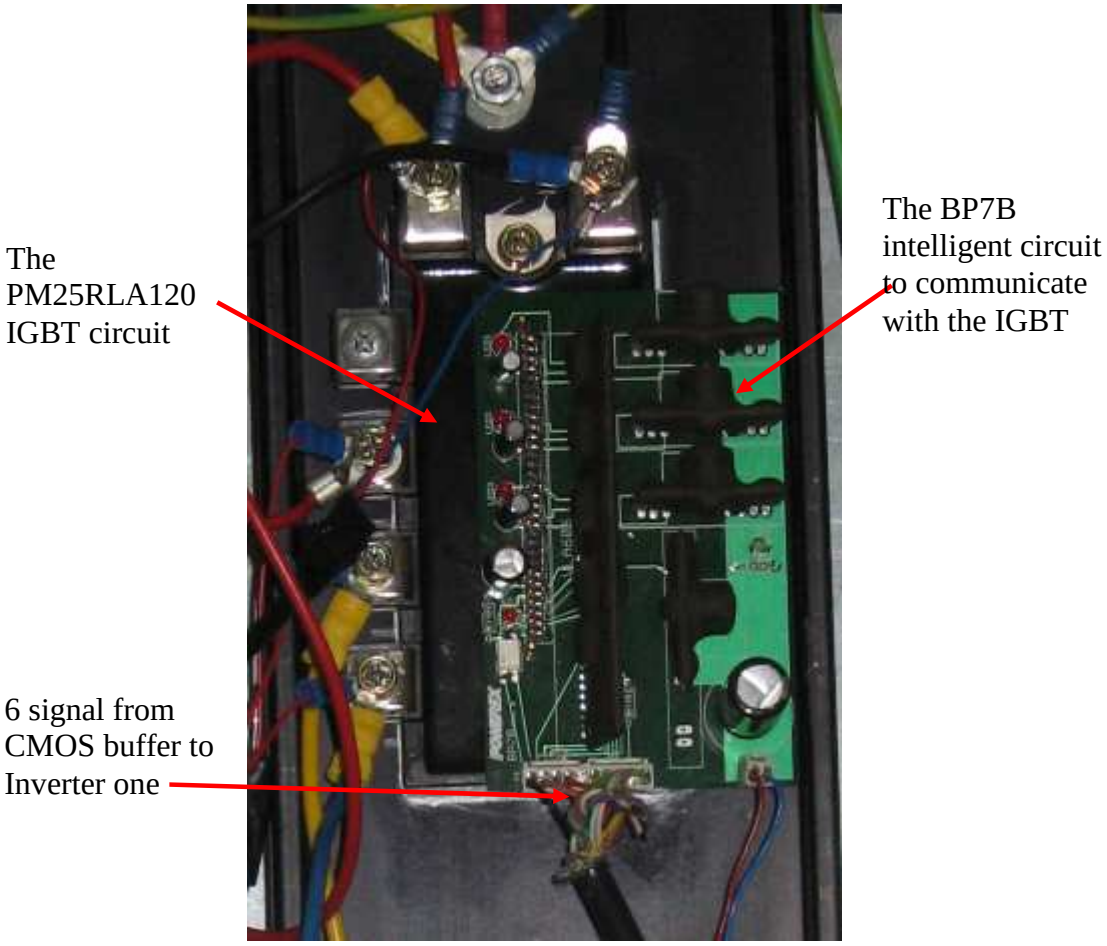

Fig. A3.20 BP7B circuit diagram.

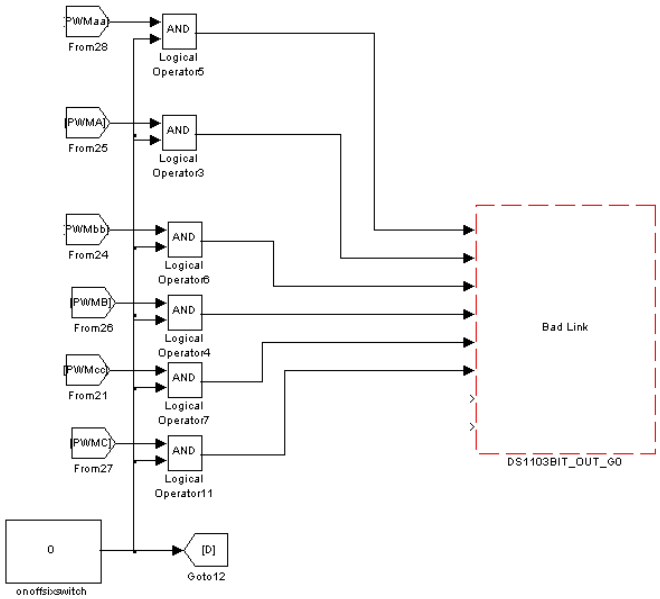

Fig. A3.21 Six switch code from DSpace to inverter.

A3.6 DSpace Model

The complete DSpace model used to implement the measured torque feedback at all speeds is shown in Fig. A3.22. The fifteen parts of the model is discussed below.

A3.6.1 Start here

The Start here block is where system starts, this block generates 5 signals, each signal is 1 s apart, the first signal is to excite phase UV, the second signal is to excite phase VW, the third signal is to excite phase WU, the fourth signal is to estimate the zero speed position and the fifth signal is to start the low speed control using measured torque feedback and then block stops. The initial signal is always set to zero which makes the machine stop. This model is illustrated on Fig. A3.23.

A3.6.2 Zero speed position estimation

The Zero speed estimation block, as discussed in Chapter 2 and 4, will take three torque inputs and estimate the initial position. The position is best when it started from stand still so that no reversal can happen. This model is illustrated on Fig. A3.24.

A3.6.3 Low speed control

The Low speed get the initial position then excites the corresponding phase, depending on the demanded speed the function increases the demanded voltage, if load is added to the block the measured torque feedback will increases or decrease the demanded voltage to keep the system from over modulation or under modulation. This model is illustrated on Fig. A3.25.

A3.6.4 Flux-linkage position estimation (a)

The flux-linkage block (a) it calculates the flux-linkage from the inputted currents and voltages, without any measured torque feedback, in Chapter 5 the results of this block is discussed. This model is illustrated on Fig. A3.26.

A3.6.5 Flux-linkage position estimation (b)

The flux-linkage block (b) it calculates the flux-linkage from the inputted currents and voltages, with measured torque feedback, in Chapter 5 the results of this block is discussed. This model is illustrated on Fig. A3.27.

A3.6.6 Flux-linkage position estimation (c)

The flux-linkage block (c) it calculates the flux-linkage from the calculated currents and voltages from a single DC current, DC voltage and with measured torque feedback, in Chapter 5 the results of this block is discussed. This model is illustrated on Fig. A3.28.

A3.6.7 Speed calculation

The speed calculation blocks takes the estimated electrical position from the flux-linkage and calculates the speed. The inputted electrical position can be either from the calculated position or from the measured position from the position sensor. This model is illustrated on Fig. A3.29.

A3.6.8 Brushless DC control

This block implements brushless DC control, the input are divided into three parts, the first part is for the zero speed estimation and the block will out the signal to the inverter to excite the three phases with 1 A excitation each and to hold the excitation for 1 s. the second part is the low speed control with measured torque feedback where after the zero position is calculated then a low speed control is implemented with measured torque feedback and the block excited the motor as a brushless DC based on the speed demanded and control the current based on the associated measured torque feedback. The third part is for over threshold speed, the flux-linkage in this motor can be calculated after 150 rpm so after the threshold speed the estimated rotor position is inputted and the motor is excited every 120 degrees. This model is illustrated on Fig. A3.30.

A3.6. 9 Current control

The current control either control the current from the measured or from the calculated current from the DC current control. The demanded current is compared to either current and the error is in putted into a PI controller. The PI control output is compared to a triangle waveform to either increase or decrease the duty ratio. The demanded duty ratio output foes to the inverter. This model is illustrated on Fig. A3.31.

A3.6.10 Inverter

The output of the current control is used as the input to the inverter, which from will give the communication signal to the real IGBT. This model is illustrated on Fig. A3.32.

A3.6.11 Torque input

This block is used to input the torque signal into DSpace where is will be used in the zero, low and flux-linkage position control. This model is illustrated on Fig. A3.33.

A3.6.12 Position sensor input

This block is used to input the incremental pulses of the position sensors used and also the index signal is this position sensor there are 5000 pulses per mechanical revolution. The electrical and mechanical position in degrees and radians can be calculated. The measured position here is used to be compared with the calculated position. This model is illustrated on Fig. A3.34.

A3.6.13 Input current

This block is used to input the measured three phase currents and the DC current into DSpace where the will be used to control the BLPM machine. This model is illustrated on Fig. A3.35.

A3.6.14 Calculated current

This block is used to calculate the three phase currents and from the measured DC current where these calculated current will be used to control the BLPM machine. This model is illustrated on Fig. A3.36.

A3.6.15 Input voltage

This block is used to input the measured three phase voltages and the DC voltage into DSpace where the will be used to control the BLPM machine. This model is illustrated on Fig. A3.37.

A3.6.16 Calculated voltage

This block is used to calculate the three phase voltages and from the measured DC voltage where these calculated current will be used to control the BLPM machine. This model is illustrated on Fig. A3.38.

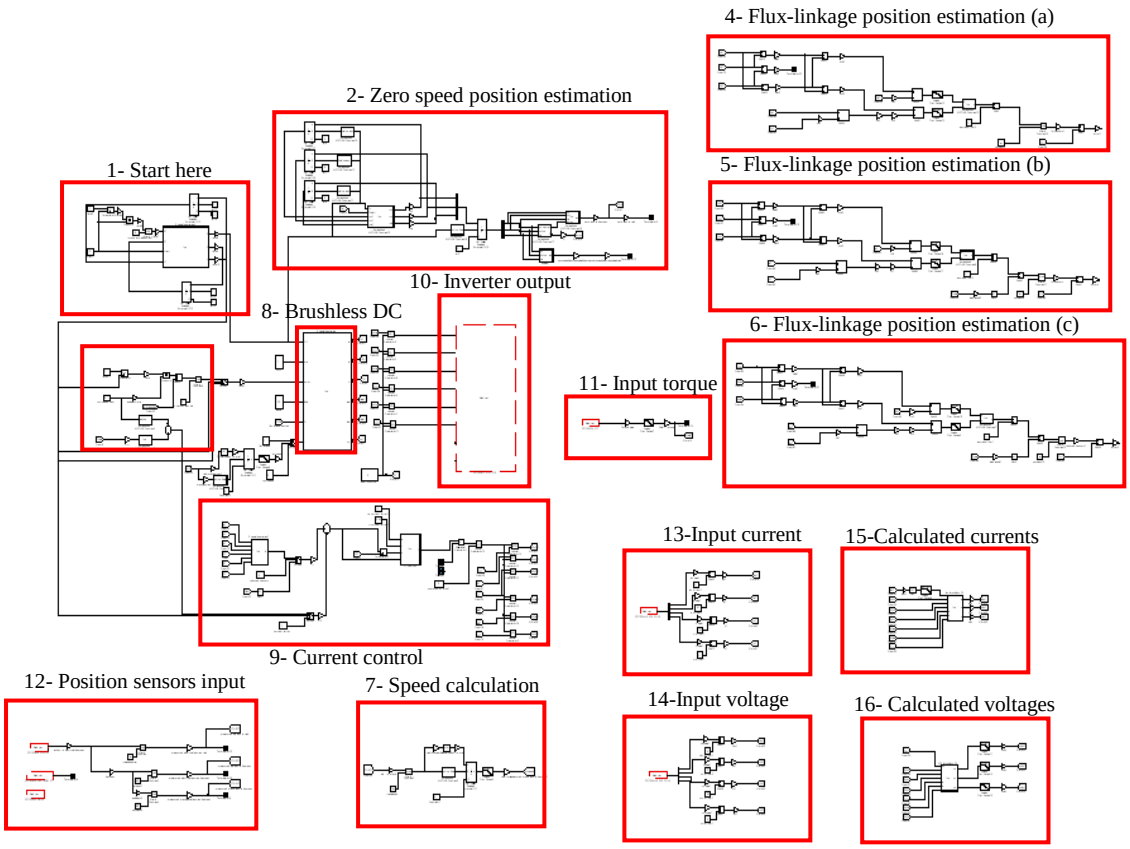

Fig. A3.22 Measured torque feedback control.

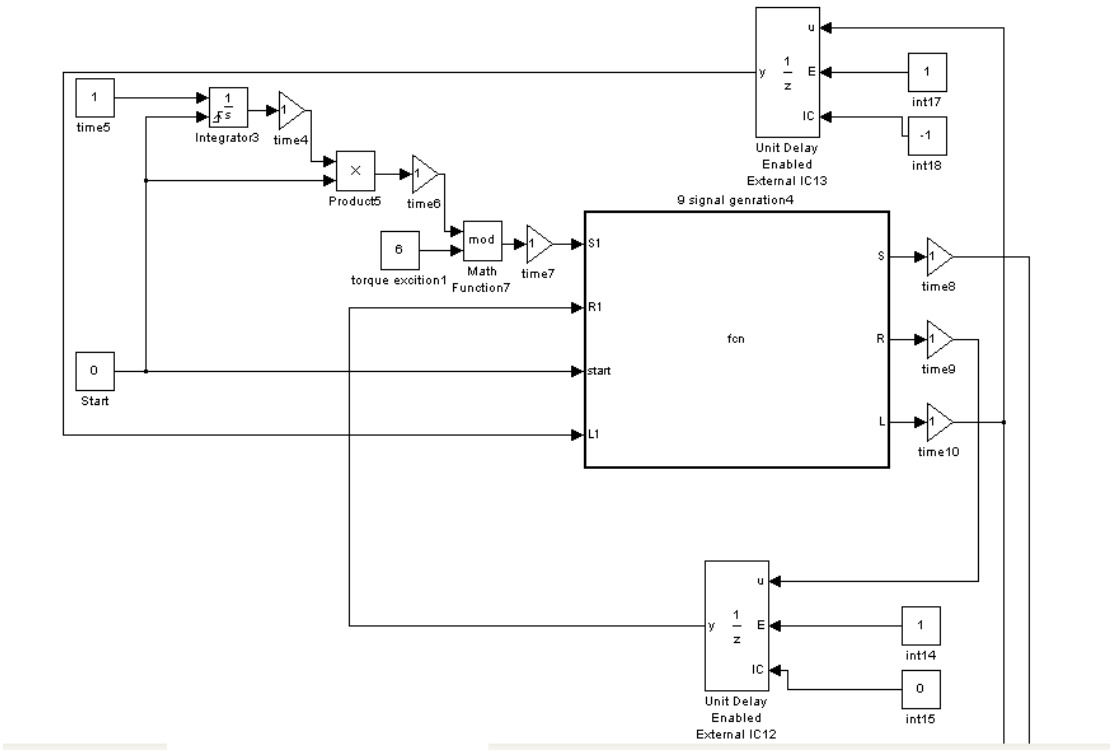

Fig. A3.23 Start up block.

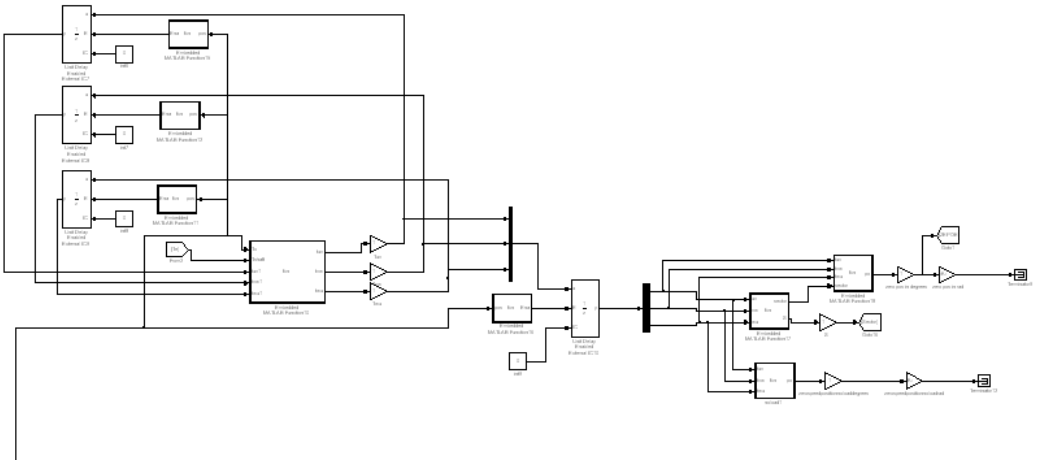

Fig. A3.24 Zero speed estimation.

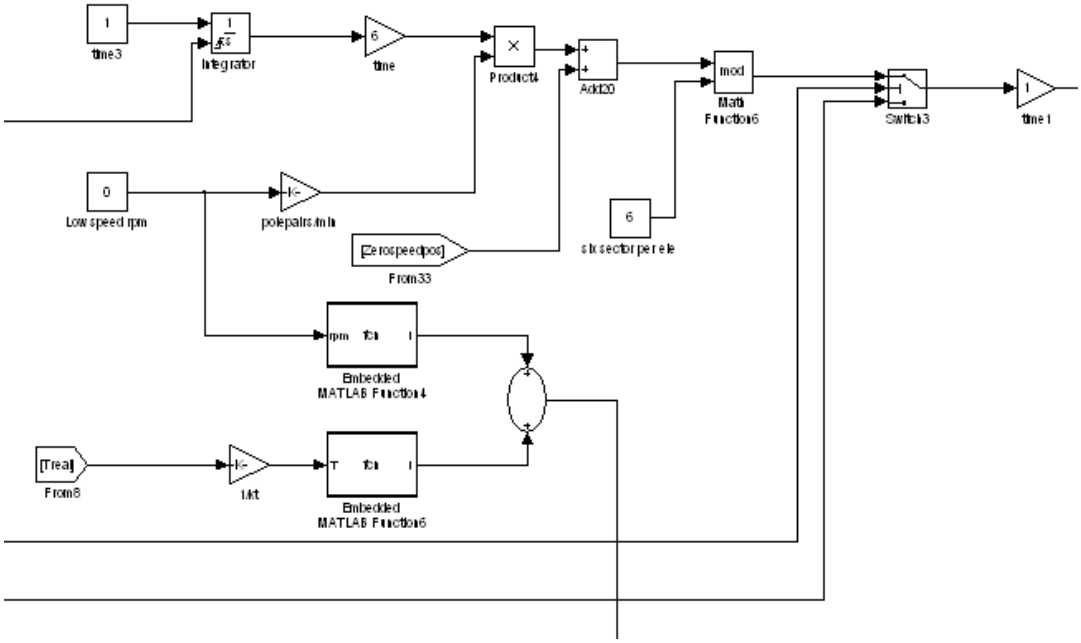

Fig. A3.25 Low speed control.

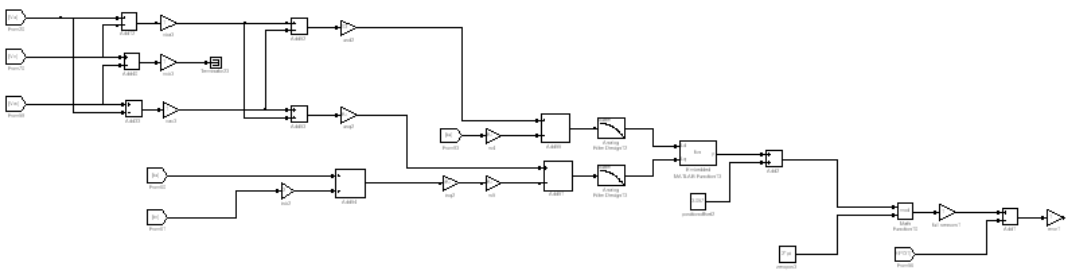

Fig. A3.26 Flux-linkage position estimation with no torque feed-back.

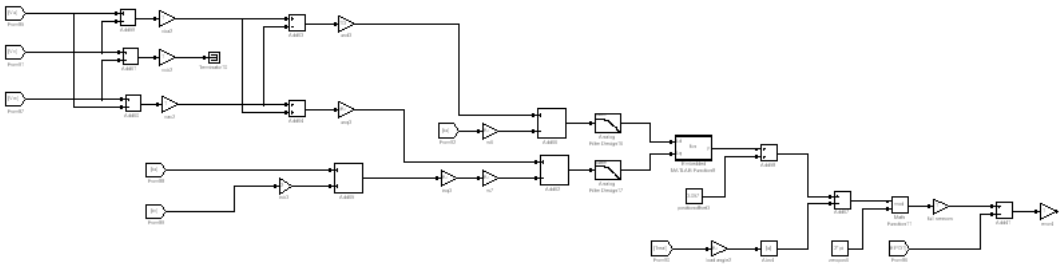

Fig. A3.27 Flux-linkage position estimation with torque feed-back.

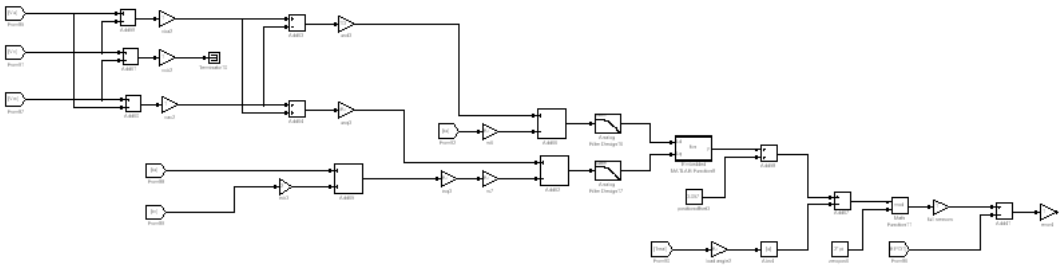

Fig. A3.28 Flux-linkage position estimation with torque feed-back and calculated currents.

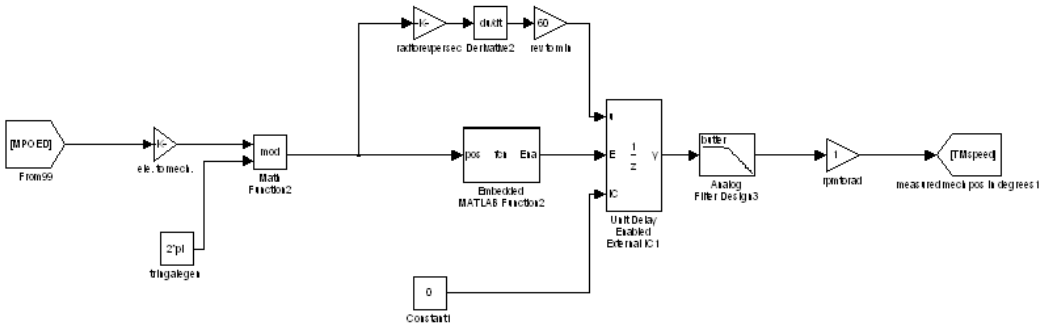

Fig. A3.29 Speed calculation.

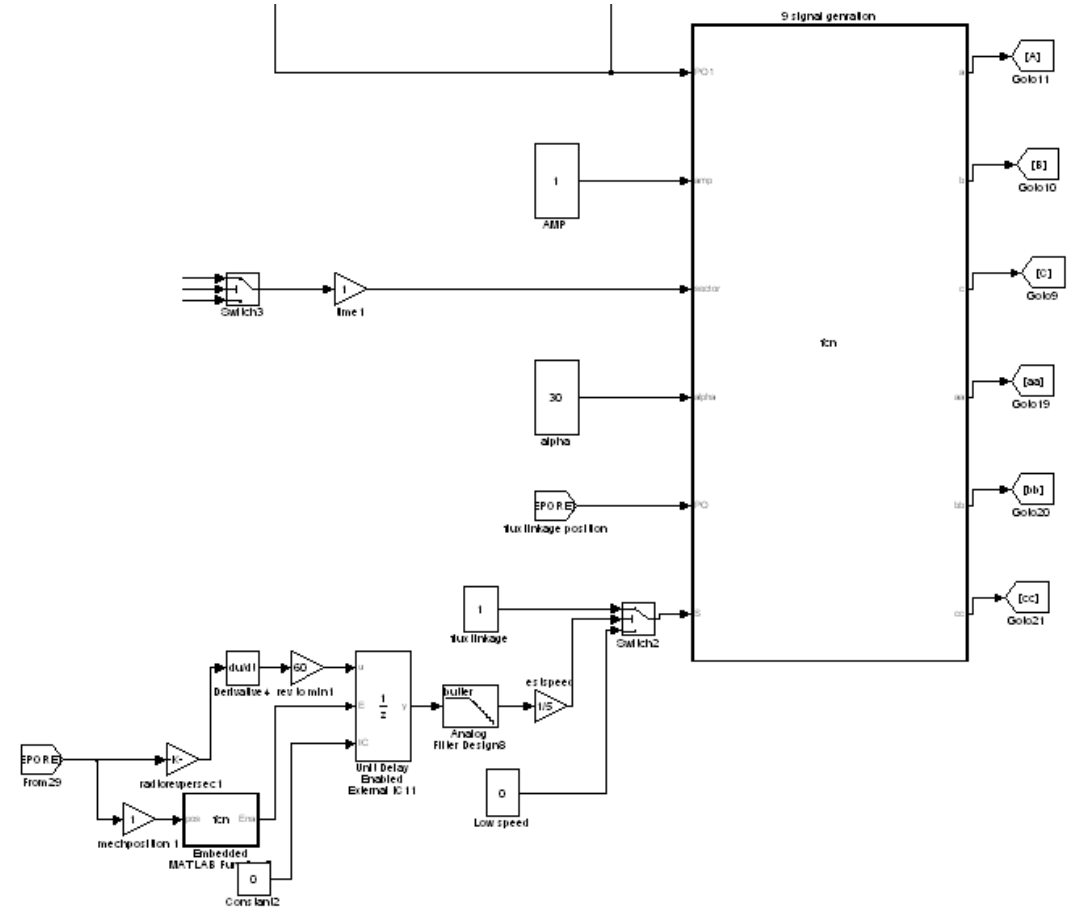

Fig. A3.30 Brushless DC control.

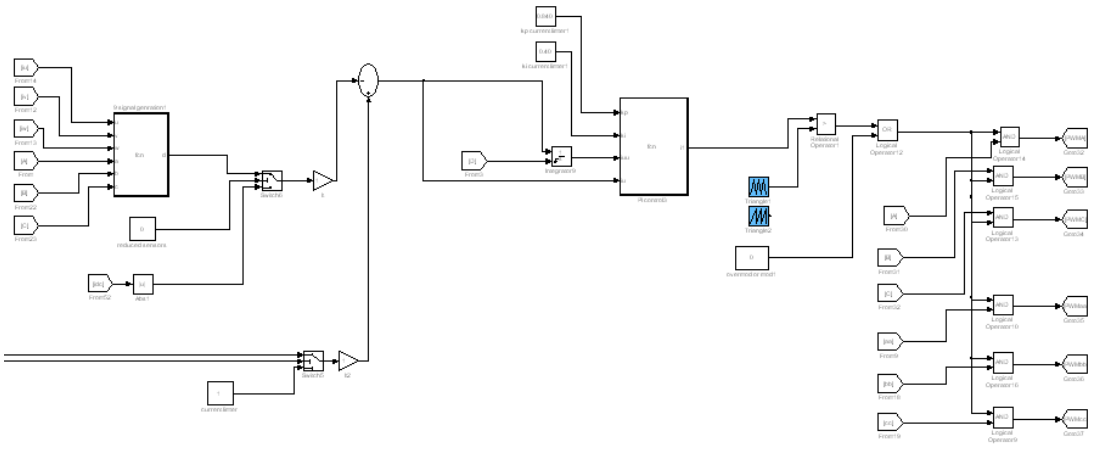

Fig. A3.31 Current control.

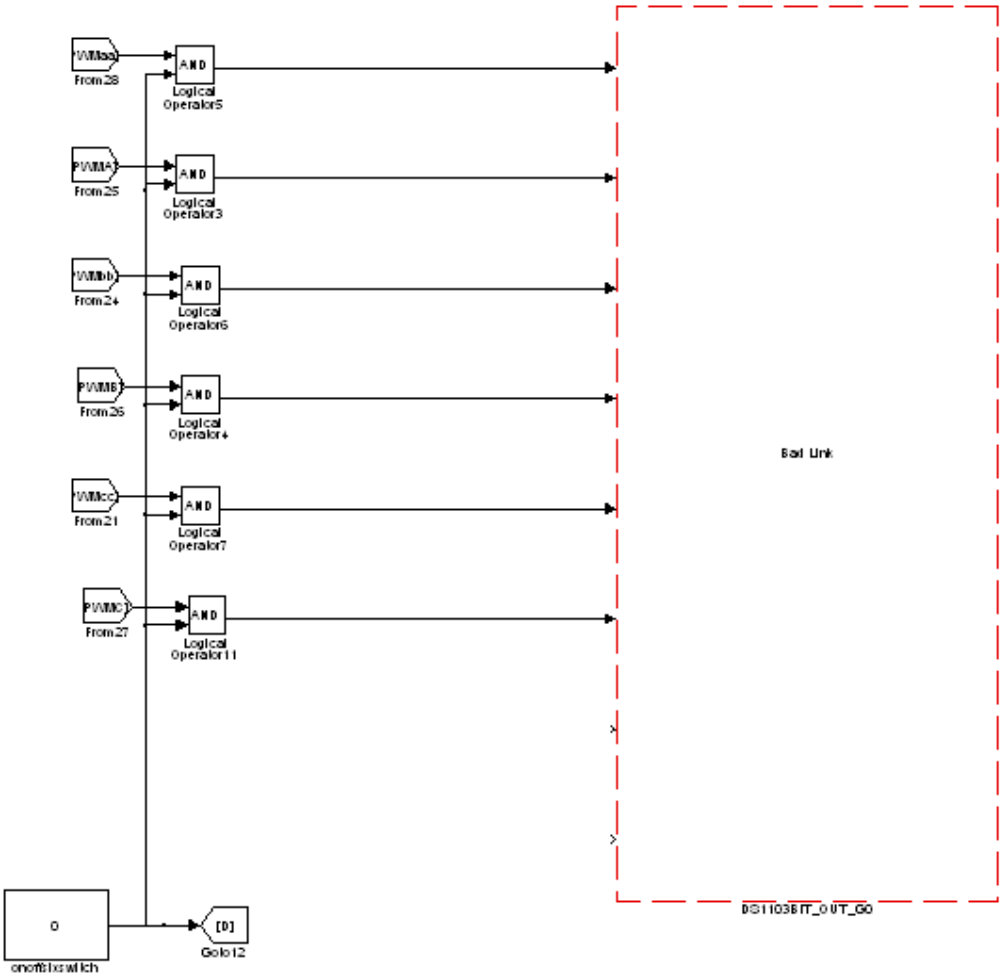

Fig. A3.32 Inverter output block.

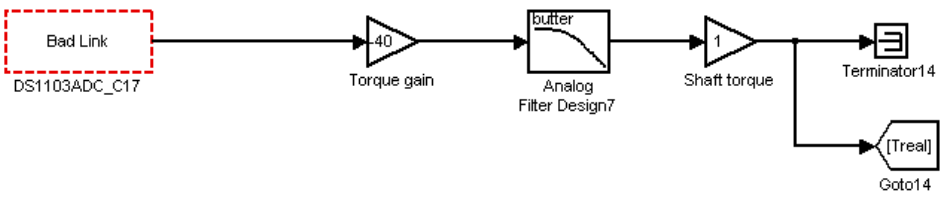

Fig. A3.33 Torque input block.

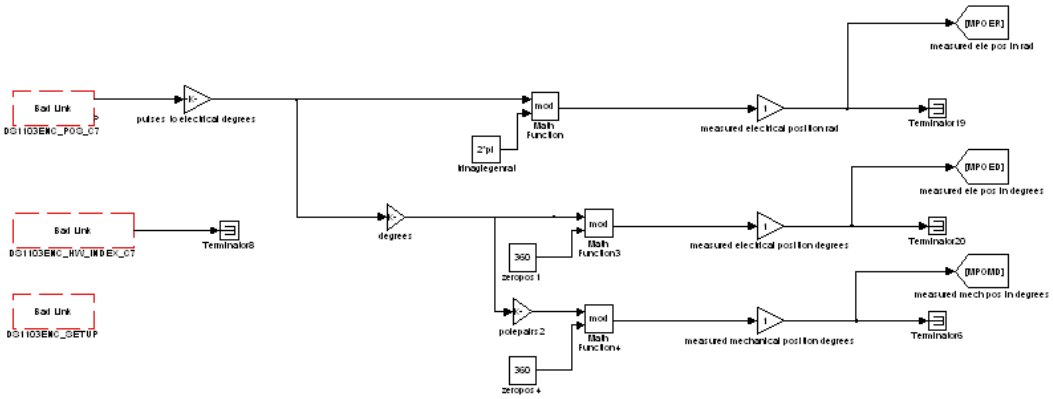

Fig. A3.34 Position sensor input block.

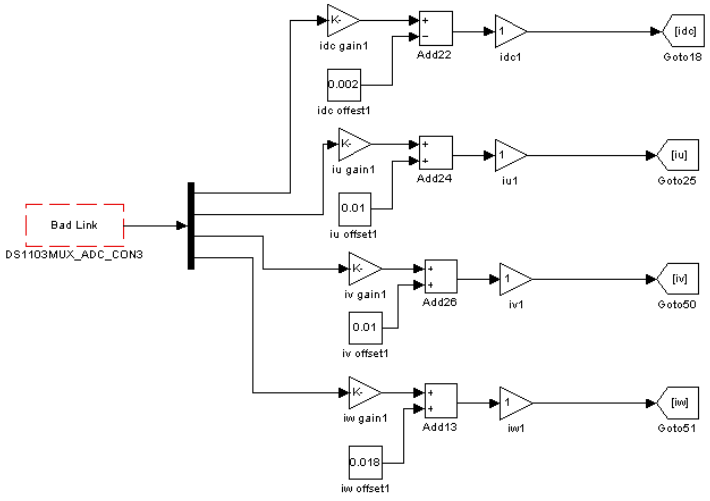

Fig. A3.35 Input current block.

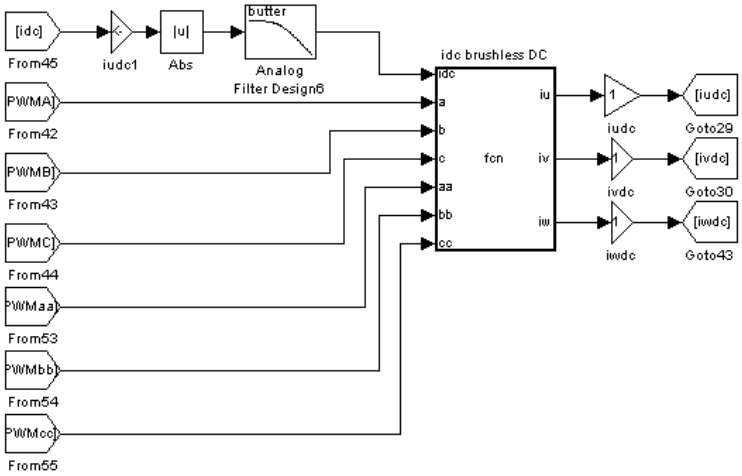

Fig. A3.36 Calculated current block.

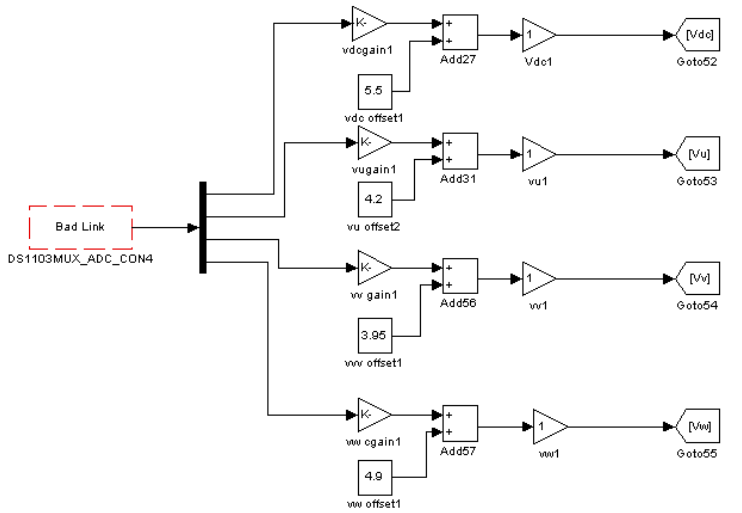

Fig. A3.37 Input voltage block.

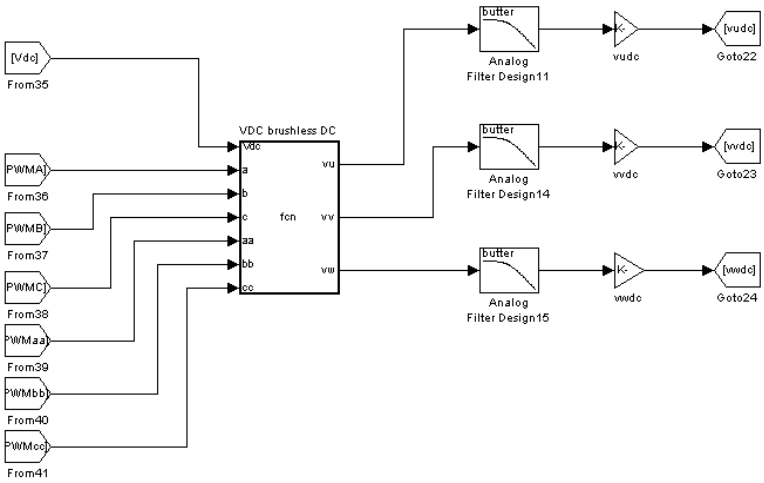

Fig. A3.38 Calculated voltage block.